FINITE ELEMENT AND CENTRIFUGE MODELING OF FROST HEAVE AND THAW CONSOLIDATION SETTLEMENT OF PIPELINES IN COLD REGIONS

By

© Rajith Dayarathne

A Thesis submitted to the

School of Graduate Studies

in partial fulfillment of the requirements for the degree of

Doctor of Philosophy

Faculty of Engineering and Applied Science

Memorial University of Newfoundland

May 2021

St. John's Newfoundland and Labrador Canada

ABSTRACT

Frost heave and thaw settlement are two main issues that need to be considered in the design of pipelines in cold regions. Operating a chilled gas pipeline in unfrozen ground or a warm oil pipeline in frozen ground could create a frost or thaw bulb in the soils around the pipeline, which could cause significant ground movement that may impose unacceptable loads on the pipeline, especially in the proximity of thermal interfaces. Modelling of such ground movement and corresponding pipeline–soil interaction may become more complex due to seasonal variation of air temperatures and operating conditions of the pipeline (e.g., pressure and temperature at the compressor stations), which may induce freeze-thaw cycles in the soils downstream areas. The frost heave and thaw settlement around the pipeline under constant and cyclic temperatures at the pipeline and ground surfaces are the focus of the present study.

An experimental investigation of displacement of pipelines buried in frost susceptible soils subjected to freeze-thaw cycles is presented first. The effectiveness of cyclic variation of pipeline operating temperatures as a frost heave mitigation measure is evaluated by analyzing 14 model pipes' tests in a geotechnical centrifuge. Based on the experimental results, five types of possible freeze-thaw induced vertical displacement responses of the pipeline during operation have been identified. The cyclic pipeline operation (sub-zero in the winter and above-zero in the summer months) could reduce the heave rate and total heave compared to those observed in the tests operated under continuous sub-zero pipe temperatures.

Secondly, a two-dimensional fully coupled thermo-mechanical finite element (FE) model is developed using Abaqus FE software for simulating the frost heave around chilled gas pipelines buried in frost susceptible soil. The mechanical behaviour of frozen and unfrozen soils is defined using elastic-plastic models that recognize the key influencing factors, including temperature and

volumetric ice content in the frozen soil. The Konrad–Morgenstern segregation potential model and the mechanical behaviour of soil are implemented in Abaqus using user subroutines. The FE calculated results are compared with the Calgary full-scale experimental results of two pipe sections buried at different depths, namely control and deep-burial sections. The FE calculated frost front penetration, frost heave, and moisture growth agree well with the experimental results, which indicates that the present FE model can successfully simulate the frost heave around buried pipelines. The long-term frost heave (up to 20 years) is simulated. The decrease of heave rate after the formation of the final ice lens and associated warming at its leading edge is highlighted. The effects of key factors on frost heave and challenges in FE modelling of such large displacements are evaluated. The factors include the water migration modelling approach, soil properties, seasonal ground surface temperatures and operating conditions.

Finally, a large-strain coupled thermo-hydro-mechanical FE model is developed using Abaqus FE software to simulate thaw consolidation. The variations of hydraulic conductivity, compressibility, and thermal properties of thawed soils during consolidation are implemented. One-dimensional FE simulations are performed first to verify the FE modelling approach and to show the limitations of the existing small-strain linear thaw consolidation model. Nonlinear variation of void ratio–effective stress–hydraulic conductivity is then considered for improved modelling of thaw consolidation. Finally, a two-dimensional FE modelling of thaw consolidation around a warm pipeline buried in permafrost is presented. The highly nonlinear void ratio–effective stress and void ratio–hydraulic conductivity relationships, specifically the high hydraulic conductivity at large void ratios and low effective stresses after thawing, cause pore water flow along the thaw front, instead of vertical flow in simplified one-dimensional thaw consolidation models, as assumed in previous studies.

ACKNOWLEDGEMENTS

First and foremost, I would like to express my sincere gratitude to my supervisor, Dr. Bipul Hawlader, Professor and Research Chair in Seafloor Mechanics of Memorial University of Newfoundland, for his supervision. Dr. Hawlader always encouraged me to be the best version of myself and steered me in the right direction whenever he felt I needed it. Without his persistent support, the goal of my research could only have been a dream.

I would also like to thank my co-supervisors, Dr. Ryan Phillips, Principal Consultant, C-CORE, NL, Canada and Dr. Dilan Robert, Senior Lecturer, RMIT University, Australia, for their invaluable suggestions and comments provided throughout my Ph.D. program.

I would not have accomplished the goal of my study without the financial support of InnovateNL, formerly RDC, Equinor Research Chair, Natural Sciences and Engineering Research Council of Canada, and the School of Graduate Studies, Memorial University. I also thank C-CORE for providing me with a perfect working space to carry out my studies throughout the program.

I owe a debt of gratitude to all the teachers who taught me, from kindergarten to the university level. As a person who comes from a low-income family, I am forever grateful to the free education system of Sri Lanka which brought me to this road of success.

Furthermore, I wish to express my very profound gratitude to my parents, family and friends for their continuous encouragement and support. Last but not least, I would like to thank my lovely wife Isuru and our precious baby boy who is growing inside her. Isuru, without your unconditional love and years of understanding, I would not have been able to complete my Ph.D. This dissertation stands as a testament to your unconditional love and encouragement.

Table of Contents

ABSTRACT ..... **ii**

ACKNOWLEDGEMENTS ..... **iv**

List of Figures ..... **x**

List of Tables ..... **xv**

List of Symbols ..... **xvi**

CHAPTER 1: INTRODUCTION **1-1**

1.1 General 1-1

1.2 Rationale 1-5

1.3 Objectives 1-6

1.4 Thesis Organization 1-8

CHAPTER 2: LITERATURE REVIEW **2-1**

2.1 Introduction 2-1

2.2 Laboratory Tests 2-2

2.2.1 Laboratory frost heave tests 2-3

2.2.2 Laboratory thaw consolidation tests 2-5

2.2.3 Freeze-thaw laboratory tests 2-7

2.3 Full-Scale Experiments 2-8

2.3.1 Full-scale frost heave experiments 2-8

2.3.2 Full-scale thaw settlement experiments 2-10

2.4 Centrifuge Frost Heave and Thaw Settlement Tests 2-11

2.5 Frost Heave/Thaw Settlement Experience in Existing Pipelines 2-13

2.6 Modelling of Frost Heave and Thaw Settlement of Buried Pipelines 2-21

2.6.1 Heat transfer analysis and thermal properties of soils 2-21
2.6.1.1 Soil freezing characteristic curve 2-22
2.6.1.2 Thermal conductivity of soils 2-24
2.6.1.3 Heat capacity and latent heat of soils 2-25
2.6.2 Frost heave modelling 2-26
2.6.2.1 Stress–strain behaviour of frozen soils 2-31
2.6.3 Thaw settlement modelling 2-33
2.6.3.1 Residual stress and hydromechanical behaviour of thawed soils 2-34
2.7 Summary 2-39
CHAPTER 3: Centrifuge Modelling of Gas Pipelines Undergoing Freeze–Thaw Cycles .. 3-1
3.1 Abstract 3-1
3.2 Introduction 3-2
3.3 Problem Statement 3-5
3.4 Centrifuge Modelling 3-7
3.4.1 Materials 3-8
3.4.2 Centrifuge model 3-9
3.4.3 Sample preparation 3-10
3.4.4 Model pipe and instrumentation 3-11
3.4.5 Initial ground temperature and centrifuge test setup 3-13
3.4.6 Centrifuge tests 3-13
3.4.7 Post-test investigation 3-14
3.5 Experimental Results 3-15
3.5.1 Case-1 3-15
3.5.2 Case-2 3-22

3.5.3 Case-3 3-24
3.6 Implications for Frost Heave Prediction and Pipeline Design 3-25
3.7 Conclusions 3-26
CHAPTER 4: Two-Dimensional Finite Element Modelling of Long-Term Frost Heave Beneath Chilled Gas Pipelines 4-1
4.1 Abstract 4-1
4.2 Introduction 4-2
4.3 Problem Statement 4-6
4.4 Modelling of Frost Heave and Thawing 4-8
4.5 Finite Element Modelling 4-11
4.5.1 Temperature boundary conditions 4-12
4.6 Numerical Implementation 4-12
4.7 Soil Properties 4-16
4.7.1 Freezing characteristics 4-16
4.7.2 Stress–strain behaviour of unfrozen silt 4-17
4.7.3 Stress–strain behaviour of frozen silt 4-18
4.8 Results 4-20
4.8.1 Frost heave and frost front penetrations 4-20
4.8.2 Heave at stable and retreating frost front 4-20
4.8.3 Temperature gradient in the frozen fringe 4-23
4.8.4 Ice growth 4-25
4.9 Conclusions 4-27

CHAPTER 5: Factors Affecting Frost Heave of Chilled Gas Pipelines 5-1

5.1 Abstract 5-1

5.2 Introduction 5-2

5.3 Problem Statement 5-5

5.4 Finite Element Modelling 5-6

5.5 Modelling of Thermo-Mechanical Behaviour of Soil 5-6

5.6 Results 5-10

5.6.1 Ground surface and initial ground temperature 5-10

5.6.2 Segregation-freezing temperature 5-13

5.6.3 Stress effect on segregation potential 5-15

5.6.4 Segregation potential with zero applied pressure (SP_0) 5-17

5.6.5 Shear strength of frozen soil 5-18

5.6.6 Pipe temperature 5-19

5.7 Conclusions 5-21

CHAPTER 6: One- and Two-Dimensional Finite Element Modelling of Thaw Consolidation 6-1

6.1 Abstract 6-1

6.2 Introduction 6-2

6.3 Problem Definition 6-5

6.4 Finite Element Modelling 6-6

6.5 Stress–Strain Behaviour 6-8

6.6 Thermal Properties 6-12

6.7 Set-I Results: 1-D Analysis with a Linear Soil Model 6-13

6.7.1 Analytical solution 6-14
6.7.2 Consolidation with a surcharge 6-15
6.7.3 Consolidation without surcharge 6-16
6.8 Set-II Results: 1-D Analysis with a Nonlinear Soil Model 6-18
6.8.1 1-D Simulation of laboratory thaw consolidation test 6-19
6.9 Set-III Results: 2-D Thawing Around a Pipeline 6-21
6.9.1 Dissipation of excess pore water pressure 6-23
6.9.2 Effect of nonlinear variation of hydraulic conductivity 6-24
6.10 Conclusions 6-26
CHAPTER 7: Conclusions and Recommendations for Future Research 7-1
7.1 Conclusions 7-1
7.2 Recommendations to Future Research 7-4
REFERENCES R-1
APPENDIX A A-1
APPENDIX B B-1

List of Figures

Fig. 1.1. Schematic of: (a) frost heave around a chilled pipeline buried in the unfrozen ground; and (b) thaw settlement around a warm pipeline buried in permafrost (after Wang et al. 2018)..... 1-3

Fig. 1.2. Differential movements at the thermal interfaces (after Nixon et al. 1990): (a) frost heave; and (b) thaw settlement..... 1-4

Fig. 2.1. Schematic of ice lenses formation in frost cell tests: (a) step freezing test; and (b) ramped freezing test (after Konrad 1994)..... 2-4

Fig. 2.2. Typical compression curve in thaw consolidation test (modified from Andersland and Ladanyi 2004)..... 2-6

Fig. 2.3. Variation of pipe temperatures in cold regions pipelines: (a) Norman Wells oil pipeline (after Nixon and Burgess 1999); and (b) Urengoy-Nadym gas pipeline in Nadym-Pur-Taz natural gas production complex (after Seligman 2000)..... 2-16

Fig. 2.4. Schematic of unfrozen water formations in frozen soil (after Rempel et al. 2004) 2-23

Fig. 2.5. Volumetric compression of frozen soils on thawing (modified from Dumais 2019) 2-36

Fig. 3.1. Variation of pipe temperature between compressor stations: (a) in pipeline; (b) at point A 3-35

Fig. 3.2. Particle size distribution of materials..... 3-36

Fig. 3.3. Centrifuge model: (a) typical test package set-up; (b) top view of test CF2 after completion of centrifuge test..... 3-37

Fig. 3.4. Typical instrument setup..... 3-38

Fig. 3.5. Vertical displacements of pipe for case-1 tests..... 3-39

Fig. 3.6. Soil temperature below the pipe: (a) pipe A1; (b) pipe A2; (c) pipe A3; (d) pipe B2 3-40
Fig. 3.7. Development of seasonal thaw and frost bulb 3-41
Fig. 3.8. Cross-sectional views of test CF2: (a) pipe A2; (b) pipe B2 3-41
Fig. 3.9. Vertical displacements of pipe for case-2 tests 3-42
Fig. 3.10. Soil temperature below pipe A4 3-42
Fig. 3.11. Soil temperature below pipe A7 3-43
Fig. 3.12. Vertical displacements of pipe for case-3 tests 3-43
Fig. 3.13. Summary of pipe displacement responses 3-44
Fig. 4.1. Frost heave of chilled gas pipeline: (a) schematic view and nomenclature; and (b) typical section after centrifuge test (C-CORE 2005) 4-39
Fig. 4.2. Finite element mesh used in two-dimensional analysis 4-40
Fig. 4.3. Implementation of model using user subroutines 4-41
Fig. 4.4. Comparison between FE and Calgary full-scale deep burial section test results: (a) frost heave; and (b) frost front penetration 4-42
Fig. 4.5. Comparison between FE and Calgary full-scale control section test results: (a) frost heave; and (b) frost front penetration 4-43
Fig. 4.6. Temperature gradient variation with time in typical soil elements in frozen zone for deep burial section 4-44
Fig. 4.7. Comparison of observed and predicted temperature gradient in segregation freezing temperature with time for deep burial section 4-45
Fig. 4.8. Comparison of observed and predicted temperature profile for deep burial section after 1000 days 4-46

Fig. 4.9. FE calculated and observed moisture content below pipe invert for deep burial section 4-47

Fig. 4.10. Volumetric ice content (%): (a)–(c) control section; and (d)–(f) deep-burial section 4-48

Fig. 4.11. Total moisture content (%): (a)–(c) control section; and (d)–(f) deep-burial section 4-49

Fig. 4.12. Volumetric strain increment due to ice lens formation in frozen fringe after 1000 days in deep burial section (Δt = 10 days) 4-50

Fig. 5.1. Schematic of frost heave of a chilled gas pipeline buried in unfrozen soil 5-32

Fig. 5.2. Finite element mesh used in the analysis 5-33

Fig. 5.3. Effect of initial ground temperature and ground surface temperature: (a) deep burial; and (b) shallow burial 5-34

Fig. 5.4. Frost front distribution of at different time intervals: (a) & (b) shallow burial; and (c) & (d) deep burial 5-36

Fig. 5.5. Temperature gradient variation with time in typical soil elements in the frozen zone for deep burial section: (a) $T_s = T_{sm}$; and (b) $T_s = T_{sv}$ 5-37

Fig. 5.6. Effects of segregation freezing temperature (T_{sf}): (a) T_g = +5 °C; and (b) T_g = +2 °C 5-38

Fig. 5.7. Temperature below pipe invert for different initial ground temperatures 5-39

Fig. 5.8. Effects of stress parameter (p_e): (a) T_g = +2 °C; and T_g = +5 °C 5-40

Fig. 5.9. Stress in frozen fringe after 4 years for T_g = +5 °C; (a) σ_n/σ_{ov}; and (b) p/σ_{ov} 5-41

Fig. 5.10. Effects of segregation potential at zero applied pressure (SP_0): (a) T_g = +2 °C; and T_g = +5 °C 5-42

Fig. 5.11. Effects of shear increase parameter of frozen soils (α): (a) T_g = +2 °C; and T_g = +5 °C 5-43

Fig. 5.12. Effects of pipe temperature (T_p): (a) T_g = +2 °C; and T_g = +5 °C 5-44

Fig. 6.1. Schematic of thaw consolidation: (a) 1-D thawing of a frozen soil column; and (b) permafrost thawing through a buried warm pipeline 6-36

Fig. 6.2. FE mesh used in two-dimensional thawing around pipeline 6-37

Fig. 6.3. Modified Drucker–Prager Cap material model: (a) yield surface; and (b) void ratio–effective stress relationship of thawed soil 6-38

Fig. 6.4. Surface settlement in the simulations with a surcharge 6-39

Fig. 6.5. Comparison of FE calculated excess pore water pressure with analytical solution for case S4: (a) without surface settlement; and (b) considering surface settlement 6-40

Fig. 6.6. Excess pore water pressure under self-weight in case S3: (a) generation during thawing; and (b) dissipation during post-thaw consolidation 6-41

Fig. 6.7. Comparison of present FE results with previous study: (a) temperature distribution; (b) void ratio; (c) excess pore water pressure; and (d) thaw settlement 6-42

Fig. 6.8. Two-dimensional thawing around pipe: (a) thaw settlement; and (b) thaw front penetration 6-43

Fig. 6.9. Location of thaw front at different time 6-44

Fig. 6.10. FE calculated mean effective stress and hydraulic conductivity of an element directly below the pipe center at y_0 = 0.9 m 6-45

Fig. 6.11. Pore water flow vectors at different time intervals (e_{max} = 1.2 and k_{max} = 3.3×10^{-7} m/s) 6-48

Fig. 6.12. Excess pore water pressure around the pipe after 50 days 6-49

Fig. 6.13. Pore water flow vectors at different time intervals (e_{max} = 1.47 and k_{max} = 1.94×10^{-4} m/s) 6-52

List of Tables

Table 2.1. Frost heave/thaw settlement experience in cold region pipelines 2-17

Table 2.2. Summary of frost heave modelling of buried chilled pipelines 2-29

Table 2.3. Summary of available thaw consolidation models 2-37

Table 3.1. Soil bed and model pipes used in centrifuge modelling 3-45

Table 3.2. Experimental conditions of centrifuge tests 3-46

Table 4.1. Parameters used in finite element simulation 4-51

Table 5.1. Parameters used in finite element simulation 5-45

Table 6.1. Mechanical properties used in Set-II and Set-III analysis with nonlinear soil model 6-53

Table 6.2. Thermal properties used in FE analysis 6-55

Table 6.3. Parameters used in one-dimensional Set-I analysis with linear soil model 6-56

List of Symbols

As the thesis is written in manuscript format, the symbols used in this study are listed at the end of each chapter (Chapters 3–6).

CHAPTER 1:

INTRODUCTION

1.1 General

With the increase in global oil and gas demand and the potential of major discoveries, the development of oil and gas fields in the Arctic has significantly increased in the last few decades, although the engineering constructions in the region are challenging due to the harsh environmental conditions and unique geotechnical issues. Parson Lake and Arctic Islands are examples of hydrocarbon discoveries in the Canadian Arctic. According to the United States Geological Survey, 13–30% of global undiscovered oil and gas reserves can be found in the Arctic (Gautier et al. 2009). Pipeline transmission is identified as one of the most efficient ways to transport the recovered oil and gas from the northern fields to southern markets. In most cases, transmission pipelines may traverse a long distance through a wide variety of geotechnical terrains and climatic conditions that are unique to the region and not commonly experienced in typical pipeline projects in warm regions. For example, the 328-mm diameter, 869-km long Norman Wells oil pipeline in Canada, which carries the oil from Norman Wells to Zama, is completely buried in discontinuous permafrost terrain where thermal interfaces frequently exist between unfrozen and frozen ground (Nixon and Burgess 1999).

Under such geotechnical conditions, the integrity of the pipeline highly depends on its interactions with the surrounding geotechnical terrains. Undesirable conditions during the construction and operation could trigger many geohazards, including frost heave, thaw settlement, and large ground movements (e.g., slope failures). To minimize the risk associated with these geohazards while meeting the design, construction and production requirements, pipeline route selection, installation method (e.g., buried or above-ground pipelines), and operating conditions

(e.g., temperature and pressure) need to be carefully planned. Note that ‘pipeline’ refers to buried pipeline throughout this thesis unless otherwise mentioned.

An accepted design philosophy for the pipelines in the north is to operate the pipeline at or close to ambient temperatures, which makes it less interactive with surrounding geotechnical systems (Nixon and Burgess 1999). In other words, if the ground is frozen, sub-zero pipeline temperatures are preferred and vice versa for unfrozen ground. This, however, is not always possible due to the unique properties of hydrocarbons, frequent changes in geotechnical conditions in a pipeline’s path, the economics of the project, spans of oil/gas processing facilities, and deviations of operating conditions from start-up after some time of operations.

Sub-zero temperatures in the unfrozen ground freeze the soil around the pipeline, which results in frost heave due to the freezing of in-situ and migrated water (Fig. 1.1(a)). This could be very significant when the pipeline passes through highly frost susceptible soils (e.g., clayey silt) (Konrad and Morgenstern 1984). However, warm operations of pipelines buried in frozen fine-grained soils or ice-rich permafrost could melt volumetric ice inclusions and cause thaw settlement (Fig. 1.1(b)). Therefore, frost heave and thaw settlement are some of the major design considerations for northern pipelines.

If the ground movement is uniform, it is unlikely to generate significant stresses on the pipeline. The key factors that govern the structural response of the pipeline are the magnitude of differential heave/settlement and pipeline–soil interaction in the vertical and axial directions. However, in discontinuous permafrost, it is common to see thermal interfaces between frozen and unfrozen grounds or soils with different frost susceptibilities. For example, Nixon et al. (1991) reported through ditch wall records that there are 2–10 thermal interfaces per kilometre along the route of the Norman Wells oil pipeline in Canada. At these locations, the unfrozen region is quite

active for frost heave compared to the frozen region, while the frozen region is active for thaw settlement; this leads to the differential movements at the thermal interface when a warm or chilled pipeline is operating (Fig. 1.2). These movements could cause unacceptable stresses on the pipeline, which may sometimes cause failure (Carlson et al. 1982; Paulin et al. 2002). The pipe's structural response is often estimated using the free-field frost heave or thaw settlement that occurs sufficiently far from the thermal interface (Rajani and Morgenstern 1994; Selvadurai et al. 1999; Hawlader et al. 2006).

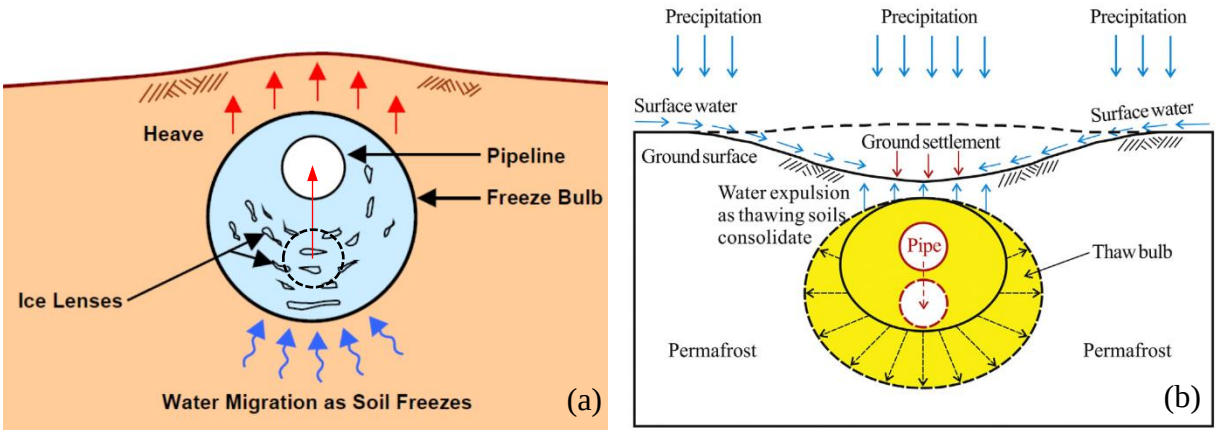

Fig. 1.1. Schematic of: (a) frost heave around a chilled pipeline buried in the unfrozen ground; and (b) thaw settlement around a warm pipeline buried in permafrost (after Wang et al. 2018)

In the field, the soil around the buried pipelines is subjected to freeze-thaw cycles with seasonal changes in pipe discharge and air temperatures, which alter the pipeline–soil interactions and soil properties. Also, a change in the pipeline layout during the life cycle of the project is possible. For example, there may be commissioning or decommissioning of compressor stations after some time of operations to increase or decrease the throughput. These changes could cause significant thermal disturbance to some areas which had been stable. For example, Seligman (2000) reported the complex pipeline–soil thermal interactions in the Nadym–Pur–Taz gas

production complex in Russia due to commissioning compressor stations after several years of operation without any compressor stations.

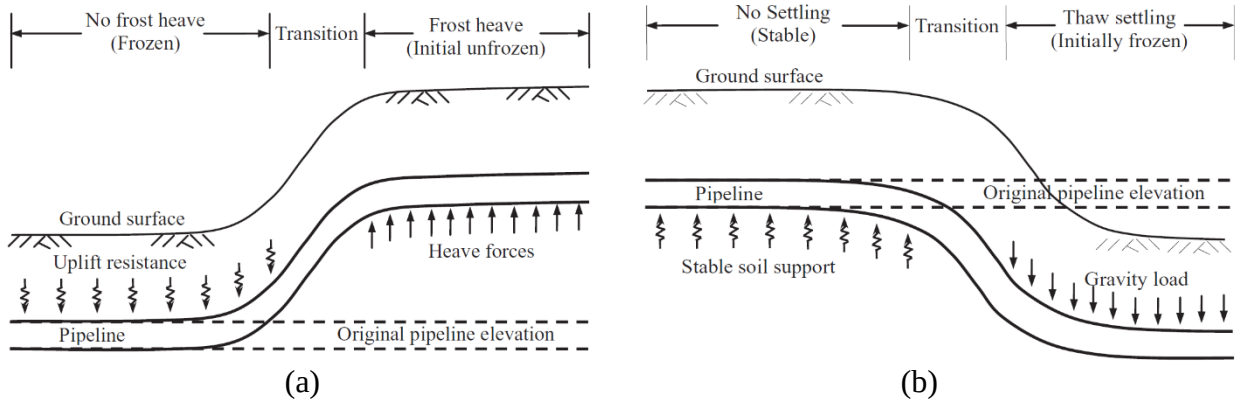

Fig. 1.2. Differential movements at the thermal interfaces (after Nixon et al. 1990): (a) frost heave; and (b) thaw settlement

In the last few decades, considerable effort has been taken to study the frost heave and thaw settlement around buried pipelines. One-dimensional laboratory frost heave tests (e.g., Taber 1929; Miller 1972; Konrad 1980) and thaw consolidation tests (e.g., Smith 1972 and Nixon 1973) were conducted for a wide range of conditions, which facilitated the development of some empirically-based predictive models (e.g., segregation potential model for frost heave calculation); however, laboratory studies with small specimens are limited to one-dimensional heat and mass flow conditions and unable to replicate the ground's freezing and thawing around the buried pipelines. Therefore, experiments were conducted using small to medium scale physical models (e.g., geotechnical centrifuge) and full-scale experimental facilities (e.g., Calgary and Inuvik pipeline experimental facilities) to understand frost heave and thaw settlement mechanisms around buried pipelines and pipeline–soil interactions, and to further investigate the possible mitigation measures. These experimental studies provided valuable information for developing and

calibrating the predictive models to understand and calculate the frost heave and thaw settlement around buried pipelines for a wide range of conditions.

The available numerical programs for frost heave and thaw settlement considered several aspects, including the magnitude of displacement (small/large), duration (long-term or seasonal freezing/thawing), modelling domain for heat transfer and mass diffusion (one- to three-dimensional), modelling approach (fully coupled/decoupled), soil constitutive model, and approaches for water diffusion.

1.2 Rationale

Despite many previous experimental and numerical studies on frost heave and thaw settlement around buried northern pipelines, the following areas that need to be addressed to properly evaluate the effects of these geohazards on the pipeline have been identified.

a) Most of the small- to full-scale studies are limited to frost heave/thaw settlement of pipelines under fixed pipeline temperatures (e.g., Slusarchuck et al. 1973, 1978; Morgan et al. 2004). It is, however, identified that the pipeline temperatures vary seasonally due to the change in discharge temperatures at processing facilities and air temperatures at the ground surface, which could induce freeze-thaw cycles downstream (Nixon and Burgess 1999; Seligman 2000). The response of pipelines when subjected to freeze-thaw cycles is less investigated.
b) Operation of freeze-thaw cyclic pipe temperatures was proposed as one of the possible frost heave mitigation measures considering unique experiment conditions (e.g., Morgan et al. 2006; Zhou et al. 2009). However, the effectiveness of this approach under a wide range of operating conditions is not well understood.

c) It is observed in existing gas pipelines that line operating conditions could also change with installing new compressor stations to increase the capacity (Nixon and Burgess 1999; Seligman 2000). The effects of such changes in existing pipelines on ground movements around pipelines are not well studied.

d) Although heat and mass diffusion at freezing or thawing around buried pipelines is two-dimensional, the existing frost heave and thaw settlement predictive models have often simplified the problem into one-dimensional and used closed-form heat transfer solutions before the mass diffusion analysis without evaluating the effects of ground movements on heat transfer (e.g., Morgenstern and Nixon 1971; Konrad and Morgenstern 1984; Nixon 1986). Although some coupled models are available, they, however, are limited to a short simulation time compared to the designed life cycle of the project, and some require complex input parameters that are difficult to estimate (e.g., Nishimura et al. 2009).

e) The constitutive relationships of frozen and thawed soils used in some predictive models are mostly based on the typical experimental conditions (e.g., Morgenstern and Nixon 1971 and Konrad and Shen 1996). However, frost heave and thaw settlement of pipelines induce unique loading conditions (e.g., the low-strain rate in frost heave of pipelines and low-stress conditions at the thawing of frozen soil).

1.3 Objectives

Frost heave and thaw settlement are two major geohazards of northern buried pipelines and could displace pipelines significantly, resulting in undesirable stresses on the pipeline unless they are not evaluated carefully in the design, construction, and operational stages. The operating conditions, especially pipeline temperatures, could change seasonally and after some time of

operation. The effects of these varying conditions on pipeline displacement response should be evaluated.

The available numerical techniques often analyze the frost heave and thaw settlement one-dimensionally using closed-form solutions; however, heat and mass flow around pipelines at freezing and thawing are two-dimensional and involve coupled thermal-hydro-mechanical processes.

The objectives of this research are to:

1. Investigate the pipeline displacement response under freeze-thaw cycles, which involves the following tasks.
    - Improve the understanding of frost heave and thaw settlement mechanisms around buried pipelines when a pipeline is operated at freeze-thaw cyclic temperatures.
    - Assess the effectiveness of cyclic pipeline temperatures as a frost heave mitigation measure.
2. Develop a fully coupled two-dimensional finite element (FE) model to simulate the frost heave mechanism of chilled pipelines buried in the unfrozen ground.
    - Implement the in-situ heave and segregational heave calculations in a FE model to simulate the long-term heave.
    - Implement material models that are appropriate in frost heave simulations of buried pipelines considering the soil type and loading conditions (e.g., temperature and low strain rates and confining pressure).
    - Identify the factors that influence the frost heave of buried pipelines.
3. Develop a fully coupled two-dimensional numerical model to simulate the thaw consolidation mechanism around a warm pipeline buried in frozen ground.

- Develop a large-strain fully coupled thermo-hydro-mechanical FE thaw consolidation model.
- Identify the advantages of two-dimensional FE modelling over one-dimensional models for determining excess pore water dissipation around a pipeline during thaw consolidation.

1.4 Thesis Organization

This thesis is prepared in manuscript format. The outcome of the study is presented in seven chapters and two appendices (A and B).

The current chapter describes the general information of the problem and the rationale and objectives of the present study.

Chapter 2 presents a general literature review. As the thesis is prepared in manuscript format, the problem-specific literature reviews are provided in Chapters 3–6 and Appendices A and B.

Chapter 3 presents an experimental evaluation of the response of pipelines which undergo freeze-thaw cycles and the effectiveness of freeze-thaw cycles as a frost heave mitigation measure, using the tests conducted in a geotechnical centrifuge. This chapter has been submitted to a journal as a technical paper for review.

Chapter 4 presents the development of a finite element modelling technique to simulate the long-term frost heave around buried pipelines. Using the developed FE model, the frost heave and moisture growth around two pipeline sections of the Calgary full-scale experiment facility are simulated. This chapter is prepared as a manuscript for a journal paper. As part of the material modelling in this study, an experimental study on stress–strain behaviour of clayey silts is

conducted, which has been published earlier in the 68th Canadian Geotechnical Conference (GeoQuebec 2015), Quebec City, Quebec, Canada, 2015 (Appendix A).

Chapter 5 evaluates the key factors that could influence the long-term frost heave of chilled pipelines for up to 20 years using the developed FE model in Chapter 4. Some of the critical components, such as modelling of frozen soil, frozen fringe and stress effects on segregation potential, are also discussed. This chapter is prepared as a manuscript for a journal paper.

Chapter 6 presents the development of a finite element modelling technique to simulate the thawing around a buried warm pipeline. This chapter is prepared as a manuscript for a journal paper. A part of this study has been published previously in the 72nd Canadian Geotechnical Conference (GeoSt.John's 2019), St. John's, NL, Canada, 2019 (Appendix B).

Note that displacement responses observed under cyclic pipe temperatures in chapter 3 were not directly compared in Chapters 4–6.

Chapter 7 presents the overall conclusions of the thesis and recommendations for future studies. The problem-specific conclusions are presented at the end of Chapters 3–6 and in Appendices A and B.

The studies cited in Chapters 1 and 2 are listed in the "References" chapter at the end of the thesis. The problem-specific references are presented at the end of Chapters 3–6 and in Appendices A and B.

CHAPTER 2:

LITERATURE REVIEW

2.1 Introduction

Frost heave and thaw settlement are common geotechnical issues in cold regions and involve complex processes of heat and mass flow. Frost heave occurs naturally at the ground surface every year in the winter months due to cold air temperatures, followed by thawing in spring months with warm air temperatures, which is commonly referred to as the frost action of soils. Frost heave and thaw settlement could also occur when artificial freezing and thawing are induced through buried pipelines that transport chilled gas and warm oil.

When saturated unfrozen fine-grained soil is subjected to freezing (e.g., around a chilled gas pipeline), volumetric expansion occurs due to freezing of in-situ pore water and migrated water. The former is called the in-situ heave, and the latter is the segregational heave (Miller 1978; Konrad and Morgenstern 1980). Segregational heave occurs due to ice lens formation with the progress of freezing. Based on idealized one-dimensional laboratory tests, conceptual approaches and mathematical models have been proposed to explain the process of ice lens formation (e.g., Miller 1978; Gilpin 1980; Konrad and Morgenstern 1980; Penner 1986; Rempel 2007; Arenson et al. 2008). It is generally accepted that ice lens formation occurs due to temperature-induced suction (cryogenic suction) which draws free water from nearby unfrozen soils to the segregation freezing temperature where the migrated water freezes (Konrad and Morgenstern 1980; Konrad 1994). A partially frozen zone, known as the frozen fringe, forms between the in-situ freezing temperature (the maximum temperature at which ice can exist in soil pores) and segregation freezing temperature (Miller 1972). The segregation freezing temperature and in-situ freezing temperature are sometimes referred to as the freezing front and frost front, respectively, as used in this thesis.

The growth of ice lenses could displace the surrounding soil, thereby causing heaving of the structures, which could be very significant if they are constructed in highly frost susceptible soils (Konrad 1994).

On the other hand, volumetric ice inclusions melt when frozen fine-grained soil or ice-rich permafrost is subjected to warm temperatures (i.e., operating a warm pipeline in permafrost), resulting in an excess amount of water over the soil's absorption capacity, which increases the pore water pressure. Settlement occurs with the dissipation of excess pore water pressure under self-weight or combined self-weight and applied loads, which is commonly known as the thaw consolidation (Morgenstern and Nixon 1971, 1975). In addition to thaw consolidation settlement, the generated excess pore water pressure could reduce the shear strength of thawed soils (referred to as thaw weakening), which might cause the failure of slopes and foundations (Morgenstern and Nixon 1971; Nixon and Morgenstern 1973a).

Experimental, theoretical, and numerical studies were conducted to study the mechanisms of frost heave and thaw settlement and to develop the predictive tools to calculate the displacements (heave/settlement). The literature review presented in this chapter focuses on the frost heave and thaw settlement around buried pipelines. Note that the problem-specific literature is presented in Chapters 3–6 and Appendices A and B, as the thesis is written in manuscript format. This chapter aims to present the additional information relevant to the current study, which could not be presented in manuscripts due to the space limitation.

2.2 Laboratory Tests

Extensive laboratory tests were conducted to understand the frost heave and thaw settlement mechanisms and to develop and calibrate the predictive models using appropriate input parameters. The following sections provide a review of the available experimental studies.

2.2.1 Laboratory frost heave tests

The laboratory frost cell tests involve one-dimensional (1-D) freezing of an instrumented unfrozen soil column between a relatively cold and a warm plate with or without a surcharge applied on the top surface. The test represents 1-D heat and mass flow conditions. Different types of tests were conducted, mainly by controlling the temperature at the end plates.

1. Step freezing tests: Freezing the specimen by a step change at a cold plate temperature (sub-zero) while maintaining the warm plate at an above-zero temperature.
2. Ramped freezing tests: Freezing the specimen by a linear change of cold and warm plate temperatures from initial values.
3. Japan Geotechnical Society freezing tests (JGST-freezing tests): This is a combined approach of step and ramped freezing tests, where the cold plate temperature is linearly reduced while the warm plate maintains a constant temperature slightly above 0 °C.

The step freezing test initially shows a fast frost front penetration and no visible ice lens as the water does not have enough time to migrate. Some water expulsion and settlement may occur due to the consolidation of unfrozen soil adjacent to the frozen fringe, especially in compressible soils (Konrad 1994; Konrad and Seto 1994). Ice lenses start to form horizontally which causes surface heave when the frost front penetration is slow enough for water to migrate to the freezing front. The thickness of the ice lenses and spacing between them increases with the progress of freezing until the final ice lens forms at the thermal steady state (Fig. 2.1 (a)). The heave rate decays gradually to a small value (or zero) after a sufficient freezing time (Konrad 1988, 1994). This type of test results has been used for frost heave model development and to characterize the frost susceptibility of a wide range of soils (e.g., Konrad 1980, 1999; Konrad and Morgenstern 1980, 1981).

The ramped freezing test has more control in the freezing process than the step freezing test, which typically gives a constant frost front penetration and temperature gradient. Therefore, the ice lenses form horizontally at regular intervals (Fig. 2.1(b)). Different frost front penetrations can be achieved by controlling the ramp rate (i.e., temperature change with time). However, compared to step freezing tests, this test takes a long time, as temperatures vary slowly, and sample height and the cooling rate dictate the maximum duration of the test. The heave curve in the ramped freezing test is typically concave upwards, i.e., the heave rate increases gradually (Penner 1986; Konrad 1988, 1994; Fukuda et al. 1997).

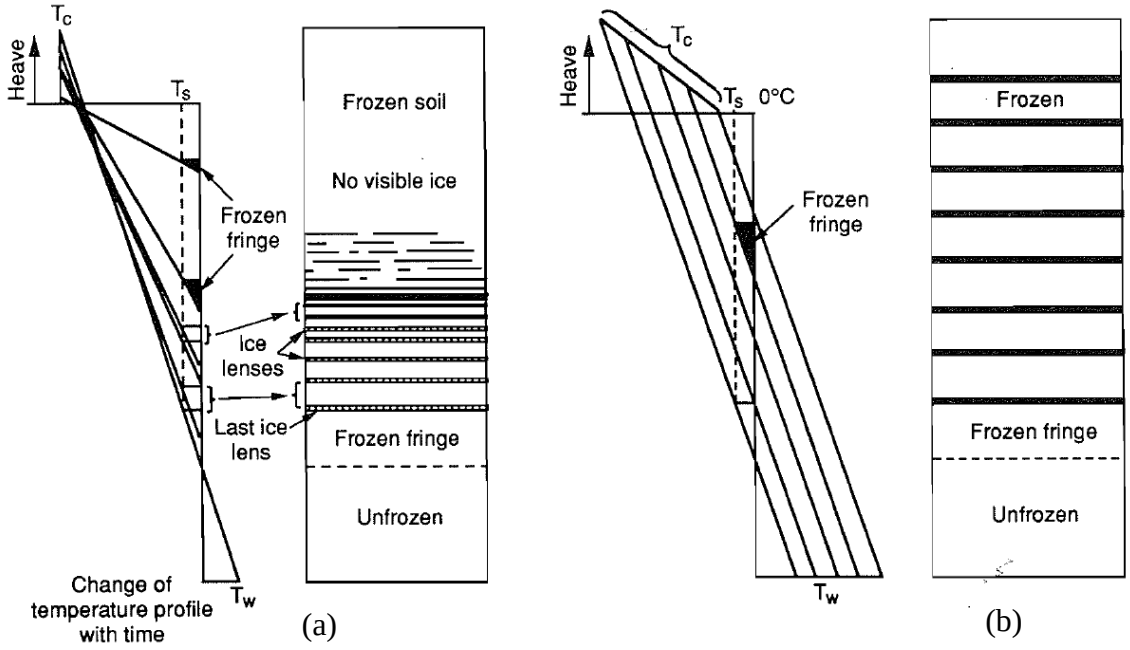

Fig. 2.1. Schematic of ice lenses formation in frost cell tests: (a) step freezing test; and (b) ramped freezing test (after Konrad 1994)

Further, the JGST-freezing test is widely used in Japan but is not common in other parts of the world (Japanese Geotechnical Society 2003). Based on the availability of an external water source for freezing, laboratory tests can also be classified as closed-system freezing (i.e., no water provided externally) and open-system freezing (i.e., water source provided externally). In closed-

system freezing, mainly the in-situ heave occurs (e.g., Konrad and Samson 2000), whereas both in-situ and segregational heave occur in open-system freezing (e.g., Chamberlain and Gow 1979 and Konrad 1980).

Laboratory specimens are, however, significantly smaller than the freezing extent in field problems (e.g., freezing around a buried chilled gas pipeline). Therefore, the temperature distribution in frozen and unfrozen regions is almost linear (i.e., constant temperature gradients), which is not the case in the field (Konrad 1994). Also, temperature gradients and cooling rates during the transient state, especially in step freezing tests, are significantly higher than those of real freezing problems; it is, however, argued that freezing conditions in laboratory step freezing tests at the thermal steady state with a warm plate temperature close to 0 °C and ramped freezing tests with a very small ramp rate are comparable with field freezing conditions (Penner 1986; Konrad 1987b, 1988, 1994). Apart from studying the frost heave mechanisms and characterizing the frost susceptibilities of different soils, some empirical models were also developed using these frost cell tests to estimate the displacements (e.g., segregation potential model).

2.2.2 Laboratory thaw consolidation tests

Thaw consolidation tests are conducted using undisturbed or remoulded frozen soil specimens placed in an oedometer type apparatus (e.g., Smith 1972 and Nixon 1973). Thawing is typically introduced by applying a step increase of temperature at the top surface from an initial sub-zero temperature to an above-zero temperature. The excess water generated upon thawing will drain out through the top surface, and settlement occurs subsequently. Similar to laboratory frost cell tests, 1-D heat and mass flow conditions are maintained (Tsytovich 1965; Smith 1972; Morgenstern and Smith 1973; Nixon 1973; Nixon and Morgenstern 1974). Figure 2.2 shows a

typical consolidation curve of a thaw consolidation test under a surcharge applied at the top surface.

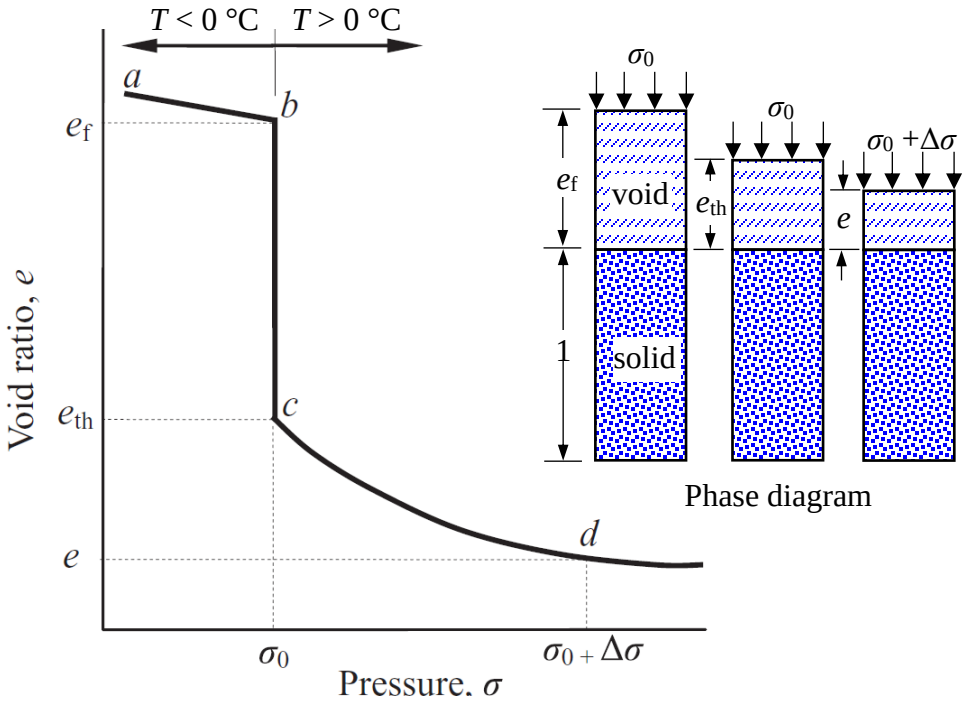

Fig. 2.2. Typical compression curve in thaw consolidation test (modified from Andersland and Ladanyi 2004)

Experimental test results could be used to estimate the total 1-D thaw settlement (Andersland and Ladanyi 2004) as:

$$\Delta H = A_0 H_f + m_v \Delta\sigma H_{th} \tag{2.1}$$

where ΔH is the thaw settlement, H_f and H_{th} are the height of the frozen and thawed soil column, respectively, m_v is the volume compressibility of thawed soils, and A_0 is the thaw strain parameter, which is defined as:

$$A_0 = \frac{e_f - e_{th}}{1 + e_f} \tag{2.2}$$

where e_f and e_{th} are the frozen and thawed void ratios, respectively.

With a known external load and thaw depth, Eq. (2.1) could be used to estimate the total thaw settlement at the completion of thaw consolidation assuming 1-D heat and mass flow, but it does not provide any information regarding the thaw settlement rate and excess pore water pressure generation and dissipation. Further, in typical field thaw consolidation problems (e.g., thawing around a warm pipeline), thaw depth penetration is time-dependent and total stress is constant unless an extra load is applied during thawing. At the instant of thawing, the effective stress in discrete soil layers reduces from a higher value to a lower value (Nixon and Morgenstern 1973a; Chamberlain and Gow 1979).

2.2.3 Freeze-thaw laboratory tests

Soils around the pipeline are typically subjected to freeze-thaw cycles due to the seasonal variation of pipe and air temperatures. Note that more discussion on freeze-thaw cycles around pipelines is presented later in this chapter in the "Frost heave/thaw settlement experience in existing pipelines" section. The freeze-thaw-induced change in some soil properties (e.g., hydraulic conductivity and compressibility) have been examined through laboratory tests (Chamberlain and Gow 1979; Konrad 1989a, b; Eigenbrod 1996; Eigenbrod et al. 1996; Konrad and Samson 2000). Experimental results show a significant increase in hydraulic conductivity and change in compressibility depending on the soil type and particle size distribution. For example, Chamberlain and Gow (1979) showed that the freeze-thaw cycles increase the hydraulic conductivity of fine-grained soils regardless of the particle size distribution, while the compressibility changes as a function of clay particle distribution among coarser silt particles. Freeze-thaw cycles could also influence the soil uplift and lateral resistances applied on structures (Carlson and Nixon 1988; Aldaeef and Rayhani 2018).

Konrad (1989a) showed that freeze-thaw cycles could alter the structure of highly frost susceptible clayey silt and reduce the frost susceptibility significantly within the first few cycles. Zhou et al. (2009) and Zhou and Zhou (2012) also investigated the effect of cyclic temperatures on frost heave using frost cell tests with sub-zero cyclic temperatures at the cold plate and observed a reduction of heave rate and total heave, as compared to that of continuous freezing, which suggested that freeze-thaw cycles could reduce the total heave. However, sub-zero to above-zero cyclic pipe temperatures occur around buried pipelines, as discussed later in this chapter, which is not well studied.

2.3 Full-Scale Experiments

Small-scale laboratory studies are limited to 1-D heat and mass flow conditions and unable to replicate the freezing and thawing and associated pipeline–soil interactions around buried pipelines. Therefore, full-scale pipeline experiments were conducted where frost heave and thaw settlement mechanisms were studied separately.

2.3.1 Full-scale frost heave experiments

Parallel to the design of major chilled gas pipelines, several full-scale experiments were conducted to study the free-field frost heave, differential heave and pipeline–soil interactions at the thermal interfaces and investigate the possible frost heave mitigation measures.

The Calgary full-scale experimental facility has been constructed parallel to the design of the proposed Mackenzie Gas Pipeline in 1974 on the premises of the University of Calgary in Canada by Canadian Arctic Gas Study Ltd. It consisted of six pipe sections which were operated between 3 to 12 years. With respect to a control pipe section, the effectiveness of several frost heave mitigation measures was investigated, which include: (i) increase of overburden pressure by increasing the burial depth and applying a soil berm on the ground above the pipe; (ii) replacement

of frost susceptible soil bed by non-frost susceptible soils; (iii) anchoring the pipeline to restrain the heave; and (iv) insulation of the pipeline to minimize the ground freezing. More details of the test sections and experiment results are reported by Slusarchuck et al. (1978), Carlson et al. (1982) and Carlson and Nixon (1988).

Parallel to the Alaska Gas Pipeline Project, another experimental facility was constructed in 1979 in Fairbanks, Alaska, by Northwest Alaskan Pipeline Company and Foothill Pipeline (Yukon) Ltd. Ten pipeline sections were operated for 500–1000 days, which investigated the effectiveness of several frost heave mitigation measures, similar to the Calgary full-scale experiment. One section of this experiment was particularly designed to investigate the pipeline–soil interactions due to differential heave when the pipeline passes through a thermal interface between permafrost and unfrozen frost susceptible ground (Northwest Alaskan Pipeline Company 1981; Colt-KBR 2003; Kim 2011).

Subsequently, several other full-scale test facilities were constructed, which include: (i) Canada–France experimental facility in a temperature-controlled chamber in Caen, France as a joint project between Canada and France in the 1980s and 1990s to study the pipeline–soil interactions under differential frost heave (Dallimore 1985; Selvadurai et al. 1999); and (ii) the reactivated Fairbanks experimental facility as a joint project between University of Alaska Fairbanks, USA and Hokkaido University, Japan, which operated from 1999 to 2003, to study pipe's structural response under the differential frost heave and the effects of air temperature and location of water table on frost heave (Huang et al. 2004; Oswell and Tcheekhovski 2005).

Based on the publicly available information for these full-scale experiments, the following observations can be found.

1. Frost heave of chilled pipelines could be minimized by taking several mitigation measures, which include the replacement of the soil bed by non-frost susceptible soil, insulation of the pipeline, anchoring the pipeline, and increasing the effective overburden pressure by increasing burial depth, lowering the water table, and applying a soil berm above the pipeline.
2. For insulated chilled pipelines buried in the unfrozen ground, freeze-thaw cycles that occur due to the variation of air temperatures could reduce the long-term heave.
3. Frost heave rate varies with time, soil bed material, operating conditions, and interactions with the groundwater table.
4. Differential frost heave occurs at the thermal interfaces between frozen ground and unfrozen frost susceptible ground or soils with different frost susceptibilities where pipe movements are restrained by the relatively less heaving side; therefore, higher stresses are induced on the pipeline near the interface.

2.3.2 Full-scale thaw settlement experiments

Similar to full-scale frost heave experiments, field pipeline experiments were also conducted to study the thaw settlement around pipelines. In 1971, Mackenzie Valley Pipeline Research Limited and the Division of Building Research of the National Research Council Canada jointly built an uninsulated warm pipeline near Inuvik, NWT, Canada, to study the effects of warm buried pipeline operations on permafrost. A 0.61-m diameter and 27-m long pipeline section was buried in the ice-rich permafrost, and thawing was introduced by circulating warm oil at +71 °C. Thaw settlement, pore water pressure and temperature distribution were monitored to obtain the pipe and surface settlement, excess pore water generated due to thawing, and thaw front penetration, respectively. A large bowl-shaped thaw bulb developed quickly around the pipeline, and a

significant pipe and ground surface settlement occurred within a short period (about 1 m settlement within the first 40 days of operation). Excess pore water pressure generation was also observed below the pipe, which dissipated quickly at upper layers compared to soils at greater depths. More details on the test facility, soil profile, installation procedure and test results are presented by Slusarchuk et al. (1973) and Watson et al. (1973). Note that the same test site was previously used to study the effects of warm above-ground pipeline operation on permafrost (Rowley et al. 1973).

Apart from the Inuvik test, the researcher did not find any complete full-scale pipeline experiments in the literature in which warm pipelines triggered the thaw, although some full-scale test results are available for surface-induced thawing (i.e., thawing from warm air temperatures) (e.g., Caen-France full-scale test) or thawing occurring accidentally due to the malfunction of the chilled gas pipelines in frost heave tests some time after operation (e.g., deep burial section in the Calgary full-scale test). Nonetheless, it is clear from the Inuvik full-scale test that operating a warm pipeline in permafrost could cause significant thaw settlements.

2.4 Centrifuge Frost Heave and Thaw Settlement Tests

In addition to the full-scale tests, relatively less expensive and time-consuming geotechnical centrifuge tests were conducted. The geotechnical centrifuge modelling technique was widely used to study the stress-dependent behaviour of soils in typical geotechnical engineering problems (e.g., slope instability and foundations failure). Miller (1990) found from the scaling analysis that centrifuge modelling can also be used to study cold region problems such as frost heave and thaw settlement. In addition to the scaled-down model, centrifuge modelling also provides an accelerated time frame for frost heave and thaw settlement problems, as the water flux towards the freezing front during freezing and water outflow during thaw consolidation are scaled proportionally to the square of the gravitational field. In other words, the time of water diffusion

in the prototype scale can be reduced in the centrifuge model by the squared time of the gravitational field. The accuracy of the scaling laws in centrifuge modelling for frost heave problems was presented by Ketcham et al. (1997) and Yang and Goodings (1998).

Phillips et al. (2001, 2002) and Clark and Phillips (2003) have successfully replicated the frost heave response of two pipeline sections in the Calgary full-scale test facility using a geotechnical centrifuge located at C-CORE, Canada. Several studies were conducted subsequently using this centrifuge facility to study the frost heave and thaw settlement around pipelines, under several industrial contracts. Limited information about these tests is available publicly, and includes the investigation of: (i) the effects of soil type on frost heave (Morgan et al. 2004); (ii) frost heave mitigation using cyclic pipeline temperatures (Morgan et al. 2006); (iii) the effects of water table location on frost heave (Piercey et al. 2011); (iv) thaw bulb formation around a warm pipeline buried in permafrost (C-CORE 2012; Wang et al. 2016); and (v) the mitigation of thaw settlement using thermosyphon cooled sandbags as a foundation (C-CORE 2012; Li et al. 2018).

The findings of these geotechnical centrifuge frost heave and thaw settlement tests on buried pipelines suggest that:

1. Long-term frost heave and thaw settlement around buried pipelines can be successfully simulated using a geotechnical centrifuge in a scaled-down physical model with an accelerated time frame (Phillips et al. 2001, 2002; Clark and Phillips 2003).
2. Frost heave of a chilled pipeline can be reduced by increasing the burial depth, as observed in the Calgary full-scale experimental facility (Phillips et al. 2001, 2002; Clark and Phillips 2003).
3. Total frost heave and heave rate of chilled pipeline vary with silt to clay ratio in fine-grained soils (Morgan et al. 2004).

4. Cyclic pipeline temperatures may reduce the frost heave and heave rate and alter the pipeline–soil interaction, relieving the stress on the pipeline (Morgan et al. 2006).
5. The location of the water table with respect to the initial pipe invert position could affect the frost heave and heave rates of pipelines at the beginning of freezing, but the effect may diminish some time after the operation (Piercey et al. 2011).
6. An air void may form above the pipeline when a warm pipeline operates in the frozen ground due to the volume reduction of the ice in the phase change (C-CORE 2012; Wang et al. 2016).
7. The use of thermosyphon cooled sandbags under a warm pipeline as a foundation could reduce the thaw settlement and thaw bulb expansion (C-CORE 2012; Li et al. 2018).

2.5 Frost Heave/Thaw Settlement Experience in Existing Pipelines

Several long-distance oil and gas pipelines have been proposed and some constructed in the Canadian arctic and cold regions around the world. In most cases, the pipelines were designed to withstand several geohazards that are unique to the region, especially frost heave and thaw settlement. A review of the frost heave and thaw settlement experience of these pipelines and success or failure stories could help to identify any areas that need to be improved or any potential gaps that need future research. Reviews of geotechnical hazards in some northern pipeline projects have been reported in the literature (e.g., Nixon et al. 1990; Nixon and Burgess 1999; Oswell 2011; Li et al. 2019). Considering their works and other literature, Table 2.1 lists some of the major pipelines in cold regions which demonstrate frost heave and thaw settlement.

In summary, the following information can be found.

1. Oil/gas flow rates and temperatures are typically controlled along the route using several processing facilities: compressor or pump stations to control the flow and chilling or

heating stations to control the temperature (e.g., Norman Wells oil pipeline and Nadym-Pur-Taz natural gas production complex).

2. Seasonal variations of pipe temperatures occurred at the discharge of processing facilities. The pipe temperatures dropped significantly downstream of the processing stations and showed seasonal fluctuations, especially in gas pipelines, due to the Joule–Thomson effect (see Fig. 2.3).
3. In some projects, changes in operating conditions and compressor stations' layout from start-up conditions have been observed to reduce the production cost and to increase/decrease the throughput after some time of operation. These changes sometimes caused significant frost heave or thaw settlement in some sections of the pipeline, which were previously stable (e.g., Nadym–Pur–Taz gas production complex and Norman Wells oil pipeline).
4. Differential movement at the thermal interfaces with frost heave or thaw settlement is identified as one of the major design considerations for cold region pipelines (Colt-KBR 2003; Oswell 2011).
5. Frost heave in some pipeline projects caused some initial out-of-alignment, which triggered the upheaval buckling in some sections (e.g., Norman Wells oil pipeline and Golmud-Lhasa oil pipeline).
6. Thawing of ice-rich permafrost around some gas pipelines caused water ponding, which leads pipelines to completely float up due to the uplift forces (e.g., Nadym–Pur–Taz gas production complex).
7. Some secondary thaw is observed around pipelines buried in permafrost due to the disturbances that occurred during the construction and with the degradation of permafrost

due to climate change (e.g., China Russia crude oil pipeline and Golmud-Lhasa oil pipeline).

8. Pipeline design and construction practices, and continuous maintenance in some projects, helped the pipe to perform well under the frost heave and thaw settlement (e.g., Trans-Alaska oil pipeline).

(a)

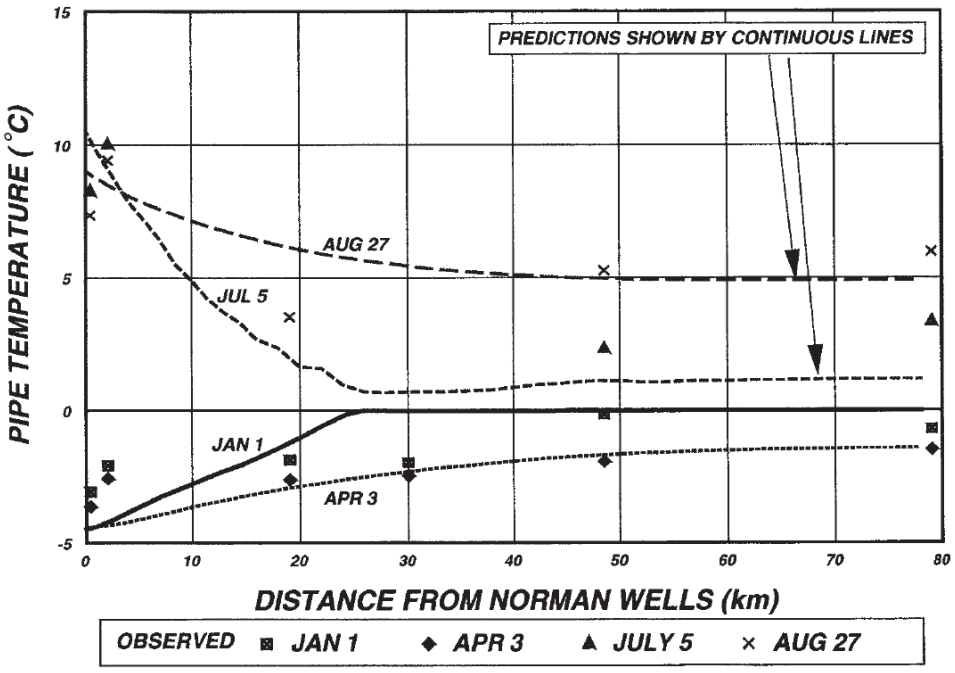

(b)

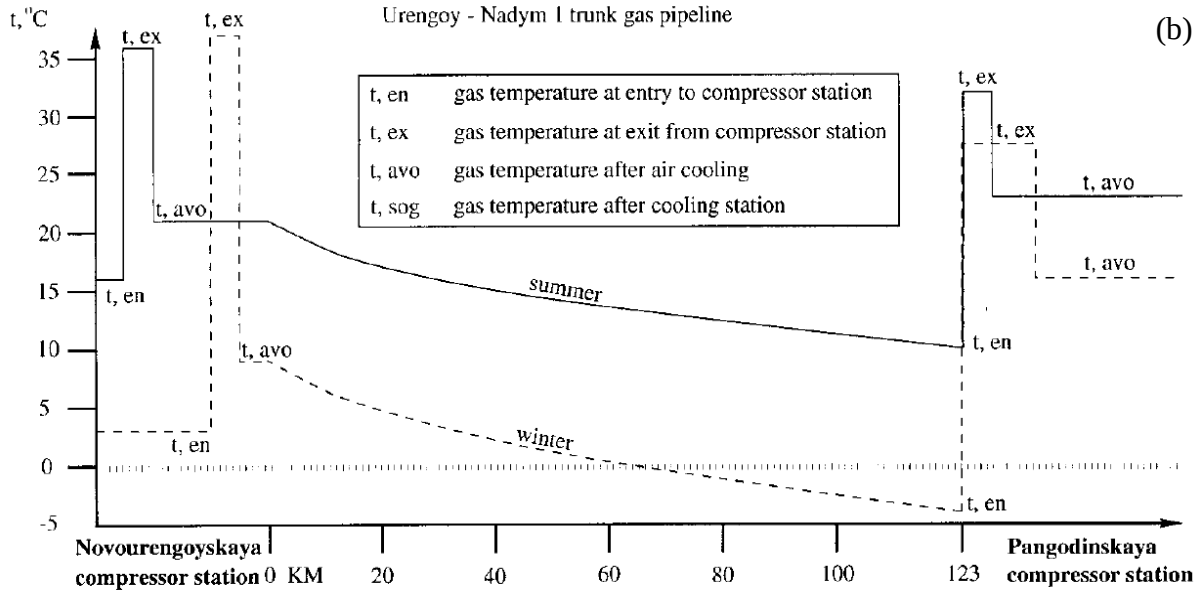

Fig. 2.3. Variation of pipe temperatures in cold regions pipelines: (a) Norman Wells oil pipeline (after Nixon and Burgess 1999); and (b) Urengoy-Nadym gas pipeline in Nadym-Pur-Taz natural gas production complex (after Seligman 2000)

Table 2.1. Frost heave/thaw settlement experience in cold region pipelines

Pipeline	General information and Frost heave/thaw settlement experience	Reference(s)
CANOL oil pipeline	–Diameter: 100 mm; Length: 960 km; Pipe temperature: -28/+32 °C; Nominal burial depth: above-ground pipeline on wooden timbers; Life cycle: Only 1 year from 1944 –Carried oil from Norman Wells, NWT to Whitehorse, Yukon in Canada –10 pumping stations along the route to regulate the flow –Operations ceased after 1 year due to several ruptures and large spills –Significant thermal disturbance to permafrost below the pipeline	Ueda et al. (1977); Johnson (1996); Oswell (2011)
Trans-Alaska oil pipeline	–Diameter: 1220 mm; Length: 1288 km; Pipe temperature: +60 °C; Nominal burial depth: 1.5 m; Life cycle: currently operating since 1977 –Carrying oil from Prudhoe Bay to Valdez in Alaska, USA –About three-fourths of the pipeline passes through permafrost –Installed above ground on vertical support members in highly thaw-unstable terrain (676 km segment) and buried conventionally in a thaw stable zone (601 km segment). An 11-km section buried in thaw-unstable permafrost with special thermal insulation and cooling pipes to minimize the permafrost thaw –11 pumping stations along the route at the maximum capacity to regulate the flow –Warm pipe temperatures caused thawing in some areas in permafrost, and excessive settlement caused the re-routing of a segment of the pipeline; however, unique pipeline design, construction practices and continuous maintenance helped the pipe to perform well beyond its initial design life of 30 years	Johnson and Hegdal (2008); Oswell (2011); Li et al. (2019)

Norman Wells oil pipeline	–Diameter: 328 mm; Length: 869 km; Pipe temperature: -2 °C for 8 years and then -4/+12 °C; Nominal trench depth: 1.1–1.2 m; Life cycle: currently operating since 1985 –Carrying crude oil from Norman Wells, NWT to Zama, Alberta in Canada –Completely buried in warm discontinuous permafrost; followed an existing disturbed corridor to minimize the interactions with the surrounding environment –One chilling station at the inlet and three pump stations along the route to regulate the flow –Chilled the oil at the inlet to a constant sub-zero temperature (-2 °C) for 8 years and then changed to seasonal cyclic temperatures (-4/+12 °C) to reduce the production cost –Seasonal variations of pipe inlet temperatures caused the freeze-thaw cycles downstream of the pipeline –Frost heave triggered upheaval buckling in one segment –Large thaw settlement observed in some sections, especially in organic terrains; however, the settlements are within the designed settlement till now	Burgess et al. (1998); Nixon and Burgess (1999); Oswell (2011)
Ikhil gas pipeline	–Diameter:168.3 mm; Length: 50 km; Pipe temperature: between -18 to -10 °C; Nominal cover depth: 1 m; Life cycle: currently operating since 1999 –Carrying natural gas from Caribou hills to Inuvik, NWT, Canada –Completely buried in continuous permafrost –Gas dried and chilled at a production facility before entering to line –No significant issues found so far in right-of-way except some minor thaw settlement in the ditch	IORVL (2004); Oswell (2011)

Nadym-Pur-Taz natural gas production complex	Several feeder, gathering and trunk gas pipeline networks were constructed, but only the long-distance trunk lines are reviewed below. –Diameter: 1220–1420mm; Total length of pipelines: over 4000 km; Pipe temperature: above-zero discharge temperatures in all compressor stations; Nominal burial depth: average 1.5–2 m; Life cycle: currently operating since 1972 –Completely buried in permafrost –No compressor stations at the start-up, but installed several compressor stations and a gas processing plant were installed after some time of operations. These changes caused significant thawing of ice-rich permafrost around the pipeline; some segments of the pipeline completely floated up due to the uplift forces induced by water ponding around the pipeline	Seligman (2000)
Golmud-Lhasa oil pipeline	–Diameter:159 mm; Length: 1076 km; Pipe temperature: -5/+9 °C; Nominal trench depth: 1.2–1.4 m; Life cycle: currently operating since 1977 –Carrying oil products (diesel, motor, and aviation fuels) from Golmud to Lhasa in Tibet, China –Fully buried using the conventional method; warm alpine permafrost through more than 50% of the route –28 pump stations at the maximum capacity along the pipeline route to regulate the flow –Significant frost heave and thawing observed in the winter and summer months –Frost heave triggered upheaval buckling in one segment –Many ruptures and spills occurred due to the excessive ground movements	He and Jin (2010); Oswell (2011)

China-Russia crude oil pipeline	–Diameter: 813 mm; Length: 1030 km; Pipe temperature: +0.4/17.9 °C; Nominal burial depth: 1.6– 2.5 m; Life cycle: currently operating since 2009 –Fully buried using the conventional method; a 518-km segment in discontinuous permafrost and 512-km segment in the seasonally frozen zone –Three pump stations along the pipeline route to regulate the flow –Seasonal thawing and refreezing of frozen soil observed around the pipeline –Significant thaw settlement observed in some ice-rich permafrost areas (e.g., over 1.4 m within 4 years of operation) –Significant thermal disturbance and thaw settlement due to removing vegetation in ROW	Wang et al. (2016); Wang et al. (2018)
Proposed Mackenzie gas pipeline	Project abandoned in 2017 mainly due to the lack of feasibility in the current market and long regulatory process. –Diameter: 760 mm; Length: 1200 km; Pipe temperature: constant sub-zero value in continuous permafrost but seasonal sub-zero to above-zero temperatures in discontinuous permafrost –Proposed to transmit gas from Inuvik area facility, NWT to northern Alberta in Canada –Fully buried in permafrost –Pipe temperature and flow will be controlled through compressor and heater stations: five compressor stations and a heater station at the start-up and 15 compressor stations at the maximum capacity –Seasonal variation of pipe temperatures predicted at the discharge of processing facilities and downstream –Differential frost heave at the thermal interfaces in discontinuous permafrost was identified as the major issue	Colt-KBR (2003, 2006); Oswell (2011)

2.6 Modelling of Frost Heave and Thaw Settlement of Buried Pipelines

In addition to the experimental studies, analytical and numerical predictive models were also developed for frost heave and thaw settlement around pipelines. In general, two important interrelated aspects are considered in the modelling: (i) heat transfer analysis to determine the frost front or thaw front penetration; (ii) mass diffusion analysis to determine the volume change in soils on freezing of unfrozen soils or thawing of frozen soils. The review of heat transfer and mass diffusion analyses in frost heave and thaw settlement models is presented below.

2.6.1 Heat transfer analysis and thermal properties of soils

When a buried pipeline operates in warmer or colder temperatures than the surrounding soil, thermal energy dissipates or is extracted gradually through different modes of heat transfer such as conduction, convection, and radiation. Typically, heat transfer by radiation is insignificant in sands and fine-grained soils (Farouki 1981b; Zhu 2006). Although some studies considered the convective heat transfer (e.g., Harlan 1973 and Dumais and Konrad 2018), it was also found negligible in fine-grained soils due to the low hydraulic conductivity. For instance, Nixon (1975) determined using a mathematical solution that the effect of convective heat transfer could be neglected without a significant loss of accuracy in one-dimensional thaw consolidation. Therefore, often only the conductive heat transfer was considered in freezing and thawing soils.

The heat transfer around the pipeline in previous studies was often performed by simplifying the problem into one-dimensional (Morgenstern and Nixon 1975; Foriero and Ladanyi 1995; Hawlader et al. 2004; Dumais and Konrad 2019) or radially symmetric (Konrad and Morgenstern 1984) or quasi-static two-dimensional frameworks (Hwang 1977; Nixon 1992), without considering the effects of ground surface temperatures. Nixon (1983) developed a two-dimensional geothermal model considering the effects of ground surface temperatures; however,

heat transfer analysis was decoupled from the mass diffusion analysis and performed first, similar to the abovementioned heat transfer approaches.

Heat dissipation from an uninsulated pipe to the surrounding soil or vice versa occurs very quickly because of the high thermal conductivity of the pipe material. Soil is, however, a multi-phase material, and heat transfer occurs gradually. This requires a consideration of some important aspects that are unique to the soil medium at freezing or thawing, which include: (i) soil freezing characteristic curve (the variation of unfrozen water content with sub-zero temperatures); (ii) variation of thermal properties (thermal conductivity and heat capacity) as a function of volumetric fractions of soil components; and (iii) latent heat released or absorbed at the phase change.

2.6.1.1 Soil freezing characteristic curve

In fine-grained soils, some water remains in its liquid form at freezing even at a temperature well below 0 ºC as a result of two mechanisms: curvature-induced premelting and interfacial premelting, as shown in Fig. 2.4. The latter is associated with repelling forces between surfaces of ice and soil particles when a thin water film is sandwiched in between, whereas the former is associated with freezing point depression due to the surface tension at the ice-water interface (Rempel et al. 2004; Nishimura et al. 2009; Ghoreishian Amiri et al. 2016).

The thermal properties and mechanical behaviour of frozen soils are strongly influenced by unfrozen water content. Also, this influences the hydraulic conductivity of the frozen fringe; therefore, it plays a crucial role in the frost heave process when water migrates to the segregation freezing front (Farouki 1981a; Rempel et al. 2004; Arenson et al. 2007; Nishimura et al. 2009; Ghoreishian Amiri et al. 2016).

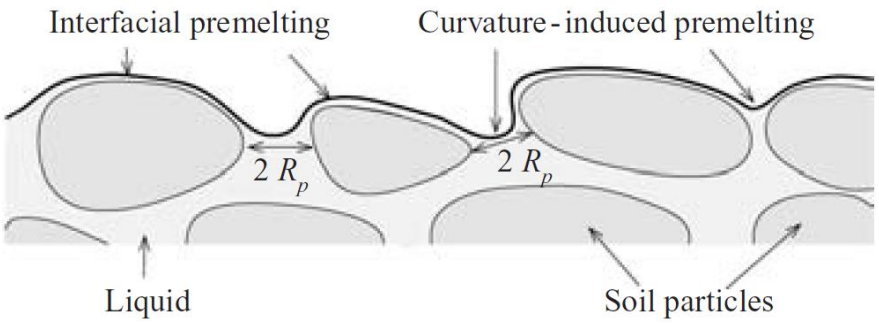

Fig. 2.4. Schematic of unfrozen water formations in frozen soil (after Rempel et al. 2004)

Sophisticated methods such as dilatometry, calorimetry, x-ray diffraction and nuclear magnetic resonance were used to measure this parameter experimentally in previous studies (e.g., Anderson and Tice 1972; Anderson et al. 1973; Tice et al. 1976; Patterson and Smith 1981). Through these studies, some empirical relationships were developed that can be used easily. Anderson and Tice (1972) and Tice et al. (1976) compiled a large amount of unfrozen water content data for different soils and proposed a simple power-law for the soil freezing characteristic curve below 0 °C as:

$$w_u = \alpha T^{\beta} \tag{2.3}$$

where w_u is the unfrozen water content (by mass), T is the temperature, and α and β are characteristic soil constants. Tice et al. (1976) and Andersland and Ladanyi (2004) have summarized α and β values for an extensive range of soils.

Equation (2.3) gives the unfrozen water content only as a function of temperature but is unable to consider different in-situ water contents (i.e., water content before freezing). Nixon (1983) introduced a more versatile exponential function to relate the normalized unfrozen water content W_u ($W_u = w_u/w_0$) to temperature as:

$$W_u = \frac{P + e^{(QT+R)}}{100} \tag{2.4}$$

where P is the percentage of the total water content that remains unfrozen well below the in-situ freezing temperature; P is 0% for coarse-grained soils and could be up to 25% for fine-grained soils (Nixon 1983); the constant Q controls the rate of unfrozen water content decrease with negative temperature, which is a function of particle size (e.g., 0.16–6 for fine-grained soils (Nixon 1983, 1986; Zhu 2006)); R is related to P as:

$$R = ln(100 - P) \tag{2.5}$$

On thawing, pore ice melts gradually and unfrozen water content increases. It is found that the unfrozen water content increase in thawing is not the same as that observed in freezing; it is a steeper curve, mainly because of the supercooling effect in freezing (Patterson and Smith 1981; Zhu 2006).

2.6.1.2 Thermal conductivity of soils

The thermal conductivity of soils highly depends on the dry density and water (or ice) content of soils (Farouki 1981a, b; Côté and Konrad 2005). Several empirical and theoretical relationships have been developed to calculate the "equivalent thermal conductivity (λ_e)" for partially saturated, saturated, and frozen soils, considering their multi-phase nature (Johansen 1975; Farouki 1981a, b; Côté and Konrad 2005). However, the geometric mean method proposed by Johansen (1975) was identified as more appropriate for saturated soils because of its simplicity and accuracy (Farouki 1981a; Côté and Konrad 2005). The equivalent thermal conductivity of saturated fine-grained soils was expressed as:

$$\lambda_e = {\lambda_s}^{\theta_s} {\lambda_w}^{\theta_w} {\lambda_i}^{\theta_i} \tag{2.6}$$

where λ is the thermal conductivity, and θ is the volumetric content with subscripts *s*, *w*, and *i*, denoting soil, water, and ice phases, respectively.

Although the thermal conductivity of soil components (i.e., λ_s, λ_w, and λ_i) is constant, the equivalent thermal conductivity varies with changes in volumetric fractions of soil components. Nevertheless, the equivalent thermal conductivity of saturated soils should be within the range of thermal conductivities of pure water and ice regardless of the state (i.e., frozen or unfrozen), temperature and frost susceptibility. The ratio of frozen soil thermal conductivity to unfrozen soil thermal conductivity of saturated soils is 1–3.7 (Nixon and McRoberts 1973).

It is, however, important to note that some previous researchers used constant thermal conductivities for frozen and unfrozen soils without considering the variation of volumetric fractions of soil components at freezing or thawing (e.g., Morgenstern and Nixon 1975; Konrad and Shen 1996; Hawlader et al. 2004). The effects of such considerations on the computation of the temperature regime should be carefully evaluated, especially for fine-grained soils.

2.6.1.3 Heat capacity and latent heat of soils

Similar to the thermal conductivity, the heat capacity of saturated three-phase soil is represented by the equivalent volumetric heat capacity (C) as:

$$C = \theta_s \rho_s c_s + \theta_w \rho_w c_w + \theta_i \rho_i c_i \tag{2.7}$$

where c is the heat capacity by mass and ρ is the density with subscripts s, w, and i, denoting soil, water, and ice phases, respectively.

As discussed in the soil freezing characteristic curve, the water in soil pores freezes over a temperature range. A gradual phase change from an in-situ freezing temperature (T_f) to a residual unfrozen water content (w_f) occurs at a low temperature (T_r). The thermal energy released over this temperature range is not only a function of the heat capacity but also the latent heat of fusion.

By combining both latent heat and heat capacity, Anderson and Tice (1972) introduced the apparent heat capacity by mass (c_a) within this temperature range ($T_r < T < T_f$) as:

$$c_a = c + \frac{1}{\Delta T}\int_{T_f}^{T_r} L' \frac{\partial W_u}{\partial T} dT \tag{2.8}$$

where L' is the latent heat of pore water, and the other terms are defined earlier.

Beyond this temperature range ($T_f < T < T_r$), the latent heat of fusion is not involved in the heat transfer analysis, and the heat capacity can be divided into two segments considering the higher and lower limits of the range as the heat capacity of unfrozen soils (c_u) and frozen soils (c_f) (Nixon and McRoberts 1973) as:

$$c_u = \frac{\gamma_d}{\gamma_{bulk}}(c_s + w_0 c_w) \qquad T \geq T_f \tag{2.9}$$

$$c_f = \frac{\gamma_d}{\gamma_{bulk}}(c_m + w_0(Pc_w + (1-P)c_i)) \qquad T \leq T_r \tag{2.10}$$

where γ_d and γ_{bulk} are dry and bulk density of soil, respectively.

2.6.2 Frost heave modelling

In fine-grained soils, upon freezing, the volume expansion occurs due to the in-situ and segregational heave. In-situ heave occurs when the pore water freezes, which is typically calculated simply by evaluating the varied amount of pore water at freezing. Segregational heave, however, occurs with the water migration from nearby unfrozen soils to the freezing front and subsequent formation of discrete ice lenses, which involve complex thermo-hydro-dynamic mechanisms. In the past, different models have been developed to predict the frost heave, which can be broadly divided into several groups based on how they formulated the water migration and ice lens formation. For example, Yu et al. (2019) discussed seven such groups of frost heave modelling. Some of the models were applied to simulate the frost heave around buried chilled pipelines, as discussed later.

The capillary theory is one of the earliest attempts to consider the pressure difference at the ice-water interface as the driving force for water to flow towards the frozen soils (Penner 1959; Everett 1961; Chalmers and Jackson 1970). The Laplace surface tension formula was used to calculate the capillary suction. Despite the simplicity of this theoretical approach, several drawbacks became apparent (Peppin and Style 2013), which include: (i) the calculated frost heave pressures significantly underestimated the experimentally observed values; and (ii) no mechanism was provided for ice lens formation.

Miller (1978, 1980) proposed a model called "Rigid Ice Theory," which suggested that water migration to freezing soils and formation of ice lenses occur through the mechanism of regelation. The classical effective stress principles and the Clausius-Clapeyron equation were used to explain the ice lens initiation and to calculate the water influx. This theoretical method was widely used for one-dimensional simulation. However, it relied on several physical frozen fringe characteristics, such as hydraulic conductivity and cryogenic suction, which are challenging to determine in the relatively thin frozen fringe, having water and ice phases that are bounded to two moving boundaries (Grip 1997).

In addition to the Capillary theory and Rigid Ice Model, several other theoretical and empirically-based models were developed, which include Gilpin's (1980) physically-based model, the segregation potential model (Konrad and Morgenstern 1980, 1981), discrete ice lens theory (Nixon 1991), and porosity rate function (Michalowski 1993). Among them, Konrad and Morgenstern's (1980, 1981) segregation potential (*SP*) model became very popular, especially in North America, and has been applied widely in practice (e.g., Konrad and Morgenstern 1984; Colt-KBR 2003; CGS 2006). The water influx (v) under zero overburden pressure at and close to the steady-state thermal condition (i.e., frost front penetration rate is zero) was expressed as directly

proportional to the temperature gradient in the frozen fringe (*grad* (*T*)) and the proportionally constant segregation potential (SP_0).

$$v = SP_0 . grad(T) \tag{2.11}$$

This model was later extended to more general freezing conditions (i.e., transient or steady-state freezing with applied loads) by evaluating the effects of suction at the frost front, the cooling rate of frozen fringe, and applied pressure on the segregation potential parameter (Konrad and Morgenstern 1982a, b). In comparison with physically-based models, the *SP* model combines the frozen fringe characteristics (hydraulic conductivity and cryogenic suction) with the segregation potential parameter, which can be estimated from the reported values of SP_0 for different soils (e.g., Konrad 1999) or experimentally, using 1-D frost cell tests, soil index properties and field observations (Konrad 1987a, 1999, 2005).

Some of the models discussed above were used to model the frost heave around buried pipelines, as summarized in Table 2.2. It is commonly assumed that heat and mass flow directly below the pipe dictate the frost heave. The heat transfer analysis was often decoupled from the frost heave model and performed first, i.e., the change of geometry, boundary conditions and thermal properties with volume change were not considered in heat transfer analysis. No clear agreement in material modelling of soils, especially for frozen soils, is observed, as described further in the following sections.

Table 2.2. Summary of frost heave modelling of buried chilled pipelines

Reference	Heat transfer analysis	Frost heave model	Stress-strain behaviour of soil	Remarks
Konrad and Morgenstern (1984)	Radially symmetrical model without considering the effects of ground surface temperature	1-D segregation potential model	No material model	–Assumed that heat and mass flow directly below the pipe dictates the frost heave –Frost front penetration and temperature gradient calculated using heat transfer analysis prior to frost heave analysis –Used temperature-independent thermal properties for frozen soils –Assumed in-situ and migrated water freezing at 0 °C –Simulated Calgary, Canada full-scale frost heave experiment pipe sections –Presented parametric study for long-term frost heave
Nixon (1986)	Nixon (1983) 2-D geothermal model considering the effects of ground surface temperature	1-D segregation potential model	No material model	–Assumed that mass flow directly below the pipe dictates the frost heave, but heat flow analysis was associated with the ground surface effects –Calculated temperature gradient at the freezing front prior to frost heave analysis by fitting the temperatures into a quadratic equation –Simulated Calgary, Canada and Caen, France full-scale frost heave pipeline test sections –Presented parametric study for long-term frost heave
Carlson and Nixon (1988)	Nixon (1983) 2-D geothermal model considering the effects of surface temperatures	1-D segregation potential model	No material model	–This study was similar to the Nixon (1986) model –Simulated Calgary, Canada full-scale frost heave experiment pipe sections

Reference	Heat transfer analysis	Frost heave model	Stress-strain behaviour of soil	Remarks
Nixon (1992)	Hwang (1977) quasi-static 2-D heat transfer analysis without considering the effects of surface temperature	1-D discrete ice lens theory	No material model	–Assumed that heat and mass flow directly below the pipe dictates the frost heave –Considered the frozen fringe characteristics and simulated the discrete ice lens formation –Simulated Calgary, Canada full-scale frost heave experiment pipe sections
Konrad and Shen (1996)	2-D heat transfer model coupled with frost heave analysis	2-D segregation potential model	–Frozen soils: Bi-linear elastic –Unfrozen soil: linear elastic	–Considered anisotropic formation of ice lens around the pipeline –Calculated temperature gradient using a temporary triangular element in the frozen side adjacent to the frost front –Simulated Calgary, Canada full-scale frost heave experiment pipe sections
Colt-KBR (2003)	Nixon (1983) 2-D geothermal model considering the effects of surface temperatures	1-D segregation potential model	No material model	–This study was similar to the Nixon (1986) model –Applied the segregation potential model to predict the frost heave and subsequent strain demand predictions for the proposed Mackenzie gas pipeline
Nishimura et al. (2009)	2-D heat transfer model coupled with frost heave analysis	Using Generalized Darcy's law and Clausius–Clapeyron equation	Modified Cam-Clay model for frozen and unfrozen soils	–Fully coupled thermo-hydro-mechanical model in the effective-stress-based framework –Simulated Calgary, Canada full-scale frost heave experiment pipe sections

2.6.2.1 Stress–strain behaviour of frozen soils

The stress–strain behaviour of frozen soil depends on many factors, including temperature, volumetric ice content, confining stress, particle size distribution, strain rate, and creep (Konrad and Shen 1996; Arenson et al. 2007). Therefore, it is extremely difficult to develop a unique relationship that applies to frozen soils under different conditions.

Materials models developed with frost heave problems for frozen soils can be broadly divided into two groups: (i) effective-stress-based models; and (ii) total-stress-based models. The effective-stress-based models are typically developed based on unsaturated soil mechanics concepts in which constitutive behaviour is related to the cryogenic suction in addition to the effective stress (e.g., Nishimura et al. 2009; Thomas et al. 2009; Ghoreishian Amiri et al. 2016). The generalized Clausius–Clapeyron equation is often used to calculate the cryogenic suction, which is, however, generally valid at the base of the new ice lens where the water and ice phases are assumed to be in equilibrium (Miller 1978; Nixon 1991; Black 1995). Due to the non-equilibrium conditions at the formation of ice lenses and possible water migration beyond the warm ice lens, the applicability of the Clausius–Clapeyron equation to constitute the frozen soil behaviour is still being debated (Miyata and Akagawa 1998; Ma et al. 2015; Yu et al. 2020).

On the other hand, total-stress-based models generally consider the effects of confining pressure on the behaviour of frozen soils and are widely used because of their practical relevance compared to the effective-stress-based models. The temperature-dependent linear elastic models were used in some initial 1-D frost heave models (e.g., Coutts 1991; Ladanyi and Shen 1993; Selvadurai and Shinde 1993; Zhu 2006). Konrad and Shen (1996), however, showed that the pure linear elastic material model may not be suitable for two-dimensional frost heave problems as it reduces the growth of ice lens significantly, thereby giving less frost heave because of unrealistic

stress build-up. Considering the results of uniaxial compressive tests (Tsytovitch 1975), they proposed a bilinear elastic model for frozen soils with temperature-dependent Young's modulus and yield and post-yield strengths. Kim (2011) extended Konrad and Shen's (1996) model by introducing the long-term creep strength as the peak strength and argued that the bilinear elastic model without long-term creep characteristics may significantly underestimate the frost heave predictions.

Parameswaran and Jones (1981) observed experimentally that the ice phase dictates the stress-strain response of frozen saturated sandy soils under very low strains in the early stages, while interparticle friction plays a crucial role later. The Mohr–Coulomb model was used to explain the material behaviour. Arenson and Springman (2005) also found from a series of triaxial tests that ice-rich frozen fine-grained soil behaviour close to 0 °C can be explained using the Mohr–Coulomb model in terms of total stress parameters. They showed that the angle of internal friction decreases with increasing ice content, whereas cohesion varies with the strain rate, volumetric ice content and temperature.

Most of the experimental stress–strain responses, which were used in the abovementioned frozen soil material models, were obtained from relatively higher strain rates and subjected to lower temperatures. However, frost heave around buried pipelines is generally a very slow process, and strain rates are very small; for example, Kim (2011) reported that strain rates in the Calgary and Fairbanks full-scale frost heave experiments were between 9.3×10^{-9} s^{-1} and 1.64×10^{-8} s^{-1}. Also, pipelines are often buried at shallower depths where low confining pressure is imposed. Under such small strain rates and low confining pressures, the behaviour of frozen soils is not well understood, especially close to 0 °C.

2.6.3 Thaw settlement modelling

On thawing of fine-grained frozen soils or ice-rich permafrost, the excess amount of water liberates over the soil absorption capacity, and excess pore water pressure may be generated, depending on the imbalance between the rate of water generation and dissipation (Morgenstern and Nixon 1971). With the dissipation of excess pore water pressure, consolidation settlement occurs, which can be modelled using the conventional consolidation theories developed for unfrozen soils. However, the moving boundaries (i.e., thaw front and position of heat source) make the problem complicated. The interrelated processes such as heat transfer, excess pore water pressure generation and dissipation, and volume compressibility of thawed soils should be carefully formulated to simulate the thaw settlement properly.

Several analytical and numerical solutions have been developed in the past to model the thaw consolidation, as summarized in Table 2.3. Some solutions were used to simulate the thawing around buried warm pipelines in permafrost, as indicated in Table 2.3. However, the applicability of these solutions is limited, as discussed below.

1. Heat and Mass flow is undoubtedly 2-D in nature in thawing around buried warm pipelines; however, most of the solutions listed in Table 2.3 are in 1-D frameworks, assuming that vertical heat and mass flow dictates the process. Although Yao et al. (2012) developed a 3-D FE model, Biot's consolidation theory and linear void ratio–effective stress relationship were used, which are applicable only for small deformation problems.
2. Small-strain solutions are valid only if the settlement is insignificant compared to thaw depth. However, large thaw settlements occur around warm pipelines, especially when pipe passes through ice-rich permafrost (see Table 2.1).
3. Similar to most of the frost heave models discussed in Table 2.2, the heat transfer analysis was often decoupled from consolidation analysis and performed first without considering

the effects of heat source displacement and the variation of thermal properties during consolidation.

4. The behaviour of thawed fine-grained soils is highly nonlinear; the volume compressibility and hydraulic conductivity vary significantly during the consolidation. Although some previous large-strain models incorporated these relationships, they are limited to 1-D problems. More discussion about the nonlinear behaviour of thawed soil is provided in the following sections.

2.6.3.1 Residual stress and hydromechanical behaviour of thawed soils

When frozen fine-grained soils or ice-rich permafrost thawed the excess pore water pressure generates immediately, and the effective stress of the soil skeleton reduces to a lower value. Nixon and Morgenstern (1973a) defined this initial effective stress that was reached immediately at the thawing under undrained conditions as the residual stress of thawed soils and the corresponding void ratio as the thawed void ratio. Experimental methods were also developed to determine the residual stress using an oedometer-type apparatus. Based on the experimental results, they established a logarithmic relationship between thawed void ratio and residual stress, which is called the residual stress curve. The generated excess pore water pressure and subsequent thaw settlement were found to be dependent on the residual stress: the higher the residual stress, the lower the excess pore water pressure generation, and thereby the thaw settlement (Nixon and Morgenstern 1973a).

Morgenstern and Nixon (1971) assumed that residual stress for ice-rich soils is zero in their small-strain thaw consolidation model. In other words, the generated excess pore water pressure on thawing is the same as the effective overburden pressure. However, for lower thawed void ratios, especially in ice-poor soils, the residual stress is significant, and the generated excess pore

water pressure is not equal to the effective overburden pressure; therefore, non-zero residual stress should be used. Dumais (2019) showed that the experimental framework proposed by Nixon and Morgenstern (1973a) measured the residual stress for the bulk soil, which is valid only for ice-poor soils, not for the soil skeleton. He proposed a new framework to determine the residual stress for ice-rich soils, considering the effective stress sustained in the overconsolidated soil elements.

With the expulsion of excess water, thawed soils consolidate under self-weight or a combination of self-weight and applied loads from the thawed void ratio (at residual stress) to a lower void ratio until they reach a new equilibrium. Typically, in ice-rich soils, three-levels of volume changes occur upon thawing, as shown in Fig. 2.5. Firstly, the frozen soil void ratio (e_f) reduces by approximately 9% to the initial thawed void ratio (e_0) (i.e., $e_0 = e_f/1.09$). Secondly, the quick reduction of e (e_0 to e_{th}) occurs with the dissipation of excess water generated on thawing over soil absorption capacity. Thirdly, the consolidation of soil occurs under the effective overburden pressure, which can be determined from one-dimensional consolidation or isotropic consolidation in triaxial tests (Dumais and Konrad 2019; Dumais 2019). Note, in ice-poor soils, that the volume change in the dissipation of excess water is insignificant as the amount of water liberated on thawing is minimal, i.e., soil can absorb all the moisture; therefore, e_0 and e_{th} are not significantly different, as indicated in Fig. 2.5.

In small-strain thaw consolidation models, the linear void ratio (e)–effective vertical stress (σ_v') relationships (i.e., constant volume compressibility) were often used to explain the behaviour of thawed soils (e.g., Tsytovich et al. 1965; Morgenstern and Nixon 1971; Yao et al. 2012). However, e–σ_v' relationships of thawed fine-grained soils are highly nonlinear, especially at low stresses, and the use of linear relationships may significantly underestimate the excess pore water pressures, and thereby the thaw settlement (Nixon and Morgenstern 1973b; Foriero and Ladanyi

1995; Dumais and Konrad 2018; Dumais 2019). Therefore, nonlinear relationships were used for the compressibility of thawed soils in large-strain thaw consolidation models (e.g., Foriero and Ladanyi 1995 and Dumais and Konrad 2018).

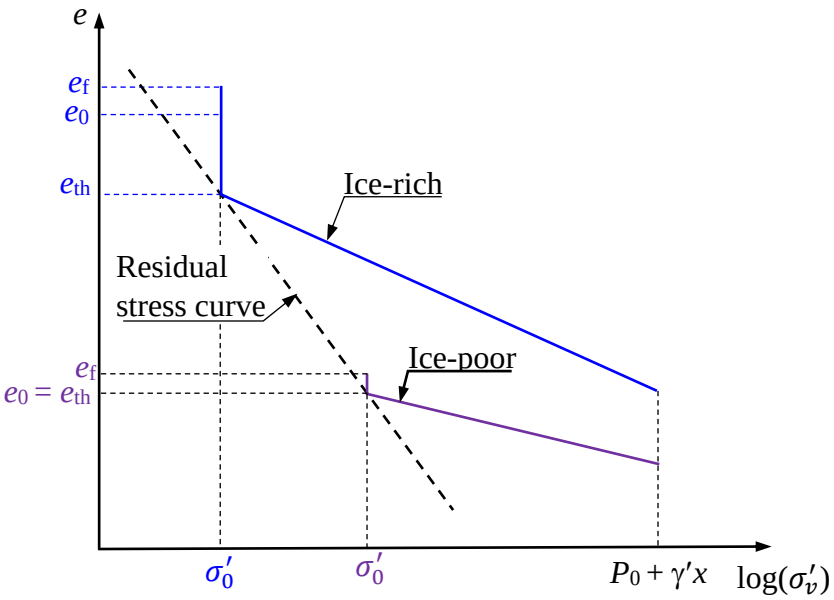

Fig. 2.5. Volumetric compression of frozen soils on thawing (modified from Dumais 2019)

The hydraulic conductivity of thawed soils (k_t) is also important in the thaw consolidation process. Experimental results show that k_t could be significantly higher than that of an unfrozen state (k). For example, Chamberlain and Gow (1979) found the ratio of k_t/k to be up to 100 for four silts and clays. Morgenstern and Nixon's (1971) small-strain solution is based on a constant k_t, although it varies nonlinearly with the void ratio (e), especially in ice-rich soils at high void ratios. Linear e–logk_t relationships, similar to those in typical unfrozen soils, were considered in some studies (Foriero and Ladanyi 1995). However, an unrealistically high k_t may be obtained if the linear e–logk_t line is extrapolated up to the large thaw void ratio, especially in ice-rich soils. Dumais and Konrad (2018, 2019) and Dumais (2019) proposed bilinear e–logk_t relationships with a threshold void ratio at which the hydraulic conductivity becomes constant.

Table 2.3. Summary of available thaw consolidation models

Model	Heat transfer analysis	Consolidation analysis	Remarks
Morgenstern and Nixon (1971) analytical solution	Neumann 1-D closed-form solution to determine thaw front penetration	Terzaghi's classical small-strain consolidation theory	–Thaw front penetration determined prior to consolidation analysis –Linear void ratio–effective stress relationship together with a constant hydraulic conductivity used for thawed soil –Frozen soil considered impermeable and incompressible –No consideration of effects of moving boundaries on heat transfer and consolidation analyses –No consideration of the volume changes due to the phase transformation from ice to water –Residual stress of thawed soil assumed to be zero –Applied to simulate the thawing around the Inuvik experimental warm pipeline one-dimensionally (Morgenstern and Nixon 1975)
Foriero and Ladanyi (1995) finite-strain model	1-D semi-empirical power law to determine thaw front penetration	Gibson's large-strain consolidation theory	–Thaw front penetration determined prior to consolidation analysis –Nonlinear void ratio–effective stress–hydraulic conductivity relationships used for thawed soils – Frozen soil considered impermeable and incompressible –Considered the moving boundaries effects for consolidation analysis –No consideration of the volume changes due to the phase transformation from ice to water –Applied to simulate the thawing around the Inuvik experimental warm pipeline one-dimensionally

Model	Heat transfer analysis	Consolidation analysis	Remarks
Yao et al. (2012) 3-D FE model	Coupled with consolidation	Biot's small-strain theory	–Developed a 3-D thaw consolidation model –Linear void ratio–effective stress relationship together with a constant hydraulic conductivity used for thawed soil –Frozen soil considered impermeable and incompressible –Valid if the thaw settlement is insignificant compared to thaw depth, which otherwise violates the small-strain assumptions
Dumais and Konrad (2018) large-strain model	Coupled with consolidation	Gibson's large-strain consolidation theory	–Nonlinear void ratio–effective stress–hydraulic conductivity relationships for thawed soils –Frozen soil considered impermeable and incompressible –Consider volume changes due to the phase transformation from ice to water –Applied to simulate the thawing around the Inuvik experimental warm pipeline one-dimensionally (Dumais and Konrad 2019)
Yu et al. (2020) large strain model	Coupled with consolidation	Gibson's large-strain consolidation theory	–Total stress and effective stress analyses used for frozen and thawed soils, respectively –Nonlinear void ratio–effective stress–hydraulic conductivity relationships for thawed soils –Consider the volume changes due to the phase transformation from ice to water and the effects of freeze-thaw cycles on hydraulic conductivity –Only applicable for 1-D thaw consolidation problems

2.7 Summary

This chapter presents a review of experimental, theoretical, and numerical studies available on frost heave and thaw settlement. The importance of frost heave/thaw settlement in existing or proposed pipelines in cold regions is also discussed. Detailed discussions are presented in each section, and the observations, drawbacks, and limitations are then summarized.

The pipeline temperature observed in the existing pipelines or predicted for the proposed pipelines shows a cyclic operating temperature due to seasonal variation of the ground surface temperature, depending on the downstream location from processing facilities and stations. Also, changes in compressor stations' layout might occur after a period of operation, which could change the thermal condition around the pipeline. The effects of cyclic pipe temperatures and changes in compressor station layout on frost heave and thaw settlement are not well understood.

In terms of the numerical modelling of frost heave and thaw settlement around pipelines, one-dimensional models are considered in most studies, assuming that heat and mass flow directly below the pipe dictate the process. The heat transfer analysis is often decoupled from the mass diffusion analysis and is performed first. Although some coupled 1-D and multi-dimensional models are available in the literature, there are some drawbacks and limitations in simulating the frost heave/thaw settlement, which are discussed above in detail.

CHAPTER 3:

Centrifuge Modelling of Gas Pipelines Undergoing Freeze–Thaw Cycles

Co-Authorship: This chapter has been submitted as a technical paper for publication in a journal as: Dayarathne, R., Hawlader, B., and Phillips, R. "Centrifuge modelling of gas pipelines undergoing freeze–thaw cycles." Most of the works presented in this chapter, including the analysis of centrifuge test results, have been performed by the first author. He also prepared the draft manuscript. The other authors supervised the research and reviewed the manuscript.

3.1 Abstract

Frost heave and thaw settlement are two critical factors that need to be considered in designing chilled gas pipelines in cold regions. Due to the variation in seasonal temperature and operating conditions (e.g., pressure and temperature at the compressor stations), the pipeline temperature in some segments might vary from subzero to above-zero during winter and summer. This study examines the freezing and thawing for cyclic and constant temperatures at the pipeline and ground surfaces based on the response of fourteen model pipes tested in a geotechnical centrifuge. The cyclic (temperature) operation reduces the frost heave rate per year and causes net settlement in some cases. When the thaw bulb resulting from an above-zero operating temperature is less than the previously developed frost bulb, upward water flow occurs through the thawed soil, which could alter the pipeline–soil interaction behaviour. Five types of freeze-thaw-induced vertical displacement of the pipe have been identified from the centrifuge test results.

3.2 Introduction

Buried pipelines transmitting natural gas from northern Canada and Alaska to a temperate market might pass through continuous permafrost, sporadic or isolated patches of discontinuous permafrost, and unfrozen areas. Maintaining the pipeline's operating temperature (i.e., gas temperature) (T_p) within a specified range is one strategy to reduce the risk associated with pipeline displacement (e.g., frost heave and thaw settlement) and ground movement (e.g., slope failure). Gas temperature decreases with downstream distance from the compression station due to a decrease in pressure, known as Joule–Thomson effect, which is an important consideration in chilled gas pipeline design (Oswell 2011). For example, Nixon (1990) showed a 10–15 °C possible drop of T_p at a distance of 200–250 km from the compressor station. This implies that, between two stations, an above-zero operating temperature on the downstream side of a compressor station may induce thawing of the soil, while a subzero temperature on the upstream of the same compressor station may result in frost heave.

An accepted design philosophy for pipelines in the continuous permafrost zone is to maintain a subzero operating temperature to reduce thermal disturbances of surrounding frozen soil. Within the discontinuous permafrost zone, an above-zero operating temperature is sometimes permitted. As an example, the Norman Wells oil pipeline in Canada was initially (1985–1993) operated at a discharge T_p of -2 °C; however, in 1993, it was allowed to operate under a cyclic temperature with a maximum of 12 °C for two months in summer and -4 °C in winter months, with a mean annual discharge temperature of -1 °C (Nixon and Maclnnes 1996). The designers of the proposed Mackenzie gas pipeline in Canada also considered a range of cyclic discharge temperatures (above-zero in summer months), depending on the terrain and location of compressor stations (Colt-KBR 2003, 2006). Based on expected pipeline temperature variation along the route, Oswell

(2011) showed that a section of the pipeline might be operated at a subzero temperature at the start-up condition with a fewer number of compressor stations; however, the pipeline temperature in that section might be greater than zero when additional compressor stations are added to operate the pipeline at full capacity.

Frost heave is one of the key design considerations for pipelines in cold regions. Chilled operation freezes the soil around the pipeline and results in heave, which is due to the freezing of in-situ and migrated water. Frost heave could be very significant when the pipeline passes through highly frost susceptible soils, such as clayey silt (Konrad and Morgenstern 1984). For example, approximately 0.6-m heave in 3 years was observed in the control section of the Calgary full-scale test (Carlson et al. 1982). Such a large vertical displacement could cause significant strain in the pipeline, especially when it passes through discontinuous permafrost areas (Razaqpur and Wang 1996; Selvadurai et al. 1999; Hawlader et al. 2006). The key factors that govern the structural response of the pipeline are the magnitude of differential heave and soil–pipeline interaction in the vertical and axial directions around the interface between the heaving and non-heaving soils. The process becomes more complex when it involves freeze-thaw cycles.

Typical laboratory frost heave tests involve one-dimensional freezing of an instrumented soil column between a relatively cold and a warm plate. Tests were conducted for monotonic (step and ramp) temperature change at these plates. Based on these test results, mathematical models have been developed, which have also been extended to 2-D conditions for predicting frost heave of chilled gas pipelines (Konrad and Morgenstern 1984; Nixon 1991; Konrad 1994; Konrad and Shen 1996; Michalowski and Zhu 2006). The performance of these frost heave models and numerical techniques has also been compared with a limited number of full-scale tests (Konrad and Morgenstern 1984; Nixon 1991; Konrad and Shen 1996; Abdalla et al. 2014). As the present

study's focus is to investigate the response of pipelines for cyclic operating temperatures, readers are referred to previous studies on frost heave under a monotonic freezing temperature for further details (e.g., Konrad 1994; Michalowski and Zhu 2006).

A varying level of frost heave in a segment of the pipeline, coupled with as-laid out-of-straightness, could increase the propensity of upheaval buckling during operation at high pressure (Nixon and Burgess 1999; Palmer and Williams 2003). The buckling potential depends on the magnitude of heave, uplift resistance, and axial movement of the pipeline (Nixon and Vebo 2005). A cyclic operative temperature (positive in summer and negative in winter) could: (*i*) reduce the frost heave, (*ii*) thaw the previously developed frost bulb, (*iii*) cause settlement of the pipe, and (*iv*) change soil properties in the freeze/thaw sections, which could also affect the pipeline–soil interaction. Recognizing that frost heave and thaw consolidation might occur simultaneously in the field, a unified framework for one-dimensional conditions has been developed by Yu et al. (2019, 2020). The combined effect of these two processes governs the resultant vertical displacement of a pipe section, as shown later in this chapter. The freeze-thaw-induced change in some soil properties (e.g., hydraulic conductivity and compressibility) have been examined through small-scale 1-D tests (Chamberlain and Gow 1979; Konrad 1989a, b; Eigenbrod et al. 1996; Konrad and Samson 2000). Experimental evidence shows a significant reduction in frozen soil strength and soil–structure interaction resistance in warmer temperatures (Yuanlin et al. 1984; Aldaeef and Rayhani 2018). Konrad (1989a) showed that, in 1-D frost heave tests, freeze–thaw cycles can alter the structure of highly frost susceptible clayey silt and reduce the heave rate significantly within a few cycles. A cyclic subzero temperature at the cold plate in 1-D freezing tests also causes a reduction of heave, as compared to that of continuous freezing (Zhou and Zhou 2012).

In summary, cycling operating temperature could have a significant influence on the pipeline response. A number of centrifuge tests were conducted previously at C-CORE in St. John's, Canada, to investigate several aspects of frost heave and potential mitigation strategies. From them, the test results of fourteen pipe sections are reanalyzed in this study to examine the effects of subzero and above-zero temperatures in winter and summer months at the pipe and ground surfaces and their practical implications in the design. Note that preliminary analyses of test results of three sections among these fourteen pipe sections have been presented in Morgan et al. (2004, 2006).

3.3 Problem Statement

Temperature cycling at the compressor station in the summer and winter months could be a mitigation strategy to reduce frost heave. Moreover, the addition of a new compressor station could also result in a cyclic pipeline temperature along the route. To maintain the desired flow rate, the pressure of the natural gas is increased at the compressor stations, which also increases the gas temperature. Within the discontinuous permafrost zone, the gas temperature may be modified to be discharged at a subzero temperature in winter and above-zero in summer months. Figure 3.1(a) presents the variation of pipe temperature (T_p) between two compressor stations. T_p generally varies nonlinearly with distance (Nixon 1990; Seligman 2000; Colt-KBR 2006); however, for the purpose of explaining the process, a linear variation is used in Fig. 3.1(a). Between two compressor stations (e.g., CS1 and CS2), only a segment of the pipeline immediately following the upstream compressor station (i.e., CS1) will have a warm flow ($T_p > 0$ °C) while a cold flow ($T_p < 0$ °C) will occur in the remaining length. Additional compressor stations might be required if the pipeline is expected to transport more gas sometime after it is put into service. For example, the Mackenzie

gas pipeline was designed with three compressor stations for the start-up condition and is expected to be operated under fourteen compressor stations at the full pipeline capacity (Colt-KBR 2006).

The addition of a new compressor station (e.g., NCS in Fig. 3.1(a)) will alter the pipeline operating temperature regime. For example, at point A in Fig. 3.1(a), the pipeline has been operated at a subzero temperature (T_p < 0 °C) for a period of time. However, the addition of a new compressor station changes the pipeline temperature, and the pipeline will be operated at average warm ($T_p = T_{cs}$) and cold ($T_p = T_{cw}$) temperatures in summer and winter months.

Figure 3.1(b) schematically shows the two phases of pipe temperature variation with time at point A. In phase-I, it is assumed in the present study that the pipe temperature remains constant ($T_p = T_{im}$ < 0 °C) for an initial freezing period (t_i); t_i depends on the time when an additional compressor station is installed. After the initial freezing (phase-I), cyclic pipe temperatures of $T_p = T_{cs}$ in the summer time (t_s) and $T_p = T_{cw}$ in the winter time (t_w) are maintained in phase-II. The transition between the summer and winter temperatures might occur gradually over a period of time; however, a step change in temperature was used in the centrifuge tests. Moreover, during the initial freezing period (i.e., in phase-I), the pipe temperature might vary in the summer and winter months; however, such variation was not considered in centrifuge tests; instead, a mean value of T_p (= T_{im}) was maintained for this period.

Centrifuge tests were also performed with an approximate mean value of the annual freezing pipe temperature in phase-II, T_{fm} ($T_{cw} < T_{fm} < T_{cs}$) (see Fig. 3.1). Although two pipe temperatures (< 0 °C) were used in phase-I and -II, these tests are called ‘continuous freezing’ tests. In these tests, the pipelines experienced only frost heave. However, in cyclic tests, the pipeline was subjected to exclusive frost heave in the initial freezing stage, but it experienced both thaw- and freezing-related displacements in the thaw- freeze stage.

The uniform free-field frost heave and thaw settlement are investigated in this study. The free-field vertical displacement is a necessary parameter for the analysis of pipelines subjected to non-uniform heaving when they pass through frost susceptible and non-frost susceptible/frozen soils (Nixon 1994; Hawlader et al. 2006).

3.4 Centrifuge Modelling

All the tests were conducted on the 5.5-m-radius beam centrifuge at C-CORE in St. John's, Canada, at n times the gravitational acceleration, where n = 55 except for one test with n = 47.9. The applicability of centrifuge testing to frost heave modelling and its limitations are available in previous studies (Ketcham et al. 1997; Yang and Goodings 1998; Phillips et al. 2001, 2002; Clark and Phillips 2003; Lawrence et al. 2005). The limitations include the concerns related to the scaling laws, primarily in the following three areas: (*i*) macro-scale ice lens and micro-scale pore ice formation, (*ii*) creep and fracture of ice, and (*iii*) uplift resistance (C-CORE 2004; Lawrence et al. 2005). A limited number of studies investigated the effects of these scaling laws. However, conducting modelling of models at three *g*-levels, Yang and Goodings (1998) showed that one-dimensional frost heave could be scaled in centrifuge tests, although they found some scatter in results which might be due to scaling law or experimental errors. Ketcham et al. (1997) also conducted modelling of model tests for constrained footings and showed an expected trend of frost front penetration and free-field heave; however, they raised concerns about the time required for uplift resistance, which was potentially due to the scaling law issues in creep and stress relaxation. Phillips et al. (2002) showed a good comparison of frost heave and frost front penetration between the centrifuge and Calgary full-scale test results. Overall, centrifuge tests provide further insights into frost heave mechanisms; however, more studies are required for further validation of scaling laws. A detailed discussion on the scaling laws is available in C-CORE (2004).

As shown in Tables 3.1 and 3.2, the centrifuge tests were conducted for the following varying conditions: (*i*) artificial and natural soils of different frost susceptibilities, (*ii*) initial moisture content (w_i), (*iii*) initial soil temperature (T_{is}), (*iv*) ground surface (T_g) and pipe (T_p) temperatures, and (*v*) the duration of freezing and thawing. Seven centrifuge tests are considered in this study (CF1–CF7, Tables 3.1 and 3.2), where two pipe sections were used in each test (pipe-A and pipe-B). The pipes are named as A1–A7 and B1–B7. The temperature of pipe A in all the tests (i.e., A1–A7) was cyclic, whereas pipe B was operated under continuous freezing except for B3 and B7. All the tests ended during a chilling phase.

A yearly weighted average of cyclic temperature in the pipe (T_{av}) was also used to represent the overall pipe temperature in phase-II.

$$T_{av} = (t_s T_{cs} + t_w T_{cw})/12 \tag{3.1}$$

where T_{cs} and T_{cw} represent the temperature in the pipe in summer (t_s) and winter (t_w) periods in a year. In the present experimental program, t_s = 5 months and t_w = 7 months in prototype scale, except for test CF7 where t_s and t_w were 4 months and 8 months, respectively. Moreover, the pipe temperature in phase-II for the continuous freezing cases (T_{fm}) was ~ T_{av} in the same test setup (T_{av} = (0.94–0.98)T_{fm}).

3.4.1 Materials

All the centrifuge tests, except for test CF7, were conducted with soil specimens prepared through a mixture of two readily available artificial materials: Sil-Co-Sil silt (S) and Speswhite China kaolin (K). These two materials were mixed in different proportions to produce a range of grain size distributions (Fig. 3.2). The grain size distribution has an important influence on frost susceptibility, in addition to its role in mechanical and thermal behaviour. The frost susceptibility of the soil used in the experimental program varied from high to very high, as per Chamberlain

(1981). The test CF7 was conducted on a natural Calgary silt, which was collected from a construction site close to the circa 1974–1985 Calgary full-scale frost heave test site (Carlson et al. 1982), which is also highly frost susceptible. Note that the Calgary silt has been used for many experimental investigations, both in the laboratory and full-scale tests (Carlson et al. 1982; Konrad and Nixon 1994; Krantz and Adams 1996; Konrad 1999).

A limited number of one-dimensional segregation potential (SP) tests were conducted. The SP values of 75S + 25K, which were used in most of the tests (CF2–CF5 in Table 3.1), are similar to the SP of Calgary silt reported by Konrad (1994). Three tests on the soil used for CF6 (60S + 40K) showed SP values higher than that of Calgary silt, and no SP tests were conducted for 50S + 50K, which were used in CF1. In the present study, frost susceptibility (high to very high) is estimated primarily based on particle size distribution, which is similar to that of Calgary silt (Fig. 3.2). However, it is understood that a full suite of SP tests for varying boundary conditions, specimen preparation and applied normal stress would be useful for a better analysis of the centrifuge test data.

3.4.2 Centrifuge model

Experiments were conducted using a thermally controlled centrifuge test package, as shown in Fig. 3.3(a), which has the following key features:

(*a*) A 670-mm deep insulated aluminum rectangular strongbox with inner dimensions of 1020 mm × 775 mm in plan view with a 50-mm thick polystyrene insulation at the base and inner walls.

(*b*) An insulated lid to cover the test package where a heat exchanger is mounted for cooling the top surface of the soil bed by recirculating glycol refrigerant to provide the ground surface temperature variation.

(*c*) A vortex tube to supply chilled air to simulate the chilled gas temperature in the pipeline.

(*d*) A thermistor panel to measure soil temperature below the pipe (inset of Fig. 3.4)

(*e*) A Mariotte tank at the corner of the model to maintain the groundwater level at the desired depth while providing additional water supply to the package during water migration due to freezing (i.e., modelling an open system freezing).

(*f*) One or two open overflow reservoirs to collect the water expelled out of the soil during the initial consolidation phase.

Further details on the development of the test package and its successful use for frost heave modelling are available in previous studies (Phillips et al. 2002; Morgan et al. 2004, 2006; Piercey et al. 2011).

3.4.3 Sample preparation

Similar to previous studies, wet compaction and slurry consolidation methods were used to prepare the soil bed in the centrifuge model test container (Ketcham et al. 1997; Yang and Goodings 1998; Han and Goodings 2006). The prepared soil bed using these two methods might be somehow different, especially the soil structure and void ratio, which could influence the water migration. The soil bed was saturated following the same procedure in both cases (i.e., flushing from the bottom, as discussed later). Full saturation was confirmed by back calculating the degree of saturation from measured moisture content. Note that slurry consolidated soil beds are typically saturated even before this flushing. Therefore, the degree of saturation effect on frost heave, as Konrad (1994) mentioned for laboratory compacted soil specimens, may not be applicable for these tests. However, the effects of soil bed preparation methods might be investigated further. A sand drainage layer of approximately 30-mm thickness was placed at the bottom of the container (connected to the Mariotte tank and overflow reservoir), and a geotextile layer was used to separate the drainage layer from the soil bed.

(*a*) Wet compaction method

The Sil-Co-Sil silt and Speswhite China kaolin were mixed at a given proportion (Table 3.1) in a dry state inside a drum type mixer until it reached a uniform mix. The dry silt-clay mixture was then further mixed with an amount of water that gives moisture content slightly above the optimum moisture content (determined previously through Standard Proctor compaction tests). The mixing was continued for 15 minutes. This wet soil was then placed in the model test container in layers of approximately 40-mm to 50-mm. Each layer was compacted manually to approximately 95% of the maximum Standard Proctor dry density using a plate compactor which was selected to provide similar compaction effort in the standard Proctor hammer.

(*b*) Slurry consolidation method

Adding deaired water to a water content of approximately twice the liquid limit, *LL* (= 40%–50%), the soil was mixed thoroughly in a drum for two hours in order to obtain a uniform slurry. The slurry was poured into a consolidation strongbox and consolidated on the laboratory floor at 1*g* up to a predefined vertical consolidation pressure (= 450 kPa, except for 200 kPa in CF7) by applying the vertical pressure in several increments. The drainage was allowed at the top and bottom boundaries. At least 90% consolidation occurred in each time increment, as verified using the square-root-of-time method. The consolidated sample was unloaded carefully and then placed into the centrifuge test container as a soil block.

3.4.4 Model pipe and instrumentation

The pipe section was fabricated from a copper tubing with an outside diameter of 22.2 mm (15.9 mm in test CF7), which represents an outside diameter of 1.2 m (0.76 m in CF7) in prototype scale for the accelerations used in this test program. It had a 400-mm horizontal section and two welded end sections, inclined at 45°–60° to the horizontal section, for connection to the inlet and

outlet (Fig. 3.3). Two pipe sections were installed in each test bed by digging trenches, which were then backfilled with the excavated soil. The pipes were sufficiently far from each other; therefore, no significant thermal interaction occurred. In a test setup, both pipes were placed at the same level maintaining the same cover depth, except for test CF3, where a step ground surface profile was created by placing a timber strip at the mid-distance between the pipes to achieve 0.75*D* and 1.5*D* cover depths for pipes A3 and B3, respectively.

Up to 64 channels were available for data acquisition. Among them, 23–27 channels recorded temperature from the thermistors: (*i*) at the pipe inlet, middle and outlet; (*ii*) in the soil body, primarily below the pipe (Fig. 3.4); and (*iii*) at and above the ground surface. The thermistors below the pipe invert were attached to a panel (see the inset of Fig. 3.4), which was inserted in the soil at the middle of the pipe. The thermistors were calibrated using an ice bath to enhance the level of accuracy, which could measure the temperature with an accuracy of ± 0.02 °C. The panel is not attached to the pipe; however, it moves up with the upward movement of the frozen soil wedge. The frictional resistance between the thermistor panel and the unfrozen soil below the frost bulb has some small effect, as discussed later. In this chapter, these thermistors are named T_d, where the subscript *d* represents the initial depth below the invert of the pipe in prototype scale in metres (Fig. 3.4). The vertical displacements of the pipe and ground surface were measured at the inlet, middle and outlet using LVDTs having an accuracy of ±0.25% of the full scale (FS). For pipes, the LVDTs were placed on the top of the pipe through plastic access tubes, as shown in Fig. 3.3(b). Three pore pressure transducers (PPTs, accuracy ±0.25% of FS) were installed in the soil bed, one directly below each pipe (Fig. 3.4) and one below the midpoint between pipes A and B but at the same horizontal level, to measure freezing-induced suction (pore water pressure below the initial hydrostatic pressure) that causes water migration towards the freezing front. The PPTs

used in this test program could successfully measure water pressure up to approximately –40 kPa without significant effects of cavitation. A third PPT was also installed immediately above the interface between the soil bed and sand drain to confirm the level of the water table. Typical instrumentation at the middle of the pipe section is shown in Fig. 3.4, except for test CF7, where a slightly different arrangement of thermistors was used, as discussed later.

3.4.5 Initial ground temperature and centrifuge test setup

The entire test container, with pipe sections and all instrumentation, was placed in a cold room to get a uniform soil temperature slightly above the freezing point. In the cold room, the model was saturated slowly for 48 hours by supplying water from the Mariotte tank to the bottom sand drainage layer. The water level was raised up to the top of the soil surface and then lowered to the targeted level (i.e., top of the pipeline in tests CF1–CF6 and the invert in CF7). Note that Yang and Goodings (1998) also used a similar procedure to saturate their compacted soil beds. The model container was then transferred to the centrifuge arm without any significant temperature change in the soil bed. The control (e.g., vortex tubes and heat exchanger) and measurement (e.g., LVDT, PPT and data acquisition) units were connected on the centrifuge platform.

3.4.6 Centrifuge tests

The test package was accelerated to 55*g* in CF1–CF6 and 47.9*g* in CF7, and the soil bed was allowed to consolidate under self-weight for 5–19 hours in order to achieve at least 90% consolidation (based on surface settlement and PPT reading). The vertical effective stress at the end of in-flight consolidation is less than the laboratory consolidation pressure applied in the slurry consolidation method, which indicates that the soil bed is overconsolidated. For the compacted soil bed, the preconsolidation pressure is expected to be increased due to suction induced by compaction (Fredlund et al. 2012; Alonso et al. 2013). Therefore, the suction-induced

consolidation of unfrozen soil during freezing in-flight is not expected to be significant. After consolidation, chilled air was supplied through the vortex tube to operate the pipe at the temperatures listed in Table 3.2. At this stage, circulating glycol refrigerant through the heat exchanger mounted under the insulated lid of test package, the ground surface temperature (T_g) was controlled as shown in Table 3.2. In phase-I, T_g was constant; however, in phase-II, T_g was constant in CF1 and CF7 while it was varied in the summer and winter months in CF2–CF6. Note that the ground surface temperature might vary significantly along the pipeline route, depending on many factors, including the seasonal variation of air temperature, snow cover, location, and vegetation. Finite element modelling shows that ground surface temperature mainly influences the response for shallow buried pipelines (see chapter 5).

3.4.7 Post-test investigation

The test container was carefully removed from the centrifuge and brought to a cold room (-5 °C) for further examination, including visual observations (e.g., surface cracks, heave and change in instruments' location). Using a handsaw and high-speed carbide tip blades, the soil block was cut into ~ 25-mm thick sections along the length of the pipe, which were photographed and x-rayed to examine ice lens formation and frost bulb growth. These sections were cut further into small cubes in a grid to determine the final moisture content (w_f). The difference between the initial (prior to self-weight consolidation in the centrifuge) (w_i) and final moisture contents provides the information of water migration during the test.

Overall, although the present centrifuge modelling is significantly less expensive than full-scale tests, the model preparation and test require some additional considerations, including temperature control at the boundaries and pipe. Also, tests require a long time compared to many

typical centrifuge tests. For example, the centrifuge spinning duration in test CF7 was more than 56 hours, including ~ 19 hours of consolidation.

3.5 Experimental Results

The pipeline response at the middle of the horizontal segment (Fig. 3.3(b)) is presented in the following sections unless otherwise mentioned. The results are presented on the prototype scale. Heave/settlement, time and temperature in prototype scale are obtained from centrifuge model scale values by multiplying n, n^2 and 1, respectively. The vertical displacement of the model pipe was measured by placing a LVDT directly on the pipe surface (Fig. 3.3(b)). The responses in the nine cyclic tests listed in Table 3.2 can be categorized into three major groups (Cases 1 to 3).

3.5.1 Case-1

a) Frost heave and thaw settlement

In this case, the initial freezing period under a constant pipe temperature (phase 1) is relatively long (t_i = 3–3.3 years), and the cyclic temperature in phase 2 causes a significant reduction of initial heave (h_i). As shown in Fig. 3.5, the cyclic tests in CF1–CF3 (pipes A1–A3 and B3 in Table 3.2) show this type of response. The pipeline heave in the continuous freezing tests in CF1 and CF2 (i.e., pipes B1 and B2 in Table 3.2) is also plotted in this figure for comparison.

Figure 3.5 shows that the measured heave at the end of the initial freezing period is comparable in both pipes in a test (e.g., h_i is ~ 430 and ~ 480 mm in pipe-A and pipe-B, respectively, in test CF2). This indicates that the soil bed and test conditions are similar for both pipes in a centrifuge test, except for continuous freezing or cyclic operation after t_i ~ 3 years. The cyclic operation causes a reduction of the initial heave, while the continuous freezing in phase-II

(T_{fm} < 0 °C) results in a gradual increase in heave. The following are the key observations in these six pipe tests in CF1–CF3.

i. A higher initial soil temperature, together with a lower pipe temperature, causes a larger heave during the initial freezing period. For example, h_i is higher in CF2 than in CF3. This could be due to a higher temperature gradient in the frozen fringe, which caused a higher segregational heave, as reported from the 1-D frost heave test (Konrad 1980; Konrad and Morgenstern 1980).

ii. An above-zero temperature in summer months during the cyclic operation caused thawing of the initially developed frost bulb, resulting in settlement of the pipe. In the subsequent winter operation under a subzero temperature at the pipe (also at the ground surface in CF2 and CF3), the freezing of the thawed soil caused heave. However, the rate of heave depends on operating conditions and the development of the thaw bulb in the previously developed frost bulb, as described below. In CF1, the settlement of the pipe in the first summer ($S_{t1)}$ was more than the initial heave (h_i), whereas $S_{t1} < h_i$ in CF2 and CF3. The potential reasons behind this are explained later in the 'freeze-thaw consolidation section.'

iii. In phase-II, three patterns of vertical displacement of the pipe were observed. Firstly, the first summer temperature in A1 caused a significant settlement; however, the subsequent cyclic temperatures resulted in only a small heave and settlement. Secondly, for pipe A2 in test CF2, the first two cycles of pipe temperature almost brought the pipe to the original position (zero resultant heave); however, in subsequent cycles, the gradual heaving continued where cyclic pipe displacement was not evident. Finally, in CF3 (pipe A3 and B3), a gradual (average) settlement of the pipe occurred where a clear cyclic pattern of heave and settlement was observed during the whole period of phase-II.

The mechanisms of the preceding response can be explained from the recorded temperature variation in the soil and resulting frost and thaw bulbs.

b) Soil temperature below the pipe

The temperature around the pipe, primarily below the invert, was recorded in all the tests. However, for brevity, temperature variation for some selected cases is presented in this chapter to explain the mechanisms. Figures 3.6(a)–3.6(c) show the variation of temperature below the pipe in three cyclic tests. The soil temperature variation in a continuous freezing test (pipe B2 in CF2) is shown in Fig. 3.6(d) for comparison.

To explain the mechanisms, the freeze-thaw process is shown schematically in Fig. 3.7 for a pipeline section upstream (e.g., point A in Fig. 3.1) at a given time in the refreezing period. A frost bulb is formed during the initial chilling period, which is then thawed during the summer operation at an above-zero pipe temperature that creates a thaw bulb. The thaw bulb will gradually refreeze from the pipe in the following winter operation and create an 'inner refrozen zone' (Fig. 3.7). If the summer operation cannot thaw the initially developed frost bulb, a 'leading frozen zone' will remain outside the thawed zone.

The temperature profile in the soil below the pipe is also shown schematically in the inset of Fig. 3.7. The depths of the leading frost front, thaw front and refreezing front (i.e., 0 °C points) are denoted as d_f, d_t and d_{rf}, respectively, and are measured from the invert of the pipe. Note that during operation, the position of the 0 °C isotherm changes continuously. For example, during the initial stage of a thawing period, the leading frost front might progress further due to temperature variation within the leading frozen zone (see the inset of Fig. 3.7), although thawing occurs near the pipe. The thickness of the leading frozen soil is denoted as t_{fl}, which also varies with radial

distance from the pipe. The shape of frost or thaw bulbs might be affected by other factors such as ground surface temperature, as observed in the present centrifuge modelling.

Figure 3.6 shows a faster temperature decrease in soil elements near the pipe (e.g., $T_{0.6}$) than in an element far from it (e.g., $T_{6.1}$), during the initial chilling period. At $t = t_i$, the frost front (T = 0 °C) penetrated to approximately 0.6 m, 1.9 m and 3.9 m below the pipe in CF1, CF2 and CF3, respectively. Here, the location of the 0 °C point below the pipe at a given time has been obtained from the temperature profile (smoothed curve) based on thermistor data. In pipe A1 (Fig. 3.6(a)), the above-zero pipe temperature (T_p) in the first summer increases the temperature in the thermistors near the pipe ($T_{0.6}$–$T_{2.8}$ to ~ 2 °C), which indicates that the initially developed frost bulb was completely thawed (at least below the pipe) and the thickness of the leading frozen zone (t_{fl}) was zero. In the subsequent cyclic operation, the soil temperature at the thermistors' locations, even in the nearest thermistor ($T_{0.6}$), did not decrease to 0 °C. This implies that the freezing and thawing occurred only in a zone near the pipe (d < 0.6 m), and the soil might be completely thawed due to summer operation. This process resulted in a cyclic nature of frost heave and thaw settlement in phase-II; however, the average annual vertical displacement was not significant (Fig. 3.5).

Cyclic pipe temperature in A2 in test CF2 showed a very different response from A1. In this case, the above-zero pipe temperature in the first summer thawed less than 0.6 m soil below the pipe ($T_{0.6}$ < 0 at the end of thawing, Fig. 3.6(b)). Moreover, the temperature in three thermistors immediately below the pipe ($T_{0.6}$, $T_{1.1}$ and $T_{1.9}$) was ~ 0 °C or less. This signifies that a thick leading frozen soil (t_{fl} ≥ 1.3 m (= 1.9 m - 0.6 m)) remained at the end of thawing due to the first summer operation. The thaw depth (d_t) increased in the subsequent summer operations, $T_{0.6}$ and $T_{1.1}$ increased and became positive at the end of each summer. However, as $T_{1.9}$ remained at subzero

temperature, the leading frozen zone always remained during the whole cyclic operation (phase-II).

Test CF3 was conducted at a lower initial soil temperature and lower pipe temperatures in the summer than those of A1 and A2 (Table 3.2). Figure 3.6(c) shows a deep frost front penetration (~ 3.9 m) at the end of the initial chilling ($T_{3.9} \sim 0$ at t_i in Fig. 3.6(c)). Also, each summer operation caused a lesser extent of thawing in this test than in A2 (compare the above-zero temperatures in the thermistors near the pipe, such as $T_{0.6}$ and $T_{1.1}$). This implies that a thicker layer of leading frost front than in A2 remained in this case. In addition to a larger cover depth ($H = 1.5D$) in B3 than in A3 ($H = 0.75D$), pipe A3 was operated at a 1 °C higher temperature, which induced less heave at the end of initial chilling (Fig. 3.5). A faster thawing was observed in the temperature–time plot in B3 than in A3; however, it did not show a significant difference between the vertical position of pipes A3 and B3 during the cyclic operation (Fig. 3.5).

c) Freeze-thaw consolidation

The vertical displacement of the pipe, presented in Fig. 3.5, is also influenced by freeze-thaw consolidation. This process has been studied using 1-D laboratory tests, and the mechanisms have been explained for open and closed systems (Nixon and Morgenstern 1973; Chamberlain and Gow 1979; Konrad 1989a, b). An unfrozen moisture reservoir should be available in the open system (Eigenbrod 1996), while only the in-situ water freezing occurs in the closed system (Nixon and Morgenstern 1973). Similar to 1-D freeze-thaw experiments in previous studies, in the present centrifuge tests, the effective stress in soil increased due to the development of suction during freezing that caused a reduction of the void ratio. The consolidation occurred primarily in the unfrozen soil and was higher in CF1 because of higher clay content (50% kaolin, Table 3.1) than in other tests. Note that, although a large portion of consolidation occurred during freezing, the

frost heave was more than the consolidation settlement, which resulted in net heave during freezing (e.g., during the initial freezing period in Fig. 3.5). The ice-rich soil thawed during the summer operation, and under a good drainage condition, the resulting excess pore pressure dissipated, and the resulting settlement was observed in the summer (Fig. 3.5). The experimental observation in CF1 could be further explained using 1*g* and centrifuge tests of Han and Goodings (2006) on clay. They showed that freezing-induced suction significantly increases the effective stress in the unfrozen soil in front of the frost front, named as the "freeze consolidated zone" because the tests on these low permeable soils behaved as a closed system although it was open. At the end of the test, the moisture content in this zone was less than the initial moisture content. The considerable amount of consolidation settlement in this zone needed to be subtracted to calculate net heave. Han and Goodings (2006) tests were only for continuous freezing. In CF1, the reduction of effective stress occurred during the thawing periods because of suction reduction; however, the void ratio does not revert to the initial value because the swelling index is less than the compression index. Therefore, a net settlement is observed in CF1 with the soil of high clay content.

In addition to the hydraulic conductivity of the unfrozen/thawed soil, the existence of the leading frost front affects the drainage of excess pore water pressure and, thereby, the freeze-thaw settlement. In the centrifuge tests, the formation of the ice lenses, especially near the leading frost front (Fig. 3.7) and reduction of the thickness of the unfrozen water film surrounding the soil particles in frozen soil reduces the permeability. This zone acted as a barrier to water flow in some tests (e.g., in A2 and A3) unless it was completely thawed (e.g., in A1). Figure 3.8 shows cross-sections of the soil block after the completion of test CF2. Mainly three types of cracks were observed in post-test investigations: (*i*) perpendicular to the heat flow direction, which is due to the formation of segregate ice lens; (*ii*) some radial cracks, which are potentially the tension cracks

due to post-test stress relaxation; and (*iii*) some tension cracks above the pipe. The last one could weaken the soil and increase the hydraulic conductivity of the soil above the pipe; however, it would not have a significant effect on ice lens formation below the pipe because the overburden pressure at the freezing front that affects water migration would not change even if these tension cracks formed. However, it could increase the thaw consolidation rate in cyclic operation. As pipe A2 was operated under a cyclic pipe temperature after the initial freezing, the summer operating temperatures thawed the previously developed ice lenses and created a thaw bulb (Fig. 3.8(a)). The formation of a thaw bulb is very clear in the x-ray (see the inset in Fig. 3.8(a)), where no marks of ice lenses are visible. However, no such zone is visible around pipe B2 (Fig. 3.8(b)) because it was operated under two uniform subzero pipe temperatures (Table 3.2).

Another observation is the accumulation of water/formation of a cavity above pipe A2 (Fig. 3.8(a)). Thawing generated excess pore water pressure in the soil in the thaw bulb. However, because of the leading frozen zone of very low hydraulic conductivity, the water migration primarily occurred in the closed thaw bulb. The water migration has been confirmed by a significant increase in moisture content (w) in the soil elements above the pipe. A similar freeze-thaw-induced water migration was also observed in pipe A3, which was also operated under cyclic pipe temperatures. Note that the upward movement of the frost bulb along with the pipe created a tension crack in the soil above the pipe in some cases (e.g., Fig. 3.8(b)) through which accumulated water could flow up easily. Therefore, a cavity was observed above the crown of the pipe in some cases in post-test observation.

In the cyclic operation period, the pipe displacement in Fig. 3.5 represents the resultant of frost heave and thaw settlement. For example, an above-zero pipe temperature in the summer could cause settlement of the pipe due to the thawing of soil near the pipe, while the frost heave could

continue in the leading frozen zone. When frost heave in the leading freezing front is larger than thaw settlement near the pipe, an upward displacement of the pipe will be observed, as occurred in pipe A2 after two summers (Fig. 3.5). Also, for the same reason, there is a time lag between pipe temperature change (e.g., winter to summer) and observed change in pipe displacement (i.e., heave to settlement). For example, in year 6, the upward vertical displacement of pipe B3 restarted ~50 days after the pipe temperature change to subzero winter conditions. In the centrifuge tests, the vertical displacement was measured only at the pipe and ground surfaces; therefore, the effects of ice lensing and thaw consolidation on the measured (resultant) displacement could not be separated.

Unfortunately, the cross-sectional view of pipe A1 and B1 (test CF1) was not taken. However, Fig. 3.6(a) shows that the frost bulb around pipe A1 was completely thawed due to cyclic summer operations (i.e., no leading frozen zone). In this case, the excess pore water pressure could also be dissipated in the unfrozen soil. Figure 3.5 shows that, at t = 3.7 years (point X), the resultant displacement of pipe A1 represents a net settlement of 57 mm from its initial position. This is potentially due to the freeze-thaw consolidation of the compressible soil (high clay content, see Table 3.1). In the following three years, only small heave and settlement occurred due to cyclic pipe temperatures.

3.5.2 Case-2

Similar to Case-1, this series of tests (CF4–CF6) was conducted for an initial chilling period (t_i) of 3 years (phase 1) with constant pipe temperature. Figure 3.9 shows that the pipes heaved 260 mm to 525 mm at the end of initial freezing. The maximum heave occurred in pipe A4, which is due to a higher initial soil temperature and lower pipe temperature in this case than in other tests presented in this figure. In addition, soil type (clay and silt percentage), bed preparation technique

(wet compaction in CF5 and slurry consolidation in CF4 and CF6) and surface temperature (low in CF4) also influenced the heave.

Only in pipe A6, a considerable settlement (~ 70 mm) was observed during the first summer operation. The freeze-thaw consolidation occurred in all tests; however, as described above, the frost heave in the leading frozen zone exceeded and compensated for this settlement, which resulted in a gradual upward movement of the pipes.

To explain the potential mechanisms that resulted in different pipe displacements in Case-1 (Fig. 3.5) and Case-2 (Fig. 3.9) during cyclic operation, typical temperature variation in the soil below pipe A4 is presented in Fig. 3.10. The primary difference between Fig. 3.6 (Case-1) and Fig. 3.10 (Case-2) is that the temperature of the thermistors located at 3.9–6.1 m gradually decreased, even in the cyclic operation period. This indicates that the depth of the leading frost front (d_f) increased—for example, d_f ~ 3 m and ~ 6.1 m at t = 3 years and 12 years, respectively. However, in Case-1, d_f was almost constant during cyclic operation. This difference is because of the lower average temperature (T_{av}) (see Eq. 3.1) in Case-2 (-3.8 °C to -5.5 °C) than in Case-1 (-2.0 °C to 0.6 °C).

Pipeline design becomes more challenging when it is surrounded by a thaw bulb (Greenslade and Nixon 2000). The cyclic operation also created a thaw bulb in this case. The x-ray section of pipe A4 in the inset of Fig. 3.9 shows that an oval-shaped thaw bulb was formed near the pipe during cyclic operation. The thaw bulb is not symmetrical around the pipe; it extended less above the pipe. Note that, in the field, the shapes of the frost bulb and thaw bulb might be altered due to seasonal temperature variation at the ground surface. The dark colour immediately above the pipe represents a void where water accumulated due to freeze-thaw consolidation. A very similar shape of the thaw bulb was formed around pipes A5 and A6.

3.5.3 Case-3

Test CF7 could be used to investigate the effects of the initial freezing period (t_i) and the thermistor mounting panel. This test was conducted on natural Calgary silt. With a short initial chilling period of 8 months (3 years in previous tests), cyclic pipe temperatures, T_{cs} = 2 °C for 4 months, followed by T_{cw} = -10 °C for 8 months (i.e., T_{av} = -6 °C), were applied for 9 years. The thermistor panel was installed only under pipe A7, while pipe B7 was tested without the thermistor panel, i.e., thermistors positioned freely. All the other conditions were the same for both pipes.

The temperature variation with time below pipe A7 is similar to that in pipe A4 (Fig. 3.11). The depth of the leading frost front continuously increases with time, even in the cyclic operation phase (e.g., d_f ~ 1.5 m and ~2.5 m at t = 0.6 years and 9 years, respectively).

Figure 3.12 shows that a small heave (~ 25 mm) occurred during the initial freezing period of 8 months. A notable freeze-thaw-induced consolidation settlement occurred only in the first few years; however, it is not significant in the later years because the frost heave resulting from the leading frost front compensated the settlement, as discussed above. Figure 3.12 shows a small difference between the vertical movement of pipes A7 and B7, which indicates that the existence of the thermistor panel does not have a significant influence on the response of the pipe, as presented in this chapter.

The inset of Fig. 3.12 shows that a thaw bulb was generated near pipe A7 due to cyclic operation. However, the shape of the thaw bulb was symmetrical around the pipe (almost circular) as compared to those presented in Fig. 3.8(a) and the inset of Fig. 3.9. This might be due to a large cover depth in this test (1.3D).

3.6 Implications for Frost Heave Prediction and Pipeline Design

The average annual vertical displacement trend observed in these centrifuge tests is shown schematically in Fig. 3.13. After an initial period of operation (t_i) at a constant pipeline temperature (T_p) below 0 °C, type-I frost heave might be observed in phase-II if: (*i*) the pipeline is still operated at a constant subzero temperature but higher than the T_p in the initial freezing period, or (*ii*) the cyclic pipeline temperatures (T_{cs} and T_{cw}) and the duration of summer (t_s) are small, such that the weighted average annual operating temperature (T_{av}) is low (≤ -3 °C in the centrifuge test results presented). In the field, this might occur, for example, at a location considerably far from the compressor station (Fig. 3.1).

Higher pipe temperatures and a longer summer operation (i.e., higher T_{av}) could cause a settlement of the pipe for soils with high clay content. The rate and magnitude of settlement depend on soil type (e.g., compressibility) and operating conditions (e.g., T_{cs} and T_{cw}). If all other conditions remain the same, type-II, -III and -IV represent the cases for high, medium and low T_{av}.

After reaching the maximum settlement (point B in Fig. 3.13 for type-III), heaving might occur (segment BC), where the frost heave from the leading frozen zone is more than the settlement. This might occur after a large settlement during the initial summer operation (e.g., A2 in Fig. 3.5) or after a small settlement (e.g., A6 in Fig. 3.9). The former might occur at a higher T_{av}. The gradual settlement might continue for a longer period, as for type-IV in Fig. 3.13. After the maximum settlement, the overall pipe displacement may not be very significant, as observed in A1 (Fig. 3.5). In the field, types-II to IV responses might be observed near the compressor station, where a relatively warm flow might occur in the summer.

Finally, the type-V response (e.g., CF7) might be found for a cyclic operation without a significant period of initial chilling; for example, a section in the downstream of a compressor station that was installed at the commissioning of pipeline operation (e.g., CS1 in Fig. 3.1).

Another practical implication is that the centrifuge test results show a varying degree of reduction of frost heave if the cyclic operation is considered, which might be beneficial for pipelines in discontinuous permafrost. However, the thawing in frozen soils could cause additional issues. Existence of a thaw bulb makes the pipeline design more challenging (Greenslade and Nixon 2000) because, in addition to the change in soil properties, the water migration and pipe settlement could weaken the soil above the pipe and/or create a cavity, as observed in the present centrifuge experiments, that alters soil–pipeline interaction, and more specifically, the uplift and axial resistances.

Note that a large variation in ground surface temperature in the summer and winter months, as expected under some field conditions, was not modelled in this test program. The ground surface temperature could influence the freezing and thawing, especially in the soil above the pipeline at typical burial depths, and thereby the soil uplift resistance and frost heave.

3.7 Conclusions

The temperature variation in the summer and winter months at the pipe and ground surfaces could cause cyclic freezing and thawing of soil around a chilled gas pipeline. In the present study, freeze-induced heave and thaw settlement/consolidation are examined from fourteen pipe section tests conducted in a geotechnical centrifuge. Initially, in phase-I, the pipes were operated at a subzero temperature for a given time period. Then, in phase-II, nine of the pipes were operated at a cyclic temperature, above-zero in the summer months and subzero in the winter months, while

in the other six, a constant subzero temperature (higher than the temperature in phase-I) was maintained. The ground surface temperature was also varied.

Cyclic operating temperatures reduced the average rate of heave (per year). For the test conditions considered in the centrifuge tests, the cyclic operation caused more reduction of heave rate than that observed in the tests under the constant subzero operating temperature in phase-II. In some cases, the higher operating temperatures during cyclic operation caused the overall settlement of the pipe from its position after heaving during phase-I.

The summer operation at an above-zero temperature thaws the initially frozen soil around the pipe. If it cannot thaw all the soil in the frost bulb, a leading frozen zone forms outside the thaw bulb, which makes the process more complex. Two key factors control the overall vertical displacement of the pipe: (*i*) frost heave resulting from the leading frost front, and (*ii*) settlement due to thawing and water migration in the inner thaw bulb, where the low permeable leading frost front might work as a barrier to water flow for thaw-induced pore water pressure dissipation. The water migration within the thaw bulb could result in the accumulation of water above the pipe or could form a cavity, as observed in some centrifuge tests, which can alter the axial and uplift resistances to the pipeline. The effects of these factors need to be studied further.

Acknowledgements

The works presented in this chapter have been supported by the InnovateNL, formerly Research Development Corporation (RDC), Newfoundland and Labrador, through the ArcticTECH program. A number of individuals were involved in upgrading the C-CORE centrifuge facility for frost heave modelling and conducting tests, including Jack Clark (deceased), Vincent Morgan, Baocheng Li, Gerry Piercey, Don Cameron, Derry Nicholl and Karl Tuff.

Valuable comments from Dr. Jim Oswell at Naviq Consulting Inc. on a draft manuscript are greatly acknowledged and appreciated.

List of symbols

D	outside diameter of pipe
d_f	depth of leading frost front below pipe invert (Fig. 3.7)
d_{rf}	depth of refreezing front (Fig. 3.7)
d_t	depth of thaw front (Fig. 3.7)
g	gravitational acceleration
H	cover depth (Fig. 3.7)
h_i	heave at the end of initial freezing
LL	liquid limit
n	times of g used in centrifuge tests
S_{t1}	settlement of pipe in first summer
T_{av}	yearly weighted average of cyclic pipe temperature
T_{cs}	summer pipe temperature (Fig. 3.1)
T_{cw}	winter pipe temperature (Fig. 3.1)
T_d	thermistor at d depth below the invert (Fig. 3.4)
T_{fm}	pipe temperature in phase-II in continuous freezing (Fig. 3.1)
T_g	ground surface temperature
T_{im}	mean pipe temperature during initial freezing period (Fig. 3.1)
T_{is}	initial soil temperature
T_p	pipeline operating temperature

t pipe wall thickness

t_{fl} thickness of leading frozen soil (Fig. 3.7)

t_i initial freezing period (Fig. 3.1)

t_s summer period (Fig. 3.1)

t_w winter period (Fig. 3.1)

w_f final moisture content

w_i initial moisture content

References

Abdalla, B., Fan, C., Mckinnon, C., Gaffard, V., Audibert-Hayet, A., Coche, E., and Eltaher, A. 2014. Extended porosity rate function for frost heave. *In* Proceedings of 33rd International Conference on Ocean, Offshore and Arctic Engineering, San Francisco, California, USA, Paper No. OMAE2014-24221.

Aldaeef, A.A., and Rayhani, M.T. 2018. Impact of ground warming on pile-soil interface strength in ice-poor frozen soils. *In* Proceedings of the 71st Canadian Geotechnical Conference, GeoEdmonton, Edmonton, Alberta, Canada, 7p.

Alonso E. E., Pinyol, N.M., and Gens, A. 2013. Compacted soil behaviour: initial state, structure and constitutive modelling. Geotechnique, **63**(6): 463–478.

C-CORE 2004. Review of centrifuge testing applicability to frost heave. Report No. R-03-094-285 v3.0, St. John's, Canada. available at https://doi.org/10.4095/220958

Carlson, L.E., Ellwood, J.R., Nixon, J.F., and Slusarchuk, W.A. 1982. Field test results of operating a chilled, buried pipeline in unfrozen ground. *In* Proceedings of 4th Canadian Permafrost Conference, Calgary, Alberta, Canada, pp. 475–480.

Chamberlain, E. 1981. Frost susceptibility of soil, review of index tests, CRREL Monogr. 81-2. Hanover, NH, USA: US Army Corps of Engineers.

Chamberlain, E.J., and Gow, A.J. 1979. Effect of freezing and thawing on the permeability and structure of soils. Engineering Geology, **13(**1–4): 73–92.

Clark, J.I., and Phillips, R. 2003. Centrifuge modelling of frost heave of arctic gas pipelines. *In* Proceedings of the 8th International Permafrost Conference, Zurich, Switzerland, pp. 21–24.

Colt-KBR. 2003. Conceptual geotechnical/geothermal design basis. In conceptual and preliminary engineering for Mackenzie Gas Project, Report No. WP-005-D1-2, Rev. B. Calgary, Alberta, Canada.

Colt-KBR. 2006. Slope design methodology report – preliminary engineering design. In conceptual and preliminary engineering for Mackenzie Gas Project, Report No. WP52-D117-001. Calgary, Alberta, Canada.

Eigenbrod, K.D. 1996. Effects of cyclic freezing and thawing on volume changes and permeabilities of soft fine-grained soils. Canadian Geotechnical Journal, **33**(4): 529–537.

Fredlund, D.G., Rahardjo, H., and Fredlund, M.D. 2012. Unsaturated soil mechanics in engineering practice. John Wiley & Sons, Inc.

Greenslade, J.G., and Nixon, D. 2000. New design concepts for pipelines buried in permafrost. *In* Proceedings of International Pipeline Conference, Calgary, Alberta, Canada, pp. 135–144.

Han, S.J., and Goodings, D.J. 2006. Practical model of frost heave in clay. ASCE Journal of Geotechnical and Geoenvironmental Engineering, **132**(1): 92–101.

Hawlader, B., Morgan, V., and Clark, J. 2006. Modelling of pipeline under differential frost heave considering post-peak reduction of uplift resistance in frozen soil. Canadian Geotechnical Journal, **43**(3): 282–293.

Ketcham S.A., Black, P.B., and Pretto, R. 1997. Frost reave loading of constrained footing by centrifuge modeling. Journal of Geotechnical and Geoenvironmental Engineering, **123**(9): 874–880.

Konrad, J.-M. 1980. Frost heave mechanics. PhD thesis, University of Alberta, Edmonton, Alberta, Canada.

Konrad, J.-M. 1989a. Physical processes during freeze-thaw cycles in clayey silts. Cold Regions Science and Technology**, 16**(3): 291–303.

Konrad, J.-M. 1989b. Effect of freeze-thaw cycles on the freezing characteristics of a clayey silt at various overconsolidation ratios. Canadian Geotechnical Journal, **26**(2): 217–226.

Konrad, J.-M. 1994. Sixteenth Canadian Geotechnical Colloquium: frost heave in soils: concepts and engineering. Canadian Geotechnical Journal, **31(**2): 223–245.

Konrad, J.-M. 1999. Frost susceptibility related to soil index properties. Canadian Geotechnical Journal, **36**(3): 403–417.

Konrad, J.-M., and Morgenstern, N.R. 1980. A mechanistic theory of ice lens formation in fine-grained soils. Canadian Geotechnical Journal, **17**(4): 473–486.

Konrad, J.-M., and Morgenstern, N.R. 1984. Frost heave predictions of chilled pipelines buried in unfrozen soils. Canadian Geotechnical Journal, **21**(1): 100–115.

Konrad, J.-M., and Nixon, J.F. 1994. Frost heave characteristics of a clayey silt subjected to small temperature gradients. Cold Regions Science and Technology**, 22(**3): 299–310.

Konrad, J.-M., and Samson, M. 2000. Hydraulic conductivity of kaolinite-silt mixtures subjected to closed-system freezing and thaw consolidation. Canadian Geotechnical Journal, **37**(4): 857–869.

Konrad, J.-M., and Shen, M. 1996. 2-D frost action modeling using the segregation potential of soils. Cold Regions Science and Technology **24**(3): 263–278.

Lawrence, D.E., Smith, S.L., and Burgess, M.M. 2005. Frost heave and northern pipelines: state of the art and status of research – three contributing studies, Geological Survey of Canada, Ottawa, Canada. doi:10.4095/220958.

Krantz, W.B., and Adams, K.E. 1996. Application of a fully predictive model for secondary frost heave. Arctic and Alpine Research, **28**(3): 284–293.

Michalowski, R.L., and Zhu, M. 2006. Frost heave modelling using porosity rate function. International Journal for Numerical and Analytical Methods in Geomechanics, **30**(8): 703–722.

Morgan, V., Clark, J., Hawlader, B., and Zhou, J. 2004. Prediction of long-term frost heave of chilled gas pipelines by centrifuge modeling. *In* Proceedings of 5th International Pipeline Conference, Calgary, Alberta, Canada, pp. 2429–2435.

Morgan, V., Hawlader, B., and Zhou, J. 2006. Mitigation of frost heave of chilled gas pipelines using temperature cycling. *In* Proceedings of 6th International Pipeline Conference, Calgary, Alberta, Canada, pp. 927–931.

Nixon, J.F. 1991. Discrete ice lens theory for frost heave in soils. Canadian Geotechnical Journal, **28**(6): 843–859.

Nixon, J.F. 1994. Role of heave pressure dependency and soil creep stress analysis for pipeline frost heave. *In* Proceedings of 7th International Cold Regions Specialty Conference, Edmonton, Alberta, pp. 397–412.

Nixon, J.F., and Burgess, M. 1999. Norman Wells pipeline settlement and uplift movements. Canadian Geotechnical Journal, **36**(1): 119–135.

Nixon, J.F., and MacInnes, K.L. 1996. Application of pipe temperature simulator for Norman Wells oil pipeline. Canadian Geotechnical Journal, **33**(1): 140–149.

Nixon, J.F., and Morgenstern, N.R. 1973. The residual stress in thawing soils. Canadian Geotechnical Journal, **10**(4): 571–580.

Nixon, J.F., Sortland, K.A., and James, D.A. 1990. Geotechnical aspects of northern gas pipeline design. *In* Proceedings of the Fifth Canadian Permafrost Conference, Quebec, Canada, pp. 299–307.

Nixon, J.F., and Vebo, A.L. 2005. Discussion of "Frost heave and pipeline upheaval buckling". Canadian Geotechnical Journal, **42**(1): 321–322.

Oswell, J.M. 2011. Pipelines in permafrost: geotechnical issues and lessons. Canadian Geotechnical Journal, **48**(9): 1412–1431.

Palmer, A.C., and Williams, P.J. 2003. Frost heave and pipeline upheaval buckling. Canadian Geotechnical Journal, **40**(5): 1033–1038.

Phillips, R., Clarke, J.I., and Hanke, R. 2001. Centrifuge Modelling of Pipeline Frost Heave. *In* Proceedings of 54th Canadian Geotechnical Conference, Calgary, Canada, 8p.

Phillips, R., Clarke, J.I., and Hanke, R. 2002. Pipeline frost heave modelling. *In* Proceedings of International Conference on Physical Modelling in Geotechnics, St. John's, NL, Canada, pp. 313–318.

Piercey, G., Volkov, N., Phillips, R., and Zakeri, A. 2011. Assessment of frost heave modelling of cold gas pipelines. *In* Proceedings of 2011 Pan-Am Geotechnical Conference, Toronto, Ontario, Canada, 8p.

Razaqpur, A.G., and Wang, D. 1996. Frost-induced deformations and stresses in pipelines. International Journal of Pressure Vessels and Piping, **69**(2): 105–118.

Seligman, B.J. 2000. Long-term variability of pipeline–permafrost interactions in north-west Siberia. Permafrost and Periglacial Processes, **11(**1): 5–22.

Selvadurai, A.P.S., Hu, J., and Konuk, I. 1999. Computational modelling of frost heave induced soil–pipeline interaction: II. modelling of experiments at the Caen test facility. Cold Regions Science and Technology, **29**(3): 229–257.

Yang, D., and Goodings, D.J. 1998. Climatic soil freezing modeled in centrifuge. Journal of Geotechnical and Geoenvironmental Engineering, **124(**12): 1186–1194.

Yu, F., Guo, P., Lai, Y., and Stolle, D. (2019). Frost heave and thaw consolidation modelling. Part 1: A water flux function for frost heaving. Canadian Geotechnical Journal. doi:10.1139/cgj-2019-0218.

Yu, F., Guo, P., Lai, Y., and Stolle, D. (2020). Frost heave and thaw consolidation modelling. Part 2: One-dimensional thermohydromechanical (THM) framework. Canadian Geotechnical Journal. doi:10.1139/cgj-2019-0306.

Yuanlin, Z., and Carbee, D.L. 1984. Creep behavior of frozen silt under constant uniaxial stress. J. Glaciology Geocryology, **6**(1): 33–48.

Zhou, Y., and Zhou, G. 2012. Intermittent freezing mode to reduce frost heave in freezing soils — experiments and mechanism analysis. Canadian Geotechnical Journal, **49**(6): 686–693.

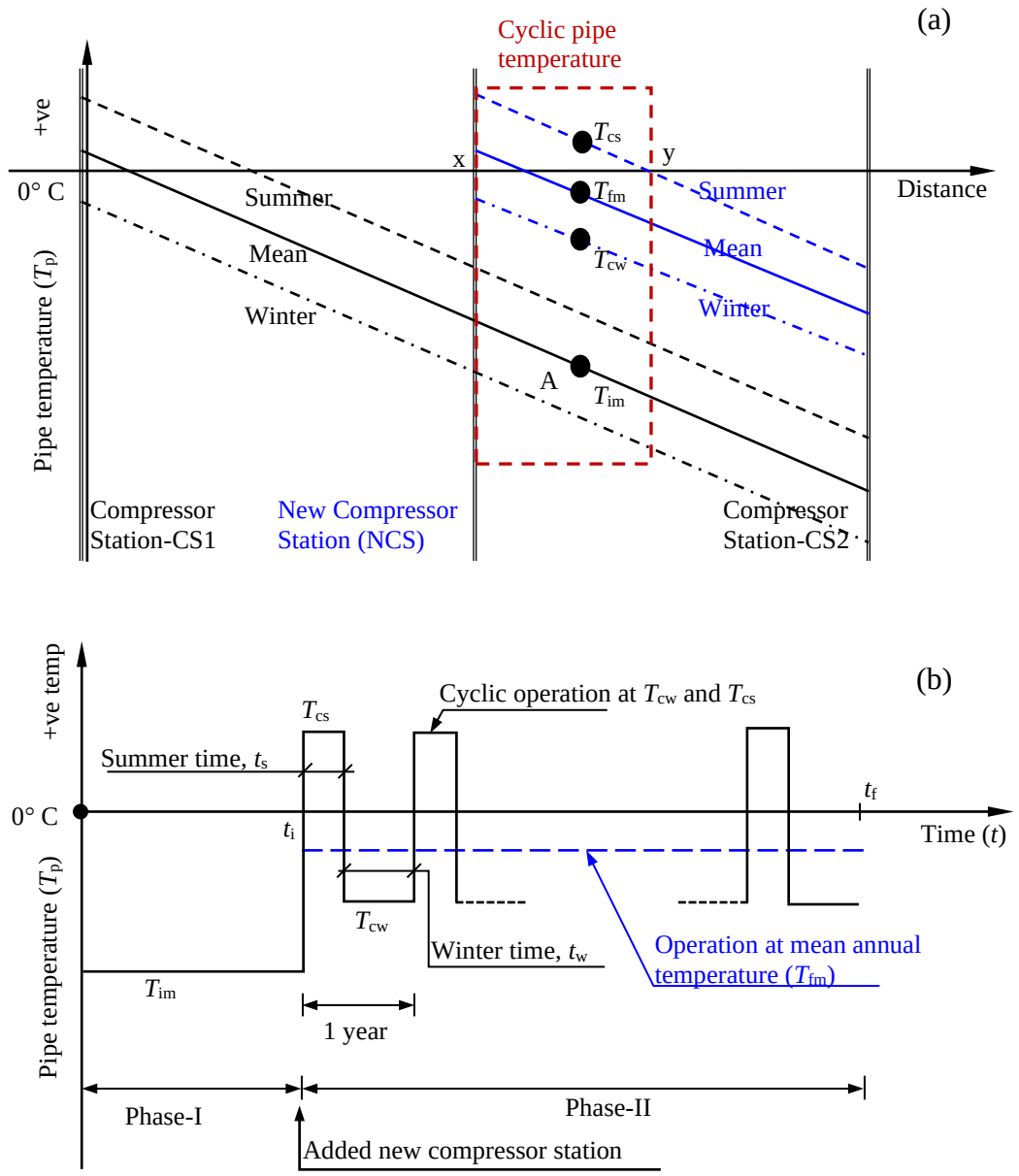

Fig. 3.1. Variation of pipe temperature between compressor stations: (a) in pipeline; (b) at point A

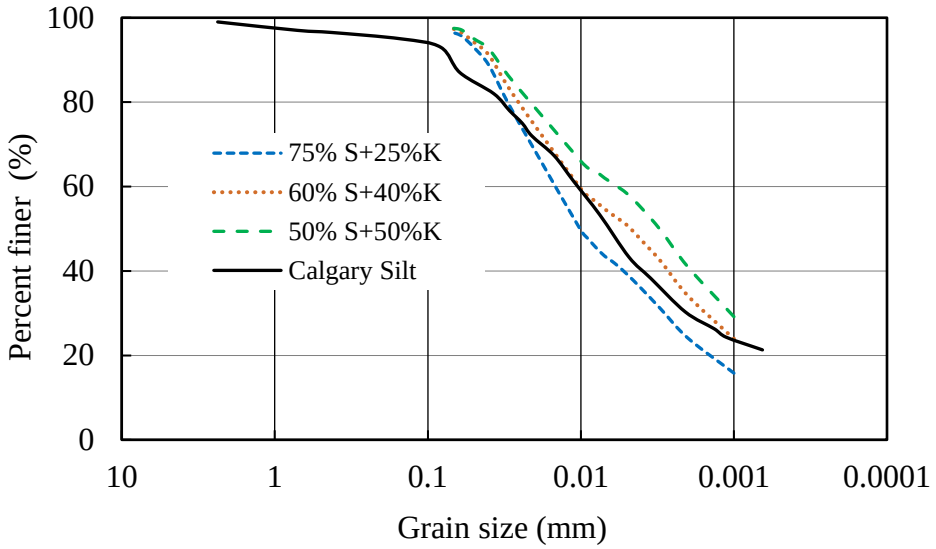

Fig. 3.2. Particle size distribution of materials

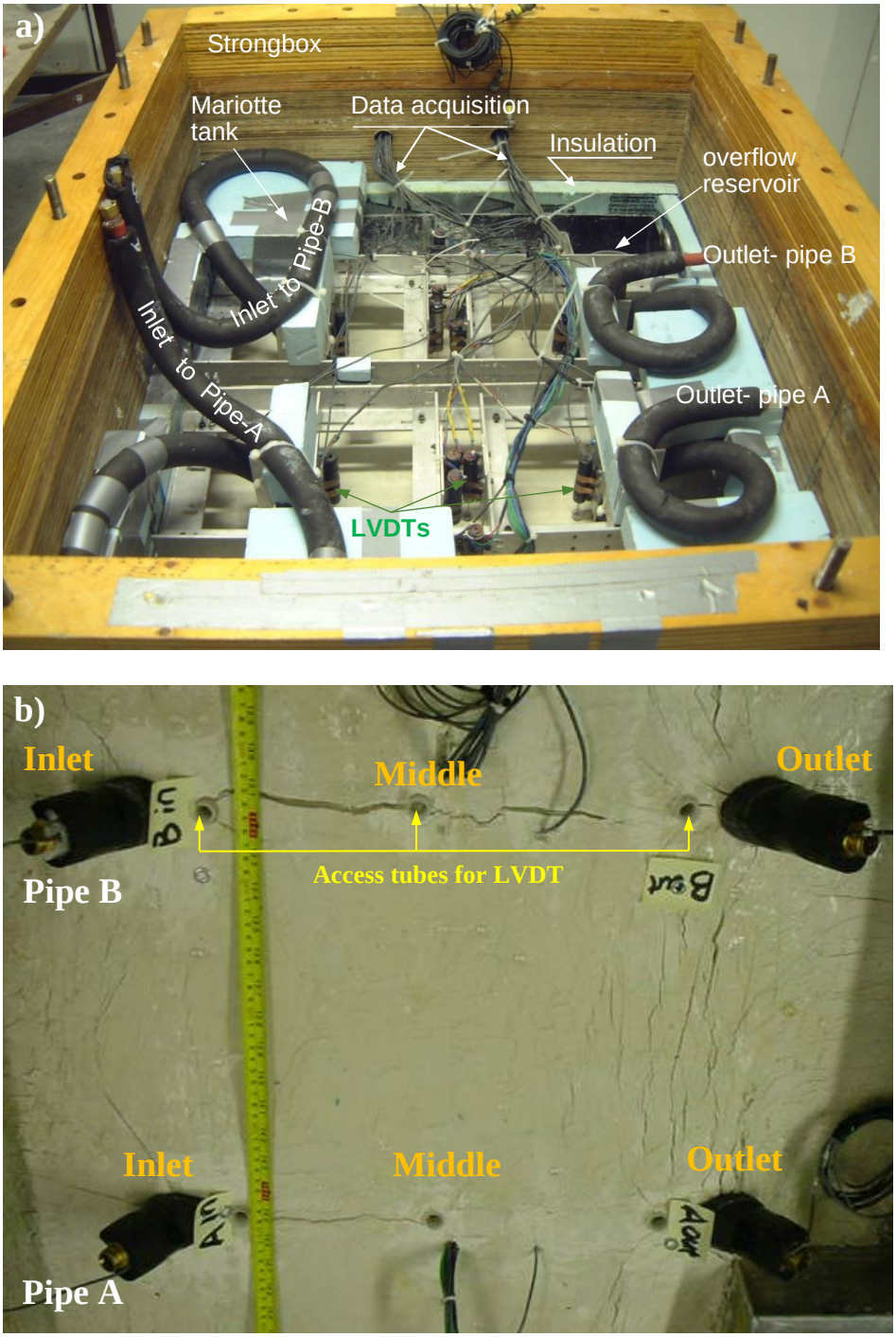

Fig. 3.3. Centrifuge model: (a) typical test package set-up; (b) top view of test CF2 after completion of centrifuge test

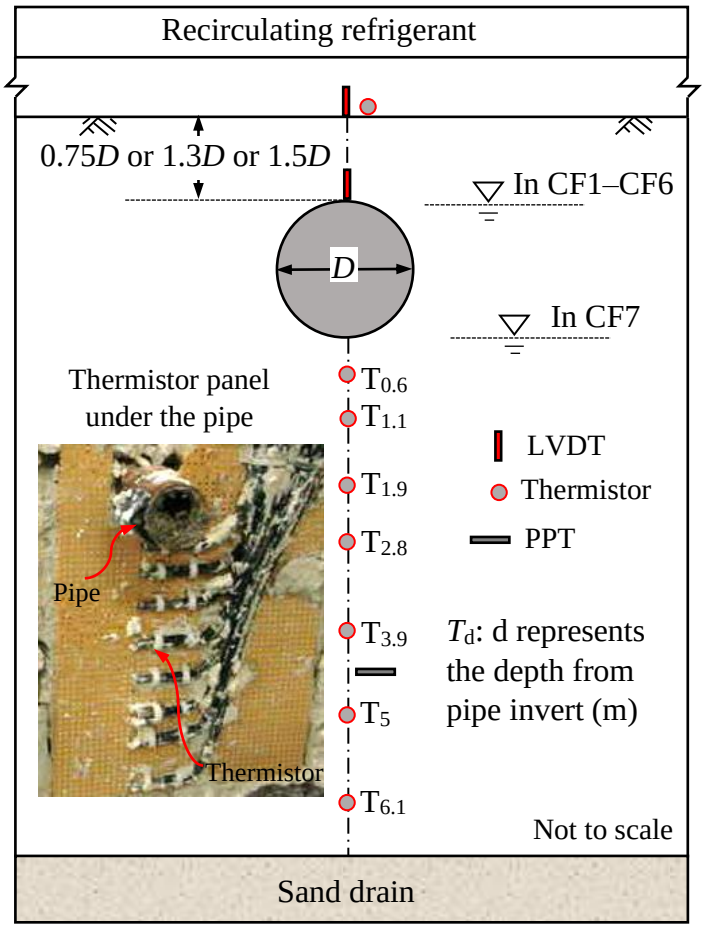

Fig. 3.4. Typical instrument setup

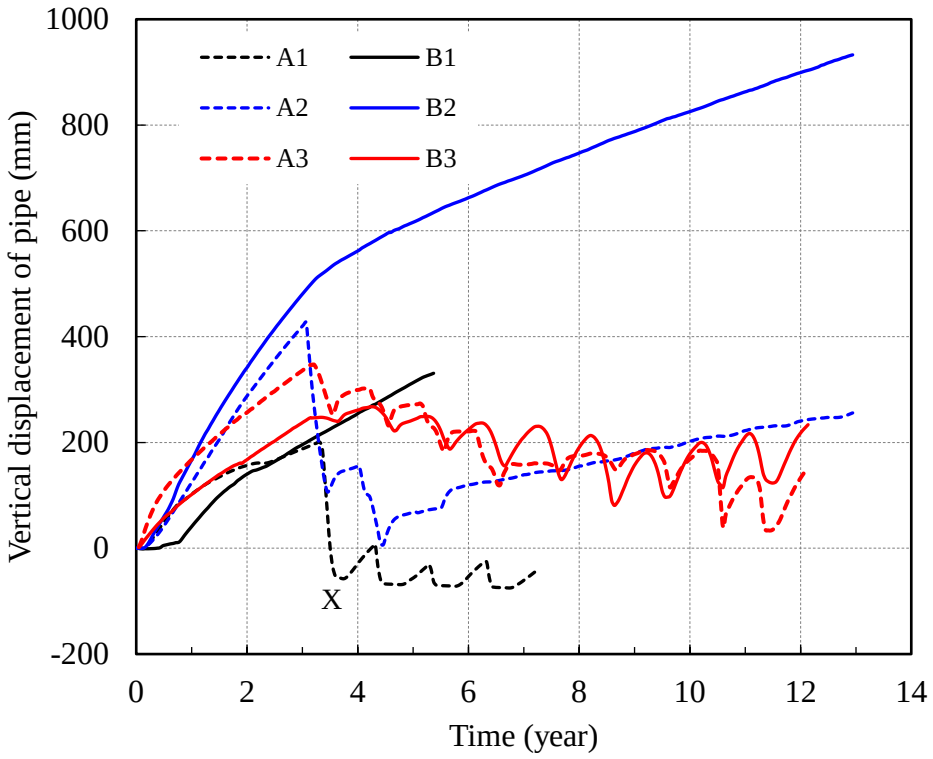

Fig. 3.5. Vertical displacements of pipe for case-1 tests

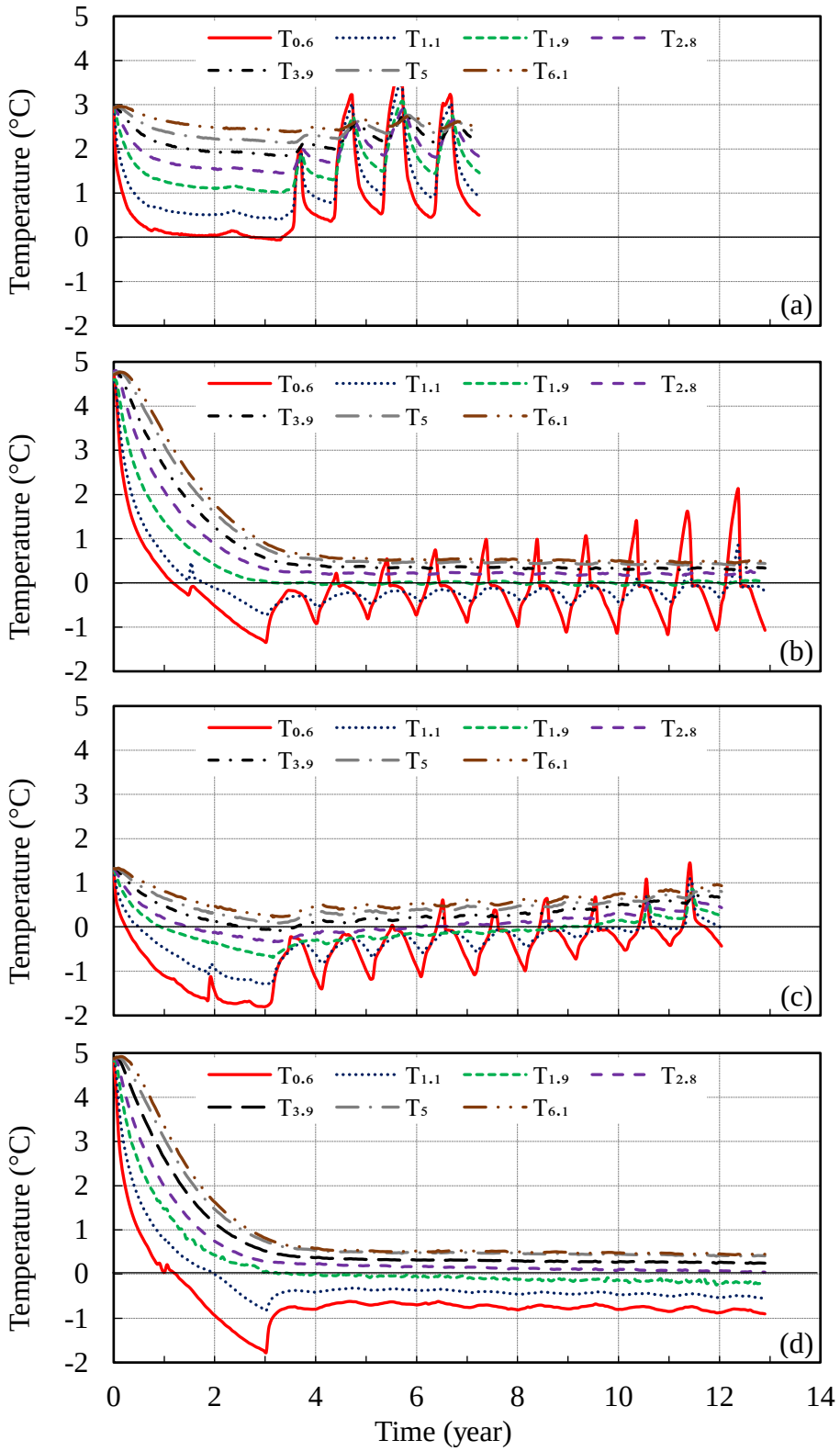

Fig. 3.6. Soil temperature below the pipe: (a) pipe A1; (b) pipe A2; (c) pipe A3; (d) pipe B2

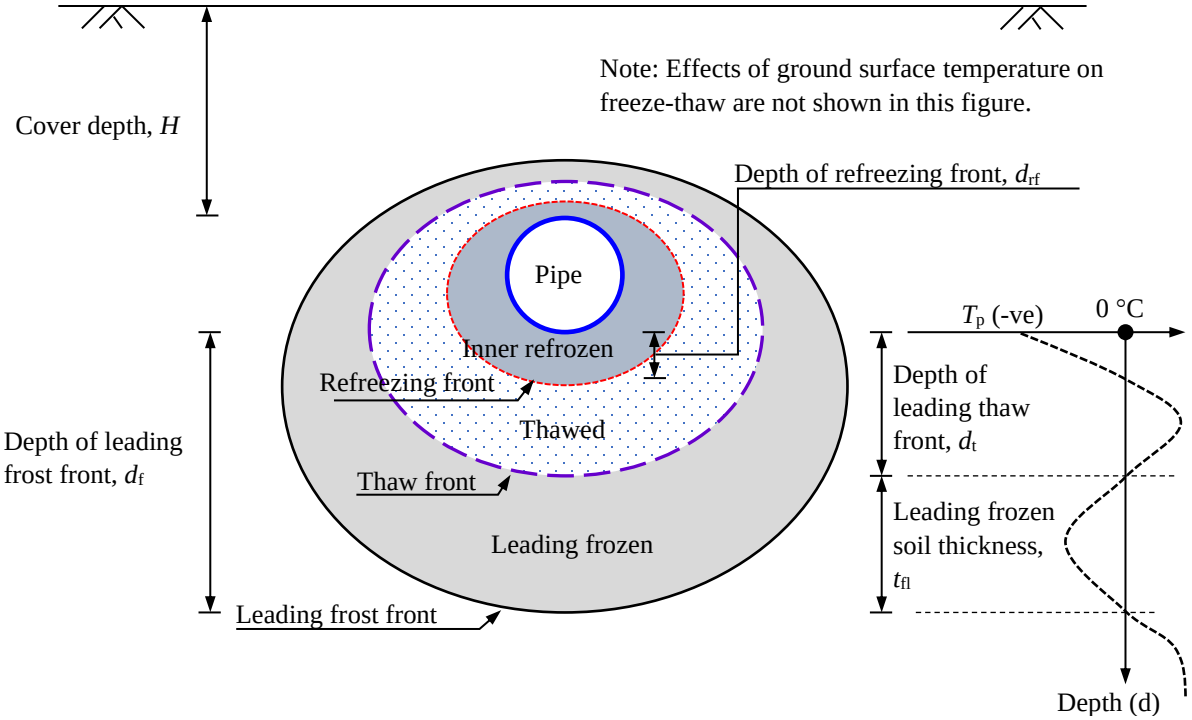

Fig. 3.7. Development of seasonal thaw and frost bulb

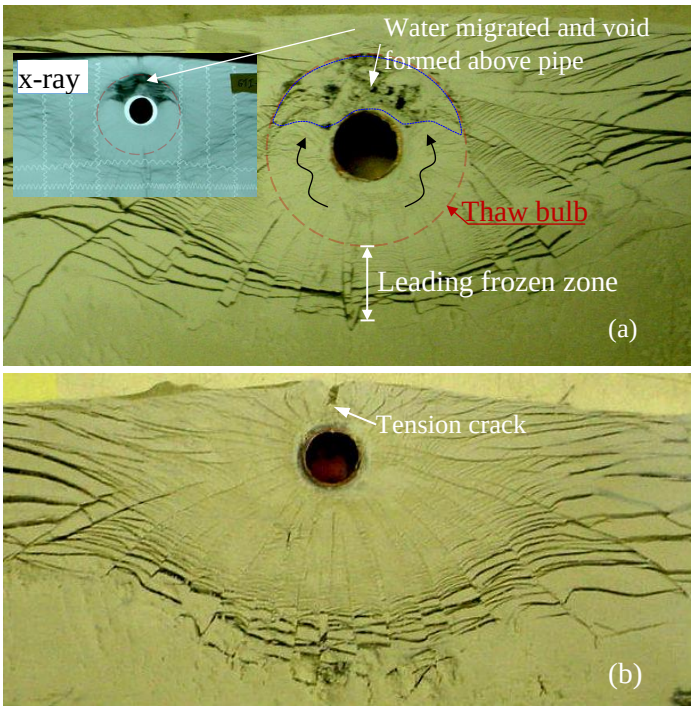

Fig. 3.8. Cross-sectional views of test CF2: (a) pipe A2; (b) pipe B2

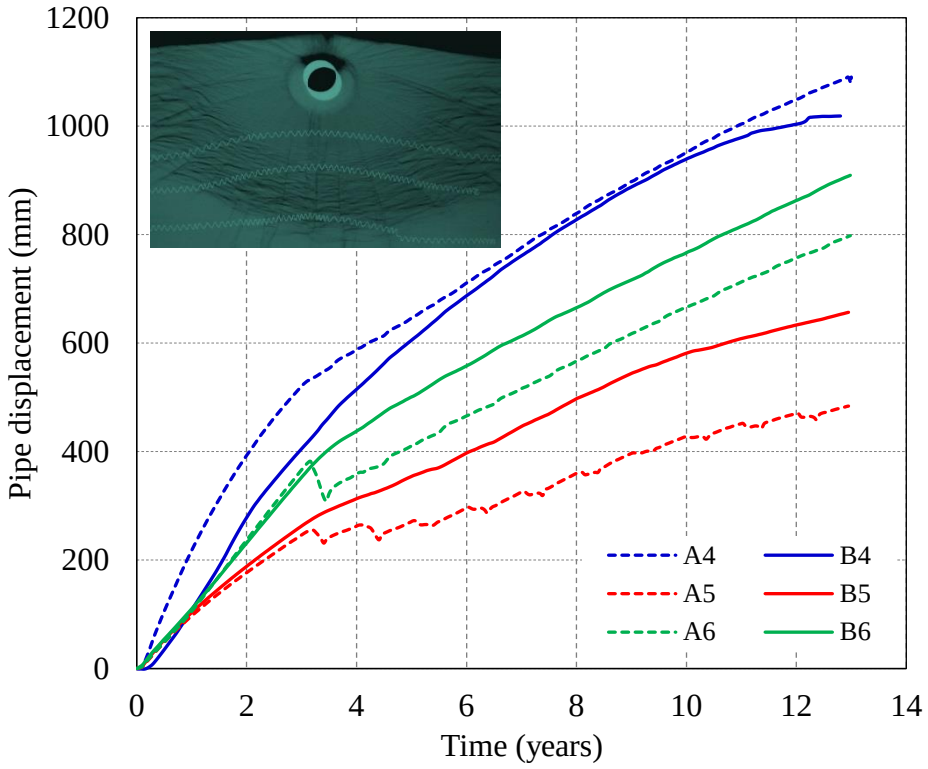

Fig. 3.9. Vertical displacements of pipe for case-2 tests

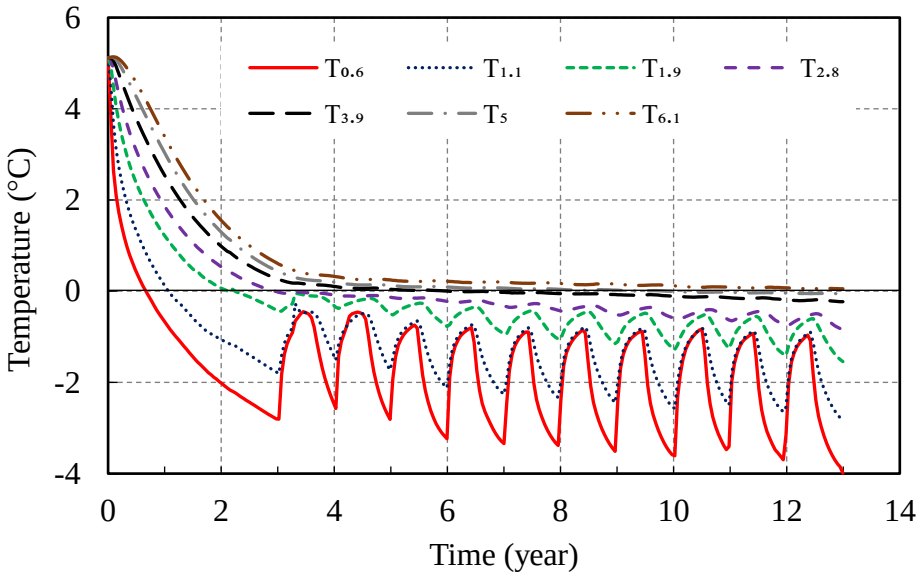

Fig. 3.10. Soil temperature below pipe A4

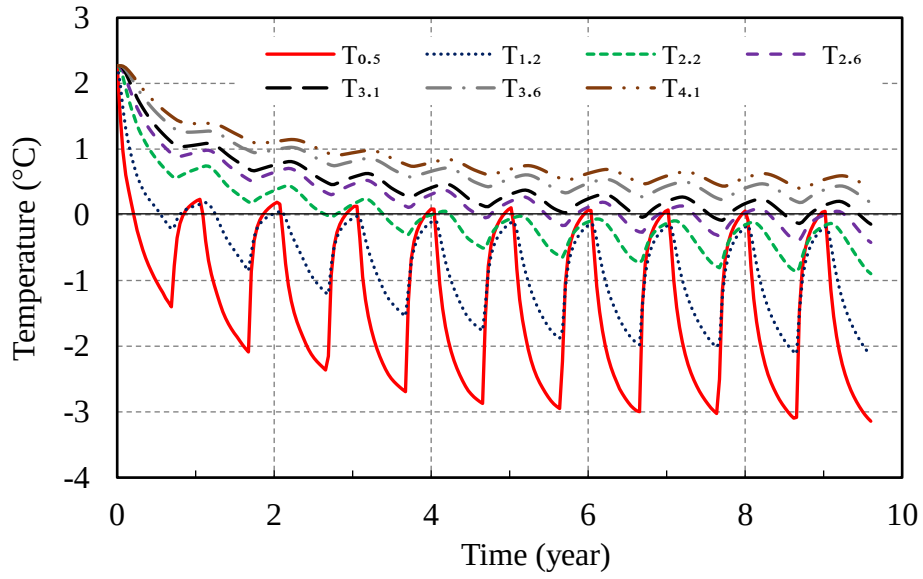

Fig. 3.11. Soil temperature below pipe A7

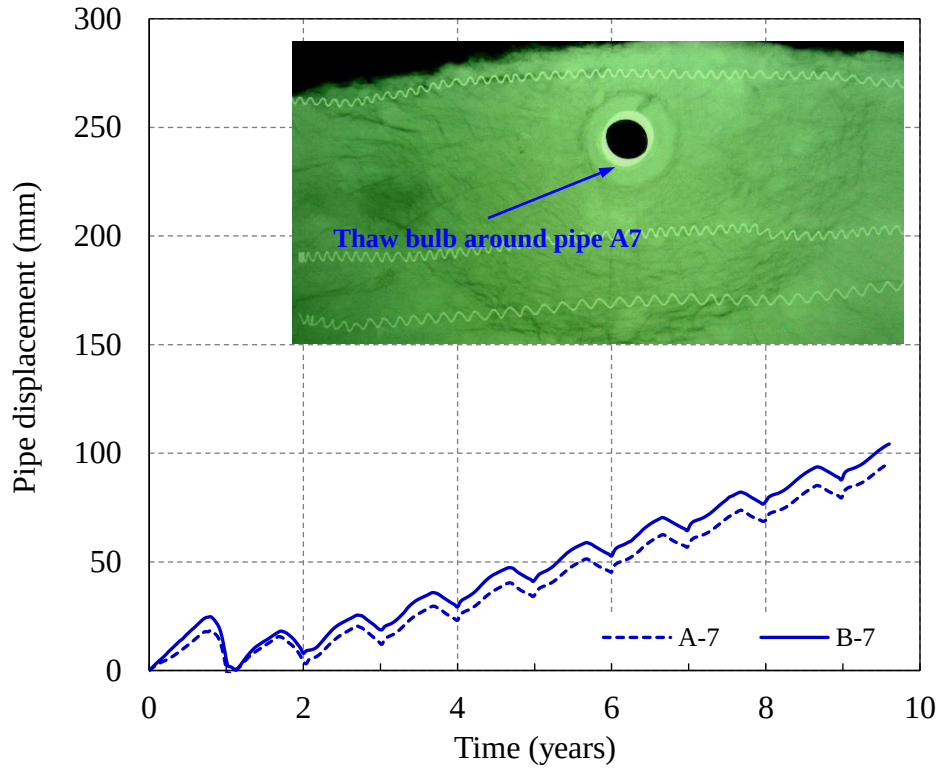

Fig. 3.12. Vertical displacements of pipe for case-3 tests

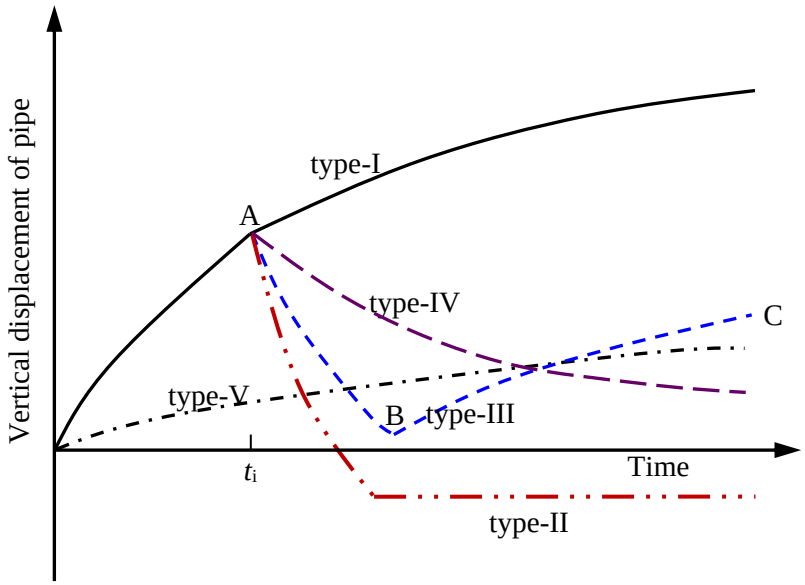

Fig. 3.13. Summary of pipe displacement responses

Table 3.1. Soil bed and model pipes used in centrifuge modelling

Test #	Soil type	Initial moisture content (%)	Soil preparation method	Model pipe diameter (mm)
CF1	50S + 50K	20	Wet compaction	22.2
CF2	75S + 25K	23	Slurry mixing	22.2
CF3	75S + 25K	16.5	Wet compaction	22.2
CF4	75S + 25K	22	Slurry mixing	22.2
CF5	75S + 25K	20	Wet compaction	22.2
CF6	60S + 40K	30	Slurry mixing	22.2
CF7	Calgary silt	18.8	Slurry mixing	15.9

S: Sil-Co-Sil silt; K: Speswhite China kaolin

Numbers in soil type represent percentage (e.g. 60S + 40K is for 60% silt and 40% kaolin)

Table 3.2. Experimental conditions of centrifuge tests

Test #	g level	Cover depth	Initial soil temp. (°C)	Surface temp. (°C)	Pipe temp. (°C)	Phase-I duration (years)	Phase-II duration (years)
CF1	55	0.75D	+3.0	$3^{(I)}$; $3^{(II)}$	A1: $-4^{(I)}$; $+5/-5^{(II)}$ B1: $-4^{(I)}$, $-4^{(II)}$	3.3	4
CF2	55	0.75D	+4.7	$-2^{(I)}$; $+2/-2^{(II)}$	A2: $-10^{(I)}$; $+8/-9^{(II)}$ B2: $-10^{(I)}$; $-2^{(II)}$	3	10
CF3	55	0.75D 1.5 D	+1.2	$+0.5^{(I)}$; $+5.5/-2^{(II)}$	A3: $-6^{(I)}$; $+6/-5^{(II)}$ B3: $-5^{(I)}$; $+7/-4^{(II)}$	3.1	9
CF4	55	0.75D	+5.0	$-2^{(I)}$; $+2/-2^{(II)}$	A4: $-10.5^{(I)}$; $+1/-10^{(II)}$ B4: $-7^{(I)}$; $-5.5^{(II)}$	3	10
CF5	55	0.75D	+1.0	$0^{(I)}$; $0.5/-6^{(II)}$	A5: $-9^{(I)}$; $+5/-10^{(II)}$ B5: $-9^{(I)}$; $-4^{(II)}$	3	10
CF6	55	0.75D	+0.5	$0^{(I)}$; $+2/-2^{(II)}$	A6: $-10^{(I)}$; $+5/-10^{(II)}$ B6: $-10^{(I)}$; $-4^{(II)}$	3	10
CF7	47.9	1.3D	+2.3	$1.5^{(I)}$; $1.5^{(II)}$	A7: -10/+2 B7: -10/+2*	0.67	9

I: phase-I; II: phase-II; *without thermistor panel; Phase I and II durations are in prototype scale

CHAPTER 4:

Two-Dimensional Finite Element Modelling of Long-Term Frost Heave Beneath Chilled Gas Pipelines

Co-Authorship: This chapter has been submitted as a technical paper for publication in a journal as: Dayarathne, R., Hawlader, B., Phillips, R., and Robert, D. “Two-dimensional finite element modelling of long-term frost heave beneath chilled gas pipelines.” Most of the research presented in this chapter has been conducted by the first author. He also prepared the draft manuscript. The other authors mainly supervised the research and reviewed the manuscript.

4.1 Abstract

Two-dimensional finite element (FE) modeling of frost heave under chilled gas pipelines buried in frost susceptible soil is presented. The Konrad–Morgenstern segregation potential (SP) model is implemented in a commercially available software using user subroutines. Simplified elastic-plastic models that recognize the key influencing factors, including temperature and volumetric ice fraction of frozen soil, are used for modeling the mechanical behaviour of soil. The present numerical approach can properly calculate the temperature gradient in the frozen fringe, which is essential in the SP model to define the volumetric expansion due to water migration to the frozen fringe. The FE calculated heave and frost front penetration are compared with the Calgary full-scale test results. The moisture content profiles obtained from FE simulation show a similar pattern as reported from a full-scale test. The challenges in modeling long-term heave resulting from continued ice accumulation in front of the final ice lens and potential warming of the leading part of the frozen bulb when the pipe moves further up are discussed.

4.2 Introduction

One of the design philosophies of buried gas pipelines in cold regions is to chill the gas to prevent excessive thermal degradation of permafrost. However, when the pipeline passes through discontinuous permafrost, freezing of frost susceptible soil in the unfrozen segment could cause heave. The differential movement between the relatively restrained frozen segment and the heaving unfrozen segment could create unacceptable strains in the pipeline. For structural analysis, the free-field heave, far from the frozen-unfrozen interface, is required (Rajani and Morgenstern 1994; Selvadurai et al. 1999; Hawlader et al. 2006), which is the focus of the present study.

One-dimensional laboratory frost heave tests were conducted for varying conditions, and mathematical models were developed based on the test results (e.g., Miller 1978; Konrad and Morgenstern 1980, 1981; Michalowski 1993). A limited number of full-scale tests were conducted in the past, which include the Calgary full-scale test (Slusarchuck et al. 1978; Carlson et al. 1982; Carlson and Nixon 1988), Canada-France pipeline experiment (Dallimore 1985; Selvadurai et al. 1999), and Fairbanks full-scale experiment (Huang et al. 2004). Geotechnical centrifuge tests were also conducted, which are relatively less expensive and time-consuming than full-scale tests (Phillips et al. 2001, 2002; Morgan et al. 2004, 2006; Piercey et al. 2011;). This information allows the numerical analysis to be developed to understand the mechanisms for varying operating conditions. Although robust software packages are commercially available for thermomechanical analysis, their built-in models are not sufficient for frost heave simulation.

The available numerical programs for frost heave simulations of buried structures in frost susceptible soil considered several aspects, including the magnitude of heave (small/large), duration (long-term/seasonal freezing), extent (one- to three-dimensional), modeling approach (fully coupled/decoupled), soil constitutive model, and approaches for water migration. Guymon et al. (1984) developed a 2-D FE method assuming the soil is nondeformable, except for volumetric

expansion in the frozen fringe due to segregate ice lens formation. Shen and Ladanyi (1987, 1991) used a similar heat and moisture transport concept to Guymon et al's (1984); however, they modeled the unfrozen soil as elastic material and considered creep in frozen soil behaviour. They simulated 1-D laboratory freezing experiments (~10 mm heave in 10 days) and the first freezing period of the Canada-France pipeline experiment (~220 mm heave in 450 days). In these studies (Guymon et al. 1984; Shen and Ladanyi 1987, 1991), the modeling of moisture migration requires hydraulic conductivity, which is one of the parameters difficult to estimate, especially in the frozen fringe. Also, this approach is suitable for the problems which experience relatively small heave. Nixon (1986) decoupled the frost heave problem; the thermal component was modeled using a finite-difference computer program which was used to find the location of the frost front and the temperature gradient at the segregation freezing temperature directly below the pipe centerline. The temperature gradient was then used to calculate the heave using the segregation potential model (Konrad and Morgenstern 1980, 1981), in addition to the heave due to the freezing of in-situ water, assuming 1-D heave without explicitly modeling the mechanical behaviour of soils and the effects of the expansion of surrounding soil due to segregate ice lens formation. The finite-difference program for geothermal modeling was revised later to incorporate the effects of ice formation on thermal properties (Colt-KBR 2003). Nixon also developed a method to predict discrete ice lens location for one-dimensional frost heave (Nixon 1991) and then extended it for simulating the frost heave beneath a pipeline (Nixon 1992); the temperature gradient was calculated by modifying a quasi-static 2-D solution for heat transfer (Hwang 1977). Again, this decoupled solution also requires the hydraulic conductivity of the frozen soil. Konrad and Morgenstern (1984) modeled heat conduction below the pipeline, assuming an axisymmetric condition of radial heat flow (no boundary effect) by developing a finite-difference computer code.

The temperature gradient at the frost front obtained from this geothermal analysis was then used to calculate the water migration to the freezing front. They also assumed that the migrated and in-situ water freezes at 0 °C.

The above studies did not consider the resistance to the upward movement of the frozen bulb during heave, although they considered overburden pressure-dependent SP values. Konrad and Shen (1996) developed a 2-D FE program for coupled thermomechanical analysis of frost heave. The numerical techniques to define water migration based on the SP model and anisotropic distribution of volumetric strain resulting from the freezing of migrated water were presented. Their FE calculated results were compared with the Calgary full-scale test results, primarily for the deep burial section, for 1,500 days. Michalowski and his co-workers developed a FE modeling technique incorporating the "porosity rate function" for water migration (Michalowski 1993), where, similar to the work of Konrad and Shen (1996), the anisotropic expansion of soil elements due to water migration was modeled (Michalowski and Zhu 2006; Zhang and Michalowski 2013a, b). The simulations were performed for freezing problems of relatively shorter periods and less heave, such as the laboratory 1-D frost heave tests, and for retaining structures, footing and culverts in less frost susceptible soils. Nishimura et al. (2009) developed a coupled thermo-hydro-mechanical FE model; the mechanical behaviour of soil was modeled in the critical state framework. From the theoretical point of view, the effective stress approach provides better insight into soil behaviour; however, the selection of soil parameters is challenging, especially for evaluating effective stresses and hydraulic conductivity of partially frozen soil in the frozen fringe with ice and water in the pores. They compared the simulation results with the Calgary full-scale test results only for the first 1,000 days.

Laboratory 1-D experiments show that, after the formation of the final ice lens, continued heave could move the cooling source (cold plate) further away from this lens (Konrad 1980; Konrad and Morgenstern 1980). Therefore, warming might occur at the leading edge of the final ice lens, which could stop the frost heave and even thaw of some frozen soil below the pipe. The decoupled geothermal analyses did not consider the effects of pipe movement (e.g., Konrad and Morgenstern 1984 and Nixon 1986). The retreat of the frost front, however, was recognized in the modeling with seasonal ground surface temperature variation and indicated a reduction of the predicted heave based on 1-D modeling by an amount proportional to the frost depth reduction (Colt-KBR 2003). The effect of such warming is more significant for shallow burial depths, higher ground and pipe temperatures, and seasonal ground surface temperature variation. Therefore, a thaw module is also needed for long-term frost heave prediction in some cases.

Various factors could affect the numerical prediction of frost heave, such as the constitutive behaviour of frozen and unfrozen soil, modeling of water migration and operating conditions (e.g., pipeline, soil, and ground surface temperatures). At a relatively low ice content, frozen soil shows dilatant behaviour during shearing at a low strain rate ($\dot{\gamma}$) while it could be brittle at high $\dot{\gamma}$; however, the soil might behave as a ductile material if it has high ice content (Arenson et al. 2007). For typical ice content and strain rate in frost heave of a pipeline, the frozen soil could be modeled as a frictional material. Previous numerical studies modeled the soil as linear or bilinear elastic material (Shen and Ladanyi 1987; Coutts 1991; Konrad and Shen 1996; Michalowski and Zhu 2006), elastic-plastic material (Tiedje 2015), and critical state framework (Nishimura et al. 2009; Thomas et al. 2009; Zhang and Michalowski 2013b; Ghoreishian Amiri et al. 2016). The soil behaviour was not modeled explicitly in some cases (Guymon et al. 1984; Konrad and Morgenstern 1984; Nixon 1986). The selection of the soil model has a significant effect on frost

heave calculation because it directly controls the resistance to the upward movement of the frost bulb and SP value.

Several mathematical models have been proposed to calculate water migration to the freezing front, such as the rigid ice model (Miller 1978), segregation potential model (Konrad and Morgenstern 1980, 1981), discrete ice lens theory (Nixon 1991), and porosity rate function (Michalowski 1993). In the present study, the SP model is used because it incorporates many complex features in a simple form, as explained by Konrad and his co-workers in several studies, and has been applied in practice (e.g., Konrad and Morgenstern 1984; Colt-KBR 2003; CGS 2006).

This discussion shows that the existing coupled FE simulations are limited to the problems of relatively low heave or shorter periods, even in the modeling of chilled gas pipelines. The long-term frost heave after the formation of the final ice lens could warm some segments of the leading face of the frost bulb, which is not generally encountered in a shorter period of simulation. In the present study, 2-D coupled thermomechanical FE modeling of long-term (up to 20 years) frost heave of a chilled gas pipeline is presented. Implementation of water migration and soil constitutive models in a FE program, and challenges in modeling large heave, in the order of a meter in some cases, are discussed.

4.3 Problem Statement

A pipeline of diameter D, buried at H and operating at a negative chilled gas temperature of T_p is modeled (Fig. 4.1(a)). Here, the pipe represents a rigid thermal boundary (T_p), and the pipe–soil interaction is not simulated. The initial ground temperature at the start of the operation is T_g, which is assumed to be uniform although it is understood that it might vary with depth. A constant (positive) ground surface temperature (T_s) is used in this study; however, the effects of seasonal variation of ground surface temperature on the frost heave are discussed in chapter 5. Trench

backfilling, seasonal effects and desiccation could alter the soil properties near the ground surface. In the present study, the soil layer below the pipe center is saturated and highly frost susceptible, while the soil above it is unsaturated and non-frost susceptible. The initial groundwater table is at the level of the pipe center. The location of any point is denoted as (x_0, y_0) and (x, y) with respect to the center of the pipe at the initial position and current position after a heave of h, respectively (Fig. 4.1(a)), where the subscript 0 represents the initial condition, and y_0 and y are positive for vertically downward locations from the center. The polar coordinates (r_0, β_0) and (r, β) are also used to explain the process, where $\beta_0 = \tan^{-1}(x_0/y_0)$ and $\beta = \tan^{-1}(x/y)$ are for the initial and current positions, respectively (Fig. 4.1(a)). Segregate ice formation could lift a soil wedge upward resulting in pipeline and ground surface heave, as shown in Fig. 4.1(b), where a chilled pipe buried at 0.75D in a frost susceptible artificial soil (25% Sil-Co-Sil silt and 75% Speswhite China kaolin) was operated for 10.4 years (in prototype scale) in a geotechnical centrifuge at C-CORE (C-CORE 2005). Decoupled analyses (e.g., Konrad and Morgenstern 1984 and Nixon 1986) do not consider the resistance to the upward motion of the frozen bulb.

Heat transfer is assumed to occur only by conduction, neglecting the advection that could have a very small effect (Nixon 1975; Dumais and Konrad 2018). The vertical distance from the initial pipe invert position to the frost front (assumed to be the 0 °C isotherm) represents the depth of the frost front (Y_0). The frost front is at a distance of Y (= Y_0 + h) from the current position of the pipe invert (Fig. 4.1(a)). The frost bulb is almost concentric initially; however, it becomes non-concentric after some time, depending upon ground surface temperature and burial depth (Fig. 4.1(a)). Similarly, the isotherm of segregation freezing temperature (T_{sf}) also becomes non-concentric. Therefore, the thickness of the frozen fringe (t_{ff}) is not the same around the pipe and is higher below the pipe for a constant ground surface temperature condition.

The following assumptions are made: (i) the frost susceptible soil is fully saturated; (ii) heat transfer in soil occurs only by conduction with an isotropic equivalent thermal conductivity; (iii) soil particles are incompressible and do not expand or shrink due to temperature change; (iv) the in-situ freezing temperature (i.e., the warmest temperature at which ice can exist in soil pores) (T_f) and segregation freezing temperature (i.e., the temperature at the base of the growing ice lens) (T_{sf}) are constant for a given soil although T_{sf} might vary with overburden pressure (Konrad and Morgenstern 1982); (v) ice lens forms perpendicular to the direction of heat flow.

4.4 Modelling of Frost Heave and Thawing

The segregation potential model is used to calculate the velocity of water migration to the base of the active ice lens (v_m) as (Konrad and Morgenstern 1984):

$$v_m = (SP_0 . e^{-ap_e}) grad T_{ff} \quad (4.1)$$

where $SP_0 . e^{-ap_e}$ is the current value of stress-dependent segregation potential; SP_0 is the segregation potential with zero applied pressure; gradT_{ff} is the temperature gradient at the segregation freezing temperature.

Initially, the temperature in the frozen zone continually decreases, and the frost front moves further away from the pipe. Once the final ice lens is formed, the heave occurs simply due to water migration to this active ice lens. However, continued heaving moves the chilled pipe further away from the final ice lens, which could cause warming of the front part of the final ice lens. Thaw back is more significant when the seasonal variation of ground surface temperature is considered, which could also cause refreezing of thawed and unfrozen soil. These issues are discussed further in chapter 5. In the current chapter, the warming of the ice lens occurs only due to the pipe's upward movement. However, for completeness, the numerical implementation of all these processes is discussed.

One-dimensional laboratory experiments show that warming of the final ice lens could reduce the heave rate with time and eventually cause the heave rate to become negligible or zero (Konrad 1980; Konrad and Morgenstern 1980). Nixon (1986) assumed pure ice formation below the active ice lens at this stage, and the heave rate was set equal to the rate of frost advancement into pure ice. In a two-dimensional case, the heaving might continue even though the frozen fringe directly below the pipeline reaches the condition of warming, because the water migration to soil elements in the frozen fringe at higher β (Fig. 4.1(a)) might still occur, which could push the pipe further up. If the pipe moves sufficiently far, the temperature in the frozen fringe in front of the so-called final ice lens could become positive and thaw, as discussed later.

There is no well-defined model for water migration during such warming of the final ice lens. The decoupled one-dimensional model does not explicitly consider the warming effect (Konrad and Morgenstern 1984). There is a negative temperature gradient with radial distance in the current frozen fringe even during warming which could attract some water. However, the hydraulic conductivity of the soil in the current frozen fringe and in front of it is drastically reduced for the following reasons. During the formation of the previous final ice lens, continuous or isolated ice forms in the pore space (Gilpin 1980; O'Neill and Miller 1985), which may not melt completely due to this temperature increase and may reduce the flow of water. The suction-induced effective stress increase in unfrozen soil immediately below the frozen fringe could reduce the void ratio. In other words, these processes will reduce the rate of water migration.

Various potential options were examined for thaw back and refreezing due to seasonal temperature to capture the trend observed in field tests (Colt-KBR 2003). The thaw settlement was either neglected or partly considered, and heaving restarts only when the frost bulb penetrates further from the previous maximum frost bulb extent. It will be shown later that if the warming

effect is not considered (i.e., no consideration for reduction or a stop of water migration during warming), the pipe might experience excessive heave in some cases, even after the formation of the final ice lens.

If the temperature in the thaw back zone increases sufficiently (> 0 °C), volumetric compression is expected due to thawing. As the process is generally very slow, the complete dissipation of the thaw-induced pore water pressure could be assumed. The thawing of frozen soil is a temperature-dependent process, unlike pure ice thawing at 0 °C. Experimental studies are not available on the thawing of ice lenses with the existence of a temperature gradient (potential suction) in the frozen fringe due to freezing. Therefore, in the present numerical analysis, the following two conditions are used. Firstly, no water migration occurs if the temperature change with time (dT/dt) is greater than zero in the frozen fringe (warming). Secondly, a gradual thawing of segregate ice with temperature occurs as Eq. (4.2) (Zhang 2014). Note that thaw consolidation is a time-dependent process, as discussed in chapter 6. However, coupled thermo-hydro-mechanical modeling of both freezing and thawing is a very challenging task.

$$\theta_{is} = \frac{\theta_{is\_max}}{1 + e^{k(T - T_{50})}} \tag{4.2}$$

where θ_{is} is the current volumetric fraction of segregate ice; θ_{is_max} is the maximum θ_{is} prior to the start of thawing; k is constant and defines the rate of thawing with temperature increase (higher k represents faster thawing); T_{50} represents the temperature at the highest rate of thawing. In the present study, k = 5 and T_{50} = 1 °C are used. The selection of T_{50} > 0 °C would compensate for some potential heave due to water migration, even at dT/dt > 0 in the frozen fringe. This also makes numerical implementation easier (frost heave at $T \leq 0$ °C and thaw settlement T > 0 °C) and gives a conservative estimation of thaw. Note, however, that the thawing of pore ice fraction (θ_{ip}) follows the unfrozen water content function used during freezing, as described below, although pore ice

thawing generally follows a steeper curve around 0 °C than that of freezing (Patterson and Smith 1981; Oliphant et al. 1983; Zhu 2006).

4.5 Finite Element Modelling

Abaqus/Standard FE software (Abaqus 2014) is used for numerical analysis. The simulations are performed for the geometry of the control and deep burial sections of the Calgary full-scale test. Figure 4.2 shows the FE mesh. Taking the advantages of symmetry, only the right half of the problem is modeled. A 1.22-m-diameter pipe buried at either H = 2.3 m or H = 1.4 m for the deep burial and control sections, respectively, are modeled. Further details of these tests are available in previous studies (Slusarchuck et al. 1978; Carlson et al. 1982; Carlson and Nixon 1988). A finer mesh is used close to the pipe (see the inset of Fig. 4.2) where frost front penetration and segregate ice lens formation are expected. The right and bottom boundaries are placed sufficiently far from the pipe to avoid boundary effects. Zero heat flux is applied at the vertical and bottom boundaries. All the vertical faces are restrained for horizontal displacement while the bottom boundary is restrained for both horizontal and vertical displacements.

The soil domain is discretized using the 4-node bilinear coupled temperature-displacement plane strain elements (CPE4T in the software). The pipe is modeled as a rigid body by defining the nodes along the outer periphery of the pipe as tie-type nodes, with a reference point at the pipe center. Modeling of the pipe by tie nodes saves computational costs and does not require the definition of pipe–soil interface behaviour. The pipe is allowed to displace vertically without rotation. The vertical displacement of the reference point represents the frost heave. The thermal conductivity of the pipe material is considerably higher than that of the surrounding soils; therefore, the chilled gas temperature is directly applied to this pipe node-set.

4.5.1 Temperature boundary conditions

Analyses are performed for the initial ground temperature T_g of +5 °C. The pipe temperature (T_p) is decreased, first instantly from +5 °C to -3.2 °C, and then linearly from -3.2 °C to -8.5 °C during the first 50 days, to simulate the Calgary full-scale test operating conditions (Konrad and Morgenstern 1984; Konrad and Shen 1996). After that period, T_p remains constant. Analyzes are also performed for an instant reduction of pipe temperature from +5 °C to -8.5 °C and a linear decrease of T_p from +5 °C to -8.5 °C over 50 days; however, no significant change in overall response is found, except for a slight change in heave and frost front penetration rate, only for an initial period.

The ground surface temperature can be estimated using the *n*-factor approach (Goodrich and Gold 1981; Andersland and Ladanyi 2004), although the surface energy balance method can be used for a rigorous analysis (Colt-KBR 2003). The *n*-factor depends on several parameters such as vegetation, topography, snow cover and soil thermal properties, which vary significantly along the pipeline route. Using the *n*-factor approach, the annual mean ground surface temperature is approximated as +5 °C, based on the mean monthly air temperatures reported by Environment Canada for five years (1974–1979) at the Calgary International Airport, which is in close proximity to the Calgary full-scale test site. A detailed parametric study of these factors (e.g., T_s, T_p, and T_g) is presented in chapter 5.

4.6 Numerical Implementation

Two-dimensional FE analyses in plane strain conditions are performed using Abaqus/Standard FE software (Abaqus 2014). The software has other FE modeling techniques to handle large deformations, such as Lagrangian-based explicit and Coupled Eulerian-Lagrangian (CEL) approaches; however, they do not support the subroutine “UEXPAN” that can be used to

model thermal volumetric expansion, which occurs due to freezing of the in-situ and migrated water. The software also does not have any built-in model to simulate frost heave. Therefore, the user subroutines SDVINI, UMATHT, USDFLD and UEXPAN are developed using Fortran computer code to implement the segregation potential model and to incorporate the solution-dependent thermal and mechanical behaviour. These subroutines interact with each other through the main program to transfer the variables (see Fig. 4.3).

The FE simulations involve two steps. In the first step, the following initial conditions are given: (i) in-situ stress through geostatic loading, (ii) initial ground temperature (T_g), and (iii) initial values of the solution-dependent variables (e.g., porosity (n), moisture content (w), cohesion of unfrozen soil (c_{un}) and angle of internal friction of unfrozen soil (ϕ_{un})), using the user subroutine SDVINI. The porosity is used to calculate the volumetric fractions of soil components. The second step represents the thermo-mechanical analysis when chilled gas transmission starts. The ground surface temperature (T_s) is also applied in this step. The SP model and solution-dependent mechanical and thermal properties are given using the following subroutines.

In the subroutine UMATHT, the current value of the volumetric fractions of the soil particles (θ_s), unfrozen water (θ_w) and ice ($\theta_i = \theta_{is} + \theta_{ip}$) are calculated, and then used to calculate the equivalent thermal conductivity (λ_e) (Côté and Konrad 2005) and the apparent volumetric heat capacity (C_a) (Nixon 1983; Colt-KBR 2003):

$$\lambda_e = \lambda_s^{\theta_s} \lambda_w^{\theta_w} \lambda_i^{\theta_i} \tag{4.3}$$

$$C_a = \theta_s \rho_s c_s + \theta_w \rho_w c_w + \theta_i \rho_i c_i + Lw\rho_d(\partial Wu/\partial T) \tag{4.4}$$

where λ, ρ and c represent the thermal conductivity, density, and specific heat, respectively; the subscript s, w and i are used for soil particles, water, and ice, respectively; L is the latent heat of water, ρ_d is the dry density of soil, and W_u represents the fraction of total water that remains

unfrozen (i.e., W_u=w_u/w_0), where w_u and w_0 are the current unfrozen and initial soil water contents, respectively (Nixon 1983). Note that no ice fraction is involved in the calculation of unfrozen soil thermal properties (i.e., θ_i = 0 and $\partial W_u/\partial T = 0$). Based on the calculated thermal properties, thermal energy balance calculations are performed. The heat flux of the soil elements in the frozen fringe in the horizontal and vertical directions (q_x and q_y) are called which are used to calculate the temperature gradients dT/dx = q_x/λ_e and dT/dy = q_y/λ_e, and then the temperature gradient parallel to heat flow direction.

$$\text{grad}T_{ff} = \sqrt{(dT/dx)^2+(dT/dy)^2} \tag{4.5}$$

The direction of heat flow (φ) is calculated as $\varphi = \tan^{-1}(q_x/q_y)$ (see point B in Fig. 4.1(a)).

The volumetric strain increments of soil elements due to freezing of in-situ ($d\varepsilon^i$) and migrated ($d\varepsilon^m$) water are calculated in the subroutines USDFLD and UEXPAN. The following unfrozen water content function proposed by Nixon (1983) is used for the freezing of pore water.

$$W_u = (P + e^{(QT+R)})/100 \tag{4.6}$$

where T is the temperature in °C and P is the percentage of the total water content that remains unfrozen well below the in-situ freezing temperature; P is 0 for coarse-grained soils and could be up to 25% for fine-grained soils (Nixon 1983); the constant Q controls the rate of unfrozen water content decrease with negative temperature, which is a function of particle size (e.g., 0.16–6 for fine-grained soils (Nixon 1983, 1986; Zhu 2006)); R is related to P as $R = ln(100 - P)$. The change in w_u in each time increment (Δw_u) is calculated based on temperature, which is used to calculate the volumetric strain due to pore water freezing.

$$d\varepsilon^i = 0.09\theta_w\ (\Delta w_u/w_u) \tag{4.7}$$

To calculate the volumetric strain increment due to migrated water ($d\varepsilon^m$), the effective overburden pressure at the integration point is obtained, which is used for p_e in Eq. (4.1) to

calculate the velocity of migrated water (v_m). Multiplying v_m by the equivalent area perpendicular to the direction of heat flow (A_e) and time increment (Δt), the amount of water moved to elements in the frozen fringe (ΔQ_w) is calculated. Considering unit thickness perpendicular to the plane strain section, A_e can be calculated as ~ l_c.1, where l_c is the characteristic length of the finite element. The volumetric strain increment due to the freezing of this migrated water ($d\varepsilon^m$) is $(\rho_w/\rho_i)(\Delta Q_w/V_e)$, where V_e is the volume of the freezing element (V_e ~l_c^2.1). Theoretically, this strain increment should occur in front of the active ice lens (T_{sf}). However, for numerical implementation, the elements in the frozen fringe are given a strain increment ($d\varepsilon^{m\_e}$) of $d\varepsilon^m l_c/t_{ff}^*$, where t_{ff}^* is the approximate thickness of frozen fringe estimated from gradT_{ff} of that element (Eq. (4.5)) as: $(T_f - T_{sf})/gradT_{ff}$. In this way, the volumetric strain due to water migration is distributed in all the soil elements in the frozen fringe instead of lumping at a discrete temperature, which could create numerical issues.

In 1-D frost cell tests, the segregate ice lens displaces the soil only in the axial direction (Konrad 1980, 1994). In the present 2-D simulations, it is assumed that the ice lens orientation is aligned with the frost front. Note that ice lenses primarily aligned along the horizontal directions were observed in the post-test excavation of a section of the Calgary full-scale tests (Carlson and Nixon 1988), which is potentially due to local soil stratigraphy. The segregated ice generates anisotropic strains. Therefore, $d\varepsilon^{m\_e}$ of each element in the frozen fringe is distributed in the direction parallel ($d\varepsilon_1^{m\_e}$) and perpendicular ($d\varepsilon_2^{m\_e}$) to the heat flow direction (Fig. 4.1) as $d\varepsilon_1^{m\_e} = [\xi + 0.5\mu(1-\xi)]d\varepsilon^{m\_e}$ and $d\varepsilon_2^{m\_e} = 0.5(1+\mu)(1-\xi)d\varepsilon^{m\_e}$ (a detailed derivation is available in Konrad and Shen 1996 and Michalowski and Zhu 2006). Here, μ is the Poisson's ratio and ξ is a parameter that defines anisotropic distribution (ξ = 1/3 for isotropic expansion). In the present study, ξ = 0.9 is used to ensure that the ice lenses primarily expand the soil elements

parallel to the direction of heat flow. For each element in the frozen fringe, $d\varepsilon_1^{m\_e}$ and $d\varepsilon_2^{m\_e}$ are then transformed to the strain increments in the *x*-*y* axis using the strain transformation equations with angle φ (Fig. 4.1(a)), which gives the volumetric expansion due to migrated water. For strain increments due to in-situ pore water freezing in frozen soil ($d\varepsilon_1^{i}$), ξ = 1/3 (isotropic expansion) is used.

4.7 Soil Properties

Chapter 2 presents a detailed discussion of various approaches proposed in previous studies to estimate the properties required in the present FE analysis, such as thermal properties of soils, segregation potential and unfrozen water content. A brief summary is presented below.

4.7.1 Freezing characteristics

The soil at the Calgary full-scale test site consisted of highly frost susceptible low to medium plastic clayey silt (13% sand, 64% silt and 23% clay). Freezing characteristics and index properties of this soil are available in previous works (e.g., Slusarchuck et al. 1978; Carlson et al. 1982; Konrad and Morgenstern 1984; Carlson and Nixon 1988). The input parameters used in the present FE analysis (see Table 4.1) are obtained from those studies unless otherwise mentioned. For the Calgary silts, SP_0 = 180×10^{-5}–300×10^{-5} mm^2/s°C and a is ~9.5 MPa^{-1} (Konrad and Morgenstern 1984). The thermal conductivity and specific heat of soil particles, water and ice are selected from previous studies (Johansen 1975; Farouki 1981, 1982). Depending upon ice content, the ratio between the thermal conductivity of frozen and unfrozen soil is 1.0–3.7 (Nixon and McRoberts 1973). The segregation freezing temperature (T_{sf}) of fine-grained material varies between -0.1 and -0.8 °C (Konrad and Shen 1996). However, T_{sf} = -1 °C is used in the present analysis, such that at least one finite element exists in the frozen fringe, which also reduces some numerical issues if the

volumetric strain increment is concentrated into a very small zone. The use of a slightly lower value of T_{sf} does not affect the heave in the simulations presented in this study. Note, however, that T_{sf} could influence the heave, especially for a low initial ground temperature, which is discussed further in chapter 5. The in-situ freezing temperature (T_f) of 0 °C is used and the effects of freezing point depression are neglected.

4.7.2 Stress–strain behaviour of unfrozen silt

Compared to clay and sand, silt behaviour has been less investigated, even for the unfrozen state. Depending upon fine content, a transitional response of silt between clean sand and clay has been observed (Nocilla et al. 2006). Low plastic silts are highly frost susceptible. For a comprehensive physical modeling of frost heave using a geotechnical centrifuge, artificial materials were prepared with Sil-Co-Sil silt (S) and Speswhite China kaolin (K), and it was found that 75%S + 25%K gives the particle size distribution and frost heave behaviour similar to the Calgary clayey silt (Clark and Phillips 2003). Further details of centrifuge frost heave tests are available in previous studies (Phillips et al. 2001, 2002; Morgan et al. 2004, 2006; Piercey et al. 2011) and in chapter 3.

Four consolidated drained and four consolidated undrained triaxial tests were conducted on the same soil used for centrifuge tests (75%S + 25%K), which is low-plastic clayey silt having the following properties: specific gravity = 2.65, liquid limit = 27%, plastic limit = 22%. A reconstituted soil block was prepared, first by mixing silt and kaolin with water at twice the liquid limit, and then normally consolidated on the laboratory floor. Samples were collected from the soil block using a Shelby tube, which were then used for one-dimensional consolidation and triaxial tests. In the triaxial tests, the specimens were isotropically consolidated to 100 kPa–640 kPa before shearing under drained or undrained conditions. Further details can be found in Dayarathne and

Hawlader (2015). The stress paths of the undrained and drained tests give the slope of the critical state line of ~1.2. The volumetric strain in the drained tests and pore water pressure in the undrained tests show a slightly dilative response. Similar pressure-dependent stress–strain and volume change behaviour were also observed in natural low plastic silts (Ferreira and Bica 2006; Nocilla et al. 2006; Georgiannou et al. 2018). In the present numerical study, it is assumed that the drained behaviour of unfrozen soil governs the response, because frost heave is a slow process. The unfrozen soil is modeled as a frictional material using the Mohr–Coulomb failure criterion with an angle of internal friction (ϕ_{un}) of 30° (correspond to the critical state line slope of ~1.2) together with small cohesion (c_{un}) of 10 kPa and dilation angle (ψ_{un}) of 5°. A Young's modulus (E_{un}) of 11.2 MPa and Poisson's ratio (ν_{un}) of 0.25 are used.

4.7.3 Stress–strain behaviour of frozen silt

Pore ice in frozen soil could act as a bonding (cohesive) agent and gives an apparent cohesion at zero or low confining pressures (Arenson et al. 2007). When the volumetric ice fraction (θ_i) is less than 0.6, the soil-ice mixture behaves as a frictional material, and the strength increases with confining pressure (Arenson and Springman 2005; Arenson et al. 2007). In some studies, effective stress-based models with an elliptical yield surface similar to modified Cam-clay have been used to model the frozen soil (Nishimura et al. 2009; Thomas et al. 2009; Zhang and Michalowski 2013b; Ghoreishian Amiri et al. 2016). In those studies, an evolution law is given to calculate the development of a pseudo preconsolidation pressure as a function of the soil parameters required in the Cam-clay model and other state variables (e.g., cryogenic suction and pore ice ratio), based on the unsaturated soil mechanics concept. The calculation of effective stress is a challenging task because of difficulties in the proper estimation of suction in frozen soil. Moreover, such an increase in effective stress will not result in significant volumetric strain because of the low compressibility

of frozen silt. Therefore, the frozen soil is modeled as a frictional material using the Mohr–Coulomb model in the total stress framework, as suggested by Arenson and Springman (2005).

Experimental studies show that unconfined compressive strength of frozen silt increases with a decrease in temperature (T) below 0 °C, which can be expressed as a function of $|T|^m$, where m is a soil parameter (m ~ 0.5–0.7) (Yuanlin and Carbee 1984; Li et al. 2003). The shear strength also reduces with a decrease in the shear strain rate. For example, Yuanlin and Carbee (1984) showed that the unconfined compressive strength at a strain rate of 1.1×10^{-6} /s is approximately one order smaller than that at a strain rate of 6.2×10^{-2} /s. The frost heave is generally a very slow process; the strain rate could be less than 10^{-9} to 10^{-8} /s for the cases analyzed in this study (Carlson et al. 1982; Kim 2011). Therefore, a lower range of strength parameters should be considered unless the creep effect is explicitly modeled because a higher shear strength of frozen soil gives a lower heave, as discussed in chapter 5. Arenson and Springman (2005) showed that cohesion of frozen soils ($c_{fr,}$ in terms of total stress) increases with ice content, and the rate of increase of c_{fr} is large at high ice content (e.g., θ_i > 0.6). Therefore, for a lower ice content in typical frost heave problems (less than about 60%), a linear increase in cohesion with θ_i is defined empirically as: $c_{fr}(\text{kPa}) = c_{un}(1 + 5\theta_i)\,|T|^{0.5}$ for T ≤ -1 °C.

Unlike cohesion, the friction angle of frozen soil (ϕ_{fr}) does not depend significantly on strain rate and temperature but is strongly related to ice content (Andersland and Alnouri 1970; Ladanyi 1972). Arenson and Springman (2005) also found that ϕ_{fr} decreases from the unfrozen state to zero for pure ice as $\phi_{fr} = \phi_{un}(1 - \theta_i^{2.6})$. This relationship has been used in the present study. Dilatancy could have some influence on shear strength at low ice contents (Nishimura et al. 2009). Although the dilation angle of frozen soil (ψ_{fr}) could be a function of θ_i, a constant value of ψ_{fr}=

5 ° is used. A temperature-dependent Young's modulus (E_{fr}) as $13.75|T|^{1.18}$ MPa (Ladanyi and Shen 1993) and Poisson's ratio (ν_{fr}) of 0.25 are used.

4.8 Results

4.8.1 Frost heave and frost front penetrations

Figures 4.4 and 4.5 show the comparison between FE calculated and measured frost heave (h) and depth of frost front (Y_0) for the deep burial (H = 2.3 m) and control sections (H = 1.4 m) of the Calgary full-scale tests, respectively. Heave occurs quickly during the first 3–5 years, and then the rate of heave ($\dot{h} = dh/dt$) decreases. Similarly, rapid frost penetration occurs during the first 3–5 years. The frost front continues to penetrate until 5–8 years and then remains almost constant at Y_0 = 3.1 m and Y_0 = 2.4 m for the deep burial and control sections, respectively. During the first few years, heave occurs quickly in the control section as compared to the deep burial section; for example, at t = 5 years, heave is 0.72 m and 0.58 m for the control and deep burial sections, respectively. The reduction of SP due to the increase of overburden pressure and more resistance to uplift the soil wedge (Fig. 4.1) reduces the heave in the deep burial case.

The insets of Figs. 4.4 and 4.5 show the locations of the frozen fringe at t = 5.5 years, which are different in the control and deep burial sections. At least one or more finite elements in the frozen fringe perpendicular to the frost front ensures proper calculation of volumetric expansion due to segregate ice formation. The positive ground surface temperature has more influence on the freezing process in the control section (shallow burial); therefore, less frost penetration occurs.

4.8.2 Heave at stable and retreating frost front

Figure 4.4(b) shows that the frost front penetration is negligible after 8 years. The water migration still continues at this stable frost front location at a constant rate. With further upward

movement of the pipe, warming (instead of cooling) occurs ($dT/dt > 0$) in the lower part of the frozen fringe. In the present study, the warming effect is considered by setting a zero water migration rate when $dT/dt > 0$, and incorporating thaw-induced volumetric strain (compression) due to the change in the segregate ice content ($1.09\Delta\theta_{is}$) using Eq. (4.2). A discussion of available approaches, especially on warming due to seasonal temperature variation at the ground surface, is presented above and available in Colt-KBR (2003). When the warming effect is neglected, a large long-term heave is calculated (e.g., 1.02 m versus 1.44 m after 20 years with and without warming effects). The frost front also moves up ~0.3 m during the period of 10–20 years if the warming effect is not considered, while it remains almost at the same depth otherwise. A more significant effect of warming has been found in similar analyses for the control section, because the frost front penetration stops earlier (~5 years) as the pipe is located closer to the ground surface. Significant mesh distortion occurs in this case, without the warming effect, and the calculation stops at 10 years for such a large heave. Note that the warming effect also depends on initial ground temperature, as discussed in chapter 5. In summary, a significant thaw back and a large heave might be obtained if the warming effect is not considered. Therefore, the analyses presented in the following sections are performed considering the warming effects.

The phenomenon of warming at the base of the final ice lens was observed in laboratory experiments (Konrad 1980; Konrad and Morgenstern 1980). Also, a separate mathematical function based on heat deficit was proposed to calculate the heave rate when the final ice lens forms, considering the variation of geometrical boundary conditions with time, due to the increase in the thickness of the final ice lens (Konrad and Morgenstern 1984).

The long-term heave rate also depends on burial depth. Figures 4.4 and 4.5 show that after a period of freezing, a considerable drop in heave rate occurs when some of the elements directly

below the pipeline reach warming conditions. However, water migration is still continued in the elements of large β (e.g., along AB in Fig. 4.1(a)). The effects of segregate ice formation at large β do not have much influence on pipe heave in the shallow burial case (Fig. 4.5(a)), compared to the deep burial condition (Fig. 4.4(a)), because the ground surface is relatively close to these elements, and therefore any expansion of these elements is primarily accommodated by the vertical movement of the soil elements above it, without influencing the displacement of the pipe. However, for the deep burial conditions, any expansion of soil elements along AB also influences the pipe movement because the resistance from the upper soil layer is high. Moreover, the positive ground surface temperature reduces the heave rate and increases the warming of the frozen bulb when a sufficient amount of heave brings the pipe closer to the ground surface in the shallow burial case. Finally, the volumetric expansion of the soil elements around the curved frost front (ABC in Fig. 4.1) increases the mean stress in the unfrozen soil and thereby the shearing resistance to the upward movement of the frozen bulb. Due to these factors, the long-term heave rate is considerably reduced in the control section as compared to the deep burial section. Therefore, the calculated total heave after 20 years is less in the control section than in the deep burial section. Previous coupled FE analyses did not report this phenomenon because such long-term frost heave was not modeled.

The deep burial section of the Calgary full-scale test was operated for ~12 years; however, ice blockage occurred in the duct of cold air flow which raised the operating temperature and caused significant thawing after ~7 years (Carlson and Nixon 1988). The present FE simulations are continued for 20 years. As shown in these figures, the present FE results compare well with the field test results, although the calculated heave is slightly lower and frost front penetration is slightly higher than the measured values, which is potentially due to the selection of soil

parameters, especially *SP* values and modeling of its dependency on stress, and non-uniformity of thermal and material properties in the field. Results are also comparable with other solutions available in the literature, which simulated the same test sections of Calgary full-scale test facility (Konrad and Morgenstern 1984; Hawlader et al. 2004). The semi-analytical solution of Hawlader et al. (2004) is based on 1-D heat transfer analysis and over predicts the long-term frost front penetration; therefore, the results are shown for only 5 years.

4.8.3 Temperature gradient in the frozen fringe

The prediction of heave using the SP model is very sensitive to the temperature gradient in the segregation-freezing front, gradT_{ff} (Eq. (4.1)). The freezing of migrated water, which is the main source of heave, occurs within this thin frozen fringe. Moreover, thermal and mechanical properties change around this area. Several attempts have been made to calculate the gradT_{ff} precisely. Nixon (1986) fitted the temperature in three elements located near the frost front—one on the unfrozen side and the other two on the frozen side—using a quadratic function, and the slope of this function at the segregation freezing temperature is considered as gradT_{ff}. The accuracy of this method depends on mesh density and variation of temperature within the frozen fringe, and also on the alignment of the integration points of these three elements perpendicular to the frost front. Shen and Konrad (1993) calculated gradT_{ff} by creating a temporary triangular element in the frozen side adjacent to the frost front. Searching nodes for this element would increase the computational cost, and the accuracy of the calculated gradT_{ff} depends on the mesh density close to the frost front. Nixon (1992) used a two-dimensional quasi-static method, developed by Hwang (1977), to define the nonlinear temperature variation, and calculated gradT_{ff} based on that temperature profile. Hawlader et al. (2004) developed an analytical solution to calculate the temperature gradient in the frozen fringe, which applies only to the 1-D frost heave simulation. In

the present study, the heat flux of the soil elements in the frozen fringe in the horizontal and vertical directions is obtained, and used to calculate gradT_{ff}, as discussed in the "Numerical Implementation" section.

Figure 4.6 shows the calculated temperature gradient of the soil elements with time at a radial distance of r_0 = 2.7 m from the pipe center at β_0 = 0° (vertically below pipe invert), 45° and 70° for the deep burial section. The temperature gradient increases from zero (initial uniform ground temperature) to the maximum value and then decreases with time. Very little oscillation occurs in the calculated temperature gradient due to FE discretization, which is an objective of an effective simulation technique (Shen and Konrad 1993). The decrease in temperature in these elements with time is also shown in this figure, which can be used to identify the period when the element is in the frozen fringe (symbol Δ: at T = 0 °C and ○: at T = -1 °C) and associated temperature gradient, which refers to the gradT_{ff}. The temperature gradient, including gradT_{ff}, is higher in the elements close to the pipe (less radial distance) and large β_0 (away from the vertically downward direction). At a given time after a period of freezing, gradT_{ff} is lower in the soil elements below the pipe because the frost front is further away from the pipe, as shown in the inset of Figs. 4.4 and 4.5.

Figure 4.7 shows the comparison between the FE calculated gradT_{ff} below the pipe and observed temperature gradients in the frozen fringe for the Calgary deep burial section, which were obtained from the readings of the thermistor strings placed 1 m offset to the pipe's centerline (Carlson and Nixon 1988). Note that the FE model calculates the gradT_{ff} in each element within the frozen fringe as described before, and the average value is presented in this figure. The temperature gradient decreases quickly with time after the commencement of the chilled gas operation and then slowly when the frost front penetrates further. The FE calculated gradT_{ff} is slightly lower than the interpreted values presented by Carlson and Nixon (1988) based on field

measurements, especially in t = 250–1500 days, which is a potential cause of lower calculated heave than field results, as shown in Fig. 4.4(a). However, considering the uncertainties in the selection of soil parameters (e.g., SP, and thermal and mechanical properties) and boundary conditions (e.g., T_p, T_s, T_g) this difference is not significant. Figure 4.7 also shows the calculated gradT_{ff} using Nixon's (1986) geothermal model and Hawlader et al's (2004) 1-D semi-analytical model. The former approach gives lower, while the latter one gives higher gradT_{ff} than the present FE results.

Figure 4.8 shows the calculated temperature profile with depth below the current position of the pipe invert at t = 1000 days for the deep burial section for a horizontal offset (x) of 0 (vertically below pipe invert), 1 m and 2.5 m from the pipe center. As expected, the temperature decrease is less in the soil elements far from the center. The temperature remains positive in most soil elements at 2.5-m offset. Figure 4.8 also shows the temperature observed in the field, which shows a good agreement with FE calculated results.

4.8.4 Ice growth

Carlson and Nixon (1988) reported the total moisture content (i.e., $w_t = w_u + w_i$, where w_i is the ratio between the mass of ice and dry soil) below the level of pipe invert for the deep burial section, which was obtained by excavating the test site at the end of the operation (~ 12 years). Note that there was a ~0.6 m thaw back of the frost bulb below the pipeline over a period of 3 years from 1981 (after ~7 years of operation) due to the blockage of chilled air flow in the duct. Chilled operations restarted in late 1983 and the frost bulb penetrated almost back to its same position before the thaw back. The present study does not model this thaw back and refreezing after ~7 years of operation. Instead, continuous freezing (i.e., constant pipe temperature) was maintained. Figure 4.9 shows the FE calculated moisture content after 5.5, 10 and 20 years. Carlson

and Nixon (1988) reported that ice lens growth in the field was mainly in the horizontal direction due to the local stratigraphic factors, regardless of heat flow direction. The measured moisture contents were also scattered. Figure 4.9 shows that the FE calculated moisture content for the deep burial section was within the lower bound of measured value, which could be because of the selected *SP* values, other soil properties and boundary conditions. However, the trend of moisture growth with frost front penetration is in agreement with measured values. After 5.5 years, moisture content primarily increased below 2 m from the initial position of the pipe invert, where the frozen fringe was located. The location of the maximum moisture content moved further away from the pipe with time because the frost front penetrated further, even after 5.5 years. However, no significant change occurred in the location of the maximum moisture during 10–20 years because the frost front remained almost constant.

For comparison, the FE calculated moisture content distribution in the control section at the end of 5.5 years is also plotted in this figure. Higher moisture content in the control section than that of the deep burial section confirms that the increase in effective stress reduces the water migration to the freezing front. A sudden increase in moisture content immediately below the pipeline is due to the initial drop of the pipeline temperature from -3.2 °C to -8.5 °C in 50 days, which was not found when T_p is decreased instantly from T_g to -8.5 °C.

Figures 4.10(a)–4.10(f) show the calculated volumetric ice content due to migrated and in-situ water freezing. The growth of ice content not only below but also around the pipe, especially for β less than 45°, influences the heave. At a given time, the maximum growth of ice occurs in the soil elements below the level of the springline (e.g., zone AB in Fig. 4.1(a)), not below the pipe, because of higher gradT_{ff}, due to smaller frozen fringe thickness and radial distance, and also due to higher SP at lower effective overburden pressure. A similar response was observed by

Nishimura et al. (2009); however, Konrad and Shen (1996) found the maximum ice growth at $\beta \sim 45°$ where they used the normal stress on the frost front as p_e. The simplified models based on one-dimensional heat flow (Hawlader et al. 2004) and radial heat flow (Konrad and Morgenstern 1984) cannot simulate this process. Figures 4.11(a)–4.11(f) show the total moisture content (w_t) for the same time periods. The pattern is very similar to the ice content, as shown in Fig. 4.10. In some areas near the final ice lens and at large β, the moisture content is greater than 100% because of significant water migration.

Typical volumetric strain increment due to the ice lens growth is shown in Fig. 4.12, which occurs primarily in the frozen fringe where the migrated water freezes. The accumulated strain has several effects on frost heave. The volumetric strains in the lower part (e.g., below the dashed line, $\beta \approx 45°$) have more influence to push the pipe upward, while the upper part may have a less direct influence on pushing the pipe upward, depending upon burial depth. However, the volumetric expansion of this zone could increase the mean stress and thereby the shear resistance of the unfrozen c-ϕ soil, through a failure wedge developing and extending up to the ground surface (Fig. 4.1(b)).

4.9 Conclusions

Commercial finite element programs are available for pure mechanical and thermal modeling, and also for thermo-mechanical analysis in some cases, including the software used in the present study. However, to simulate the frost heave of a chilled gas pipeline, additional complexities arise from the migration of water towards the frozen soil and expansion of water due to freezing. The numerical implementation of the Konrad-Morgenstern segregation potential model is presented in this study. The user subroutines are used to write computer programs to model the freezing of soil, incorporating solution-dependent thermal and mechanical properties of

the soil. The developed FE technique was used to simulate the process for a 20 year period without numerical issues, although the pipe in some cases heaved ~ 1 m or more. The FE calculated heave and frost front penetration compare well with the results of the control and deep burial sections of the Calgary full-scale test. Although the discrete segregate ice lens formation is not modeled explicitly, the moisture content obtained from the present continuum approach matches the observed behaviour in the full-scale tests.

While the elastoplastic models used for mechanical behaviour and the SP model for water migration can capture the key features, the selection of model parameters is still challenging, for instance, the temperature- and ice fraction-dependent geotechnical properties of the frozen soil and SP values. In addition, the seasonal temperature variation at the ground surface might have a significant influence on heave, especially for a shallow buried pipeline. These effects have been investigated in chapter 5.

Acknowledgements

The works presented in this chapter have been supported by the InnovateNL, formerly Research Development Corporation (RDC), Newfoundland and Labrador, through the ArcticTECH program, Equinor Research Chair, and Natural Sciences and Engineering Research Council of Canada.

List of symbols

The following symbols are used in this chapter:

A_e = equivalent area of element perpendicular to heat flow direction;

a = soil constant;

C_a = apparent volumetric heat capacity of soil;

c_{fr} = cohesion of frozen soil;

c_i = specific heat of ice;

c_s = specific heat of soil particle;

c_{un} = cohesion of unfrozen soil;

c_w = specific heat of water;

D = pipe diameter;

$d\varepsilon^i$ = volumetric strain increment due to pore water freezing;

$d\varepsilon^m$ = volumetric strain increment due to freezing of migrated water;

$d\varepsilon^{m\_e}$ = volumetric strain increment due to freezing of migrated water in a given element;

E_{fr} = Young's modulus of frozen soil;

E_{un} = Young's modulus of unfrozen soil;

g = gravitational acceleration;

$gradT_{ff}$ = temperature gradient in frozen fringe;

H = burial depth;

h = frost heave;

$\dot{h}$ = heave rate;

k = constant for thawing with temperature increase;

L = latent heat of water;

l_c = characteristic element length;

m = soil parameter;

n = porosity;

P = percentage of total water content that remains unfrozen well below 0 °C;

P_e = effective overburden pressure;

Q = factor controls unfrozen water content with temperature;

Q_w = migrated water flow to a given element;

q = heat flux;

q_x, q_y = heat flux in x and y-direction;

R = parameter related to P;

r = radial distance from current pipe center;

r_0 = radial distance from initial pipe center;

SP_0 = segregation potential at zero applied pressure;

T = temperature;

T_f = in-situ freezing temperature;

T_g = initial ground temperature;

T_p = chilled gas temperature;

T_s = ground surface temperature;

T_{sf} = segregation freezing temperature;

T_{50} = temperature at the highest rate of thawing;

t = time;

t_{ff} = thickness of frozen fringe;

V_e = volume of freezing element;

v_m = migrated water influx;

W_u = fraction of total water that remains unfrozen;

w_i = ice content basis of the dry mass of soil;

w_t = total moisture content of frozen soil basis of the dry mass of soil;

w_u = unfrozen water content basis of the dry mass of soil;

w_0 = soil water content basis of the dry mass of soil before freezing;

x, x_0 = horizontal distance measured from pipe center;

Y = depth of frost front from current pipe invert position;

Y_0 = depth of frost front from initial pipe invert position;

y = vertical distance measured from current pipe center;

y_0 = vertical distance measured from initial pipe center;

β = angle from y-axis to a point with respect to current pipe center;

β_0 = angle from y-axis to a point with respect to initial pipe center;

$\dot{\gamma}$ = strain rate;

θ_i = volumetric fraction of ice;

θ_{ip} = volumetric fraction of pore ice;

θ_{is} = volumetric fraction of segregated ice;

θ_{is_max} = maximum volumetric fraction of segregated ice prior to thawing;

θ_s = volumetric fraction of soil particle;

θ_w = volumetric fraction of unfrozen water;

λ_e = equivalent thermal conductivity of soil;

λ_i = thermal conductivity of ice;

λ_s = thermal conductivity of soil particle;

λ_w = thermal conductivity of water;

v_{fr} = Poisson's ratio of frozen soil;

v_{un} = Poisson's ratio of unfrozen soil;

ξ = parameter defines anisotropic distribution of volumetric strain;

ρ_d = dry density of soil;

ρ_i = density of ice;

ρ_s = density of soil particle;

ρ_w = density of water;

ϕ_{fr} = angle of internal friction of frozen soil;

ϕ_{un} = angle of internal friction of unfrozen soil;

φ = direction of heat flux with respect to y-axis;

ψ_{fr} = dilation angle of frozen soil; and

ψ_{un} = dilation angle of unfrozen soil.

References

Abaqus. 2014. *Abaqus documentation*. 6.14. Providence, USA: Dassault Systemes.

Andersland, O. B., and I. Alnouri. 1970. "Time-dependent strength behavior of frozen soils." *Journal of Soil Mechanics & Foundations Div*. 96 (1): 1249–1265.

Andersland, O. B., and B. Ladanyi. 2004. *Frozen ground engineering: Heat flow in soils,* 56–88. New Jersey, USA: John Wiley and Sons.

Arenson, L. U., and S. M. Springman. 2005. “Mathematical descriptions for the behaviour of ice-rich frozen soils at temperatures close to 0 °C.” *Can. Geotech. J.* 42 (2): 431–442.

Arenson, L. U., S. M. Springman, and D. C. Sego. 2007. “The rheology of frozen soils.” *Applied Rheology* 17 (1): 12147-1–12147-14.

Carlson, L. E., J. R. Ellwood, J. F. Nixon, and W. A. Slusarchuk. 1982. “Field test results of operating a chilled, buried pipeline in unfrozen ground.” In *Proc., 4th Can. Permafrost Conf.,* edited by H. French, 2–6. Calgary, Alberta: National Research Council of Canada.

Carlson, L. E., and J. F. Nixon. 1988. “Subsoil investigation of ice lensing at the Calgary, Canada, frost heave test facility.” *Can. Geotech. J.* 25 (2): 307–319.

C-CORE. 2005. *Centrifuge and Analytical Modeling of Chilled Buried Pipelines Subject to Frost Heave*. C-CORE publication R-04-087-277v2.0. St. John’s, Canada: C-CORE.

CGS (Canadian Geotechnical Society). 2006. *Canadian Foundation Engineering Manual (CFEM)*. Richmond, British Columbia: Canadian Geotechnical Society.

Clark, J. I., and R. Phillips. 2003. “Centrifuge modelling of frost heave of arctic gas pipelines.” In *Proc., 8th Int. Permafrost Conf.,* 21–24. Zurich, Switzerland.

Colt-KBR (Colt Engineering Corporation and Kellogg Brown & Root). 2003. *Conceptual geotechnical/geothermal design basis.* WP-005-D1-2, Rev. B. Calgary, Alberta, Canada: Colt Engineering Corporation and Kellogg Brown & Root.

Côté, J., and J.-M. Konrad. 2005. “A generalized thermal conductivity model for soils and construction materials.” *Can. Geotech. J.* 42 (2): 443–458.

Coutts, R. J. 1991. “Development of a two-dimensional finite element model to calculate temperatures and stresses in frost susceptible soil around a chilled pipeline.” M.Sc. thesis, Department of Earth Sciences, University of Waterloo.

Dallimore, S. R. 1985. “Observations and predictions of frost heave around a chilled pipeline.” M.A. thesis, Department of Geography, Carleton University.

Dayarathne, R. S., and B. C. Hawlader. 2015. “Stress–strain behaviour of a clayey silt in triaxial tests.” In *Proc., 68th Can. Geotech. Conf.,* p6. Quebec: Can. Geotech. Society.

Dumais, S., and J.-M. Konrad. 2018. “One-dimensional large-strain thaw consolidation using nonlinear effective stress–void ratio–hydraulic conductivity relationships.” *Can. Geotech. J.* 55 (3): 414–426.

Farouki, O. T. 1981. *Thermal properties of soils*. CRREL Monograph 81-1. Hanover, New Hampshire, USA: US Army Corps of Engineers.

Farouki, O. T. 1982. *Evaluation of methods for calculating soil thermal conductivity*. CRREL 82-8. Hanover, New Hampshire, USA: US Army Corps of Engineers.

Ferreira, P. M. V., and A. V. D. Bica. 2006. “Problems in identifying the effects of structure and critical state in a soil with a transitional behaviour.” *Géotechnique* 56 (7): 445–454.

Georgiannou, V. N., M. R. Coop, F. N. Altuhafi, and D. I. Lefas. 2018. “Compression and strength characteristics of two silts of low and high plasticity.” *J. Geotech. Geoenv. Eng.* 144 (7): 04018041-1–04018041-12.

Ghoreishian Amiri, S. A., G. Grimstad, M. Kadivar, and S. Nordal. 2016. “Constitutive model for rate-independent behavior of saturated frozen soils.” *Can. Geotech. J.* 53 (10): 1646–1657.

Gilpin, R. 1980. “A model for the prediction of ice lensing and frost heave in soils.” *Water Resources Research* 16 (5): 918–930.

Goodrich, L. E., and L. W. Gold. 1981. *Permafrost Engineering Design and Construction*: *Ground thermal analysis*, 149–172. New York: John Wiley & Sons.

Guymon, G. L., T. V. Hromadka, and R. L. Berg. 1984. “Two-Dimensional Model of Coupled Heat and Moisture Transport in Frost-Heaving Soils.” *ASME. J. Energy Resour. Technol.* 106 (3): 336–343.

Hawlader, B. C., V. Morgan, and J. I. Clark. 2004. “A simplified solution for frost heave prediction of chilled pipelines.” In *Proc., 12th Int. Spec. Conf.* 16–19. Edmonton, Canada.

Hawlader, B. C., V. Morgan, and J. I. Clark. 2006. “Modelling of pipeline under differential frost heave considering post-peak reduction of uplift resistance in frozen soil.” *Can. Geotech. J.* 43 (3): 282–293.

Huang, S. L., M. T. Bray, S. Akagawa, and M. Fukuda. 2004. “Field investigation of soil heave by a large diameter chilled gas pipeline experiment, Fairbanks, Alaska.” *J. Cold Reg. Eng.* 18 (1): 2–34.

Hwang, C. T. 1977. “On quasi-static solutions for buried pipes in permafrost.” *Can. Geotech. J.* 14 (2): 180–192.

Johansen, O. 1975. “Thermal conductivity of softs.” Ph.D. thesis, University of Trondheim, Trondheim, Norway. CRREL Draft English Translation 637. Hanover, New Hampshire, USA: US Army Corps of Engineers.

Kim, K. 2011. “Multi-dimensional frost heave modeling with SP porosity growth function.” Ph.D. thesis, Department of Civil and Env. Eng., University of Alaska Fairbanks.

Konrad, J.-M. 1980. “Frost heave mechanics.” Ph.D. thesis, Department of Civil Engineering, University of Alberta, Canada.

Konrad, J.-M. 1994. “Sixteenth Canadian Geotechnical Colloquium: Frost heave in soils: concepts and engineering.” *Can. Geotech. J.* 31 (2): 223–245.

Konrad, J.-M., and N. R. Morgenstern. 1980. “A mechanistic theory of ice lens formation in fine-grained soils.” *Can. Geotech. J.* 17 (4): 473–486.

Konrad, J.-M., and N. R. Morgenstern. 1981. “The segregation potential of a freezing soil.” *Can. Geotech. J.* 18 (4): 482–491.

Konrad, J.-M., and N. R. Morgenstern. 1982. “Effects of applied pressure on freezing soils.” *Can. Geotech. J.* 19 (4): 494–505.

Konrad, J.-M., and N. R. Morgenstern. 1984. “Frost heave prediction of chilled pipelines buried in unfrozen soils.” *Can. Geotech. J.* 21 (1): 100–115.

Konrad, J.-M., and M. Shen. 1996. “2-D frost action modeling using the segregation potential of soils.” *Cold Reg. Sci. Technol.* 24 (3): 263–278.

Ladanyi, B. 1972. “An engineering theory of creep of frozen soils.” *Can. Geotech. J.* 9 (1): 63–80.

Ladanyi, B., and M. Shen. 1993. “Freezing pressure development on a buried chilled pipeline.” In *Proc., Int. Symp. Frost in Geotech. Eng.,* 23–33. Alaska.

Li, H. P., Y. L. Zhu, and W. D. Pan. 2003. “Uniaxial compressive strength of saturated frozen silt.” In *Proc., 8th Int. Conf. Permafrost,* 679–684.

Michalowski, R. L. 1993. “A constitutive model of saturated soils for frost heave simulations.” *Cold Reg. Sci. Technol.* 22 (1): 47–63.

Michalowski, R. L., and M. Zhu. 2006. “Frost heave modelling using porosity rate function.” *Int. J. Numer. Anal. Meth. Geomech.* 30 (8): 703–722.

Miller, R. D. 1978. “Frost heaving in non-colloidal soils.” In *Proc., Int. Conf. on Permafrost,* 707–713. Edmonton, Alberta: National Research Council of Canada.

Morgan, V., J. Clark, B. Hawlader, and J. Zhou. 2004. “Prediction of long-term frost heave of chilled gas pipelines by centrifuge modeling.” In *Proc., 5th Int. Pipeline Conf.* 2429–2435.

Morgan, V., B. Hawlader, and J. Zhou. 2006. “Mitigation of frost heave of chilled gas pipelines using temperature cycling.” In *Proc., 6th Int. Pipeline Conf.* 927–931. Calgary, Canada.

Nishimura, S., A. Gens, S. Olivella, and R. J. Jardine. 2009. “THM-coupled finite element analysis of frozen soil: formulation and application.” *Géotechnique* 59 (3): 159–171.

Nixon, J. F. 1975. “The role of convective heat transport in the thawing of frozen soils.” *Can. Geotech. J.* 12 (3): 425–429.

Nixon, J. F. 1983. “Practical applications of a versatile geothermal simulator.” *Journal of Energy Resources Technology* 105 (4): 442–447.

Nixon, J. F. 1986. “Pipeline frost heave predictions using a 2-D thermal model.” *ASCE Research Transportation Facilities Cold Reg.,* 67–82: ASCE.

Nixon, J. F. 1991. “Discrete ice lens theory for frost heave in soils.” *Can. Geotech. J.* 28 (6): 843–859.

Nixon, J. F. 1992. “Discrete ice lens theory for frost heave beneath pipelines.” *Can. Geotech. J.* 29 (3): 487–497.

Nixon, J. F., and E. C. McRoberts. 1973. “A study of some factors affecting the thawing of frozen soils.” *Can. Geotech. J.* 10 (3): 439–452.

Nocilla, A., M. R. Coop, and F. Colleselli. 2006. “The mechanics of an Italian silt: an example of ‘transitional’ behaviour.” *Géotechnique* 56 (4): 261–271.

Oliphant, J. L., A. R. Tice, and Y. Nakano. 1983. “Water migration due to a temperature gradient in frozen soil.” In *Proc., 4th Int. Permafrost Conf.* 951–956.

O'Neill, K., and R. D. Miller. 1985. “Exploration of a rigid ice model of frost heave.” *Water Resources Research* 21 (3): 281–296.

Patterson, D. E., and M. W. Smith. 1981. “The measurement of unfrozen water content by time domain reflectometry: Results from laboratory tests.” *Can. Geotech. J.* 18 (1): 131–144.

Phillips, R., J. I. Clark, and R. Hanke. 2001. “Centrifuge Modelling of Pipeline Frost Heave.” In *Proc. 54th Can. Geotech. Conf.,* Calgary: Canadian Geotechnical Society.

Phillips, R., J. I. Clarke, and R. Hanke. 2002. “Pipeline frost heave modelling.” In *Proc., Int. Conf. Physical Modelling in Geotechnics,* 313–318. St. John’s, Canada.

Piercey, G., N. Volkov, R. Phillips, and A. Zakeri. 2011. “Assessment of frost heave modelling of cold gas pipelines.” In *Proc., 2011 Pan-Am Geotechnical Conf.* 8p. Toronto, Canada.

Rajani, B., and N. Morgenstern. 1994. “Comparison of predicted and observed responses of pipeline to differential frost heave.” *Can. Geotech. J.* 31 (6): 803–816.

Selvadurai, A. P. S., J. Hu, and I. Konuk. 1999. “Computational modelling of frost heave induced soil–pipeline interaction: II. Modelling of experiments at the Caen test facility.” *Cold Reg. Sci. Technol.* 29 (3): 229–257.

Shen, M., and J.-M. Konrad. 1993. “Correct use of the segregation potential concept for two-dimensional frost heaving simulation.” In *Proc. 6th Int. Conf. Permafrost,* 550–555. Beijing.

Shen., M., and B. Ladanyi. 1987. “Modelling of coupled heat, moisture and stress field in freezing soil.” *Cold Reg. Sci. Technol.* 14 (3): 237–246.

Shen, M., and B. Ladanyi, 1991. “Soil-pipe interaction during frost heaving around a buried chilled pipeline.” In *Proc.* 6th Int. *Specialty Conf.,* 11–21. Hanover, New Hampshire: ASCE.

Slusarchuk, W. A., J. I. Clark, J. F. Nixon, N. R. Morgenstern, and P. N. Gaskin. 1978. “Field test results of a chilled pipeline buried in unfrozen ground.” In *Proc., 3rd Int. Conf. Permafrost,* 878–883. Edmonton, Canada.

Thomas, H. R., P. Cleall, Y. C. Li, C. Harris, and M. Kern-Luetschg. 2009. “Modelling of cryogenic processes in permafrost and seasonally frozen soils.” *Géotechnique* 59 (3): 173–184.

Tiedje, E. 2015. “Characterization and numerical modelling of frost heave.” Ph.D. thesis, Department of Civil Engineering, McMaster University.

Yuanlin, Z., and D. L. Carbee. 1984. “Creep behavior of frozen silt under constant uniaxial stress.” *J. Glaciology Geocryology* 6 (1): 33–48.

Zhang, Y. 2014. “Thermal-Hydro-Mechanical model for freezing and thawing of soils.” Ph.D. thesis, Department of Civil and Environmental Engineering, University of Michigan.

Zhang, Y., and R. L. Michalowski. 2013a. *Multi-Scale Process of soil Freezing, Thawing, and Thaw-Settlement*. Ann Arbor, Michigan: Michigan Univ. Regents Ann Arbor Div. of Research Development and Administration, U.S. Army Research Office.

Zhang, Y., and R. L. Michalowski. 2013b. “Thermal-mechanical constitutive modeling for freezing and thawing soils.” In *Proc., 10th Int. Sym. Cold Reg. Develop.* 256–267. Alaska.

Zhu, M. 2006. “Modeling and simulation of frost heave in frost-susceptible soils.” Ph.D. thesis, Department of Civil and Environmental Engineering, University of Michigan.

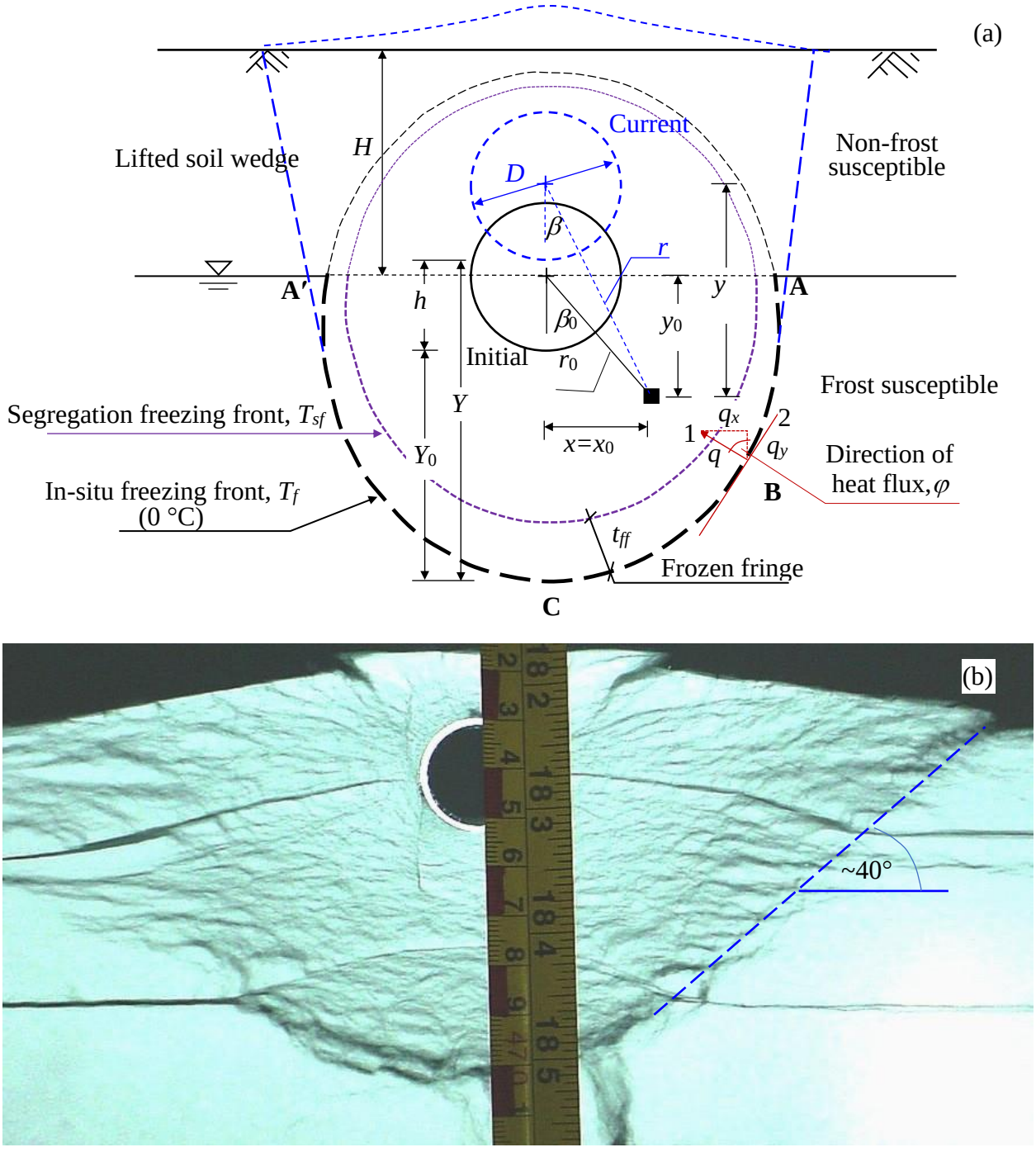

Fig. 4.1. Frost heave of chilled gas pipeline: (a) schematic view and nomenclature; and (b) typical section after centrifuge test (C-CORE 2005)

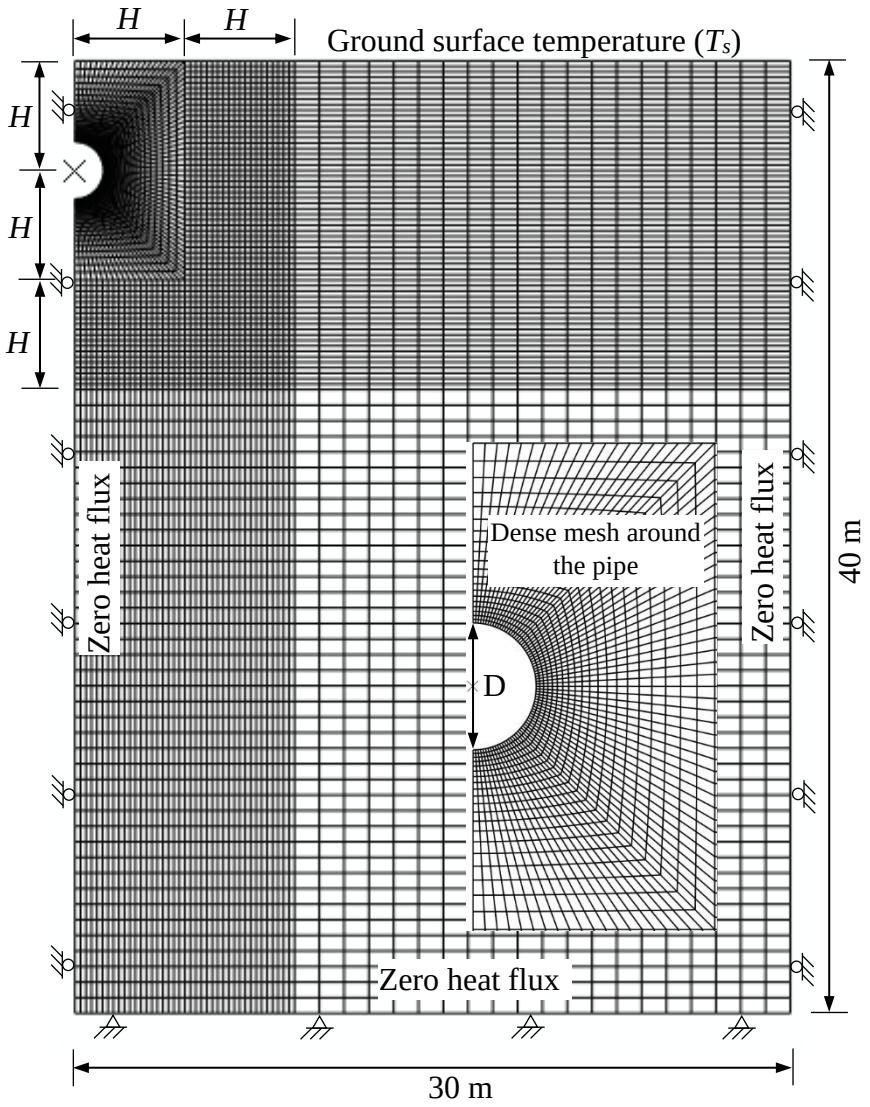

Fig. 4.2. Finite element mesh used in two-dimensional analysis

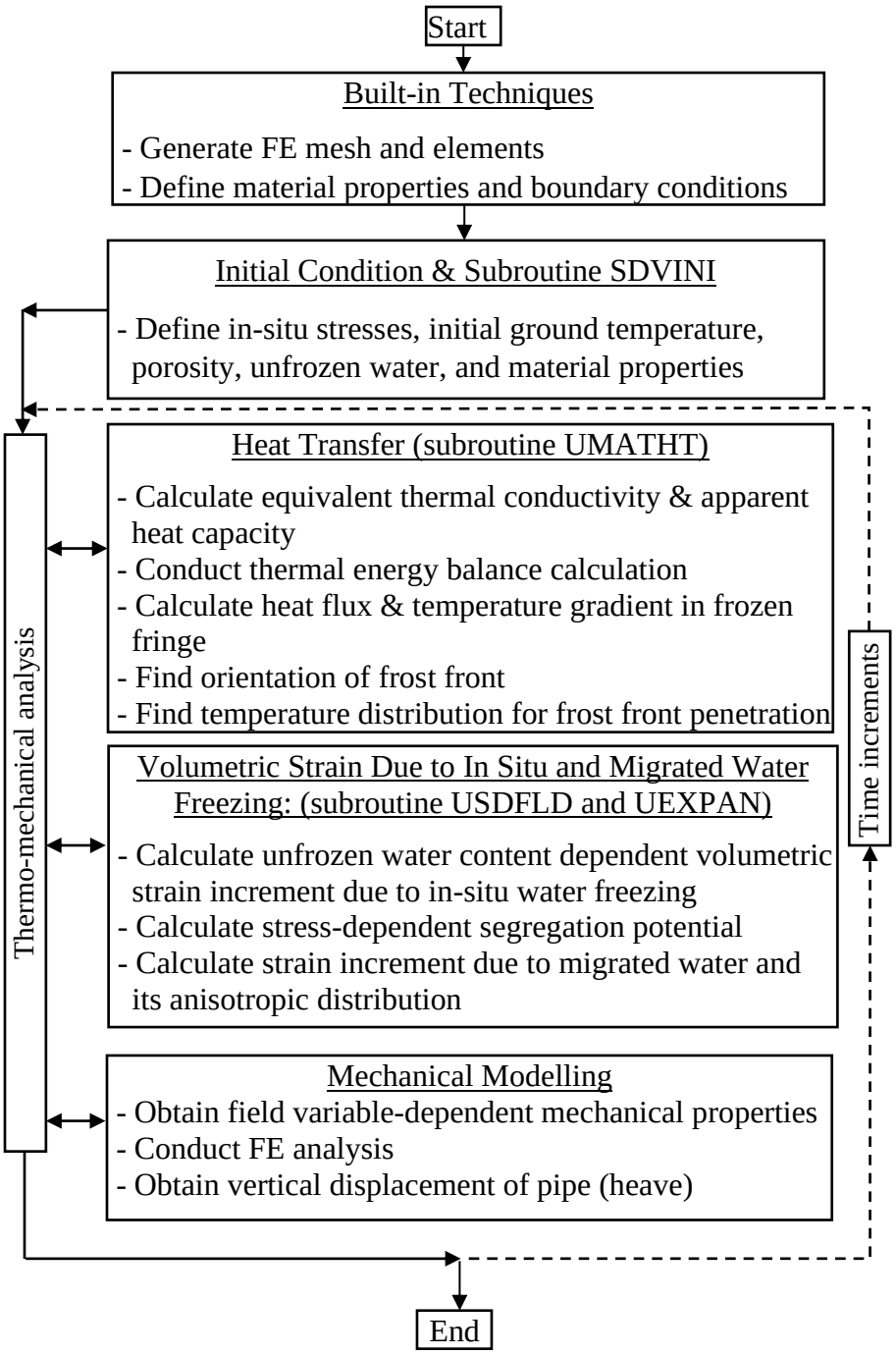

Fig. 4.3. Implementation of model using user subroutines

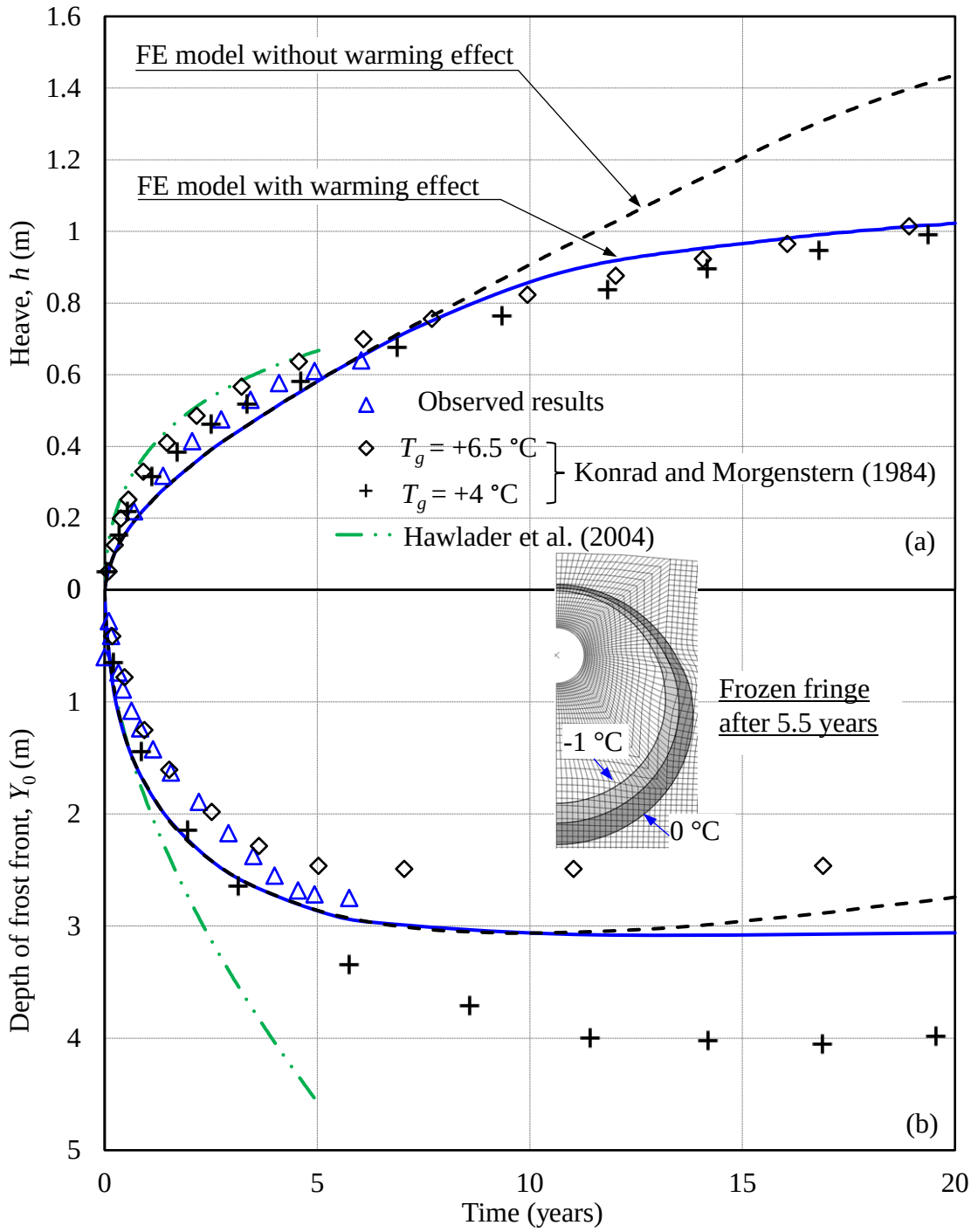

Fig. 4.4. Comparison between FE and Calgary full-scale deep burial section test results: (a) frost heave; and (b) frost front penetration

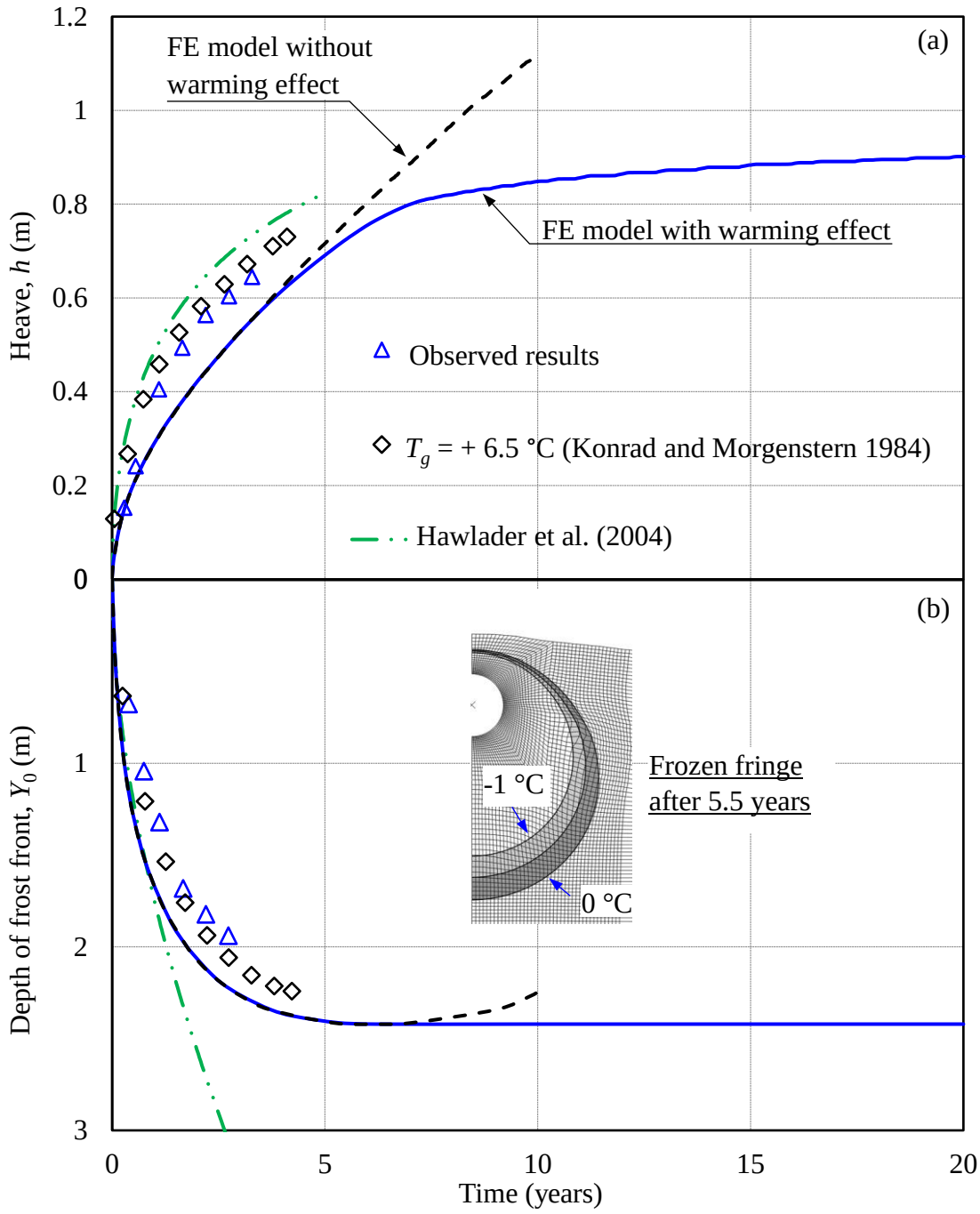

Fig. 4.5. Comparison between FE and Calgary full-scale control section test results: (a) frost heave; and (b) frost front penetration

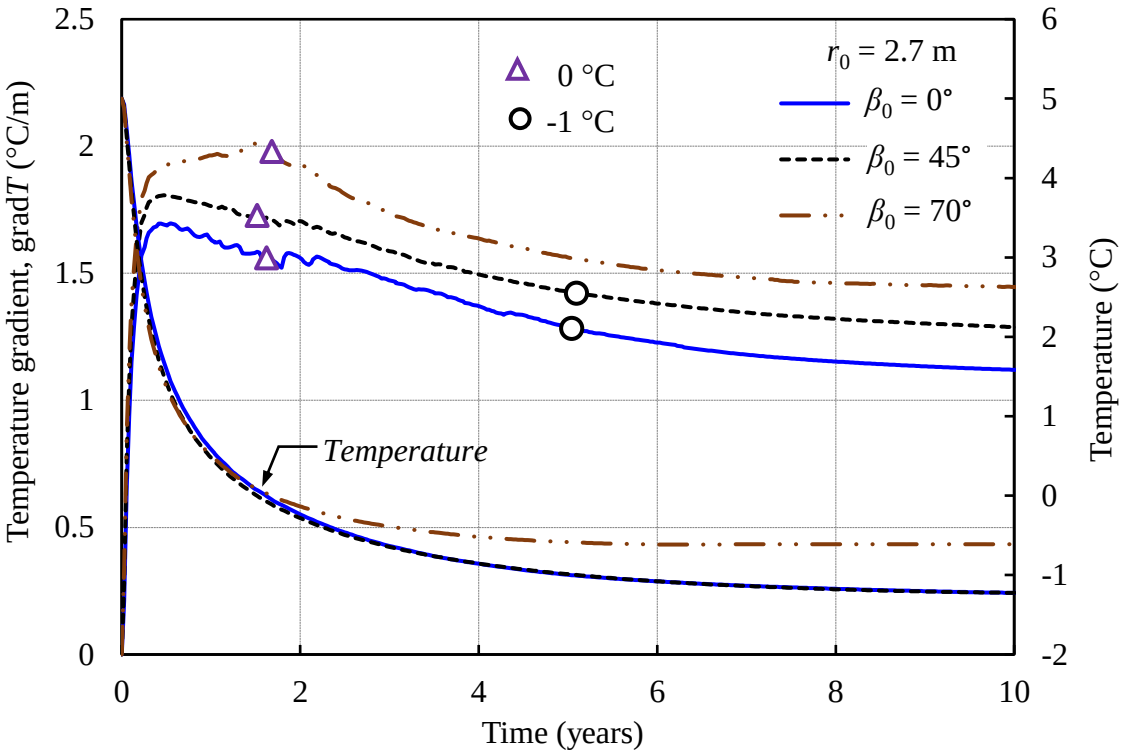

Fig. 4.6. Temperature gradient variation with time in typical soil elements in frozen zone for deep burial section

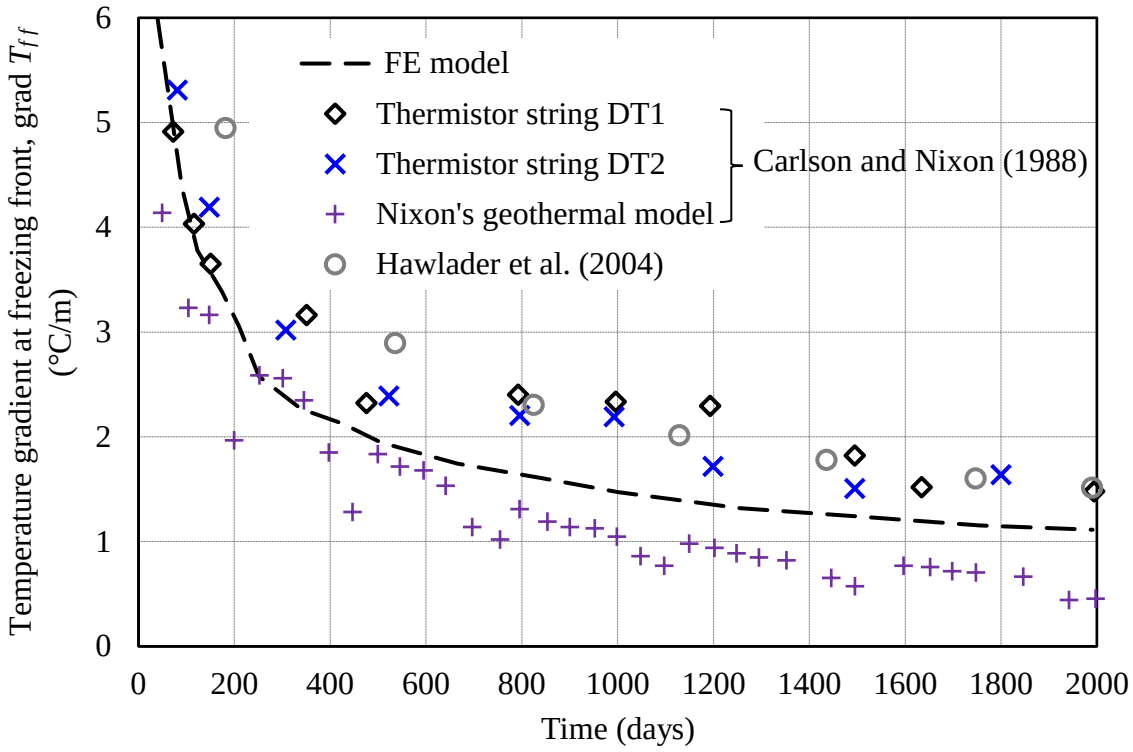

Fig. 4.7. Comparison of observed and predicted temperature gradient in segregation freezing temperature with time for deep burial section

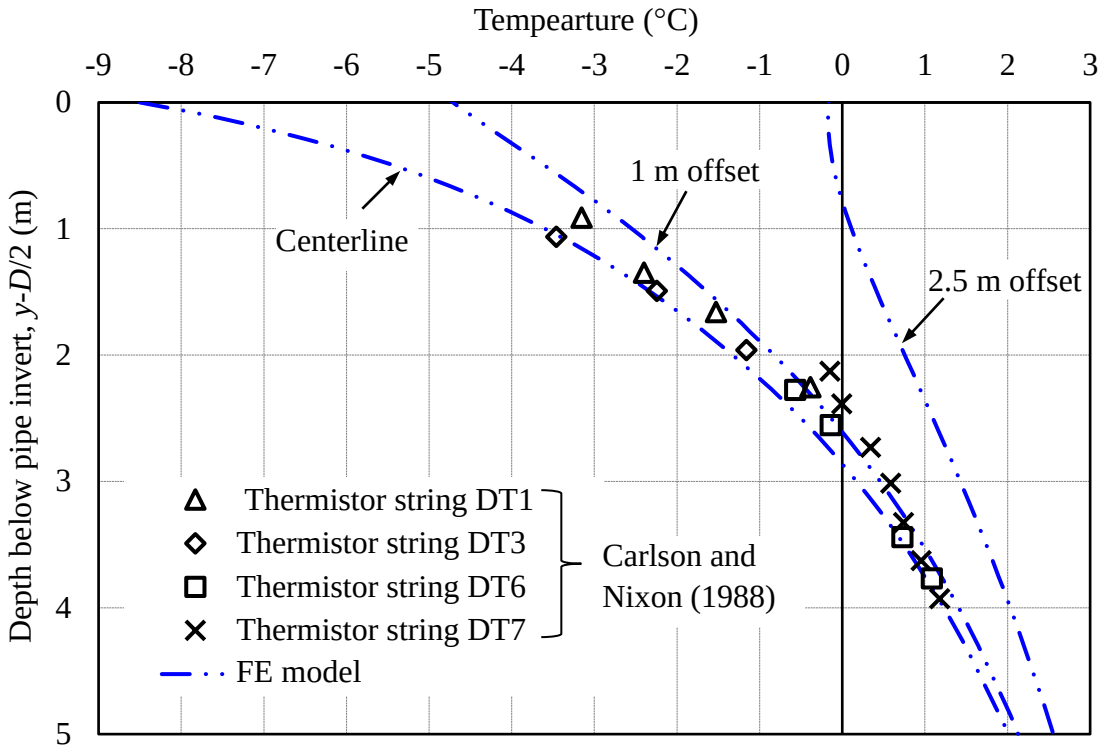

Fig. 4.8. Comparison of observed and predicted temperature profile for deep burial section after 1000 days

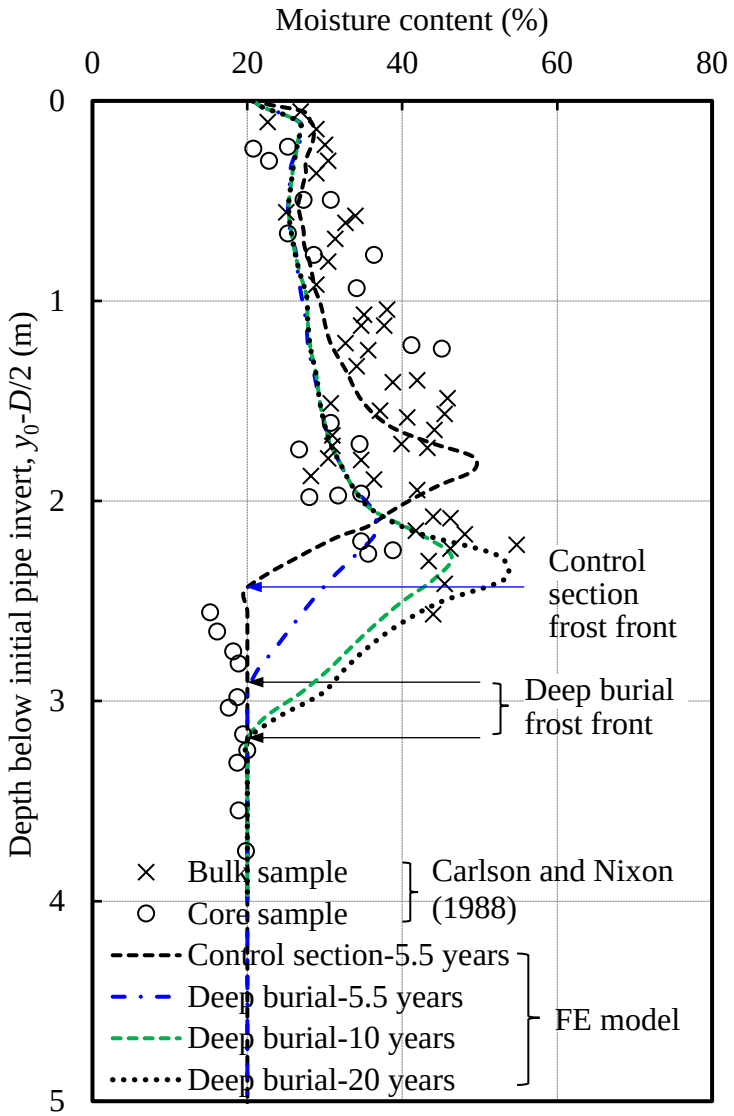

Fig. 4.9. FE calculated and observed moisture content below pipe invert for deep burial section

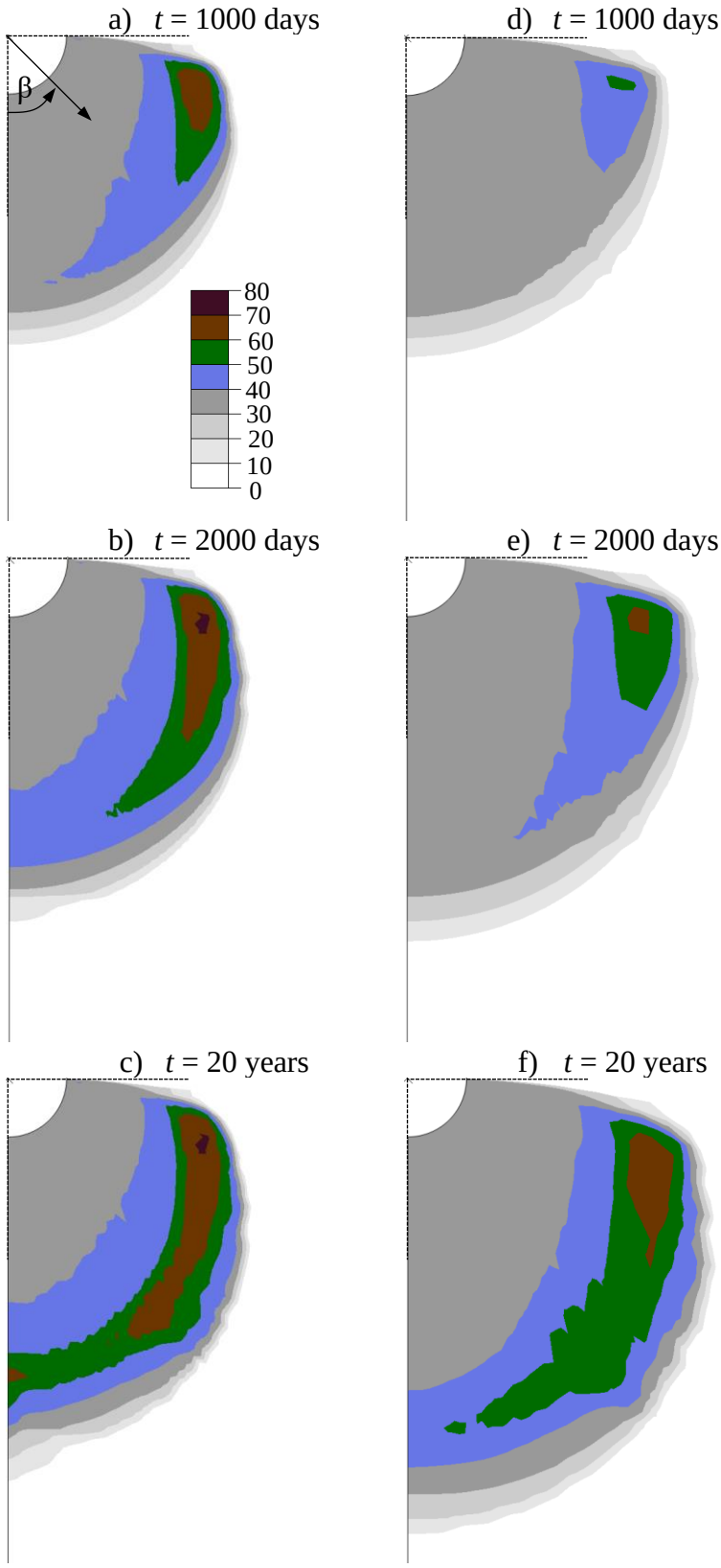

Fig. 4.10. Volumetric ice content (%): (a)–(c) control section; and (d)–(f) deep-burial section

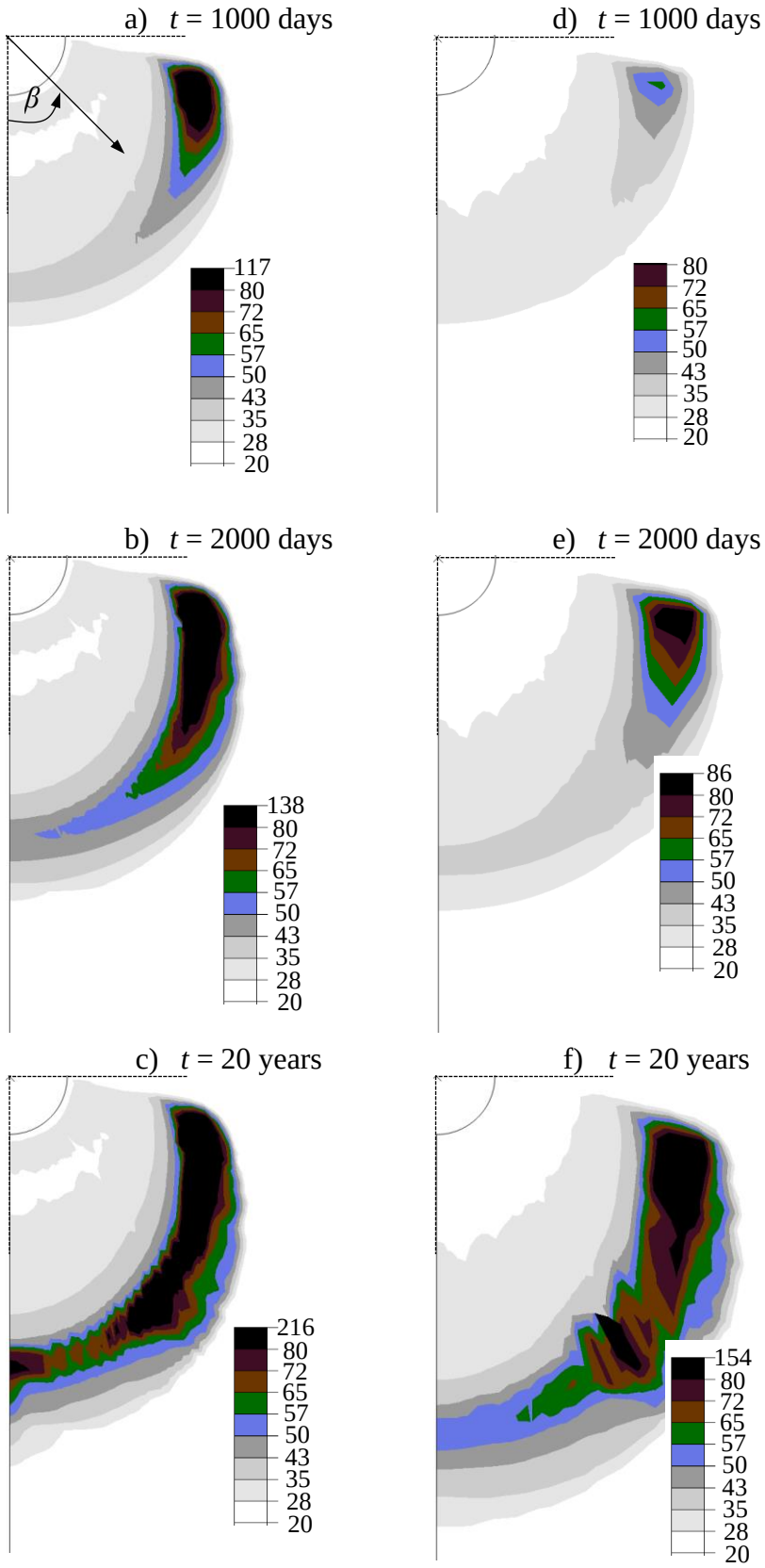

Fig. 4.11. Total moisture content (%): (a)–(c) control section; and (d)–(f) deep-burial section

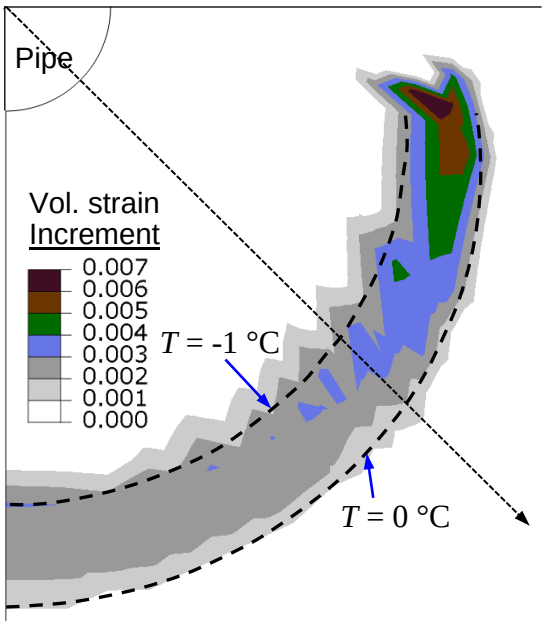

Fig. 4.12. Volumetric strain increment due to ice lens formation in frozen fringe after 1000 days in deep burial section (Δt = 10 days)

Table 4.1. Parameters used in finite element simulation

Parameter	Value/expression
Mechanical Properties	
Unfrozen soil	
Young's modulus, E_{un} (MPa)	11.2
Poisson's ratio, v_{un}	0.25
Angle of internal friction, ϕ_{un} (°)	30
Cohesion, c_{un} (kPa)	10
Dilation angle, ψ_{un} (°)	5
Frozen soil	
Young's modulus, E_{fr} (MPa)	$13.75\|T\|^{1.18}$
Poisson's ratio, v_{fr}	0.25
Angle of internal friction, ϕ_{fr} (°)	$\phi_{un}(1-\theta_i^{2.6})$
Cohesion, c_{fr} (kPa)	$c_{un}(1+5\theta_i)\ \|T\|^{0.5}$
Dilation angle, ψ_{fr} (°)	5
Freezing Characteristics	
Segregation potential	
SP_0 (mm^2/°C.s)	230×10^{-5}
a (MPa^{-1})	9.5
Unfrozen water content function	
P (%)	25
Q	1
In-situ freezing temperature, T_f (°C)	0
Segregation freezing temperature, T_{sf} (°C)	-1
Dry density of soil, ρ_d (kg/m^3)	1740
Initial water content, w_0	0.2 (0.1 for non-frost susceptible)
Initial porosity, n	0.35
Density of soil skeleton, ρ_s (kg/m^3)	2,670
Density of water, ρ_w (kg/m^3)	1,000
Density of ice, ρ_i (kg/m^3)	917
Thermal conductivity of soil skeleton, λ_s (W/m°C)	2.1
Thermal conductivity of water, λ_w (W/m°C)	0.6

Thermal conductivity of ice, λ_i (W/m°C)	2.24
Specific heat of soil skeleton, c_s (J/kg°C)	836
Specific heat of water, c_w (J/kg°C)	4,184
Specific heat of ice, c_i (J/kg°C)	2,100
Latent heat of water, L (J/kg)	334,720

CHAPTER 5:

Factors Affecting Frost Heave of Chilled Gas Pipelines

Co-Authorship: This chapter has been submitted as a technical paper for publication in a journal as: Dayarathne, R., Hawlader, B., Phillips, R., and Robert, D. “Factors affecting frost heave of chilled gas pipelines.” Most of the research presented in this chapter has been conducted by the first author. He also prepared the draft manuscript. The other authors mainly supervised the research and reviewed the manuscript.

Videos S1–S5 are available in the supplementary data submitted together with this thesis.

5.1 Abstract

Chilled gas pipelines generally traverse a long distance through a variety of soils and may operate for decades with varying temperatures of gas, surrounding soil and ground surface. The present study investigates the effects of key factors on frost heave using finite element modeling of the coupled thermomechanical process by implementing the Konrad–Morgenstern segregation potential model in a commercial software. A simplified approach is proposed to estimate the thaw back effects on long-term frost heave. The seasonal variation of ground surface temperature significantly affects the heave, especially for pipelines at shallow burial depths and for long-term heaving. An increase in cohesion of the frozen soil and reduction of initial ground temperature reduce the heave. Modeling of frozen fringe and stress effects on segregation potential are discussed. Sub-zero gas temperature has a smaller effect on heave for lower initial ground temperature; however, it significantly affects long-term heave for higher ground temperatures.

5.2 Introduction

Chilling gas to increase throughput and reduce permafrost degradation is a preferred option for the operation of buried gas pipelines, not only in continuous but also in discontinuous permafrost areas. When a chilled gas pipeline passes through frost susceptible unfrozen soils in discontinuous permafrost zones, differential frost heave could cause unacceptable strains in the pipeline near the interface between frozen and unfrozen soils or soils with different frost susceptibilities. Proper estimation of free-field frost heave that occurs sufficiently far from the interface is required to analyze the response of a pipeline (Rajani and Morgenstern 1994; Selvadurai et al. 1999b; Hawlader et al. 2006). A pipeline generally passes through soils of varying frost susceptibility and mechanical behaviour. The ground surface and pipeline temperatures, and also the ground temperature prior to pipeline operation, vary along the route (Konrad and Morgenstern 1984; Nixon 1986; Colt-CBR 2003; Oswell 2011). The effects of these factors on frost heave prediction can be evaluated using numerical tools calibrated with full-scale and reduced-scale test results.

Studies are available on the freezing of soil, including heat transfer, frost susceptibility and mechanical behaviour of frozen soils. Thermal properties of soils (e.g., thermal conductivity, specific heat and latent heat) depend on volumetric ice and water fractions and the dry density of soils (Johansen 1975; Farouki 1981a, b; Côté and Konrad 2005). The mechanical behaviour of frozen and unfrozen soils (e.g., elastic, elastoplastic and creep) is also related to ice and water fractions, in addition to temperature, strain rate and confining pressure (Arenson et al. 2007). The migration of water to the frozen fringe and formation of ice lens behind the frost front also depend on soil type; for example, clayey silts are highly frost susceptible (Andersland and Ladanyi 2004).

Mathematical models have been developed for thermal, mechanical and water migration processes in frost heave, and have also been implemented in advanced numerical techniques to

predict the frost heave (Guymon et al. 1984; Konrad and Morgenstern 1984, Nixon 1986, 1992; Selvadurai et al. 1999a; Michalowski 1993; chapter 4 in the current thesis). Studies of full-scale tests (e.g., Calgary full-scale test (Slusarchuck et al. 1978; Carlson et al. 1982; Carlson and Nixon 1988), Canada-France pipeline experiment (Dallimore 1985; Selvadurai et al. 1999b), and Fairbanks full-scale experiment (Huang et al. 2004)) and centrifuge tests (Phillips et al. 2001, 2002; Morgan et al. 2004, 2006; Piercey et al. 2011; chapter 3 in the current thesis) are also available, including the calibration of numerical approaches with these experimental results. The present study focused on identifying the key factors that influence frost heave based on coupled finite element (FE) analyses.

Finite element and finite-difference modeling techniques were developed to solve the complex thermo-hydro-mechanical processes of frost heave by idealizing the problem in different ways. A summary of available numerical approaches was provided in chapters 2 and 4. The migration of water that forms the ice lens was modeled in several ways (frost heave model), including the use of Darcy's law and the Clausius-Clapeyron equation, and in a more practical way, using the "segregation potential" model (Konrad and Morgenstern 1980, 1981) and "porosity rate function" (Michalowski 1993). Early numerical work assumed soil was non-deformable except for the volumetric expansion of the soil in the frozen fringe due to segregate ice lens formation (Guymon et al. 1984). In some "decoupled" analyses, a geothermal analysis was conducted first to find temperature distribution, which was then used in the one-dimensional frost heave model to calculate the long-term (20–30 years) heave (e.g., Konrad and Morgenstern 1984; Nixon 1986; Colt-KBR 2003). Coupled thermo-mechanical analyses were also performed with different constitutive models of frozen and unfrozen soils considering elastic and plastic properties, also recognizing the creep effect on frozen soil behaviour (Konrad and Shen 1996; Michalowski

and Zhu 2006; Kim 2011). In these studies, water migration is modeled using the empirical functions: SP-model and porosity rate function. Fully coupled thermo-hydro-mechanical analysis was also attempted; however, such an approach requires additionally complex constitutive relations and soil properties, including hydraulic conductivity and suction-induced pore water flow (Nishimura et al. 2009; Thomas et al. 2009; Zhang and Michalowski 2013b; Ghoreishian Amiri et al. 2016).

The existing coupled analyses were limited to a relatively small period of freezing as compared to the design life of a pipeline or simulated the response of buried structures that might experience relatively less heave. For example, although the design life of a pipeline could be more than 20 years, the FE results were compared with the Calgary full-scale test results for less than 1,500 days (Konrad and Shen 1996; Nishimura et al. 2009; Tiedje 2015). Other studies focused on the simulation of laboratory one-dimensional frost heave tests, and retaining structures, footing and culverts in less frost susceptible soils (Michalowski and Zhu 2006; Zhang and Michalowski 2013a, b).

Frost heave of a pipeline needs to be evaluated for a wide range of geotechnical and geothermal conditions. For example, some sections of the Norman Wells oil pipeline passed through two to ten frozen–unfrozen thermal interfaces per kilometre in the discontinuous permafrost areas, where a large variation in soil properties and temperature conditions was reported (Nixon et al. 1991; Colt-KBR 2003). Nixon's geothermal modeling together with SP-based heave calculation shows that some parameters, such as ground temperature, segregation freezing temperature and segregation potential (*SP*) values, could significantly affect the heave (Nixon 1986; Colt-KBR 2003).

In chapter 4, a coupled FE modeling approach to calculate frost heave using Abaqus FE software is developed, which has also been calibrated against full-scale test results. The objective of the present chapter is to identify the key factors that could influence the long-term heave (up to 20 years) of chilled gas pipelines using that numerical technique. Attention is given to potential thawing at the front part of the frost bulb, especially after a long-term operation and under seasonal variation of the ground surface temperature. Some of the critical components, such as modeling of frozen soil, frozen fringe and stress effects on segregation potential, are also discussed.

5.3 Problem Statement

A pipeline of diameter D, buried at H and operating at a negative chilled gas temperature of T_p is modeled (Fig. 5.1). The pipe–soil interaction is not modeled; instead, the pipe represents a rigid body of the thermal boundary of T_p. The initial ground temperature at the start of the operation is T_g. The soil layer below the pipe center is saturated and highly frost susceptible, while the soil above it is unsaturated and non-frost susceptible. The groundwater table is at the level of the pipe center. The location of any point is denoted by (x_0, y_0) and (x, y) with respect to the center of the pipe at the initial condition and current positions, respectively (Fig. 5.1), where y_0 and y are positive for vertically downward locations from the center. The polar coordinates (r_0, β_0) and (r, β) are also used; $\beta_0 = \tan^{-1}(x_0/y_0)$ and $\beta = \tan^{-1}(x/y)$ are for the initial and current positions, respectively (Fig. 5.1). Segregate ice formation could lift a soil wedge resulting in ground surface heave. It is assumed that heat transfer occurs only by conduction because the advection effect is not significant (Nixon 1975; Dumais and Konrad 2018). The vertical distance from the initial pipe invert position to the frost front (assumed to be the 0 °C isotherm) represents the depth of the frost front (Y_0).

5.4 Finite Element Modelling

Frost heave of a two-dimensional pipeline section in plane strain condition is modeled using Abaqus/Standard FE software (Abaqus 2014). Figure 5.2 shows the typical FE mesh. Taking the advantage of symmetry, only the right half of the problem is modeled. A finer mesh is used close to the pipe (see Inset 1 of Fig. 5.2) where the frost front penetration and segregated ice lens formation are expected. The right and bottom boundaries are placed sufficiently far from the pipe to avoid boundary effects. Zero heat flux is applied at the vertical and bottom boundaries. Constant temperature or sinusoidal seasonal temperature variation (see Inset 2 of Fig. 5.2), as discussed later, is given to the ground surface. All the vertical faces are restrained for horizontal displacement while the bottom boundary is restrained for both horizontal and vertical displacements.

The soil domain is discretized using the 4-node bilinear coupled temperature-displacement plane strain elements (CPE4T in Abaqus 2014). The pipe is modeled as a rigid body by defining the nodes along the outer periphery of the pipe as tie-type nodes with a reference point at the pipe center. Modeling of the pipe by tie nodes saves computational costs and does not require a definition of pipe–soil interface behaviour. The pipe is allowed to displace vertically without rotation. The vertical displacement of the reference point represents the frost heave (h in Fig. 5.1). The thermal conductivity of pipe material is considerably higher than that of surrounding soil; therefore, the chilled gas temperature is directly applied to this pipe node-set. The pipe temperature (T_p) was decreased linearly from T_g to a targeted value within the first 50 days and then remained constant.

5.5 Modelling of Thermo-Mechanical Behaviour of Soil

The software used in this study does not have any built-in technique to model the frost heave processes, as discussed below; therefore, user subroutines have been developed in FORTRAN to

implement the SP-model and the temperature- and solution-dependent thermal and mechanical properties. The details of FE implementation have been presented in chapter 4. A summary is provided in the following sections.

a) The velocity of water that migrated to the frozen fringe to form ice lenses (v_m) is calculated as (Konrad and Morgenstern 1984):

a) The velocity of water migrated to the frozen fringe to form ice lenses (v_m) is calculated as (Konrad and Morgenstern 1984):

$$v_m = (SP_0 . e^{-ap_e}) grad T_{ff} \quad (5.1)$$

where $SP_0 . e^{-ap_e}$ is the current value of stress-dependent segregation potential; SP_0 is the segregation potential with zero applied pressure; gradT_{ff} is the temperature gradient at the segregation freezing temperature (T_{sf}).

Multiplying v_m by an equivalent area perpendicular to the direction of heat flux (see Fig. 5.1) and time increment, the amount of water flowing to an element in the frozen fringe is calculated. The frozen volume (= 1.09 times of the migrated water) is used to calculate the volumetric strain increment in the frozen fringe, which is distributed in the elements in the frozen fringe (i.e., the thickness of t_{ff} in Fig. 5.1) anisotropically in the directions parallel and perpendicular to the heat flow direction by 90% and 10%, respectively (Konrad and Shen 1996; Michalowski and Zhu 2006).

It is assumed that the water migration will not occur when the temperature change (dT/dt) in the frozen fringe is positive. This occurs during the seasonal variation of ground surface temperature and also when the pipe moves sufficiently far from the final ice lens. However, during refreezing in the winter period, dT/dt becomes negative again and the water migration continues.

b) The normalized unfrozen water content W_u (i.e., $W_u = w_u/w_0$) is calculated as (Nixon 1983):

$$W_u = (P + e^{(QT+R)})/100 \quad (5.2)$$

where w_u is the current unfrozen water content; w_0 is the initial water content; T is the negative temperature in °C; P is the percentage of the total water content that remains unfrozen well below the in-situ freezing temperature (T_f); the constant Q defines the steepness of W_u–T curve; $R = ln(100 - P)$. The volume change due to the freezing of this water is given as isotropic expansion.

c) Equivalent thermal conductivity (λ_e) and apparent volumetric heat capacity (C_a) are calculated as:

$$\lambda_e = \lambda_s^{\theta_s} \lambda_w^{\theta_w} \lambda_i^{\theta_i} \quad (5.3)$$

$$C_a = \theta_s \rho_s c_s + \theta_w \rho_w c_w + \theta_i \rho_i c_i + Lw\rho_d(\partial Wu/\partial T) \quad (5.4)$$

where λ, ρ and c represent the thermal conductivity, density, and specific heat, respectively; the subscript s, w and i are used for soil particles, water, and ice, respectively; L is the latent heat of water, ρ_d is the dry density of soil (Nixon 1983; Colt-KBR 2003; Côté and Konrad 2005).

d) Both unfrozen and frozen soils are modeled as frictional materials using the Mohr–Coulomb failure criterion. The mechanical properties are represented by a subscript "f" for the frozen and without it for the unfrozen soils. The cohesion of frozen soil (c_f) increases with increasing volumetric ice fraction and decreasing temperature. The effect is more significant at higher ice fractions and lower temperatures (Arenson and Springman 2005). In this study, c_f is expressed as:

$$c_f \text{ (kPa)} = c(1 + \alpha\theta_i)\,|T|^{0.5} \quad (5.5)$$

where $|T|^{0.5}$ represents the temperature's effect on cohesion; α is the rate of increase of c_f with θ_i, and c is the cohesion of unfrozen soil. The friction angle of frozen soil (ϕ_f) is decreased from the unfrozen value (ϕ) to zero for pure ice as $\phi_f = \phi(1 - \theta_i^{2.6})$ (Arenson and Springman 2005). The dilatancy has some influence on stress–strain behaviour of highly frost susceptible unfrozen silts and clayey silts, even for the frozen state at a low ice fraction (Nishimura et al. 2009; Dayarathne

and Hawlader 2015). Therefore, a dilation angle of 5° is used for both unfrozen (ψ) and frozen (ψ_f) soils.

e) For the seasonal ground surface temperature variation, the positive summer temperature could thaw some frozen soil. The thawing of pore ice reduces the volume of the soil. The isotropic volume change due to pore ice thawing is modeled as a reverse process of volume change due to pore water freezing (see Eq. (5.2)), although it is understood that the pore ice thawing with temperature increase is different from pore water freezing (Patterson and Smith 1981; Oliphant et al. 1983; Zhu 2006).

The thawing of an ice lens could generate excess pore water pressure near the thaw front. It is assumed that the excess pore water pressure dissipates completely to the nearby unfrozen soil because the thaw front retreat is a slow process, as discussed later. The volumetric strain due to thawing of segregated ice is $1.09\Delta\theta_{is}$, where $\Delta\theta_{is}$ is the decrease in the volume fraction of segregate ice. Unlike thawing of pure ice at 0 °C, the thawing of segregate ice in the soil is expected to occur over a range of temperatures, and is defined as (Zhang 2014):

$$\theta_{is} = \frac{\theta_{is\_max}}{1 + e^{k(T - T_{50})}} \tag{5.6}$$

where θ_{is} is the current volumetric fraction of segregate ice; θ_{is_max} is the maximum θ_{is} prior to the start of thawing; k is a constant that defines the rate of thawing with temperature increase; T_{50} represents the temperature at the highest rate of thawing. In the present study, k = 5 and T_{50} = +1 °C is used. In the FE program, implementing thawing over a temperature range reduces some numerical issues. The maximum value of the volumetric fraction of segregated ice during freezing is recorded as a state variable (θ_{is_max}), which is then used to calculate $\Delta\theta_{is}$ based on two temperatures at the start and end of a time increment, using Eq. (5.6). Finally, the calculated volumetric strain is assigned to that soil element anisotropically using the UEXPAN subroutine.

5.6 Results

The performance of the present FE modeling and its verification using the Calgary full-scale test have been discussed in chapter 4. In the following sections, the effects of some key parameters on the frost heave of chilled gas pipelines are shown. The analyses are performed by varying one parameter while the other parameters are kept constant, as listed in Table 5.1 unless otherwise mentioned. FE simulations are performed for two burial depths: H = 1.4 m and H =2.3 m, which are called “shallow burial” and “deep burial” sections, respectively.

5.6.1 Ground surface and initial ground temperature

The ground temperature varies with many factors, including local weather conditions, geographical location, elevation, ground surface condition (e.g., vegetation, snow cover), geological conditions and depth. For example, the mean annual ground temperatures of the unfrozen sections in the discontinuous permafrost zone of the proposed Mackenzie gas pipeline route vary between 0 °C and +2 °C, which is lower than the ground temperature in the Calgary full-scale tests (Konrad and Morgenstern 1984; Colt-KBR 2003).

The ground surface temperature (T_s) also depends on many local factors, including air temperature, snow cover, vegetation, wind velocity and solar radiation. Surface energy balance analysis could be performed for a better estimation of the ground surface temperature at a given location based on observed climate data (Colt-KBR 2003; Oswell and Nixon 2015). Another simplified way to estimate T_s is the use of the n-factor approach which multiplies the observed mean monthly air temperature by a site-specific factor (Goodrich and Gold 1981; Andersland and Ladanyi 2004), which is used in this study. Two types of ground surface temperature are used: a mean annual ground surface temperature ($T_s = T_{sm}$), and a seasonal ground surface temperature variation ($T_s = T_{sv}$). In one case (T_g = +5 °C), the air temperature in the proximity of the Calgary

full-scale experiment (at Calgary Airport) is obtained, which is multiplied by the *n*-factor and then fitted by a sinusoidal curve to obtain T_{sv} (Inset 2 of Fig. 5.2). The weighted average of this T_{sv} gives T_{sm} = +5 °C. To simulate a colder climate, this T_{sv} curve is shifted down by 3 °C, which gives T_{sm} = +2 °C. Similar to the Calgary full-scale tests, the simulation started in March, which is important for $T_s = T_{sv}$ cases. The long-term air temperature increase due to climate change is not considered.

The simulations are performed for a combination of two initial ground temperatures (T_g = +2 °C & +5 °C), two burial depths (H = 1.4 m & 2.3 m) and two types of ground surface temperatures (T_{sm} & T_{sv}). Frost heave and frost front penetration of these analyses are shown in Fig. 5.3. The dotted lines represent the simulations with seasonal ground surface temperatures, whereas solid lines are for the mean annual ground surface temperatures. To examine the role of the seasonal retreat and advancement of the frost bulb with seasonal ground surface temperatures, the two simulations are also performed for deep and shallow burial sections without the thawing effect (Eq. (5.6)). Following are the key observations from these analyses:

a) Heave increases significantly with an increase in initial ground temperature. For example, the calculated heave for the deep burial section after 10 years under a constant mean ground surface temperature is 0.54 m and 0.86 m for the ground temperature of +2 °C and +5 °C, respectively (Fig. 5.3(a)). The frost front penetrates more in the cases of lower ground temperature, which reduces the gradT_{ff} and *SP* due to the increased overburden stress and thereby the segregational heave.

b) For T_g = +2 °C, an increase in burial depth reduces the long-term heave. For example, heave is 0.89 m and 0.74 m after 20 years for the shallow and deep burial sections, respectively, with mean ground surface temperature. However, the long-term trend for the higher T_g and T_s (= +5 °C) is not the same because the effect of warming of the base of the final ice lens

(i.e., $dT/dt > 0$) is higher in the shallow burial section. This warming effects have been discussed in detail in chapter 4.

c) For the cases analyzed, the seasonal variation of ground surface temperature (T_{sv}) gives a lower long-term heave and higher frost front penetration than the heave obtained with T_{sm}, except for the long-term response of the shallow burial section ($t > 8.5$ years) with a higher T_g (= +5 °C). Moreover, the effects of ground surface temperature variation are more significant for a higher ground temperature and a lower burial depth.

d) If the thawing effect is not considered (see Eq. (5.6)) in the seasonal surface temperature variation cases, the frost heave might be overestimated.

Figures 5.4(a)–5.4(d) show the location of the frost front for the shallow and deep burial conditions for T_g = +5 °C under two different ground surface temperature definitions (T_{sv} and T_{sm}). The results are shown on the non-deformed geometry for the purpose of illustration at the maximum summer (Figs. 5.4(a) & 5.4(c)) and minimum winter (Figs. 5.4(b) & 5.4(d)) temperature conditions for the seasonal ground surface temperature variation case (see Inset 2 of Fig. 5.2). The corresponding frost front locations for $T_s = T_{sm}$ for the same time are also shown in these figures for comparison. The variation of frost bulb extents for the different ground surface temperatures and burial depths are also available in Videos S1–S4 in the supplemental data. A considerable thawing of the soil elements at the leading edge of the frost bulb at higher β occurs due to the positive summer temperature, especially for the shallow burial section and a higher ground temperature (Video S1).

As shown, the seasonal T_s alters the temperature distribution significantly near the ground surface up to the approximate level of the initial pipe invert position in the shallow burial case (Figs. 5.4(a) & 5.4(b)) and up to the initial springline level in the deep burial case (Figs. 5.4(c) &

5.4(d)). Below that, 0 °C isotherm locations for both surface temperature conditions follow closely during the first few years. However, the size of the frost bulb for the $T_s = T_{sv}$ case is larger than that of $T_s = T_{sm}$ in the later years, especially for the deep burial section. Therefore, the increased overburden pressure effect on *SP* and reduced temperature gradient, together with the thawing of the leading edge of the frost bulb at higher β_0, give a lower long-term heave for the seasonal T_s variation cases. A closer examination of the moisture content shows that the seasonal ground surface temperature variation reduces the ice growth at higher β as compared to that of mean T_s, especially for higher T_g. Therefore, the calculated heave for $T_s = T_{sv}$ case is less than that of $T_s = T_{sm}$ in Fig 5.3(a). A similar trend has been found for the shallow burial case for $t < 8.5$ years (Fig. 5.3(b)).

Equation (5.1) shows that the heave is directly proportional to temperature gradients (grad*T*). Figure 5.5 shows temperature gradients of typical soil elements with time at a radial distance $r_0 =$ 2.7 m from the pipe center and $\beta_0 = 0°$, 45° and 70°. The calculated grad*T* shows almost no oscillation in the simulation with the constant ground surface temperature (Fig. 5.5(a)); however, it oscillates when the seasonal surface temperature variation is given (Fig. 5.5(b)). The oscillation in grad*T* is more in the soil elements closer to the ground surface (i.e., larger β_0); however, it has less influence on calculated heave and shows a small amount of oscillation (Figs. 5.3(a) & 5.3(b)).

In the following sections, all the simulations are performed for the deep burial condition with a constant mean annual ground surface temperature.

5.6.2 Segregation-freezing temperature

The migrated water forms ice lenses at the segregation freezing temperature (T_{sf}), which varies between -0.8 °C and -0.1 °C (lower values are for finer materials) (Konrad and Shen 1996). Konrad and Morgenstern (1984) assumed that the freezing of migrated water occurs at 0 °C. Based

on the calculation of gradT_{ff} from the fitted temperature distribution line near 0 °C and the SP-model, Nixon (1986) and Colt-KBR (2003) calculated a significant increase in heave with lowering T_{sf}. In the present study, gradT_{ff} is calculated based on heat flux and the resulting volumetric expansion due to freezing of migrated water is distributed over the thickness of the frozen fringe, defined by T_{sf} and the in-situ freezing temperature T_f (= 0 °C) isotherms (t_{ff} in Fig. 5.1). The effects of T_{sf} (i.e., frozen fringe thickness) on frost heave calculations for different T_g (= +2 °C & +5 °C) are shown in Fig. 5.6. Figure 5.6(a) shows no significant variation in calculated heave and frost front penetration with T_{sf} = -1 °C to -0.3 °C for the initial ground temperature of +5 °C. However, if a very small value of T_{sf} (= -0.1 °C) is used, a very different heave and frost front penetration are calculated because a sufficient number of elements do not exist within the frozen fringe in this case, especially at the initial stage of freezing (t < 5 years), when the thickness of the frozen fringe is small. When the volumetric expansion due to migrated water occurs within such a relatively thin frozen fringe, significant mesh distortion might occur, especially in the long-term simulation when the frost front does not penetrate significantly with time.

Figure 5.6(b), however, shows that the calculated heave significantly increases with a decrease in T_{sf} for the initial ground temperature of +2 °C in contrast to T_g = +5 °C, although the frost front penetration shows no significant difference, which can be explained by the temperature distribution. Figure 5.7 shows the calculated temperature variation directly below the pipe center for t = 1 years and t = 5 years with T_{sf} = -1 °C. The slope of temperature versus depth line (i.e., temperature gradient) near 0 °C (within the frozen fringe) is smaller for T_g = +2 °C than that of +5 °C, which reiterates that heave increases significantly with an increase in initial ground temperature (compare Figs. 5.6(a) and 5.6(b)). In the case of T_g = +2 °C, the temperature gradient in the frozen fringe considerably decreases with an increase in temperature with depth, whereas

no such variation is found in the case of T_g = +5 °C. In other words, $gradT_{ff}$ is not very sensitive to T_{sf} for a higher value of T_g; therefore, less effect of T_{sf} on heave is found (Fig. 5.6(a)). An increase in heave with a decrease in T_{sf} has also been reported in previous studies (Nixon 1986; Colt-KBR 2003). In summary, T_{sf} affects the calculated heave for a lower ground temperature; however, the effects are not significant for a higher ground temperature.

5.6.3 Stress effect on segregation potential

The stress effect on frost heave is defined by a reduction factor, e^{-ap_e} (Eq. (5.1)). Several 1-D and 2-D analyses used p_e equal to the initial effective overburden pressure at the base of the frost front (σ_{ov}) to calculate the heave using the SP-model (Konrad and Morgenstern 1984; Nixon 1986; Colt-KBR 2003; Kim 2011). Carlson and Nixon (1988) used the vertical stress at the base of the frost bulb, considering the weight of the soil and shear resistance along the two inclined surfaces of the uplifted soil wedge. The first stress invariant was also used to reduce the porosity rate (a parameter similar to *SP*) with stress (Michalowski 1993; Michalowski and Zhu 2006; Zhang and Michalowski 2013a, b). Konrad and Shen (1996) replaced p_e with the normal stress acting on the frost front in their 2-D FE simulation.

Figures 5.8(a) and 5.8(b) show the calculated heave for three different approaches of modeling p_e but with the same value of a (= 9.5) for two ground temperatures (i.e., T_g = +2 °C and +5 °C). The calculated heave with the effective mean stress (p) and normal stress (σ_n) is smaller than that of the effective overburden pressure (σ_{ov}). For the cases analyzed here, no significant difference in heave is found when the stress effect on *SP* is calculated based on the mean and normal stresses. Figures 5.9(a) and 5.9(b) show σ_n/σ_{ov} and p/σ_{ov} within the frozen fringe in the simulation with $p_e = \sigma_{ov}$ at t = 4 years and T_g = +5 °C. The values of σ_n/σ_{ov} and p/σ_{ov} greater than 1.0 indicate the higher reduction of *SP* in the simulations with $p_e = p$ and $p_e = \sigma_n$, which reduces

the segregational heave. Therefore, although p and σ_n might incorporate the effects of additional stress components on water migration, the parameter a (see Eq. (5.1)) might be different from that obtained from one-dimensional laboratory frost heave tests. Figures 5.8(a) and 5.8(b) show approximately 15% and 25% smaller heave at 20 years for $p_e = \sigma_n$ than that of $p_e = \sigma_{ov}$, respectively, which implies that appropriate stress needs to be considered in the two-dimensional analysis.

Using $p_e = \sigma_n$ and a bilinear stress–strain relationship for frozen soil, Konrad and Shen (1996) showed a higher moisture content (in-situ plus migrated) around $\beta_0 = 45°$ at the end of their simulation (t = 4.1 years). In the present FE modeling with $p_e = \sigma_n$, a similar trend is found during the progress of freezing (Video S5), which is because of the combined effects of stress-dependent SP values and temperature gradient; however, after a long-term simulation (e.g., t = 20 years), the present analysis shows higher moisture content in the soil elements at β_0 = 0–40°. A considerable moisture content increase also occurs in the soil elements at β_0 = 70°–90° because the frost penetration is negligible in this range of β_0 after t ~5 years but the moisture migration continues over the whole period. Note that moisture growth in these elements does not have a significant effect on pipe heave.

The *SP* reduction parameter (a) decreases with increasing clay content. For example, Jessberger and Jagow (1989) reported a of 10–18 MPa^{-1} and 0–6 MPa^{-1} for clay fractions of <1% and 50%, respectively. A trend of increasing a with average grain size (d_{50}) was also reported (Konrad 1999, 2005). To show the effect of this parameter, two more analyses were performed for a = 5 and 15 MPa^{-1} with $p_e = \sigma_{ov}$ for a ground temperature of +2 °C with the same SP_0 (= 230×10^{-5} $mm^2/(°C.s)$ (Fig. 5.8(a)). The heave increased significantly with decreasing this parameter. Note, however, that not only the parameter a, but also SP_0, changes with soil type—for example, Konrad

(1999) showed that Fairbanks silt has a significantly lower SP_0 and higher a than that of Calgary silt. The effect of this parameter (SP_0) is discussed further in the following section.

Generally, the stress effect on SP is obtained from one-dimensional laboratory frost heave tests where the specimen is laterally restrained, and the expansion is possible only in the axial direction (Konrad 1980; Konrad and Morgenstern 1982). This system might be improved further for triaxial loading conditions maintaining constant lateral stress, as attempted in some previous studies (Ryu et al. 2016; Amanuma et al. 2017), which might give different SP_0 and a values.

Carlson and Nixon (1988) reported horizontal ice lens orientation in the Calgary full-scale test, which was thought to be due to the variation of local stratigraphy. Therefore, the overburden pressure could be used to define the stress-dependency of SP unless the dependency on other stress components is examined with advanced laboratory tests and a suitable mathematical model is developed.

5.6.4 Segregation potential with zero applied pressure (SP_0)

Konrad (1999) reported a wide range of SP_0 of 60×10^{-5} to 500×10^{-5} mm^2/(s.°C) for different soils depending upon d_{50}, moisture content, liquid limit and specific surface area. A wide range of SP was also used to assess the free-field frost heave of the proposed Mackenzie Gas pipeline (Colt-KBR 2003). Figures 5.10(a) and 5.10(b) show the calculated heave and frost front penetration for different values of SP_0. Heave increases with SP_0; however, it is not simply proportional to SP_0 because other factors such as stress effects on SP, resistance to the upward movement of the frozen bulb and temperature boundary effects influence the heave. Figure 5.10(a) shows a continuous increase in heave with time; however, Fig. 5.10(b) shows a significant drop in heave rate after a period of freezing (e.g., after 10 years for $SP_0 = 300\times10^{-5}$ mm^2/(s.°C)). This is due to the warming of the base of the frost bulb for a higher ground temperature when the pipe moves sufficiently far

from the final ice lens and the frost front does not penetrate further. Previous coupled FE analyses did not report this phenomenon because the simulations have been performed for a shorter period.

5.6.5 Shear strength of frozen soil

An increase in cohesion (c) and decrease in friction angle (ϕ) with an increase in volumetric ice fraction (θ_i) were observed in experimental studies, where θ_i have more significant effects on c than ϕ. For example, Arenson and Springman (2005) found c > 240 kPa for frozen granular soils with θ_i > 66%; however, c is zero for the same soil upon thawing. For highly frost susceptible clayey silt, a small value of c at the unfrozen state (c = 10 kPa) is used in the present study. For frozen soil, c is increased with volumetric ice fraction by a factor α (see Eq. (5.5)). Figures 5.11(a) and 5.11(b) show that the heave decreases with an increase in α for both initial ground temperatures (T_g = +2 °C & +5 °C). A closer examination of the displacement of the soil elements shows that a larger wedge of soil moves up when a larger value of α is used because of the increase in shear strength of frozen soil, especially in the elements near the frozen fringe. However, a negligible difference in calculated heave is found when a large value of α (= 17.5 or 40) is used because the frozen soil is strong in this case and most of the soil elements are within the elastic limit.

The shape of the frost heave curves is different in Figs. 5.11(a) and 5.11(b). Larger heave occurs for a higher ground temperature and a lower shear strength (e.g., T_g = +5 °C and α = 0.1), which moves the pipe further up, resulting in warming of the bottom of the frost bulb that decreases the rate of heave significantly after 10 years (Fig. 5.11(b)). However, for T_g = +2 °C, the heave and frost front penetration continue without a significant decrease in rate, even after 10 years.

Figures 5.11(a) and 5.11(b) show no significant change in frost front penetration under the pipeline due to the variation in frozen soil properties. However, the calculated heave is very different depending upon frozen soil strength. For example, at t = 20 years, heave is 0.65 and 0.85 m for α = 0.1 and α = 40, respectively when T_g = +2 °C. Using a bilinear model for frozen soil, Konrad and Shen (1996) also showed that a higher slope of the post-yield stress–strain curve for frozen soils reduces the heave.

The current numerical simulations clearly show the importance of the frozen soil model to predict frost heave. The pure elastic behaviour of frozen soil might significantly underpredict the heave. The Mohr–Coulomb model can simulate the process better; however, the soil parameters, especially cohesion, should be selected for a low strain rate because the frost heave is a slow process. Analyses are also performed for varying unfrozen soil properties; however, no significant effect on heave is found.

5.6.6 Pipe temperature

The mean annual gas temperature might vary with discharge temperature and the distance from the compressor station in the downstream direction. Figures 5.12(a) & 5.12(b) show that the frost front penetration (Y_0) increases with a decrease in T_p and initial ground temperature (T_g). For T_g = +5 °C, the rate of frost front penetration is almost negligible after some period of freezing. The time required to reach the maximum Y_0 increases with decreasing pipe temperature. For example, frost penetration almost stops at t ~ 4.5 years for T_p = -5 °C while the penetration continues until ~15 years for T_p = -10 °C (see Fig. 5.12(b)). However, for a lower T_g (= +2 °C), the frost penetration does not stop and penetrates to a large depth (e.g., Y_0 ~ 8 m at t = 20 years for T_p = -10 °C).

Figure 5.12(a) shows that the heave rate is higher for a lower pipe temperature initially because of the higher temperature gradient in the frozen fringe while the other conditions are almost the same. However, the long-term heave rate depends on the depth of the frost front. For a higher pipe temperature (T_p = -3 °C), frost front penetration does not occur after t = 12 years. However, continued heaving moves the pipe up which results in warming of the base of the frost bulb ($dT/dt > 0$) which reduces the heave rate significantly. For pipe temperatures of -10 °C to -5 °C, the frost front penetration is continued without warming; therefore, the heaving continues. Lowering pipe temperature increases the depth of the frost front, which reduces *SP*, due to an increase in overburden pressure in the frozen fringe. Therefore, the long-term heave rate is less for T_p = -10 °C than T_p = -5 °C.

For T_g = +5 °C, no significant difference in heave for different T_p is found for the first 5 years (Fig. 5.12(b)). A lower pipe temperature increases the depth of the frost front, which increases the heave due to in-situ water freezing, but reduces the *SP*, due to the increase in p_e. These two compensating effects, together with the change in gradT_{ff}, give almost the same heave up to 5 years. When the frost front becomes almost stable after 5 years, the rate of heave is higher for a lower pipe temperature.

A significant increase in heave with decreasing T_p, even at the initial period of freezing, was found by Konrad and Morgenstern (1984) based on radial heat transfer analysis for T_g = +2 °C. However, the calculation with the modified Nixon's geothermal simulator showed a small increase in heave with decreasing T_p (Colt-KBR 2003). The present FE analyses show a small effect of T_p (i.e., gas temperature) on heave for a lower T_g (Fig. 5.12(a)) but a significant long-term effect for a higher T_g (Fig. 5.12(b)).

5.7 Conclusions

Coupled thermomechanical FE simulations of frost heave of chilled gas pipelines are presented; the moisture migration is modeled using the Konrad-Morgenstern segregation potential approach. The analyses are performed for a range of soil properties, burial depths, and thermal boundary conditions, as expected in the field. The underlying effects of various factors on the resultant heave are discussed. With a close examination of the FE results, the following conclusions can be drawn for the range of soil proprieties and other conditions considered in this study.

a) Frost heave increases with the initial ground temperature (T_g). For a lower T_g, the long-term heave increases with a decrease in burial depth; however, the trend is different for higher T_g because of the warming of the front part of the frozen bulb.

b) Seasonal ground surface temperature variation gives a lower long-term heave than that with a mean ground surface temperature. The effect is more significant for a higher ground temperature and a lower burial depth.

c) Segregation-freezing temperature T_{sf} does not have a significant effect on heave for a higher T_g; however, the heave increases with decreasing T_{sf} for a lower T_g.

d) Modeling stress effects on *SP* using the effective overburden pressure gives 15%–25% more heave than that obtained with effective mean stress and normal stress on the frost front. The parameters for *SP* reduction with stress (a) might be different from those obtained from the one-dimensional frost heave test.

e) An increase in cohesion of the frozen soil decreases the heave; however, the unfrozen soil properties do not have a significant effect.

f) Chilled gas temperature between -10 °C and -5 °C does not have a significant effect on frost heave for a lower T_g; however, the lower gas temperature increases the long-term heave for a higher T_g.

Acknowledgements

The works presented in this chapter have been supported by the InnovateNL, formerly Research Development Corporation (RDC), Newfoundland and Labrador, through the ArcticTECH program, Equinor Research Chair, and Natural Sciences and Engineering Research Council of Canada.

List of symbols

The following symbols are used in this chapter:

a = soil constant;

C_a = apparent volumetric heat capacity of soil;

c = cohesion of unfrozen soil;

c_f = cohesion of frozen soil;

c_i = specific heat of ice;

c_s = specific heat of soil particle;

c_w = specific heat of water;

D = pipe diameter;

E = Young's modulus of unfrozen soil;

E_f = Young's modulus of frozen soil;

$gradT$ = temperature gradient;

$gradT_{ff}$ = temperature gradient in frozen fringe;

H = burial depth;

h = frost heave;

k = constant for thawing with temperature increase;

L = latent heat of water;

n = porosity;

P = percentage of total water content that remains unfrozen well below 0 °C;

P_e = stress parameter for segregation potential;

p = effective mean stress;

Q = factor controls unfrozen water content with temperature;

q = heat flux;

q_x, q_y = heat flux in x and y-direction;

R = parameter related to P;

r = radial distance from current pipe center;

r_0 = radial distance from initial pipe center;

SP_0 = segregation potential at zero applied pressure;

T = temperature;

T_f = in-situ freezing temperature;

T_g = initial ground temperature;

T_p = pipe temperature;

T_s = ground surface temperature;

T_{sf} = segregation freezing temperature;

T_{sm} = mean annual ground surface temperature;

T_{sv} = seasonal ground surface temperature;

T_{50} = temperature at the highest rate of thawing;

t = time;

t_{ff} = thickness of frozen fringe;

v_m = migrated water influx;

W_u = fraction of total water that remains unfrozen;

w_u = unfrozen water content basis of the dry mass of soil;

w_0 = soil water content basis of the dry mass of soil before freezing;

x, x_0 = horizontal distance measured from pipe center;

Y_0 = depth of frost front from initial pipe invert position;

y = vertical distance measured from current pipe center;

y_0 = vertical distance measured from initial pipe center;

α = rate of increase of cohesion of frozen soil with ice content;

β = angle from y-axis to a point with respect to current pipe center;

β_0 = angle from y-axis to a point with respect to initial pipe center;

θ_i = volumetric fraction of ice;

θ_{is} = volumetric fraction of segregated ice;

θ_{is_max} = maximum volumetric fraction of segregate ice lens prior to start of thawing;

θ_s = volumetric fraction of soil particle;

θ_w = volumetric fraction of unfrozen water;

λ_e = equivalent thermal conductivity of soil;

λ_i = thermal conductivity of ice;

λ_s = thermal conductivity of soil particle;

λ_w = thermal conductivity of water;

v = Poisson's ratio of unfrozen soil;

v_f = Poisson's ratio of frozen soil;

ρ_d = dry density of soil;

ρ_i = density of ice;

ρ_s = density of soil particle;

ρ_w = density of water;

σ_n = effective normal stress;

σ_{ov} = effective overburden pressure;

ϕ = angle of internal friction of unfrozen soil;

ϕ_f = angle of internal friction of frozen soil;

φ = direction of heat flux with respect to y-axis;

ψ = dilation angle of unfrozen soil; and

ψ_f = dilation angle of frozen soil.

References

Abaqus. 2014. *Abaqus documentation*. 6.14. Providence, USA: Dassault Systemes.

Amanuma, C., T. Kanauchi, S. Akagawa, Z. Hao, and S. Kanie. 2017. "Evaluation of frost heave pressure characteristics in transverse direction to heat flow." *Procedia Eng.* 171: 461–468.

Andersland, O. B., and B. Ladanyi. 2004. *Frozen ground engineering.* New Jersey, USA: John Wiley and Sons.

Arenson, L. U., and S. M. Springman. 2005. "Mathematical descriptions for the behaviour of ice-rich frozen soils at temperatures close to 0 °C." *Can. Geotech. J.* 42 (2): 431–442.

Arenson, L. U., S. M. Springman, and D. C. Sego. 2007. “The rheology of frozen soils.” *Applied Rheology* 17 (1): 12147-1–12147-14.

Carlson, L. E., J. R. Ellwood, J. F. Nixon, and W. A. Slusarchuk. 1982. “Field test results of operating a chilled, buried pipeline in unfrozen ground.” In *Proc. 4th Can. Permafrost Conf.* edited by H. French, 2–6. Calgary, Alberta: National Research Council of Canada.

Carlson, L. E., and J. F. Nixon. 1988. “Subsoil investigation of ice lensing at the Calgary, Canada, frost heave test facility.” *Can. Geotech. J.* 25 (2): 307–319.

Colt-KBR (Colt Engineering Corporation and Kellogg Brown & Root). 2003. *Conceptual geotechnical/geothermal design basis.* WP-005-D1-2, Rev. B. Calgary, Alberta, Canada: Colt Engineering Corporation and Kellogg Brown & Root.

Côté, J., and J.-M. Konrad. 2005. “A generalized thermal conductivity model for soils and construction materials.” *Can. Geotech. J.* 42 (2): 443–458.

Dallimore, S. R. 1985. “Observations and predictions of frost heave around a chilled pipeline.” M.A. thesis, Department of Geography, Carleton University.

Dayarathne, R. S., and B. C. Hawlader. 2015. “Stress–strain behaviour of a clayey silt in triaxial tests.” In *Proc. 68th Can. Geotech. Conf.* p6. Quebec, Canada.

Dumais, S., and J.-M. Konrad. 2018. “One-dimensional large-strain thaw consolidation using nonlinear effective stress–void ratio–hydraulic conductivity relationships.” *Can. Geotech. J.* 55 (3): 414–426.

Farouki, O. T. 1981a. “The thermal properties of soils in cold regions.” *Cold Reg. Sci. Tech.* 5 (1): 67–75.

Farouki, O. T. 1981b. *Thermal properties of soils*. CRREL-Monograph-81-1. Hanover, New Hampshire, USA: US Army Corps of Engineers.

Ghoreishian Amiri, S. A., G. Grimstad, M. Kadivar, and S. Nordal. 2016. “Constitutive model for rate-independent behavior of saturated frozen soils.” *Can. Geotech. J.* 53 (10): 1646–1657.

Goodrich, L. E., and L. W. Gold. 1981. *Permafrost Engineering Design and Construction*: *Ground thermal analysis*, 149–172. New York: John Wiley & Sons.

Guymon, G. L., T. V. Hromadka, and R. L. Berg. 1984. “Two-Dimensional Model of Coupled Heat and Moisture Transport in Frost-Heaving Soils.” *ASME. J. Energy Resour. Technol.* 106 (3): 336–343.

Hawlader, B. C., V. Morgan, and J. I. Clark. 2006. “Modelling of pipeline under differential frost heave considering post-peak reduction of uplift resistance in frozen soil.” *Can. Geotech. J.* 43 (3): 282–293.

Huang, S. L., M. T. Bray, S. Akagawa, and M. Fukuda. 2004. “Field investigation of soil heave by a large diameter chilled gas pipeline experiment, Fairbanks, Alaska.” *J. Cold Reg. Eng.* 18 (1): 2–34.

Jessberger, H. L., and R. Jagow. 1989. “Determination of frost susceptibility of soils.” In *Proc. VTT Symp. 95,* 449–469. Saariselka, Finland: VTT Information Service.

Johansen, O. 1975. “Thermal conductivity of softs.” Ph.D. thesis, University of Trondheim, Trondheim, Norway.

Kim, K. 2011. “Multi-dimensional frost heave modeling with SP porosity growth function.” Ph.D. thesis, Department of Civil and Environmental Engineering, University of Alaska Fairbanks.

Konrad, J.-M. 1980. “Frost heave mechanics.” Ph.D. thesis, Department of Civil Eng., The University of Alberta, Canada.

Konrad, J.-M. 1999. “Frost susceptibility related to soil index properties.” *Can. Geotech. J.* 36 (3): 403–417.

Konrad, J.-M. 2005. “Estimation of the segregation potential of fine-grained soils using the frost heave response of two reference soils.” *Can. Geotech. J.* 42 (1): 38–50.

Konrad, J.-M., and N. R. Morgenstern. 1980. “A mechanistic theory of ice lens formation in fine-grained soils.” *Can. Geotech. J.* 17 (4): 473–486.

Konrad, J.-M., and N. R. Morgenstern. 1981. “The segregation potential of a freezing soil.” *Can. Geotech. J.* 18 (4): 482–491.

Konrad, J.-M., and N. R. Morgenstern. 1982. “Effects of applied pressure on freezing soils.” *Can. Geotech. J.* 19 (4): 494–505.

Konrad, J.-M., and N. R. Morgenstern. 1984. “Frost heave prediction of chilled pipelines buried in unfrozen soils.” *Can. Geotech. J.* 21 (1): 100–115.

Konrad, J.-M., and M. Shen. 1996. “2-D frost action modeling using the segregation potential of soils.” *Cold Reg. Sci. Tech.* 24 (3): 263–278.

Michalowski, R. L. 1993. “A constitutive model of saturated soils for frost heave simulations.” *Cold Reg. Sci. Tech.* 22 (1): 47–63.

Michalowski, R. L., and M. Zhu. 2006. “Frost heave modelling using porosity rate function.” *Int. J. Numer. Anal. Meth. Geomech.* 30 (8): 703–722.

Morgan, V., J. Clark, B. Hawlader, and J. Zhou. 2004. “Prediction of long-term frost heave of chilled gas pipelines by centrifuge modeling.” In *Proc. 5th Int. Pipeline Conf.* 2429–2435. Calgary, Alberta, Canada.

Morgan, V., B. Hawlader, and J. Zhou. 2006. “Mitigation of frost heave of chilled gas pipelines using temperature cycling.” In *Proc. 6th Int. Pipeline Conf.* 927–931. Calgary, Alberta, Canada.

Nishimura, S., A. Gens, S. Olivella, and R. J. Jardine. 2009. “THM-coupled finite element analysis of frozen soil: formulation and application.” *Géotechnique* 59 (3): 159–171.

Nixon, J. F. 1975. “The role of convective heat transport in the thawing of frozen soils.” *Can. Geotech. J.* 12 (3): 425–429.

Nixon, J. F. 1983. “Practical applications of a versatile geothermal simulator.” *J. Energy Res. Tech.* 105 (4): 442–447.

Nixon, J. F. 1986. “Pipeline frost heave predictions using a 2-D thermal model.” *ASCE Research on Transportation Facilities in Cold Regions* 67–82: ASCE.

Nixon, J. F. 1992. “Discrete ice lens theory for frost heave beneath pipelines.” *Can. Geotech. J.* 29 (3): 487–497.

Nixon, J. D., R. Saunders, and J. Smith. 1991. “Permafrost and thermal interfaces from Norman Wells pipeline ditchwall logs.” *Can. Geotech. J.* 28 (5): 738–745.

Oliphant, J. L., A. R. Tice, and Y. Nakano. 1983. “Water migration due to a temperature gradient in frozen soil.” In *Proc. 4th Int. Permafrost Conf.* 951–956. Fairbanks.

Oswell, J. M. 2011. “Pipelines in permafrost: geotechnical issues and lessons.” *Can. Geotech. J.* 48 (9): 1412–1431.

Oswell, J. M., and J. F. Nixon. 2015. “Thermal Design Considerations for Raised Structures on Permafrost.” *J. Cold Reg. Eng.* 29 (1): 04014010-1–04014010-13.

Patterson, D. E., and M. W. Smith. 1981. “The measurement of unfrozen water content by time domain reflectometry: Results from laboratory tests.” *Can. Geotech. J.* 18 (1): 131–144.

Phillips, R., J. I. Clark, and R. Hanke. 2001. “Centrifuge Modelling of Pipeline Frost Heave.” In *Proc. 54th Can. Geotech. Conf.,* Calgary: Canadian Geotechnical Society.

Phillips, R., J. I. Clarke, and R. Hanke. 2002. “Pipeline frost heave modelling.” In *Proc. Int. Conf. Physical Modelling in Geotechnics,* 313–318. St. John’s, Canada.

Piercey, G., N. Volkov, R. Phillips, and A. Zakeri. 2011. “Assessment of frost heave modelling of cold gas pipelines.” In *Proc. 2011 Pan-Am Geotech. Conf.,* 8p. Toronto, Canada.

Rajani, B., and N. Morgenstern. 1994. “Comparison of predicted and observed responses of pipeline to differential frost heave.” *Can. Geotech. J.* 31 (6): 803–816.

Ryu, B. H., H. W. Jin, and J. Lee. 2016. “Experimental study of frost heaving using temperature controlled triaxial cell.” *J. Korean Geoenv. Society* 17 (6): 23–31.

Selvadurai, A. P. S., J. Hu, and I. Konuk. 1999a. “Computational modelling of frost heave induced soil–pipeline interaction: I. Modelling of frost heave.” *Cold Reg. Sci. Tech.* 29 (3): 215–228.

Selvadurai, A. P. S., J. Hu, and I. Konuk. 1999b. “Computational modelling of frost heave induced soil–pipeline interaction: II. Modelling of experiments at the Caen test facility.” *Cold Reg. Sci. Tech.* 29 (3): 229–257.

Slusarchuk, W. A., J. I. Clark, J. F. Nixon, N. R. Morgenstern, and P. N. Gaskin. 1978. “Field test results of a chilled pipeline buried in unfrozen ground.” In *Proc. 3rd Int. Conf. Permafrost,* 878–883. Edmonton, Canada.

Thomas, H. R., P. Cleall, Y. C. Li, C. Harris, and M. Kern-Luetschg. 2009. “Modelling of cryogenic processes in permafrost and seasonally frozen soils.” *Géotechnique* 59 (3): 173–184.

Tiedje, E. 2015. “Characterization and numerical modelling of frost heave.” Ph.D. thesis, Department of Civil Engineering, McMaster University.

Zhang, Y. 2014. “Thermal-Hydro-Mechanical model for freezing and thawing of soils.” Ph.D. thesis, Department of Civil and Environmental Engineering, University of Michigan.

Zhang, Y., and R. L. Michalowski. 2013a. *Multi-Scale Process of soil Freezing, Thawing, and Thaw-Settlement*. Ann Arbor, Michigan: Michigan Univ. Regents Ann Arbor Div. of Research Development and Administration, U.S. Army Research Office.

Zhang, Y., and R. L. Michalowski. 2013b. “Thermal-mechanical constitutive modeling for freezing and thawing soils.” In *Proc. 10th Int. Symp. Cold Reg. Develop.* 256–267. Alaska.

Zhu, M. 2006. “Modeling and simulation of frost heave in frost-susceptible soils.” Ph.D. thesis, Department of Civil and Environmental Engineering, University of Michigan.

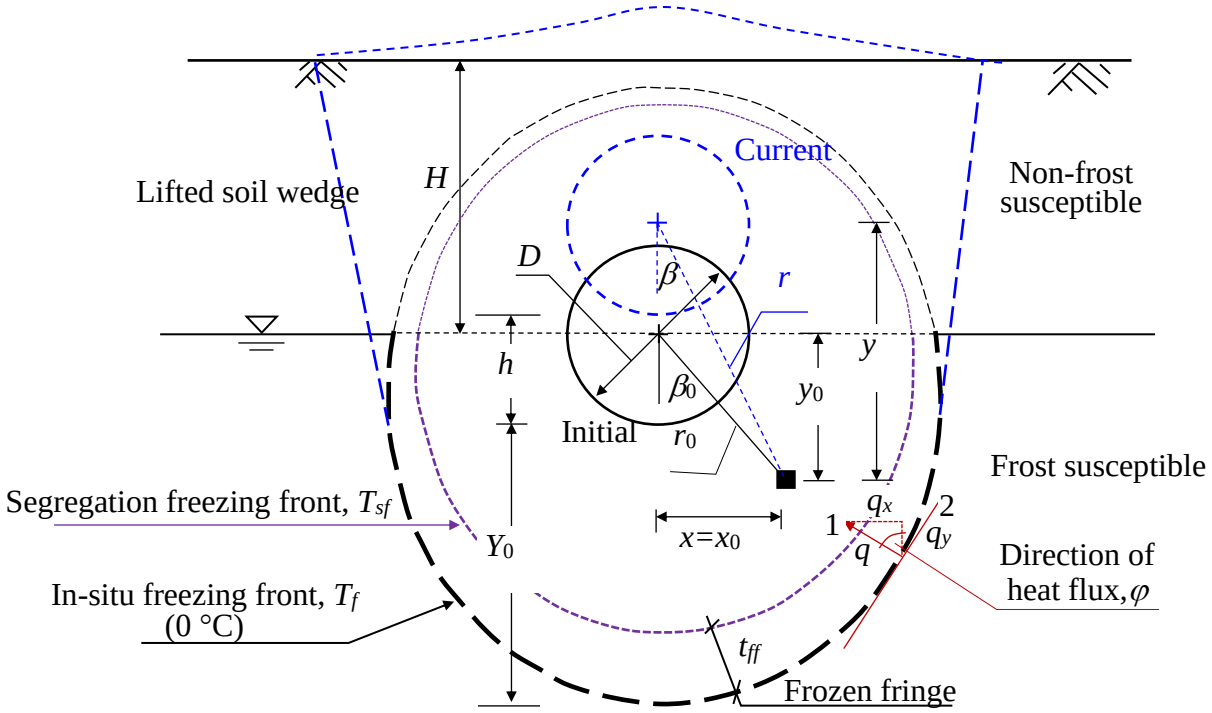

Fig. 5.1. Schematic of frost heave of a chilled gas pipeline buried in unfrozen soil

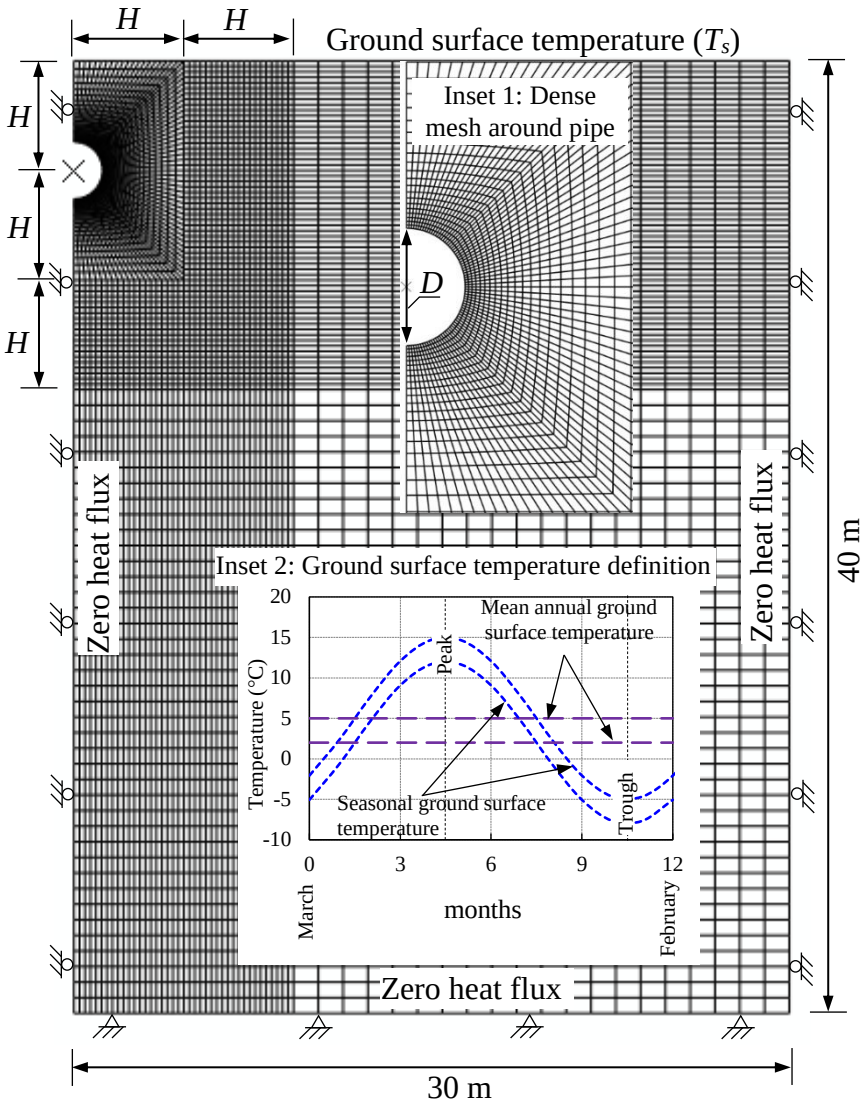

Fig. 5.2. Finite element mesh used in the analysis

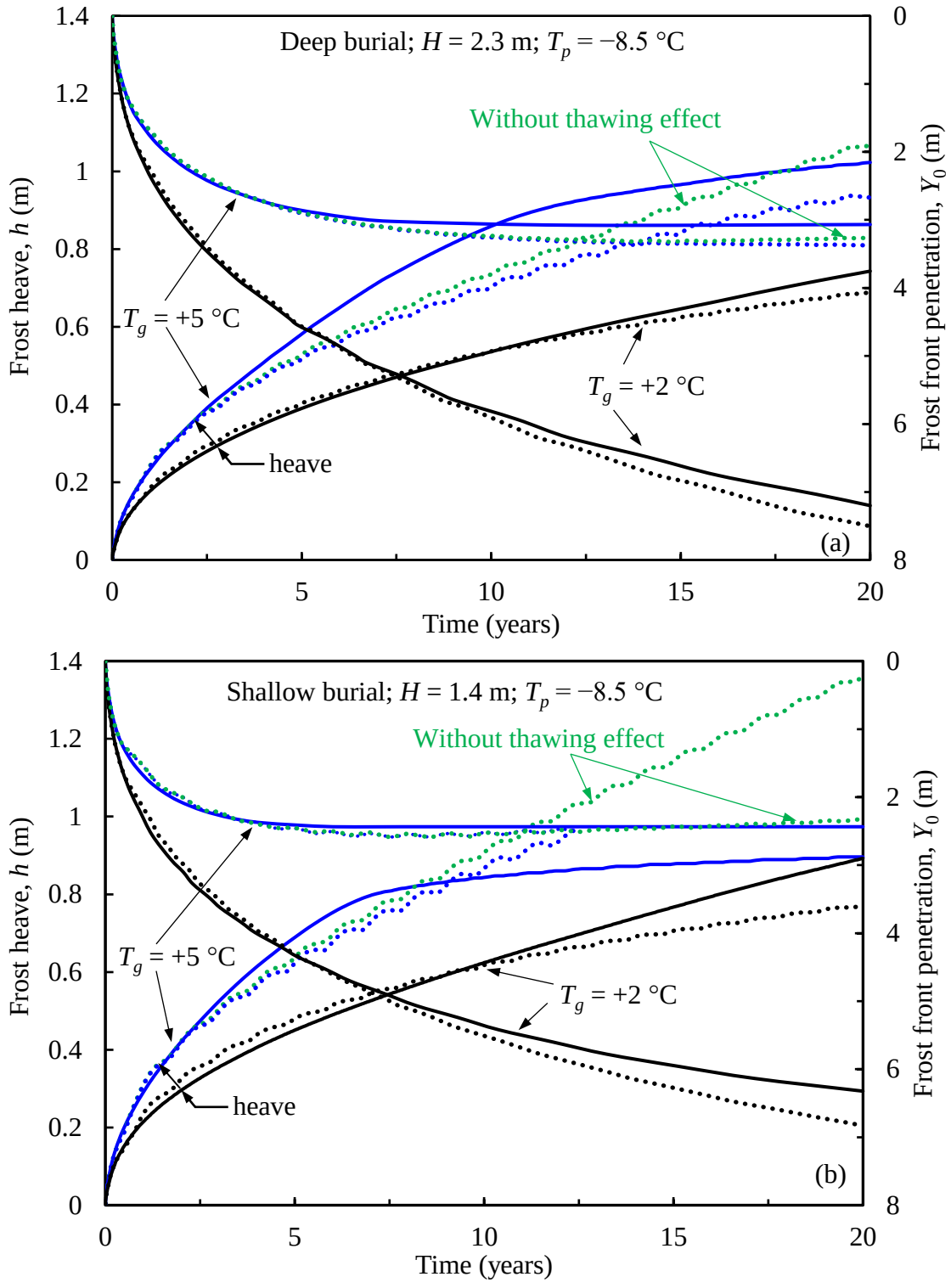

Fig. 5.3. Effect of initial ground temperature and ground surface temperature: (a) deep burial; and (b) shallow burial

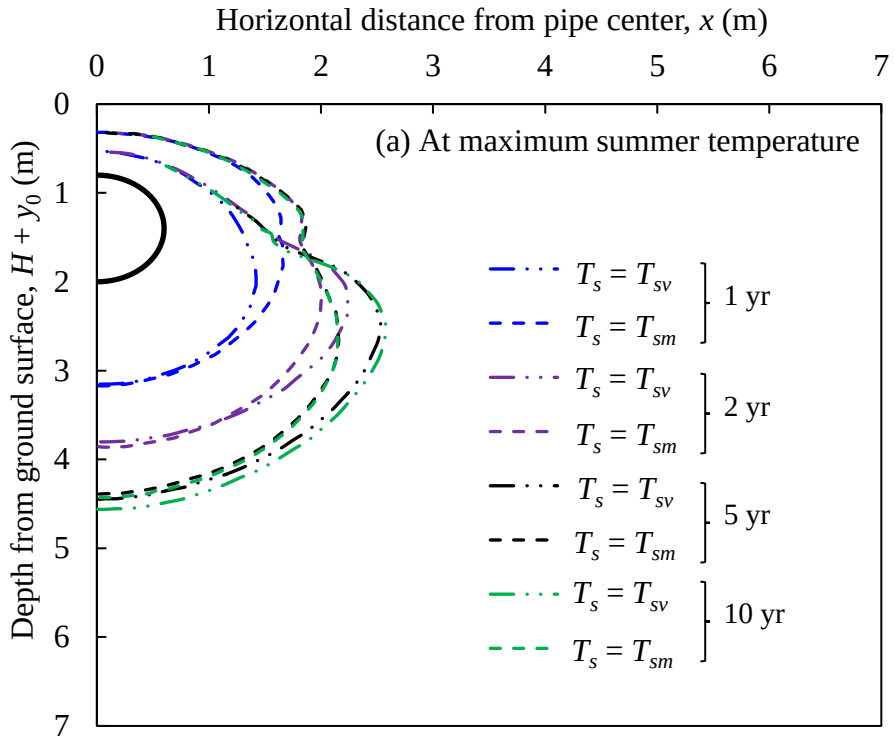
Horizontal distance from pipe center, x (m)
0
1
2
3
4
5
6
7
Depth from ground surface, H + y0 (m)
(a) At maximum summer temperature
Ts = Tsv
Ts = Tsm
1 yr
2 yr
5 yr
10 yr

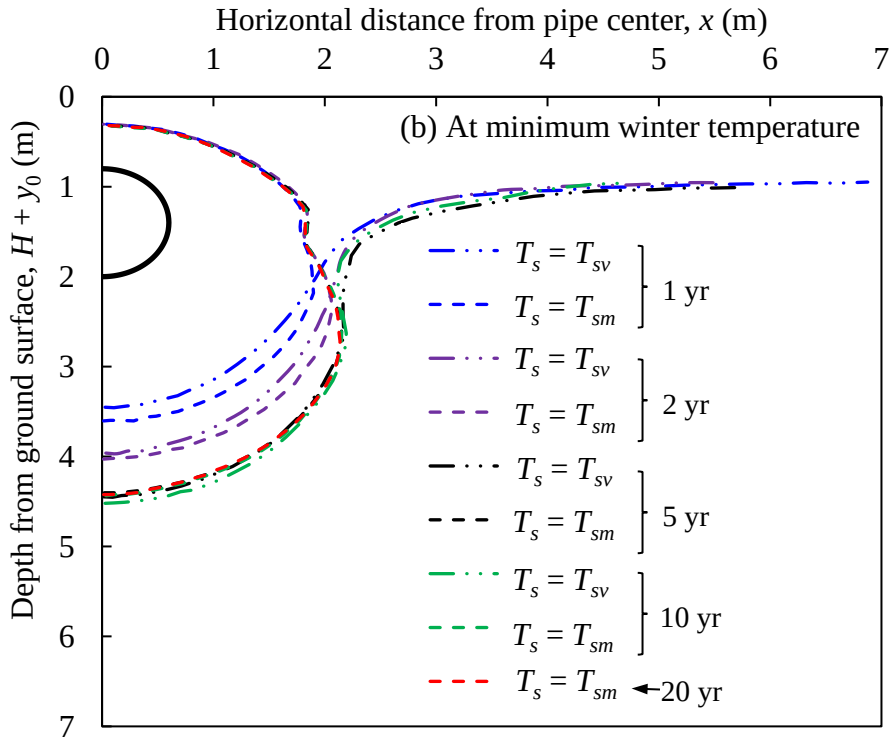
Horizontal distance from pipe center, x (m)
0
1
2
3
4
5
6
7
Depth from ground surface, H + y0 (m)
(b) At minimum winter temperature
Ts = Tsv
Ts = Tsm
1 yr
2 yr
5 yr
10 yr
20 yr

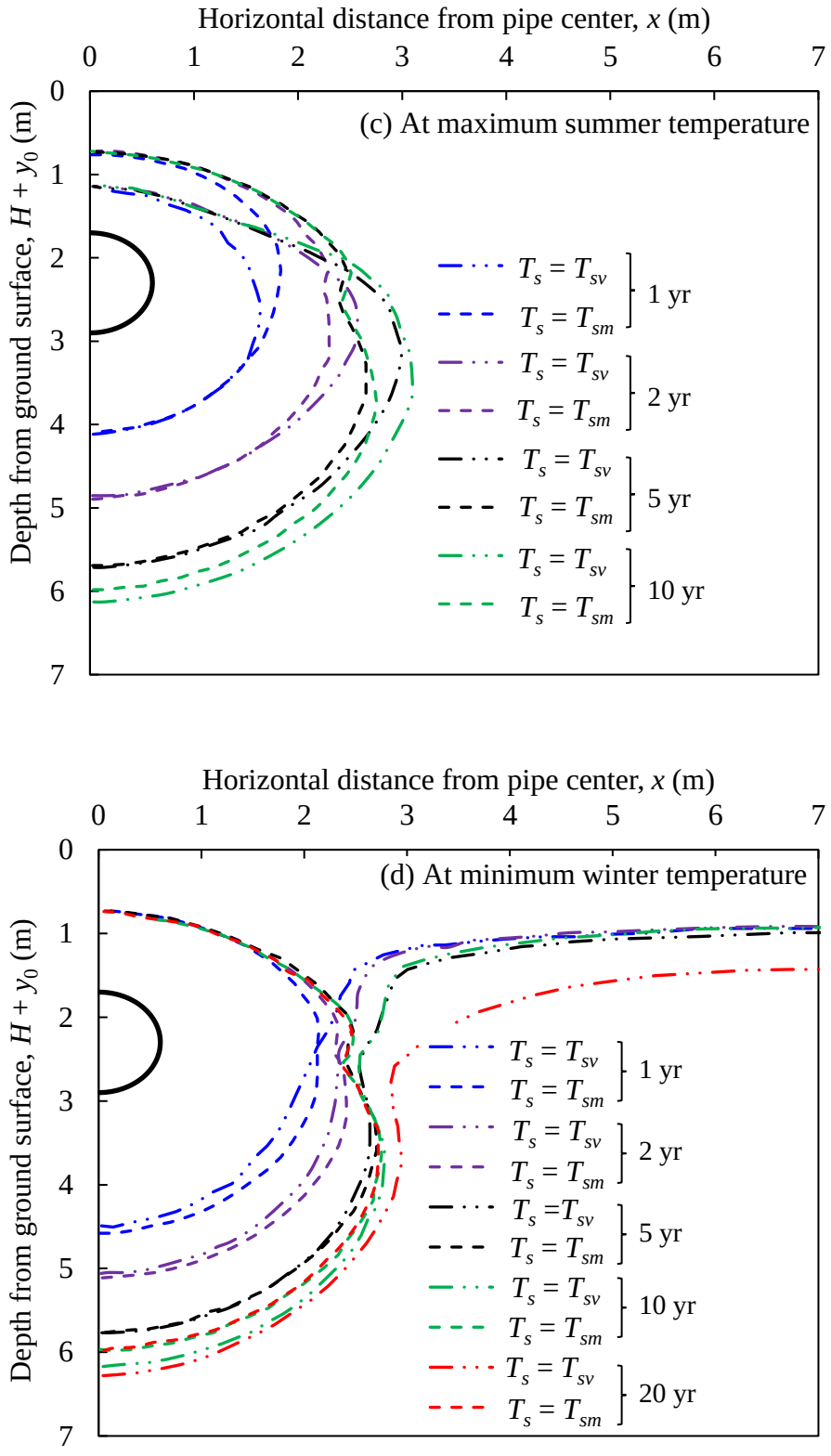

Fig. 5.4. Frost front distribution of at different time intervals: (a) & (b) shallow burial; and (c) & (d) deep burial

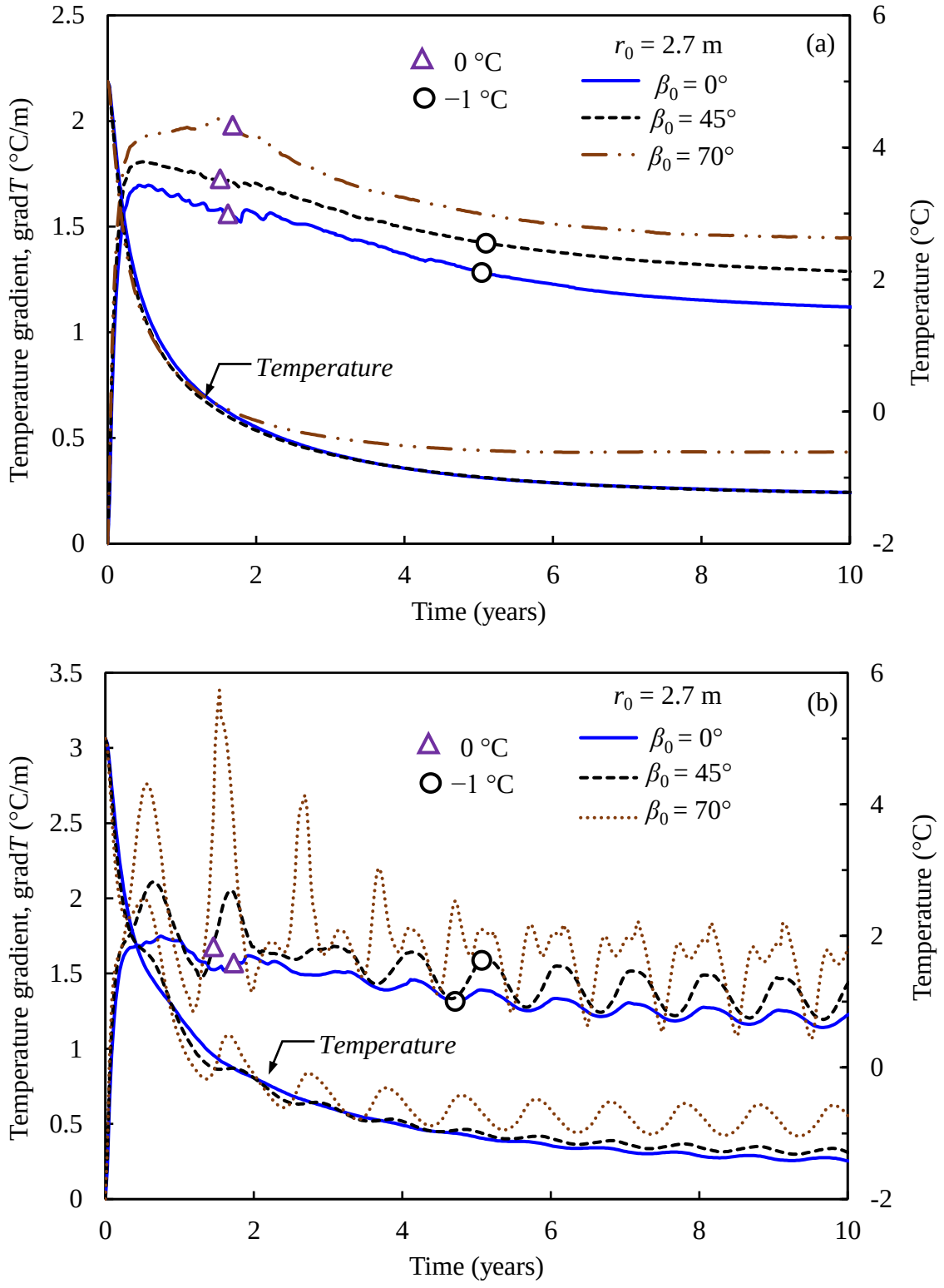

Fig. 5.5. Temperature gradient variation with time in typical soil elements in the frozen zone for deep burial section: (a) $T_s = T_{sm}$; and (b) $T_s = T_{sv}$

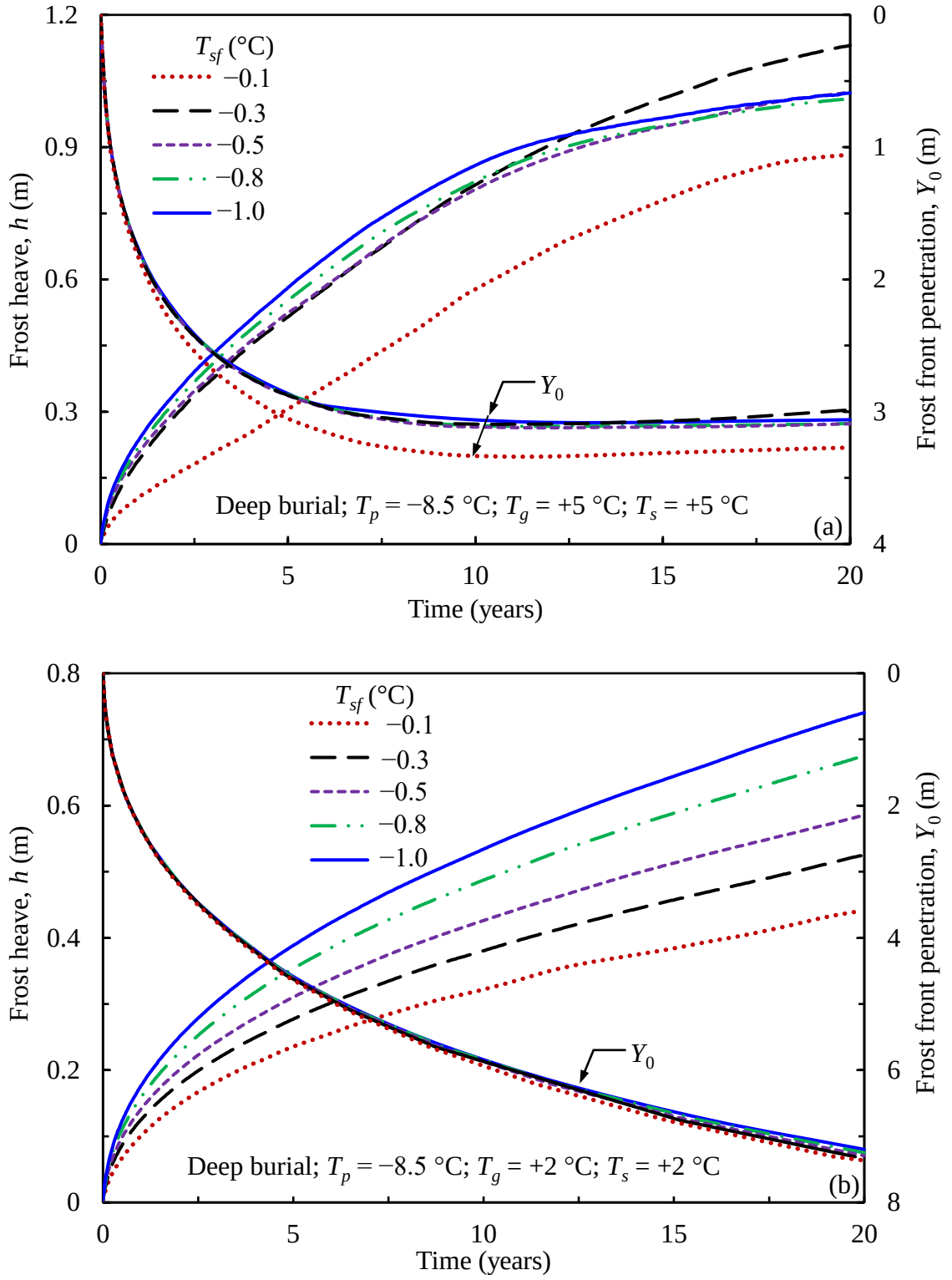

Fig. 5.6. Effects of segregation freezing temperature (T_{sf}): (a) T_g = +5 °C; and (b) T_g = +2 °C

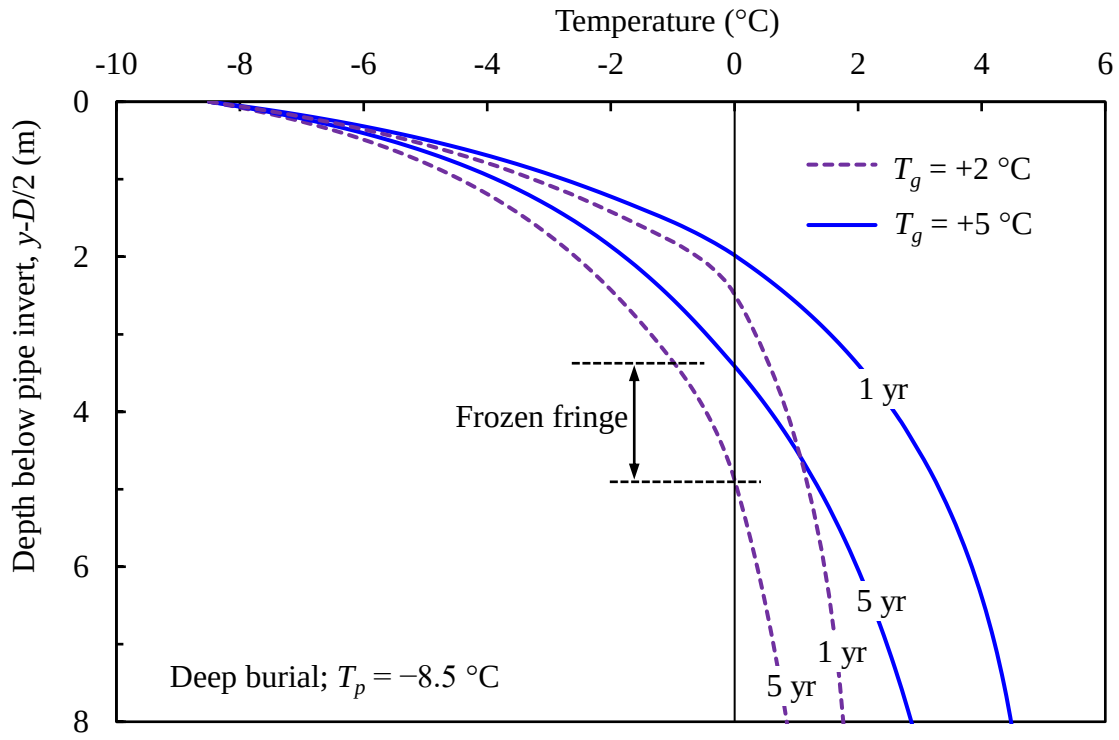

Fig. 5.7. Temperature below pipe invert for different initial ground temperatures

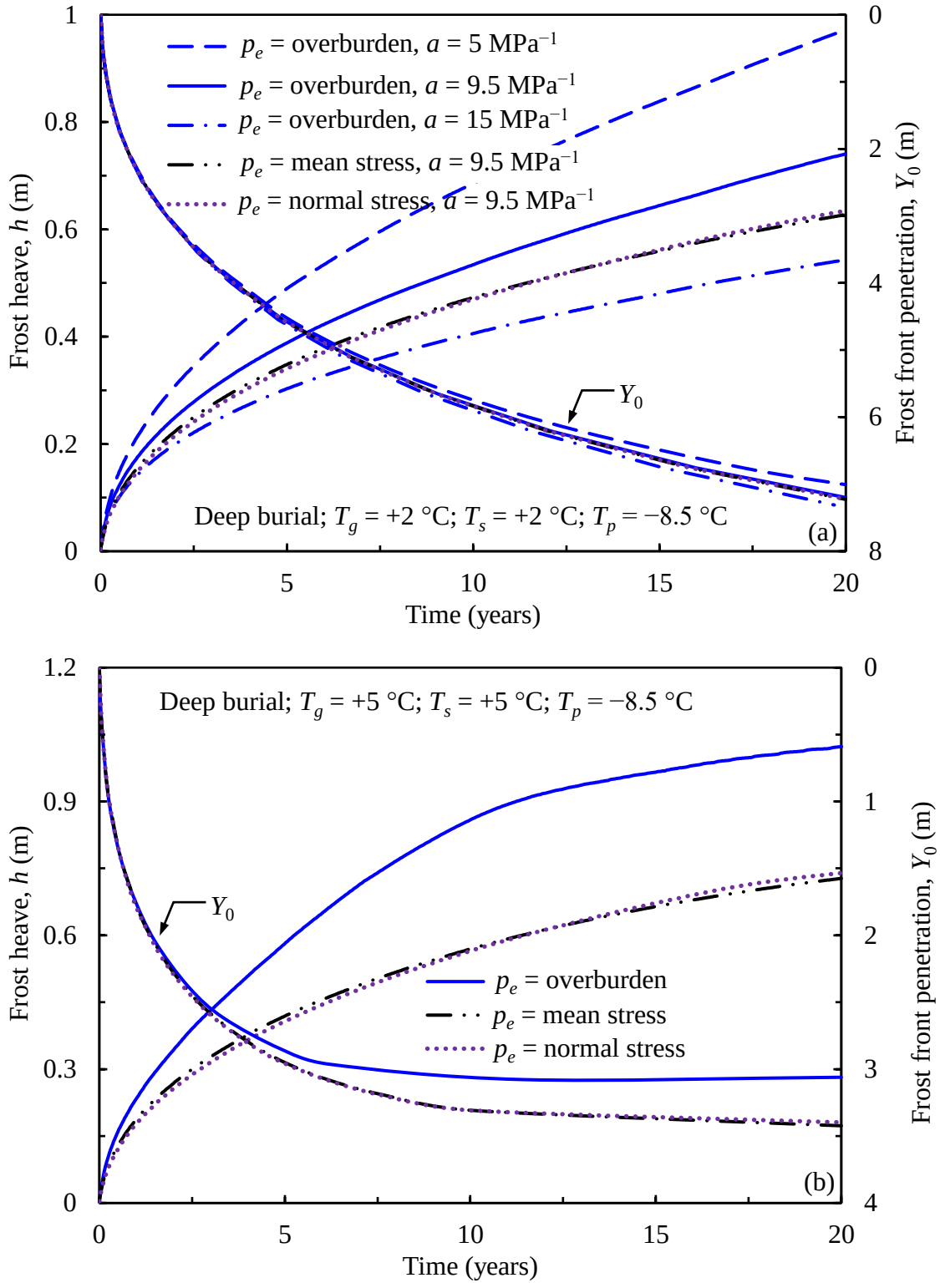

Fig. 5.8. Effects of stress parameter (p_e): (a) T_g = +2 °C; and T_g = +5 °C

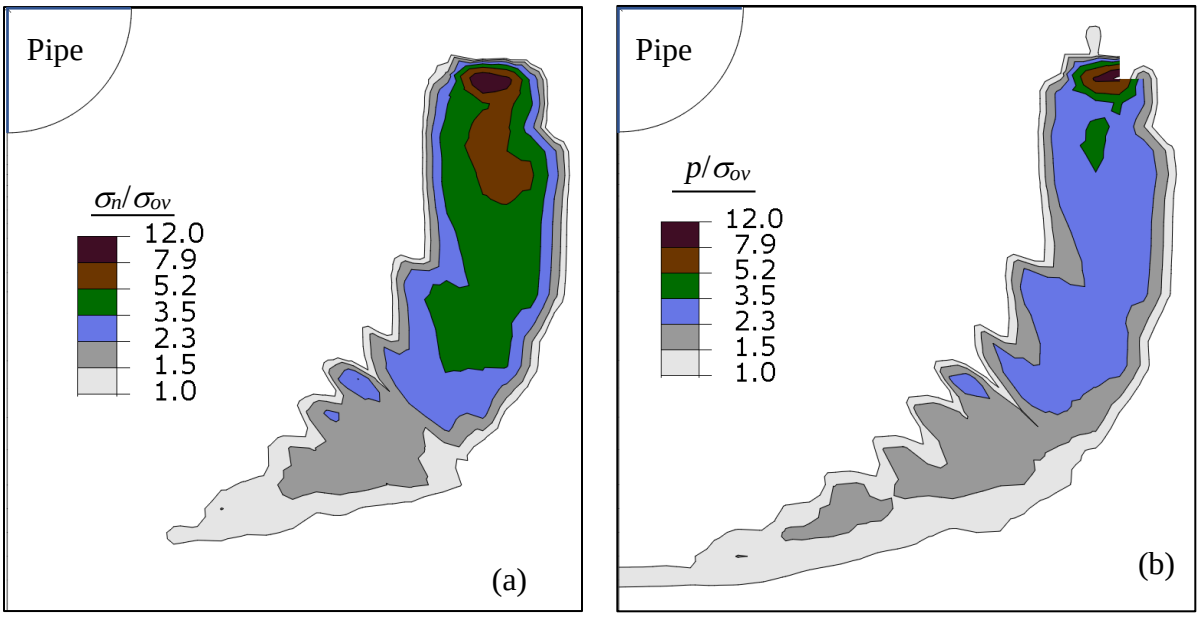

Fig. 5.9. Stress in frozen fringe after 4 years for T_g = +5 °C; (a) σ_n/σ_{ov}; and (b) p/σ_{ov}

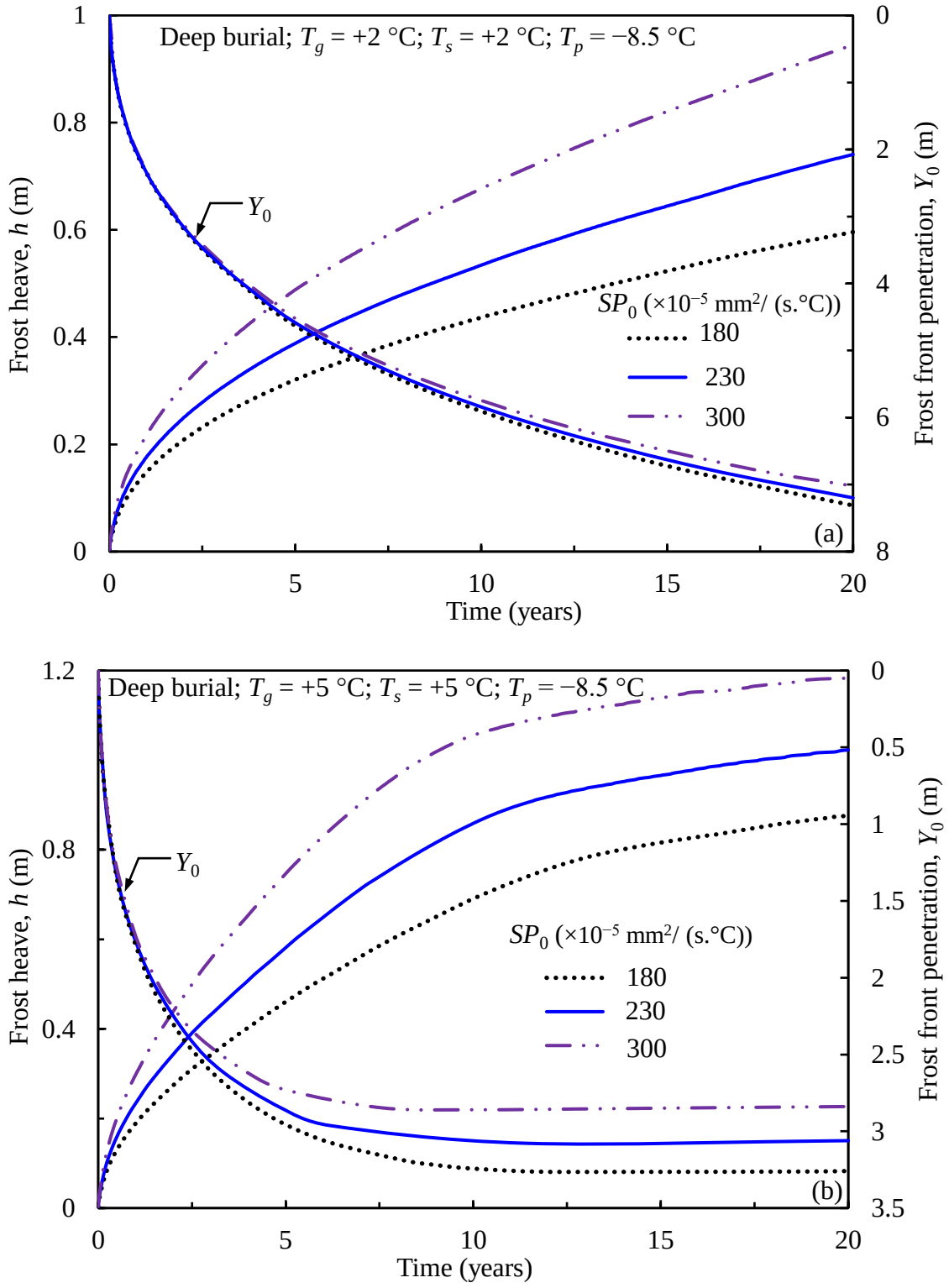

Fig. 5.10. Effects of segregation potential at zero applied pressure (SP_0): (a) T_g = +2 °C; and T_g = +5 °C

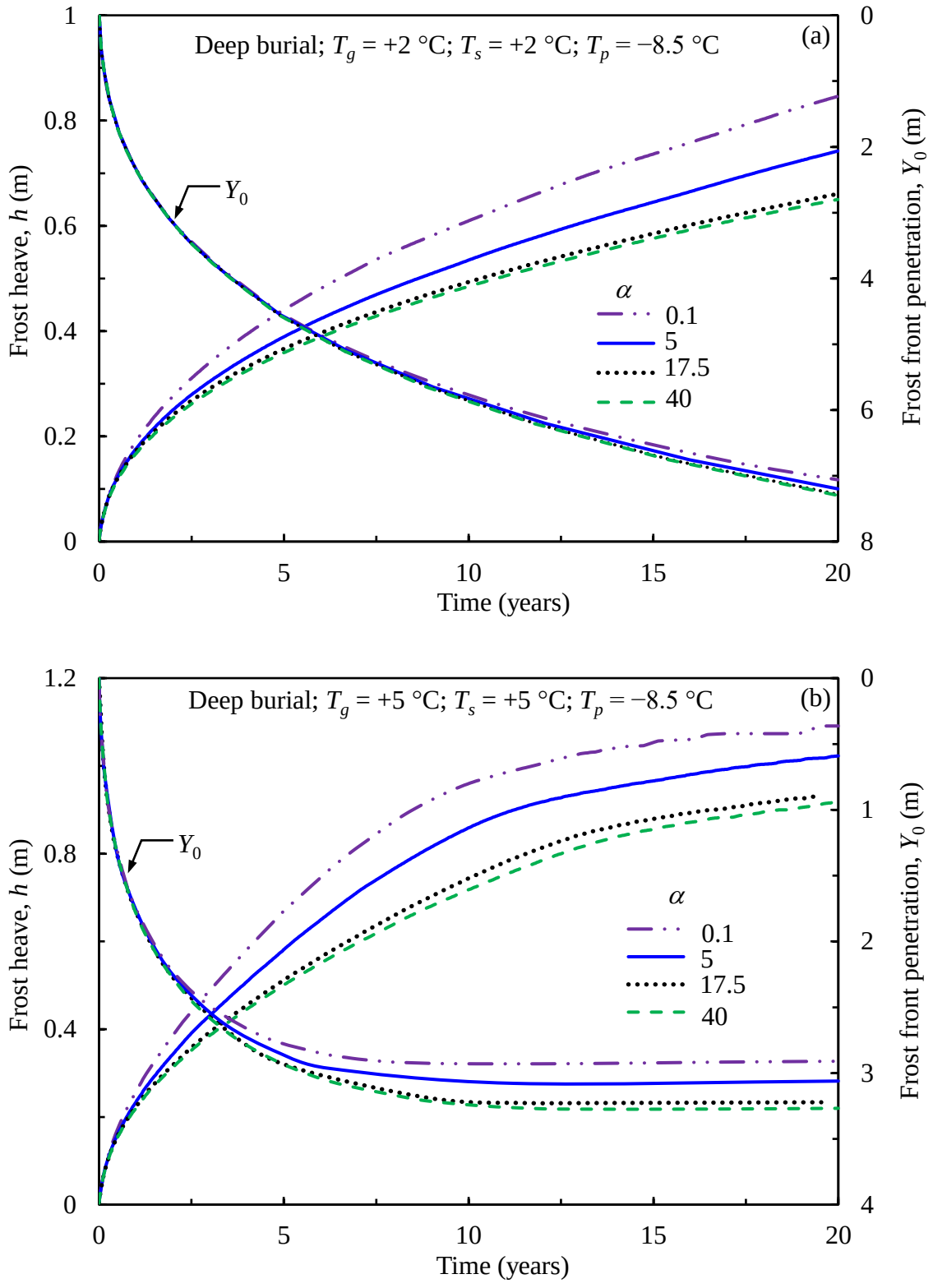

Fig. 5.11. Effects of shear increase parameter of frozen soils (α): (a) T_g = +2 °C; and T_g = +5 °C

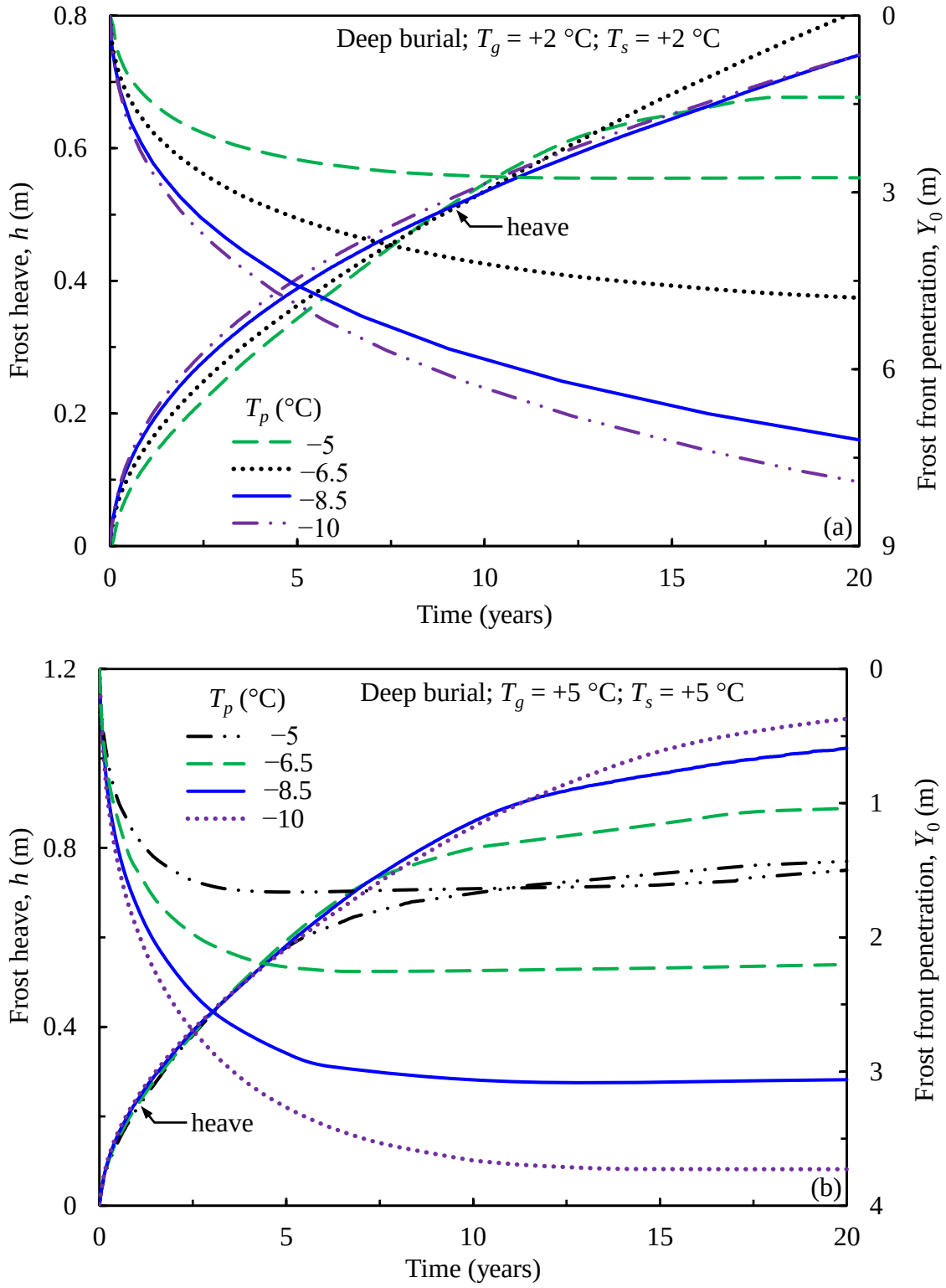

Fig. 5.12. Effects of pipe temperature (T_p): (a) T_g = +2 °C; and T_g = +5 °C

Table 5.1. Parameters used in finite element simulation

Parameter	Value/expression
Geometry	
Diameter of pipe, D (m)	1.2
Burial depth, H (m)	2.3 (1.4)
Temperature boundary conditions	
Pipe temperature, T_p (°C)	-8.5 (-3, -5, -6.5, -10)
Initial ground temperature, T_g (°C)	+2 and +5
Ground surface temperature, T_s (°C)	+2 and +5 (seasonal temperatures)
Mechanical Properties	
Unfrozen soil	
Young's modulus, E (MPa)	11.2
Poisson's ratio, v	0.25
Angle of internal friction, ϕ (°)	30
Cohesion, c (kPa)	10
Dilation angle, ψ (°)	5
Frozen soil	
Young's modulus, E_f (MPa)	$13.75\|T\|^{1.18}$
Poisson's ratio, v_f	0.25
Angle of internal friction, ϕ_f (°)	$\phi(1-\theta_i^{2.6})$
Rate of increase of frozen soil cohesion, α	5 (0.1, 17.5, 40)
Dilation angle, ψ_f (°)	5
Freezing Characteristics	
Segregation potential	
SP_0 ($\times 10^{-5}$ mm^2/°C.s)	230 (180, 300)
a (MPa^{-1})	9.5 (5, 15)
Unfrozen water content function	
P (%)	25
Q	1
In-situ freezing temperature, T_f (°C)	0
Segregation freezing temperature, T_{sf} (°C)	-1 (-0.1, -0.3, -0.5, -0.8)
Dry density of soil, ρ_d (kg/m^3)	1740
Initial water content, w_0	0.2 (0.1 for non-frost susceptible)
Initial porosity, n	0.35

Density of soil skeleton, ρ_s (kg/m^3)	2,670
Density of water, ρ_w (kg/m^3)	1,000
Density of ice, ρ_i (kg/m^3)	917
Thermal conductivity of soil skeleton, λ_s (W/m°C)	2.1
Thermal conductivity of water, λ_w (W/m°C)	0.6
Thermal conductivity of ice, λ_i (W/m°C)	2.24
Specific heat of soil skeleton, c_s (J/kg°C)	836
Specific heat of water, c_w (J/kg°C)	4,184
Specific heat of ice, c_i (J/kg°C)	2,100
Latent heat of water, L (J/kg)	334,720

Note: Values in parentheses are used in the parametric study.

CHAPTER 6:

One- and Two-Dimensional Finite Element Modelling of Thaw Consolidation

Co-Authorship: This chapter has been submitted as a technical paper for publication in a journal as: Dayarathne, R., Hawlader, B., Phillips, R., and Robert, D. “One- and two-dimensional finite element modelling of thaw consolidation.” The first author has conducted most of the research presented in this chapter. He also prepared the draft manuscript. The other authors mainly supervised the research and reviewed the manuscript.

6.1 Abstract

Coupled thermo-hydro-mechanical finite element (FE) modelling of thaw consolidation is presented. One-dimensional FE analyses are performed for thaw consolidation of a soil column due to self-weight and with a combination of self-weight and surcharge, with the linear and nonlinear void ratio–effective stress–hydraulic conductivity relationships of thawed soil. The nonlinear behaviour of thawed soil is modelled using a modified Drucker–Prager Cap model, while the hydraulic conductivity is varied with the void ratio. Finally, two-dimensional FE modelling of thaw consolidation around a warm pipeline buried in permafrost is performed. The rapid reduction of the void ratio with consolidation, especially at the low-stress level, results in a wide variation of hydraulic conductivity within the thawed zone. The significantly large hydraulic conductivity of soil elements along the curved thaw front, as compared to that of thaw consolidated soil, causes the flow of water along the thaw front, instead of a vertical flow, as assumed in previous 1-D thaw consolidation modelling of buried pipelines.

6.2 Introduction

Thawing of permafrost is one of the design issues for some infrastructure in cold regions, including roadway embankments, impoundment reservoirs, fuel storage tanks, building foundations and warm pipelines. In some cases, thawing occurs due to an elevated temperature over a relatively wide area (e.g., thawing of frozen soil under a large fuel storage tank); therefore, the heat and moisture flow can be assumed to be one-dimensional (1-D). However, thawing around a warm pipeline occurs from a relatively small heat source where at least two-dimensional (2-D) heat transfer and moisture flow occur.

Buried pipelines transmitting oil and gas in permafrost regions pass through a wide variety of soils: fine- to coarse-grained and ice-poor to ice-rich soils. Ground subsidence and pipe settlement may occur when a pipeline in ice-rich permafrost operates at above-zero temperatures. For example, significant ground subsidence was observed in some areas of a 119-km section of the China-Russia crude oil pipeline, which passes through the ice-rich continuous permafrost with oil temperatures seasonally varying between +0.4 °C and +17.9 °C (Wang et al. 2018). Also, the Inuvik experimental warm-oil pipeline (Inuvik pipeline) on highly ice-rich to ice-poor soils at different depths settled approximately 1 m within 40 days of operation at pipe temperature, T_p, of +71 °C (Watson et al. 1973). A bowl-shaped thaw front was reported, based on thermistor readings (Watson et al. 1973).

Morgenstern and Nixon (1971) developed an analytical solution for thaw consolidation based on Terzaghi's classical small-strain consolidation theory, using constant volume compressibility (m_v) and hydraulic conductivity (k) for thawed soil. They decoupled the process and solved heat transfer and consolidation separately. Morgenstern and Nixon (1975) used this linear theory of 1-D thaw consolidation to simulate the observed thaw settlement in the Inuvik

pipeline, assuming that the heat and moisture flow directly below the pipeline dictate the process. However, they recognized that the problem is undoubtedly 2-D in nature. The Morgenstern-Nixon simplified approach has been used in several later studies (e.g., Nixon 1973 and Lesage 2008).

Recognizing large thaw consolidation settlement in the field, Foriero and Ladanyi (1995) developed a 1-D finite-strain thaw consolidation model by extending Gibson's large-strain consolidation theory (Gibson et al. 1981). They also considered the variation of compressibility and hydraulic conductivity during consolidation. A semi-empirical expression was used to determine the thaw front depth prior to consolidation analysis, similar to Morgenstern and Nixon's (1971) decoupled approach.

Dumais and Konrad (2018, 2019) considered nonlinear relationships between the void ratio (e), vertical effective stress (σ_v') and hydraulic conductivity of thawed soil (k) and developed a framework for the finite-strain 1-D consolidation theory. They then solved the processes numerically using a computer program. Compiling laboratory test data on thawed Athabasca clay (Smith 1972) and Inuvik silt (Watson et al. 1972), they proposed linear e–logσ_v' and e–log$k$ relationships. Laboratory tests at very low-stress levels were not available. Therefore, they extrapolated the e–logσ_v' and e–log$k$ lines to a very low stress (residual stress, Nixon and Morgenstern 1973) at a high thawed void ratio; for example, residual stress of σ_0' = 0.0028 kPa at the thawed void ratio e = 2.6 is used for the Athabasca clay (Dumais and Konrad 2018). This 1-D model has also been used by Dumais and Konrad (2019) to simulate the Inuvik pipeline response, again based on the same assumption of Morgenstern and Nixon (1975) on idealizing the problem as one-dimensional. Yu et al. (2020) developed a one-dimensional thaw consolidation model similar to that of Dumais and Konrad (2018), incorporating the effects of freeze-thaw cycles on the hydraulic conductivity of thawed soil. Yao et al. (2012) also developed a coupled three-

dimensional finite element thaw consolidation model using Biot's 3-D consolidation theory, which is, however, limited, due to the small-strain and linear void ratio–effective stress (i.e., linear elastic) assumptions, similar to the Morgenstern and Nixon (1971) solution.

Thaw consolidation settlement might occur due to only self-weight (e.g., spring warming of the frozen ground at the surface) or under combined effects of self-weight and external loads (e.g., frozen ground warming below a heated tank). One-dimensional thaw consolidation due to only self-weight is similar to self-weight consolidation of a slurry. Hawlader et al. (2008) summarized the mathematical equations used in previous studies for slurry consolidation. For a slurry, the compressibility and hydraulic conductivity at very low-stress levels are obtained from specialized laboratory tests, such as settling column and fluidization tests (Sills 1995, 1998; Pane and Schiffman 1997; Bartholomeeusen et al. 2002). Comparing slurry consolidation test results, the extrapolation of e–logσ'_v and e–log$k$ lines to a low-stress level for thaw consolidation analysis (Dumais and Konrad 2018, 2019) is logical. However, there are two key questions:

i) Can the water flow during thaw consolidation around a warm pipeline be reasonably assumed to be one-dimensional when such highly nonlinear e–σ'_v–k soil behaviour could cause a large variation of k within the thaw bulb? The pore pressure isochrones follow the curved thaw front, unlike in typical 1-D slurry consolidation, where the pore pressure isochrones are horizontal. Outside the thaw front, the frozen soil acts as a relatively impermeable and incompressible medium because of its low hydraulic conductivity (k_f) and high strength.

ii) Can shearing of thawed soil at such low stresses occur during the settlement of the thawed soil wedge? If so, how can this soil be modelled?

These questions could be answered from the 2-D finite element (FE) simulations of the coupled thermo-hydro-mechanical process of thaw consolidation. Unfortunately, such analyses are not available in the literature and are performed in this study. The FE analyses are performed for the following conditions. Firstly, 1-D thaw consolidation is analyzed for a linear e–σ_v' relationship together with a constant hydraulic conductivity for thawed soil to verify the present FE modelling and to explain the limitations of the small-strain linear approach. Secondly, nonlinear e–σ_v'–k relationships are implemented using an advanced soil constitutive model; 1-D FE analysis is performed and then compared with previous numerical studies. Finally, 2-D thaw consolidation analyses around a warm pipeline are performed.

6.3 Problem Definition

One- and two-dimensional thaw consolidation analyses of saturated soil are performed. First, the simulations are performed for 1-D soil columns, which correspond to the thawing of a semi-infinite frozen mass and laboratory 1-D thaw consolidation tests. Initially, at time t = 0, the soil column is frozen at a constant temperature T_g (< 0 °C) (Fig. 6.1(a)). The top surface temperature is then increased to T_s (> 0 °C). Excess pore water pressure (u) is generated when the pore ice and ice lenses melt. Thaw consolidation occurs when u dissipates, which causes ground surface settlement (S). The distance of the thaw front (T = 0 °C) is Y_0 and Y from the initial and current position (after settlement) of the top surface, respectively (Fig. 6.1(a)). The frozen region below the thaw front is almost incompressible and impermeable as compared to the thawed region. Simulations are performed with and without a surcharge (P_0).

Two-dimensional modelling is also performed for a warm pipeline buried in permafrost. Figure 6.1(b) shows the 2-D pipeline section modelled in this study. The pipeline has a diameter of D and is buried at depth H. It is assumed that the initial frozen ground temperature (T_g) is

uniform, and the pipeline temperature (T_p > 0 °C) remains constant during the operation. It is, however, understood that T_g might vary with depth, and seasonal variation of T_p is possible, even at a given pipeline section. The distance of the thaw front (T = 0 °C) is Y_0 and Y from the initial and current pipe invert positions, respectively (Fig. 6.1(b)). Thawing of permafrost causes ground surface settlement (S_s) and pipe settlement (S_p).

The backfill material in the trench might be different from native frozen soil. Also, different soil layers in terms of mechanical properties and varying ice content might exist in the field, for example, as observed in the Inuvik pipeline test site (Rowley et al. 1973; Slusarchuk et al. 1973; Watson et al. 1973). Moreover, the seasonal effects could alter the soil behaviour in the active layer above the permafrost table. Rowley et al. (1973) showed that, at the Inuvik test site, the ground surface temperature, even at the base of the moss layer, remains at a subzero state for most of the year, except for about three months of the summer. Site-specific variation of soil properties and ground temperatures could be modelled using the present numerical approach with some modification; however, in the present study, a homogeneous soil and a constant ground surface temperature (T_s) slightly above 0 °C are used. An above-zero surface temperature allows excess water to flow out and ground surface to settle, as discussed further in later sections.

6.4 Finite Element Modelling

Coupled thermo-hydro-mechanical (THM) analysis is performed using Abaqus/Standard FE software (Abaqus 2014). The software has other FE modelling techniques to handle large deformations, such as Lagrangian-based explicit and Coupled Eulerian-Lagrangian (CEL) approaches; however, the currently available versions do not support the modelling of coupled pore fluid diffusion with heat transfer and stress analysis. Further, the THM modelling approach currently supports only axisymmetric and three-dimensional elements. Therefore, for 1-D

analyses, one column of 1-mm cubical elements is considered. For 2-D thawing around a pipeline, the analyses are performed with only one element of 0.1-m thickness in the out-of-plane direction to simulate the plane strain condition.

The soil is modelled using the 8-node brick fully coupled temperature–pore pressure elements with reduced integration (C3D8RPT in Abaqus 2014). Although thermal and structural interaction can be defined between pipe and soil, the 15-mm thick pipe is modelled as an integral part of the soil body to reduce the computational cost, using a different element type without pore pressure (C3D8RT in Abaqus 2014).

Figure 6.2 shows the FE mesh used for 2-D analysis. Taking the advantage of symmetry, only the left half of the problem is modelled. A 0.6-m-diameter pipe buried at H = 1.5 m is modelled. A finer mesh is used close to the pipe (inset of Fig. 6.2), where most of the thaw consolidation occurs. The left and bottom boundaries are placed sufficiently far from the pipe to avoid the boundary effects. Zero heat flux is applied at the vertical boundaries, while the temperature at the bottom boundary is fixed to the initial ground temperature ($T = T_g$). The vertical faces and bottom boundary have zero pore fluid flux boundary conditions, while the top surface is a free-drainage boundary. All the vertical faces are restrained from horizontal displacement, while the bottom boundary is restrained from both horizontal and vertical displacements (Fig. 6.2).

To model a semi-infinite medium, the soil column height considered in 1-D analyses is greater than five times the maximum expected thaw depth. Analyses are also performed with larger soil columns ($> 5Y_0$), but no significant effects on results are found. The other boundary conditions in 1-D analysis are the same as those in 2-D analysis, as mentioned above.

The FE simulation consists of the following steps. First, the in-situ stress (through geostatic loading), initial ground temperature (T_g), frozen void ratio (e_f) and degree of saturation (= 100%)

are defined. In 1-D simulations with surcharge loads, the surcharge is then applied instantly as an extra step at the top surface, which increases the pore water pressure uniformly by the same amount of applied stress. The final step represents the thermo-hydro-mechanical analysis of thawing. The top surface temperature (T_s) in 1-D and 2-D analyses and the pipe temperature (T_p) in the 2-D analysis are applied in this step. T_p is applied to the nodes on the inner surface of the pipe (Fig. 6.2); however, heat transfer occurs very quickly through the pipe to the surrounding soil because of the high thermal conductivity of the pipe material. T_s is ramped gradually in 1 min for 1-D simulations, while T_s and T_p in 2-D pipeline simulations for a longer period (5 years) are ramped for 1 hour and 10 days, respectively.

Thawing of ice in soil generally occurs over a temperature range (Patterson and Smith 1981; Zhu 2006; Zhang et al. 2020). In the present study, mechanical, hydraulic, and thermal properties of soil are changed linearly from frozen to thawed values within -0.5 °C and 0 °C.

6.5 Stress–Strain Behaviour

The following three sets of analyses are performed:

Set-I: One-dimensional thawing of a soil column for a linear e–σ_v' relationship (constant compressibility) and constant hydraulic conductivity;

Set-II: One-dimensional thawing of a soil column for varying compressibility and hydraulic conductivity (i.e., e-logp' and e-log$k$, where p' is the mean effective stress);

Set-III: 2-D analyses of thawing around a warm pipeline buried in permafrost for varying compressibility and hydraulic conductivity as in Set-II.

Set-I analyses are performed to show the performance of FE modelling, compared to the results with an analytical solution, and to show the limitations of the small-strain considerations. Set-II analyses are performed to explain the importance of the nonlinear behaviour of thawed soil.

The linear stress–strain behaviour of thawed soil for Set-I is defined by elastic properties. However, for Sets-II and -III, a modified Drucker–Prager Cap model is used, which is called simply the "cap model" in the following sections.

The stress path of the soil elements in 2-D thawing around a pipe in Set-III does not always remain on the stress path in 1-D consolidation as in Set II. However, both sets of analyses could be performed using the cap model, although, in Set-II, the stresses will always be on the cap (Fig. 6.3(a)). Note that this type of model has been used in previous studies for thaw-weakened soil under pavement systems subjected to vehicle loads (Shoop et al. 2008) and thaw settlement of embankments constructed on permafrost (Gholamzadehabolfazl 2015).

Both frozen and thawed soils are modelled using the cap model. The frozen soil is a stronger material (outer dashed line in Fig. 6.3(a)); however, the soil becomes weak once thawed (as on the inner solid yield surface in Fig. 6.3(a)). As the thawed soil mainly governs thaw consolidation, the cap model for thawed soil is discussed in detail.

The yield surface in the meridional plane is defined by the following Drucker–Prager shear failure surface (F_s), a cap surface (F_c) and a transition region between F_s and F_c.

$$F_s = t_s - p' \tan \beta_1 - d = 0 \tag{6.1}$$

where t_s is the deviatoric stress, β_1 is the slope of F_s on the meridional plane and d is the t_s intercept of F_s. Also,

$$t_s = \frac{q}{2}\left[1 + \frac{1}{K} - \left(1 - \frac{1}{K}\right)\left(\frac{J_3}{q}\right)^3\right] \tag{6.2}$$

where q is the Mises equivalent stress, J_3 is the third deviatoric stress invariant, and K defines the shape of the yield surface in the deviatoric plane, which varies between 0.778 and 1.0 to maintain convexity. $K = 1$ is used in this study. For plane strain condition, β_1 and d are related to cohesion

(c') and angle of internal friction (ϕ') as: $\beta_1 = \tan^{-1}\left(\sqrt{3}\sin\phi'/\sqrt{1+\sin^2\phi'/3}\right)$ and $d = \sqrt{3}c'\cos\phi'/\sqrt{1+\sin^2\phi'/3}$.

The cap yield surface (F_c) is expressed as:

$$F_c = \sqrt{(p' - p'_a)^2 + \left(\frac{R_1 t_s}{1+\alpha_1-\alpha_1/\cos\beta_1}\right)^2} - R_1(d + p'_a \tan\beta_1) = 0 \quad (6.3)$$

where R_1 is a parameter that controls the shape of the cap, and α_1 is a small number used to define the transition region of the yield surface (α_1 = 0, in this study). The evolution parameter (p'_a) is expressed as:

$$p'_a = \frac{p'_b - R_1 d}{1 + R_1 \tan\beta_1} \quad (6.4)$$

where p'_b is the hydrostatic yield stress of thawed soils, which varies with consolidation (Fig. 6.3(a)). Note that $p'_b = p'_{b0}$ immediately after thawing; p'_{b0} is a very small value, which is related to residual stress, as discussed later.

Three levels of volume changes occur during thaw consolidation (Dumais and Konrad 2019), as shown schematically in Fig. 6.3(b). Firstly, the frozen soil void ratio (e_f) reduces by 9% to e_0 (i.e., $e_0 = e_f/1.09$) due to the phase change. Secondly, immediately after thawing, a rapid reduction of void ratio (e_0 to e_{th}) occurs because of the expulsion of water that cannot be accommodated in the soil particles, especially in ice-rich soil. Finally, the void ratio gradually reduces with an increase in effective stress due to the consolidation ($e < e_{th}$). The first and second parts of the volume change are not explicitly modelled in this study because such rapid reduction could create numerical issues, and the water expulsion process in the second part is not well-understood. Therefore, in this study, an e-lnp' curve starting from e_f at a low p'_b ($= p'_{b0}$) with a slope of λ is used for the normal consolidation line (Fig. 6.3(b)). The slope λ should be greater than that of

consolidation only (third part) to incorporate the effects of the first and second parts, depending upon the ice content. This assumption does not significantly affect the overall thaw consolidation after a period of thawing because most of the void ratio reduction expected from these two sources is accommodated in the rapid reduction of e during a small increase in p' from the initial value. A separate function for the rapid reduction of e at low stresses (i.e., e_f to e_{th}) could be used by varying the λ with p'_b as in Dumais and Konrad (2019); however, this could create numerical issues, especially in the 2-D analysis, because of mesh distortion. Moreover, the e–p' relationship for such low stresses cannot be determined accurately from traditional laboratory tests.

Note that the initial rapid reduction of void ratio ($e_f \rightarrow e_0$ and $e_0 \rightarrow e_{th}$ in Fig. 6.3(b)) has two implications. Firstly, a smaller settlement will be calculated initially as the compression curve ad is above abcd in Fig. 6.3(b). However, the difference between the calculated settlements with these two compression curves will be reduced with an increase in effective stress. Secondly, centrifuge tests show that a void might be formed above the pipe, potentially due to volumetric reduction during the phase change from ice to water (i.e., $e_f \rightarrow e_0$) (C-CORE 2012; Wang et al. 2016). This void could create a thermal barrier and result in more lateral expansion of the thaw bulb (C-CORE 2012; Wang et al. 2016). This issue is not considered in the present analysis; instead, the soil is modelled as a fully saturated continuum.

The hardening law is given as (Wood 1990):

$$\varepsilon_v^p = \frac{\lambda - \kappa}{1 + e_f} \ln\left(\frac{p'_b}{p'_{b0}}\right) \tag{6.5}$$

where ε_v^p is the plastic volumetric strain; and $\lambda = 0.434C_c$ and $\kappa = 0.434C_s$, where C_c and C_s are the compression and swelling/recompression indexes, respectively. In this study, $\kappa = 0.1\lambda$ is used (typical range of κ/λ is 0.1 to 0.2).

Tables 6.1–6.3 show the values of the mechanical and thermal properties of the soil, respectively. In this chapter, the parameters with subscript *f* represent the frozen, and without a subscript, represent the thawed soil properties. Also, the superscripts I, II and III represent the value of a parameter used in that set of analyses (e.g., $W_u = 0.3^{(II)}$ represents the value used for Set-II). The density of the soil skeleton, water and ice are $2650^{(II)}$ ($2670^{(I,\ III)}$), 1000 and 917 kg/m^3, respectively. Constant Young's modulus of thawed (E') and frozen (E'_f) soils are used, although it is understood that E'varies with mean effective stress and E'_f with subzero temperature. In numerical analysis, simply by using a large value of p'_{bf}, the frozen soil is modelled as an elastic material. Moreover, creep plays a significant role in frozen soil behaviour. However, a complex soil model is not used for the frozen soil because the frozen soil deformation is very small compared to the thawed soil; therefore, the frozen soil model does not significantly affect thaw consolidation. Further details of the material property selection are provided later in Sets-II and -III simulation results sections.

6.6 Thermal Properties

The thermal conductivity and specific heat of soil skeleton (λ_s, c_s), water (λ_w, c_w) and ice (λ_i, c_i) are given as input parameters (Table 6.2). The software calculates the equivalent thermal conductivity and equivalent specific heat, based on the current void ratio when the void could be filled with water or ice. The values of thermal properties of the material in the void (water/ice) change linearly from the frozen to the thawed state between -0.5 °C and 0 °C, as discussed before. In the current numerical approach, the water in the thawed soil flows through the pores during consolidation; therefore, the advection also contributes to heat transfer in addition to the conduction, although the advection is not significant in thaw consolidation (Nixon 1975; Dumais and Konrad 2018).

Following the work of Nixon and McRoberts (1973), the latent heat of soil per unit mass is calculated as:

$$L = \frac{w}{1+w}(1 - W_u)L' \tag{6.6}$$

where w is the moisture content of the frozen soil (= e_f/G_s); G_s is the specific gravity of the soil, W_u is the water content that remains unfrozen in the frozen soil; and L' is the latent heat of water (= 334,720 J/kg).

The amount of unfrozen water at a given sub-zero temperature is higher in fine-grained than in coarse-grained soils (Anderson et al. 1973; Lunardini 1988; Andersland and Ladanyi 2004). In this study, W_u = 0.3 for Set-II (clay) and 0.1 for Sets-I and III (relatively coarser materials) are used. In an analytical solution, L can be lumped at 0 °C (Nixon and McRoberts 1973). However, defining the phase change over a temperature range between the solidus (T_{sw}) and liquidus temperature (T_{lw}) could avoid numerical issues. The phase change of pore water in soils in varying temperature ranges was also observed in experimental studies, especially for fine-grained soils (Lunardini 1988; Andersland and Ladanyi 2004). Note that Nixon and McRoberts (1973) showed that distributing L over a temperature range does not significantly affect thaw depth calculation and, therefore, thaw consolidation.

6.7 Set-I Results: 1-D Analysis with a Linear Soil Model

This section presents the FE simulation results with a linear e–σ_v' relationship and a constant k for 1-D thawing of a semi-infinite frozen soil medium. Table 6.3 shows the details of the four cases (S1–S4) considered in this set of analyses. The thermal parameters are shown in Table 6.2. The initial ground temperature of the soil column is -5 °C, on which different surface temperatures (T_s = 5 °C and 20 °C) are applied at the top surface. The variation of these temperatures, hydraulic

conductivity (k) and volume compressibility (m_v) give a wide range of thaw consolidation ratios (defined below), R (= 0.24–1.64) (Morgenstern and Nixon 1971). Note that a lower value of E' is used in this case than in Set-I and -II cases (Table 6.1) to capture highly compressible thawed soil behaviour with this linear elastic model.

The FE results are compared with Morgenstern and Nixon's (1971) small-strain analytical solution; therefore, the mathematical formulation and procedure to obtain the input parameters of the analytical solution are described below briefly.

6.7.1 Analytical solution

Morgenstern and Nixon (1971) calculated the excess pore water pressure (u) at time t in a thawed soil element located at y_0 below the initial position of the top surface (Fig. 6.1(a)) as:

$$u(y_0,t) = \frac{P_0}{\mathrm{erf}(R) + \frac{e^{-R^2}}{\sqrt{\pi}R}} \times \mathrm{erf}\left(\frac{y_0}{2\sqrt{c_v t}}\right) \times \mathrm{erf}\left(\frac{y_0}{2\sqrt{c_v t}}\right) + \frac{\gamma' y_0}{1 + \frac{1}{2R^2}} \tag{6.7}$$

where c_v is the coefficient of consolidation of the thawed soil, P_0 is the surcharge (Fig. 6.1(a)), γ' is the submerged unit weight of the thawed soil, and R is the thaw consolidation ratio, defined as a function of the coefficient of consolidation (c_v) that is related to m_v as:

$$R = \frac{\alpha}{2\sqrt{c_v}} \tag{6.8}$$

$$c_v = \frac{k}{m_v \gamma_w} \tag{6.9}$$

where γ_w is the unit weight of water, and the α is a constant determined from the heat transfer solution.

For linear e–σ_v' relationships, m_v is related to Young's modulus (E') in 1-D compression as:

$$m_v = \frac{(1+\nu)(1-2\nu)}{E'(1-\nu)} \tag{6.10}$$

where ν is the Poisson's ratio of the thawed soil.

Morgenstern and Nixon (1971) used the Neumann solution (Carslaw and Jaegar 1947) to calculate the thaw depth before the consolidation analysis, which is analogous to *Y* in the current analysis (Dumais and Konrad 2018) as:

$$Y = Y_0 - S = \alpha\sqrt{t} \tag{6.11}$$

The thaw depth penetration (*Y*) with time obtained from the current FE model is used to calculate α for the analytical solution. Alternatively, the analytical methods, such as Neumann and Stefan's solutions, can be used to calculate α.

6.7.2 Consolidation with a surcharge

Figure 6.4 shows the 1-D FE simulated thaw settlement (*S*) of the soil layer with time under P_0 = 15 kPa for the four cases shown in Table 6.3. The settlement increases with increasing surface temperature, hydraulic conductivity, and volume compressibility. Figure 6.5(a) shows the excess pore pressure (u) variation with depth at t = 8 h, 16 h and 58 h for Case S4, where the vertical axis represents the depth measured from the top surface of the soil block before settlement (y_0). The results from the analytical solution (Eq. (6.7)) are also plotted for comparison. Note that the thaw settlement (*S* in Fig. 6.4) is considered in plotting the present FE results. However, in the analytical solution, the settlement is not considered (small-strain assumption); therefore, all the curves start from the origin. The bottom of each curve in Fig. 6.5(a) represents the location of the thaw front, which penetrates with time. The analytical solution underestimates the thaw depth and thereby the thaw settlement because the heat source settlement is not considered. If the calculated pore water pressure using the analytical solution (Eq. (6.7)) is adapted from the current position of the top

surface based on FE calculated settlement, it follows the FE calculated u closely, as shown in Fig. 6.5(b). A similar observation was reported by Dumais and Konrad (2018).

In summary, Figure 6.5 shows that the developed FE technique can simulate the thaw consolidation and that the settlement of the top surface should be considered for better modelling.

The excess pore water pressure is not completely dissipated during the simulation period (58 hours), although it decreases with time; for example, at y_0 = 80 mm depth, u = 5.4 kPa and u = 2.75 kPa at t = 16 h and t = 58 h, respectively. Depending upon the thaw front penetration rate and hydraulic conductivity of thawed soils, the dissipation of the remaining pore water pressure might occur during a longer period of thawing when the thaw front penetrates slowly, as discussed later in the post-thaw consolidation section.

6.7.3 Consolidation without surcharge

Simulations are also performed without a surcharge ($P_0 = 0$), which represents a process similar to the self-weight consolidation. Figure 6.6(a) shows the FE calculated excess pore water pressure during thawing only due to the self-weight of the soil for the parameters of case S3 in Table 6.3. In this case, low hydraulic conductivity of thawed soil ($k = 1\times10^{-9}$ m/s) is used, which is representative of clay (Nixon and Morgenstern 1974). The upper part of the excess pore water pressure profile up to the thaw front is almost linear. The pore pressure also develops below the maximum u (thaw front), although u decreases rapidly within a small frozen zone. This is attributed to the change of mechanical, hydraulic, and thermal properties from the frozen to the thawed state over a temperature range (-0.5 °C to 0 °C in this study). As mentioned before, numerical issues may arise if a very small range is used. The Analytical solution, however, considers the thaw front as an impermeable and incompressible boundary. Nevertheless, the pore pressure development

and dissipation in this transition zone may not affect the thaw settlement significantly because it has significantly less compressibility and hydraulic conductivity than fully thawed soil.

When $P_0 = 0$, excess pore water pressure in the small-strain analytical solution (Eq. (6.7)) becomes a time-independent linear function as:

$$u(y_0) = \frac{\gamma' y_0}{1 + \frac{1}{2R^2}} \tag{6.12}$$

For the soil parameters used in this analysis, *R* is calculated using Eqs. (6.8)–(6.11) and then inserted into Eq. (6.12) to calculate *u*, which is shown by the solid line in Fig. 6.6(a). The *u* obtained from the analytical solution matches the FE calculated values, which implies that the present FE analysis can properly simulate the generation of excess pore pressure due to self-weight thawing. Note that the thaw settlement in this relatively shorter thawed zone (170 mm at t = 58 h) during self-weight thawing is very small compared to thawing with a surcharge (Fig. 6.4), which makes the FE model results in a good agreement with the small-strain analytical solution.

To simulate the post-thaw consolidation, the heat transfer in the FE analysis is stopped at t = 58 hours, and the process is continued only for consolidation. At that time, the thaw front moves ~170 mm. Figure 6.6(b) shows the pore pressure dissipation in the thawed zone with the time factor $T_v = c_v t/h^2$, where c_v = 1.22×10^{-8} m^2/s for the soil parameters used in the FE model, and h is the drainage length which is equal to the thaw depth (= 170 mm). The pore pressure dissipates with time, and the pore pressure isochrones are very similar to the self-weight consolidation of a soil layer with an impermeable bottom boundary. Note that post-thaw consolidation may occur if thaw depth becomes stationary or thaw depth reaches a maximum depth (e.g., after complete thawing of a laboratory frozen sample) or thaw depth reaches the coarse-grained soil layer, which may not generate excess pore water pressure upon thawing (e.g., Inuvik pipeline experiment).

The above simulations show that the developed FE technique can simulate the thaw consolidation for a given value of volume compressibility with and without a surcharge. Also, additional comparisons with different values of *R* in Table 6.3 have been presented in Dayarathne et al. (2019) (Appendix B in this thesis).

The linear e–σ_v' relationship and constant hydraulic conductivity are used for the thawed soils for the comparison of FE results with the linear small-strain analytical solution. However, in real thawed soils, the void ratio–effective stress–hydraulic conductivity relationships are highly nonlinear, especially at a low-stress level, which is considered in the following simulations.

6.8 Set-II Results: 1-D Analysis with a Nonlinear Soil Model

This section presents an extension of the preceding FE model to incorporate the nonlinear e–σ_v' and e–k relationships for a better simulation of thawed soil behaviour. Dumais and Konrad (2018, 2019) used the nonlinear e–σ_v' and e–k relationships for thawed soils, which can be generalized as:

$$e = e_{th} - C_c \log\left(\frac{\sigma_v'}{\sigma_0'}\right) \qquad \text{if } \sigma_v' > \sigma_0' \tag{6.13}$$

$$k = \begin{cases} k_{max} 10^{\frac{e-e_{max}}{C_k}} & \text{if } e \le e_{max} \\ k_{max} & \text{if } e_{max} < e \le e_f \end{cases} \tag{6.14}$$

where e_{th} is the void ratio at the start of thaw consolidation at a very low effective stress (σ_0') after a rapid void ratio change from the frozen void ratio, due to phase change and the expulsion of excess amount of water that cannot be accommodated in the soil pores (Fig. 6.3(b)); e is the current void ratio, and C_c is the compression index of thawed soil; C_k is the slope of the e–log$k$ curve, and k_{max} is the maximum hydraulic conductivity of thawed soil at a large void ratio of e_{max}. Freeze-thaw cycles might increase the hydraulic conductivity of thawed soil, especially in highly plastic

soils under low effective stresses, potentially due to shrinkage crack formation (Chamberlain and Gow 1979; Konrad and Samson 2000). However, the semi-logarithmic function (Eq. (6.14)) was found to be reasonably valid even for thawed soil (Konrad and Samson 2000; Yu et al. 2020).

A detailed discussion of the selection of σ_0' based on the concept of residual stress and experimental measurements is available in Nixon and Morgenstern (1973) and Dumais (2019). In a 1-D laboratory test simulation, Dumais and Konrad (2018) used extrapolated linear $e-\log\sigma_v'$ lines up to a low-stress level of σ_0' = 0.0028 kPa and e_0 = 2.6, respectively (cf. Fig. 6.3(b)), although the laboratory tests' results covered $\sigma_v' > 0.2$ kPa and $e < 1.5$ (Smith 1972). For this simulation, they also provided the variation of e and k with depth with the progress of consolidation. Based on this e–k relationship and the analysis conducted by Yu et al. (2020), k_{max} and C_k are selected.

Dumais and Konrad (2019) used σ_0' = 0.2 kPa and e_{max} equal to the void ratio corresponding to the liquid limit of thawed soils (= 1.47) for the simulation of thaw consolidation of the Inuvik pipeline. As shown later from 2-D FE simulations, e_{max} has a significant influence on thaw consolidation. Dumais and Konrad (2018, 2019) used the compression index of thawed soils (C_c) between 0.2 and 0.45; higher values are for higher e_f in ice-rich fine-grained soils.

6.8.1 1-D Simulation of laboratory thaw consolidation test

The nonlinear relationships discussed above are incorporated into the current FE model. The model performance is validated using the numerical results presented in Dumais and Konrad (2018) for a simulation of the laboratory thaw consolidation test which was conducted by Smith (1972) on a frozen Athabasca clay specimen. The 50-mm high specimen was initially frozen to T_g = -5 °C and then thawed by applying a step change of temperature at the top surface to T_s = +5 °C and allowed to consolidate under a surcharge (P_0) of 15 kPa. The complete thawing of the frozen specimen was observed after 348 minutes and then entered the post-thaw consolidation stage.

Tables 6.1 and 6.2 show the parameters used to simulate these experimental results. The simulation is performed using a 250-mm high soil column, similar to that used by Dumais and Konrad (2018). Once thawed, the hydrostatic yield stress reduces to a small value p'_{b0} from a large value in the frozen state (p'_{bf}) (Fig. 6.3(a)). For this simulation, p'_{b0}=0.003 kPa is used, which gives low vertical effective stress at the K_0 condition, similar to that in the study of Dumais and Konrad (2018). Based on the estimated value of C_c as explained in the "stress-strain behaviour" section, the parameters λ and κ in Eq. (6.5) for the cap model are obtained, as listed in Table 6.1. The other parameters in Table 6.1 are similar to those used by Dumais and Konrad (2018), based on laboratory tests on thawed Athabasca clay (Smith 1972).

Figures 6.7(a)–6.7(d) show the comparison of the present FE model results with numerical results presented by Dumais and Konrad (2018). Following are the key observations.

- Temperature profiles in the frozen zone obtained from the above two numerical techniques are slightly different (Fig. 6.7(a)). This is mainly attributed to the difference in latent heat calculations. In the present FE analysis, the total latent heat is calculated using Eq. (6.6) and uniformly distributed between -1 °C and 0 °C, whereas Dumais and Konrad (2018) incorporated the soil water freezing characteristics curve (i.e., unfrozen water content variation with temperature) to calculate the latent heat. However, this difference in latent heat calculations did not cause any significant difference in temperature profiles in the thawed zone, as stated by Nixon and McRoberts (1973).
- At a given depth, the void ratio is higher in the present FE analysis than that in the work of Dumais and Konrad (2018) (Fig. 6.7(b)), especially after a considerable time of consolidation (e.g., t = 348 min), because the e–ln(p') line in the current FE analysis is above the Dumais and Konrad (2018) one (Fig. 6.3(b)).

- No significant difference between the pore pressures obtained from these two numerical solutions is found (Fig. 6.7(c)), although the void ratio–effective stress relation is slightly different.
- After t > 300 min, settlement is higher in the present FE analysis than in the work of Dumais and Konrad (2018), although the difference is very small initially. This is due to linear variation of the soil properties from the frozen to thawed state, between -0.5 °C and 0 °C in the present study. Some soils within this temperature range also compress during thaw consolidation. To verify, a simulation is performed for the same conditions but varying the thermal and mechanical properties within -0.1 °C and 0 °C which results in a lower settlement (Fig. 6.7(d)). Note, however, that such a small temperature range could be used in this simulation because the element size is small (1 mm). However, larger elements are used in the following 2-D pipe simulations to reduce computational cost; therefore, the soil properties are varied between -0.5 °C and 0 °C.

This analysis again confirms that the developed FE modelling technique can successfully simulate thaw consolidation, even for highly nonlinear e–σ'–k cases.

6.9 Set-III Results: 2-D Thawing Around a Pipeline

Tables 6.1 and 6.2 show the parameters used in this set of simulations. The initial ground temperature of the frozen soil is -5 °C. The pipe and ground surface temperatures are then increased to T_p = +6 °C and T_s = +1 °C, respectively, using the process described in the "Finite Element Modeling" section. The thaw consolidation analysis was continued for five years. Compared to Set-II analyses (clay), a relatively granular material (silt) is considered in this set of simulations; therefore, higher k and lower λ and κ are used (Table 6.1). Also, a higher value of p'_{b0}(= 0.5 kPa)

is used because of the lower frozen void ratio used in this analysis compared to Set-II and a trend of increasing residual stress with an increase in particle size (Nixon and Morgenstern 1973).

Figure 6.8(a) shows the settlement of the pipe (S_p) and the ground surface above the pipe center (S_s) (solid lines). The pipe settlement starts immediately after the start of thawing. Figure 6.8(b) shows the thaw front penetration below the initial position of the pipe invert (Y_0). The settlement and thaw front penetration continued until the end of the simulation period (t = 5 years), although their rate decreased with time. However, a negligible ground surface settlement was found until $t \approx 120$ days, and then S_s increased rapidly up to $t \approx 500$ days. After 500 days, S_p and S_s increased approximately at the same rate with time.

The above observation can be explained from the location of the 0 °C isotherm. Figure 6.9 shows the location of 0 °C at t = 50, 100, 500 and 1,000 days. In the beginning, two thaw fronts are formed due to the warming effect of the ground surface and the pipe, which are moving closer with time, mainly above the pipe. The frozen soil between these two thaw fronts is strong and does not allow the surface to settle, although a thawed zone forms around the pipe. However, after t ~ 120 days, these thaw fronts merge, which allows the surface to settle quickly during t = 120–500 days with the dissipation of excess pore water pressures generated in the thawed region around the pipe.

Figure 6.10 shows the e-logp' and e-log$k$ curves for the soil element directly below the pipe centerline at y_0 = 0.9 m. Upon thawing at 0 °C, the p' reduces from a high value of the frozen soil to a very small value of p'on the initial cap of the thawed soil (A→B in Fig. 6.10). Thawing also increases the hydraulic conductivity drastically from a frozen ($k = 1\times10^{-14}$ m/s) to a thawed ($k = k_{max}$) value (a→b$_1$ in Fig. 6.10). Note that stress ratio (η), the ratio between deviatoric to mean (p') stress, is greater than 0; therefore, the p' at the start of thaw consolidation is less than p'_{b0} (= 500

Pa). Primarily 1-D compression occurs in this soil element without changing η; therefore, e gradually decreases with p' (B→C), which also causes a reduction of k ($b_1 \rightarrow b_2 \rightarrow c$). In this simulation, k remains constant at k_{max} (= 3.3×10^{-7} m/s) during consolidation until the void ratio reduces to the value at b_2. Note that k_{max} has a significant effect on consolidation, as discussed later. Some oscillation (i.e., reduction of $p'$from line BC) is due to an increase in pore pressure resulting from the thawing of soil elements further below this point. For the soil elements far from the vertically downward direction (e.g., around the springline level), the η changes considerably during thaw settlement and in some cases, it could reach shear failure conditions.

6.9.1 Dissipation of excess pore water pressure

Figures 6.11(a)–6.11(d) show the pore water flow vectors at different time intervals. At t = 50 days, water flow mainly occurs from the soil below the pipe to the soil above it within the concentric thaw bulb, and no noticeable water flow occurs outside this zone (Fig. 6.11(a)). The excess pore water pressure at this condition is shown in Fig. 6.12. Although excess pore water pressure is not significantly different, a gradient is formed from the soil below the pipe to the soil above, which causes dissipation of excess pore water pressure, and thereby, the settlement of the pipe.

At t = 100 days, some water flow is observed near the surface directly above the pipe as the frozen zone between two thaw fronts is thin enough to dissipate some excess pore water pressure (Fig. 6.11(b)). This dissipation accelerates when the thaw fronts merge at $t \approx 120$ days. Therefore, the pore water pressure decreases quickly, and a significant ground settlement occurs because the shear strength of the thawed soil is lower than the frozen soil. A large, thawed zone is formed above the pipe after a longer period of thawing (Figs. 6.11(c) and 6.11(d)). The pore water pressure

generated along the thaw front dissipates through the zone, and the water mainly flows in an upward direction.

Note that, in the field, this kind of water flow scenario might be created due to a positive ground surface temperature in the summer. The subzero winter temperature could again create a frozen zone near the ground surface and reduce the rate of dissipation of pore water pressure and, thereby, the settlement rate. However, the dissipation of the excess pore water pressure is expected to occur quickly in the field through the soil layer near the ground surface because of the increase in hydraulic conductivity, due to the seasonal effect. In any case, although it is not done in the present study, a site-specific seasonal ground surface temperature variation could be incorporated in the developed program for a better simulation, when required.

6.9.2 Effect of nonlinear variation of hydraulic conductivity

Estimation of hydraulic conductivity of thawed soil (k) at large void ratios is a challenging task. As described before, for slurry consolidation under self-weight, hydraulic conductivity at a very low effective stress level could be obtained from different tests, such as settling column and fluidization tests (Sills 1995, 1998; Pane and Schiffman 1997; Bartholomeeusen et al. 2002). Unfortunately, such techniques are not available for the thawed soil because the formation processes of the soil of a high void ratio during the settling in slurry and thawing of ice-rich soil are different. However, in some studies, the e–log$k$ line obtained from a relatively higher stress level is simply extrapolated to the high void ratio at low stress (Dumais and Konrad 2018, 2019). For example, test data available on thawed soil at the Inuvik test site are mostly for $e < 1.3$ and corresponding $k < 3\times10^{-7}$ m/s (Watson et al. 1972). Dumais and Konrad (2019) extrapolated the e–log$k$ line obtained from these test data to $e = 1.47$ (void ratio at the liquid limit) and calculated

the maximum k of 1.94×10^{-4} m/s, which is approximately three orders higher than the measured maximum k.

To check the effect of maximum k at higher void ratios, a simulation is performed with e_{max} = 1.47 and $k_{max} = 1.94\times10^{-4}$ m/s and then compared with the previous simulation (e_{max} = 1.2 and $k_{max} = 3.3\times10^{-7}$ m/s). The surface and pipe settlements observed for this case are presented in Fig. 6.8(a) (dashed lines), which does not show any difference from the previous analysis results, except for a slight increase of surface settlement. Figure 6.13 shows the water flow vectors at different times. A comparison of pore-water flow vectors in Figs. 6.13(a) and 6.13(b) with Figs. 6.11(a) and 6.11(b), at 50 days and 100 days, shows that the water flow directions with both k_{max} are the same (follow the thaw bulb shape). However, Figs. 6.13(c) and 6.13(d) show very different flow vectors from those shown in Figs. 6.11(c) and 6.11(d), almost vertical in Figs. 6.11(c) and 6.11(d) with a lower k_{max}, while it is along the thaw front in Figs. 6.13(c) and 6.13(d) with a higher k_{max}.

The e-logp' and e-log$k$ curves for the same soil element directly below the pipe centerline at y_0 = 0.9 m, which is discussed previously for lower e_{max}, are presented in Fig. 6.10. No significant difference in e-logp' lines is observed for two values of e_{max}; however, compared to the analysis with the lower e_{max}, a significantly large decrease in k occurs during consolidation for larger e_{max} ($b_3\rightarrow b_4\rightarrow c$), although the final k is the same in both cases (point c). This indicated that the hydraulic conductivity after a period of thawing (e.g., t = 500 and 1,000 days) is significantly higher around the thaw front than that of the consolidated zone around the pipe, which is because of rapid reduction of e with a small increase in p' that results in a rapid reduction of k (Fig. 6.10). The difference in k within the thawed zone increases with an increase in k_{max} and C_c and a decrease

in C_k. Note that higher values of C_c and k_{max} are expected for ice-rich soil with an increasing frozen void ratio.

The present 2-D simulations reveal an important aspect of thaw consolidation modelling. Conceptually, the extrapolation of e-logp' and e-log$k$ to the low-stress level is acceptable until it is proven differently from advanced experiments. A large variation in k of several orders of magnitude in the thawed zone could cause pore water flow along the thaw front. However, in 1-D thaw consolidation, both heat and moisture flow paths under the pipe are assumed to be vertical (Morgenstern and Nixon 1975; Dumais and Konrad 2019). This assumption deviates more in the ice-rich soil of higher k at low effective stress. In such a case, the 1-D analysis with linear e-logp' and e-log$k$ relationships might give a lower thaw settlement rate because of the vertical flow of pore water through the lower permeable consolidated soil below the pipe.

6.10 Conclusions

An approach for finite element modelling of thaw consolidation is presented in this study. Fully coupled thermo-hydro-mechanical simulations are performed for one- and two-dimensional thaw consolidation of saturated soil. The mechanical behaviour of thawed soil is modelled using a modified Drucker–Prager Cap model, and the hydraulic conductivity is varied with the calculated void ratio. One-dimensional FE analyses are also performed for constant volumetric compressibility, and the results are compared with a decoupled analytical solution based on small-strain linear consolidation theory.

The present FE technique can simulate 1-D thaw consolidation for a given value of volume compressibility with and without surcharge, including post-thaw consolidation. Some discrepancies in pore pressure variation with the depth between the present FE results and the analytical solution are due to allowing the displacement of the warm boundary with consolidation

in FE analysis. The value of effective stress at the start of thaw consolidation affects the progress of consolidation. If an *e*-log*k* relationship extrapolated up to a high void ratio (e.g., void ratio immediately after thawing) is used, a significant variation of *k* occurs within the thawed zone because of the high compressibility of the soil at such low stress. In a two-dimensional thawing under that condition, the pore water flows along the curved thaw front; therefore, the assumption of one-dimensional thaw consolidation below the pipe due to pure vertical heat and moisture flow becomes questionable, especially for ice-rich soil.

The present 2-D FE simulations are conducted in uniform soil. In the field, the soil near the ground surface might vary due to seasonal effects and differences in backfill materials and native soil properties. Moreover, the seasonal variation of the ground surface temperature needs to be considered. Finally, limited laboratory test results are available on thawed soil, especially at the low-stress level, to develop a constitutive model and to estimate soil properties. However, these factors could be implemented easily in the present FE modelling technique.

Acknowledgments

The works presented in this chapter have been supported by the InnovateNL, formerly Research Development Corporation (RDC), Newfoundland and Labrador, through the ArcticTECH program, Equinor Research Chair, and Natural Sciences and Engineering Research Council of Canada.

List of symbols

The following symbols are used in this chapter:

C_c compression index of thawed soil

C_k slope of e–log$k$ curve

C_s swelling/recompression index of thawed soil

c_i specific heat of ice

c_p specific heat of pipe material

c_s specific heat of soil particle

c_v coefficient of consolidation

c_w specific heat of water

c' cohesion of thawed soils

c'_f cohesion of frozen soils

D pipe diameter

d t_s intercept of F_s

E_p Young's modulus of pipe material

E' Young's modulus of thawed soils

E'_f Young's modulus of frozen soils

e void ratio

e_f void ratio of frozen soil

e_{max} void ratio at maximum hydraulic conductivity

e_{th} thawed void ratio

e_0 void ratio of thawed soils after phase change

F_c cap surface in modified Drucker–Prager model

F_s shear failure surface in modified Drucker–Prager model

G_s specific gravity

H burial depth

h drainage length

J_3 third deviatoric stress invariant

K parameter defines the shape of the yield surface in the deviatoric plane

k hydraulic conductivity of thawed soils

k_{f} hydraulic conductivity of frozen soils

$k_{\max}$ maximum hydraulic conductivity

L latent heat of soils

L' latent heat of water

m_{v} volume compressibility of thawed soils

P_0 applied surcharge

p' mean effective stress

p'_a evolution parameter in modified Drucker–Prager model

p'_b hydrostatic yield stress of thawed soils

p'_{bf} initial hydrostatic yield stress of frozen soils;

p'_{b0} initial hydrostatic yield stress of thawed soils

q Mises equivalent stress

R thaw consolidation ratio

R_1 cap shape parameter for thawed soils

$R_{1\mathrm{f}}$ cap shape parameter for frozen soils

S top surface thaw settlement in 1-D analyses

S_{p} pipe settlement

S_{s} ground surface settlement

T temperature

T_g initial ground temperature

T_{lw} liquidus temperature

T_p pipe temperature

T_s surface temperature

T_{sw} solidus temperature

T_v time factor

t time

t_s deviatoric stress

u excess pore water pressure

W_u fraction of total water that remains unfrozen in frozen soils

w moisture content of frozen soil

Y depth of thaw front from current surface (or pipe invert) position

Y_0 depth of thaw front from initial surface (or pipe invert) position

y vertical distance measured from current surface (or pipe center);

y_0 vertical distance measured from initial surface (or pipe center)

α constant determined from heat transfer solution

α_1 parameter to define transition region of yield surface

β_1 slope of F_s on the meridional plane

γ_w unit weight of water

γ' submerged unit weight of the thawed soil

ε_v^p plastic volumetric strain

η stress ratio

κ slope of e–lnp' in elastic region

λ slope of e–lnp' in plastic region

λ_i thermal conductivity of ice

λ_p thermal conductivity of pipe material

λ_s thermal conductivity of soil particle

λ_w thermal conductivity of water

v Poisson's ratio of thawed soils

v_f Poisson's ratio of frozen soils

v_p Poisson's ratio of pipe material

σ_v' vertical effective stress

σ_0' residual stress of thawed soils

ϕ' angle of internal friction of thawed soil

ϕ_f' angle of internal friction of frozen soil

References

Abaqus. 2014. Abaqus documentation. 6.14. Providence. Dassault Systemes, USA.

Andersland, O.B., and Ladanyi, B. 2004. Frozen ground engineering. John Wiley and Sons, New Jersey, USA.

Anderson, D.M., Tice, A.R., and McKim, H.L 1973. The unfrozen water and the apparent specific heat capacity of frozen soils. *In* Proceedings of Second International Conference on Permafrost, Yakutsk, USSR, pp. 289–295.

Bartholomeeusen, G., Sills, G.C., Znidarčić, D., Van Kesteren, W., Merckelbach, L.M., Pyke, R., Carrier III, W.D., Lin, H., Penumadu, D., Winterwerp, H., and Masala, S., 2002. Sidere: numerical prediction of large-strain consolidation. Géotechnique, **52**(9): 639–648.

Carslaw, H. S., and Jaegar, J.C. 1947. Conduction of heat in solids. Clarendon Press, Oxford.

C-CORE. 2012. Modelling of Thaw-settlement related to Mo'he-Daqing crude oil pipeline. C-CORE publication C-R-12-080-928. C-CORE, St. John's, Canada.

Chamberlain, E.J., and Gow, A.J. 1979. Effect of freezing and thawing on the permeability and structure of soils. Engineering Geology, **26**: 73–92.

Dayarathne, R., Hawlader, B.C., and Robert, D. 2019. An approach for finite element modeling of one-dimensional thaw consolidation. *In* Proceedings of 72nd Canadian Geotechnical Conference, Canadian Geotechnical Society, St. John's, Canada, 8p.

Dumais, S. 2019. Modelling large thaw consolidation deformations. Ph.D. thesis, University of Laval, Quebec, Canada.

Dumais, S., and Konrad, J.M. 2018. One-dimensional large-strain thaw consolidation using nonlinear effective stress–void ratio–hydraulic conductivity relationships. Canadian Geotechnical Journal, **55**(3): 414–426.

Dumais, S., and Konrad, J.M. 2019. Large-strain nonlinear thaw consolidation analysis of the inuvik warm-oil experimental pipeline buried in permafrost. Journal of Cold Regions Engineering, **33**(1): 04018014.

Foriero, A., and Ladanyi, B. 1995. FEM assessment of large-strain thaw consolidation. Journal of Geotechnical Engineering, **121**(2): 126–138.

Gholamzadehabolfazl, A. 2015. A numerical study of a highway embankment on degrading permafrost. M.Sc. thesis, University of Manitoba, Winnipeg, Manitoba.

Gibson, R.E., Schiffman, R.L., and Cargill, K.W. 1981. The theory of one-dimensional consolidation of saturated clays. II. Finite nonlinear consolidation of thick homogeneous layers. Canadian Geotechnical Journal, **18**(2): 280–293.

Hawlader, B.C., Muhunthan, B., and Imai, G. 2008. State-dependent constitutive model and numerical solution of self-weight consolidation. Géotechnique, **58**(2): 133–141.

Konrad, J.-M., and Samson, M. 2000. Hydraulic conductivity of kaolinite-silt mixtures subjected to closed-system freezing and thaw consolidation. Canadian Geotechnical Journal, **37**(4): 857–869.

Lesage, K. 2008. Experimental studies of thaw consolidation of fine grained frozen soils from the Mackenzie Valley. Ph.D. thesis, University of Ottawa.

Lunardini, V. J. 1988. Freezing of soil with an unfrozen water content and variable thermal properties. CRREL report 88-2. CRREL, Hanover, NH, USA.

Morgenstern, N.R., and Nixon, J.F. 1971. One-dimensional consolidation of thawing soils. Canadian Geotechnical Journal, **8**(4): 558–565.

Morgenstern, N.R., and Nixon, J.F. 1975. An analysis of the performance of a warm-oil pipeline in permafrost, Inuvik, NWT. Canadian Geotechnical Journal, **12**(2): 199–208.

Nixon, J.F. 1973. Thaw–Consolidation of Some Layered Systems. Canadian Geotechnical Journal, **10**(4): 617–631.

Nixon, J.F. 1975. The role of convective heat transport in the thawing of frozen soils. Canadian Geotechnical Journal, **12**(3): 425–429.

Nixon, J.F., and McRoberts, E.C. 1973. A study of some factors affecting the thawing of frozen soils. Canadian Geotechnical Journal, **10**(3): 439–452.

Nixon, J.F., and Morgenstern, N.R. 1973. The residual stress in thawing soils. Canadian Geotechnical Journal, **10**(4): 571–580.

Nixon, J.F., and Morgenstern, N.R. 1974. Thaw–consolidation tests on undisturbed fine-grained permafrost. Canadian Geotechnical Journal, **11**(1): 202–214.

Pane, V., and Schiffman, R.L. 1997. The permeability of clay suspensions. Géotechnique, **47**(2): 273–288.

Patterson, D.E., and Smith, M.W. 1981. The measurement of unfrozen water content by time domain reflectometry: Results from laboratory tests. Canadian Geotechnical Journal, **18**(1): 131–144.

Rowley, R.K., Watson, G.H., Wilson, T.M., and Auld, R.G. 1973. Performance of a 48-in. warm-oil pipeline supported on permafrost. Canadian Geotechnical Journal, **10**(2): 282–303.

Shoop, S., Affleck, R., Haehnel, R., and Janoo, V. 2008. Mechanical behavior modeling of thaw-weakened soil. Cold Regions Science and Technology, **52**(2): 191–206.

Sills, G.C. 1995. Time dependent processes in soil consolidation. *In* Proceedings of the International Symposium on Compression and Consolidation of Clayey Soils, *Edited by* H. Yoshikuni and O. Kusakabe, A. A. Balkema, Rotterdam, pp. 875–890.

Sills, G.C. 1998. Development of structure in sedimenting soils. Philosophical Transactions of the Royal Society of London. Series A: Mathematical, Physical and Engineering Sciences, **356**(1747): 2515–2534.

Slusarchuk, W.A., Watson, G.H., and Speer, T.L. 1973. Instrumentation around a warm oil pipeline buried in permafrost. Canadian Geotechnical Journal, **10**(2): 227–245.

Smith, L.B. 1972. Thaw consolidation tests on remoulded clays. M.Sc. thesis, University of Alberta.

Wang, Y.P., Li, G.Y., Jin, H.J., Lu, L.Z., He, R.X., and Zhang, P. 2016. Thermal state of soils in the active layer and underlain permafrost at the kilometer post 304 site along the China-Russia Crude Oil Pipeline. Journal of Mountain Science, **13**(11): 1984–1994.

Wang, F., Li, G., Ma, W., Mu, Y., Zhou, Z., and Mao, Y. 2018. Permafrost thawing along the China-Russia crude oil pipeline and countermeasures: a case study in Jiagedaqi, northeast China. Cold Regions Science and Technology, **155**: 308–313.

Watson, G.H., Rowley, R.K., and Speer, T.L. 1972. Inuvik frozen core testing. Mackenzie Valley Pipeline Research Limited. Calgary, Alberta, Canada.

Watson, G.H., Rowley. R.K., and Slusarchuk, W.A. 1973. Performance of a warm oil pipeline buried in permafrost. *In* Proceedings of Second International Conference on Permafrost, Yakutsk, USSR, pp. 759–766.

Wood, D. M. 1990. Soil behaviour and critical state soil mechanics. Cambridge university press, Cambridge.

Yao, X., Qi, J., and Wu, W. 2012. Three dimensional analysis of large strain thaw consolidation in permafrost. Acta Geotechnica, **7**(3): 193–202.

Yu, F., Guo, P., Lai, Y., and Stolle, D. 2020. Frost heave and thaw consolidation modelling. Part 2: One-dimensional thermohydromechanical (THM) framework. Canadian Geotechnical Journal, **57**(10): 1595–1610.

Zhang, M., Zhang, X., Lai, Y., Lu, J., and Wang, C. 2020. Variations of the temperatures and volumetric unfrozen water contents of fine-grained soils during a freezing–thawing process. Acta Geotechnica, **15**(3): 595–601.

Zhu, M. 2006. Modeling and simulation of frost heave in frost-susceptible soils. Ph.D. thesis, Department of Civil and Environmental Engineering, University of Michigan.

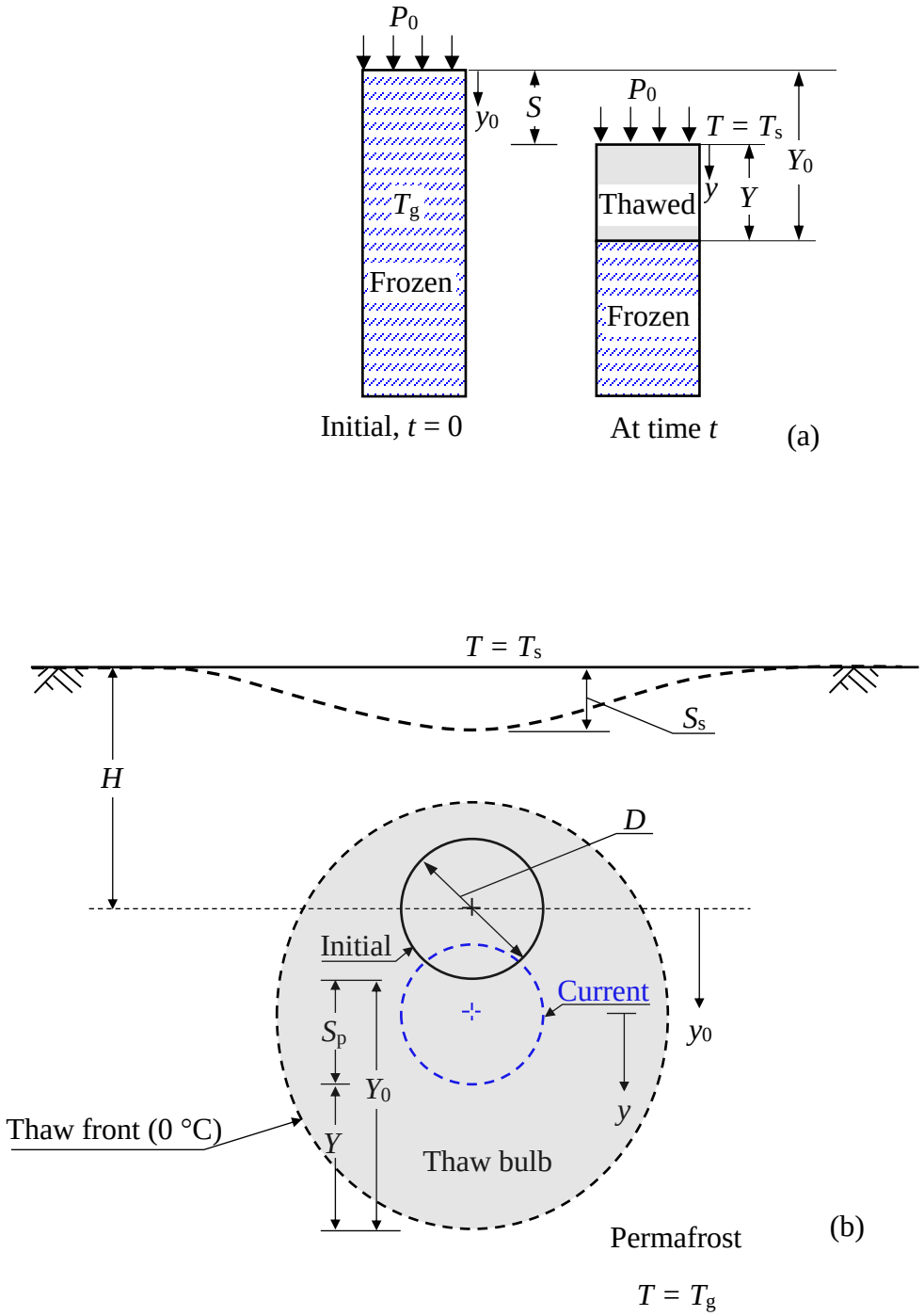

Fig. 6.1. Schematic of thaw consolidation: (a) 1-D thawing of a frozen soil column; and (b) permafrost thawing through a buried warm pipeline

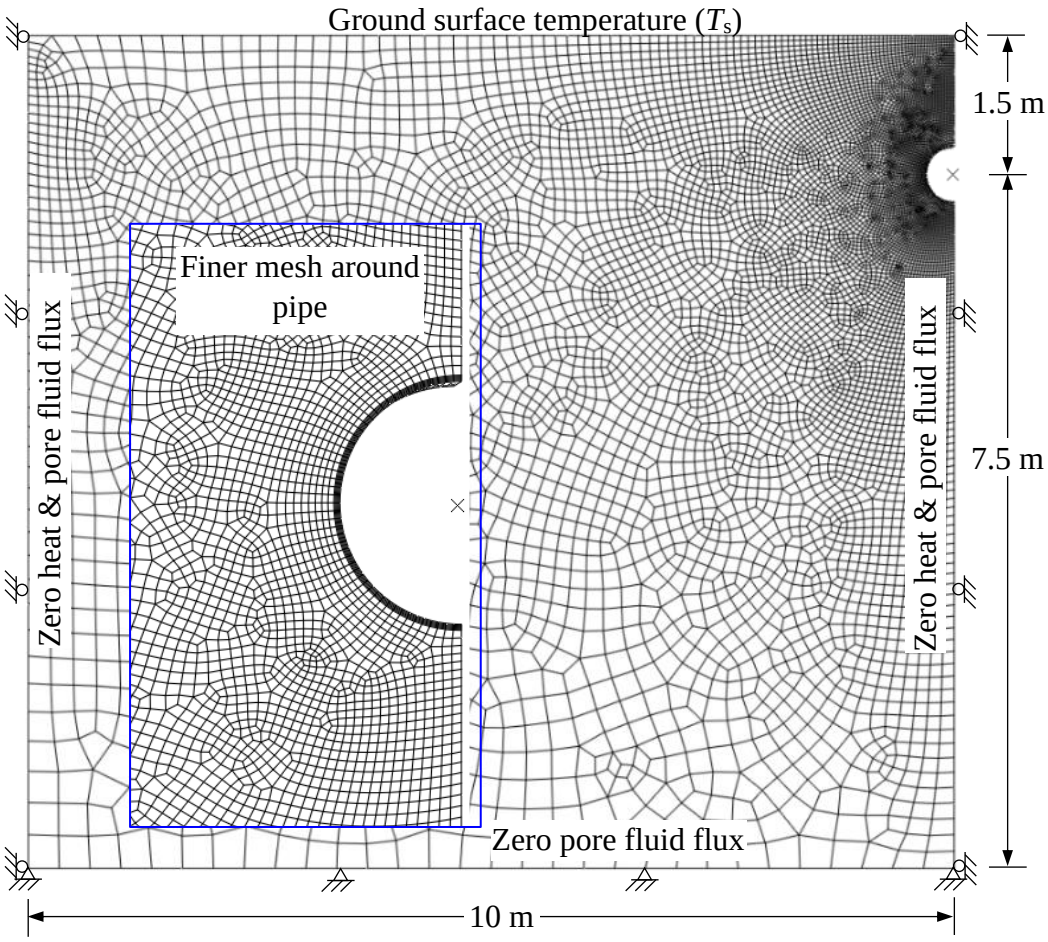

Fig. 6.2. FE mesh used in two-dimensional thawing around pipeline

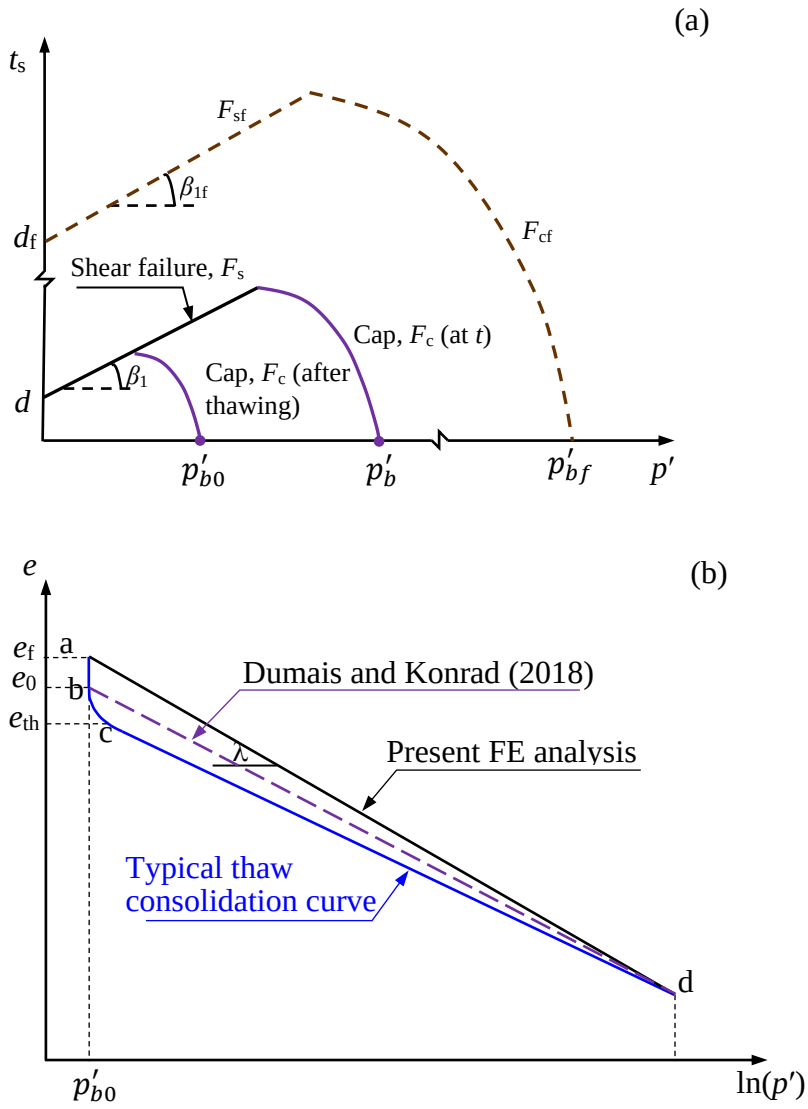

Fig. 6.3. Modified Drucker–Prager Cap material model: (a) yield surface; and (b) void ratio–effective stress relationship of thawed soil

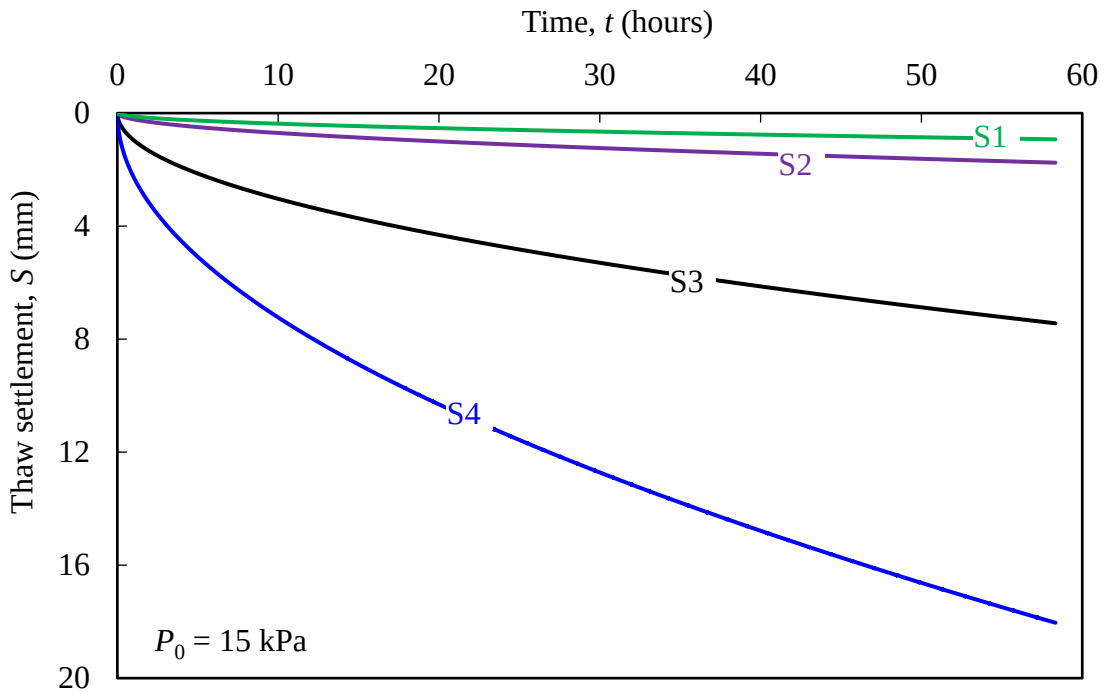

Fig. 6.4. Surface settlement in the simulations with a surcharge

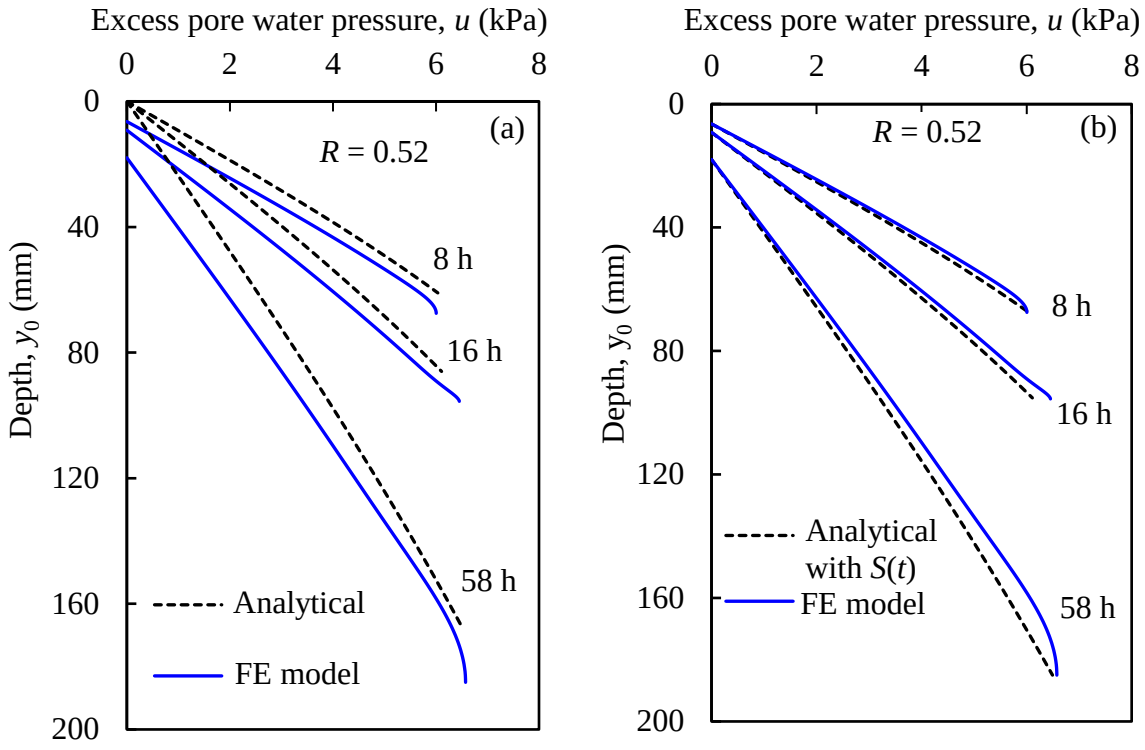

Fig. 6.5. Comparison of FE calculated excess pore water pressure with analytical solution for case S4: (a) without surface settlement; and (b) considering surface settlement

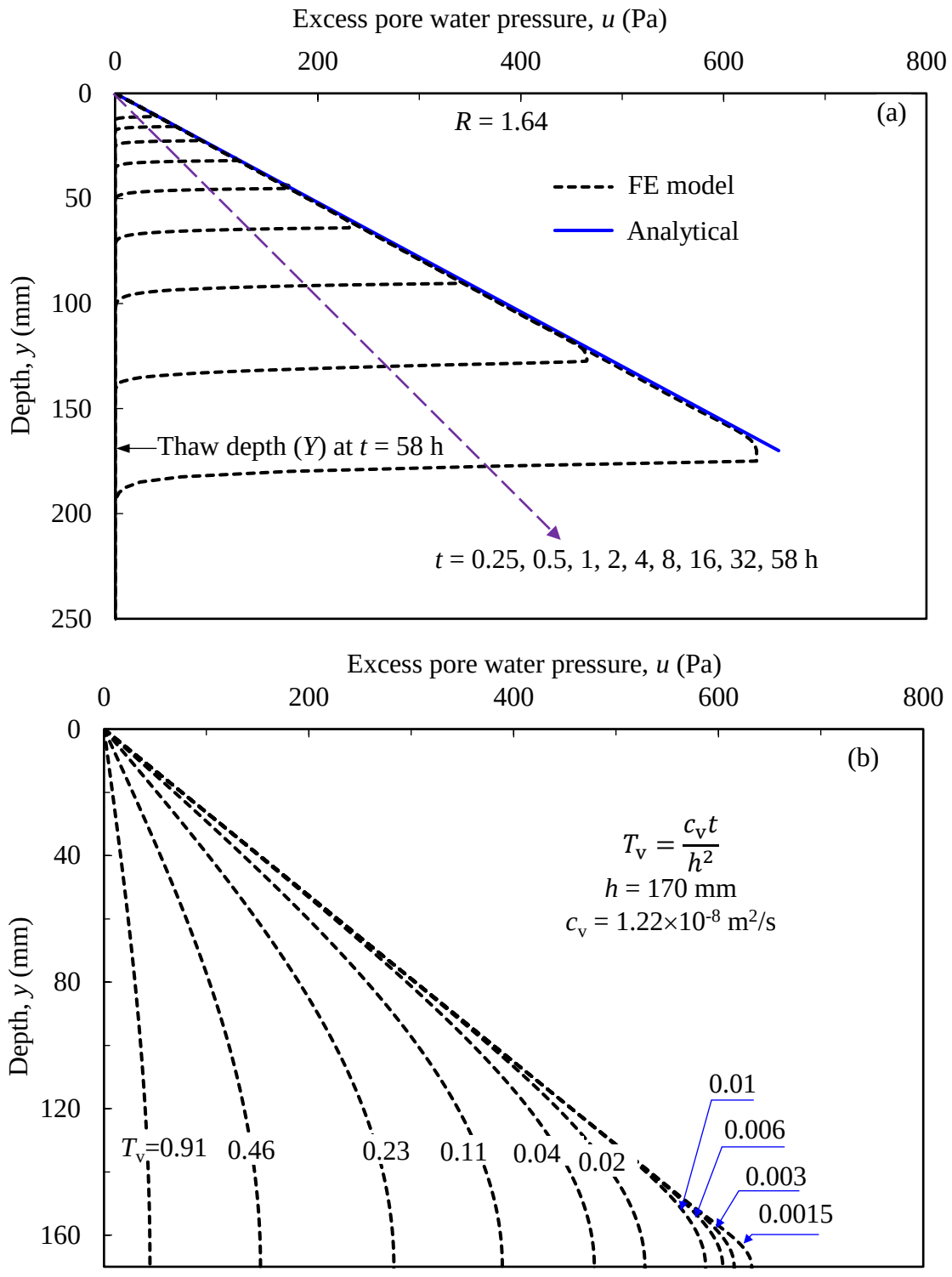

Fig. 6.6. Excess pore water pressure under self-weight in case S3: (a) generation during thawing; and (b) dissipation during post-thaw consolidation

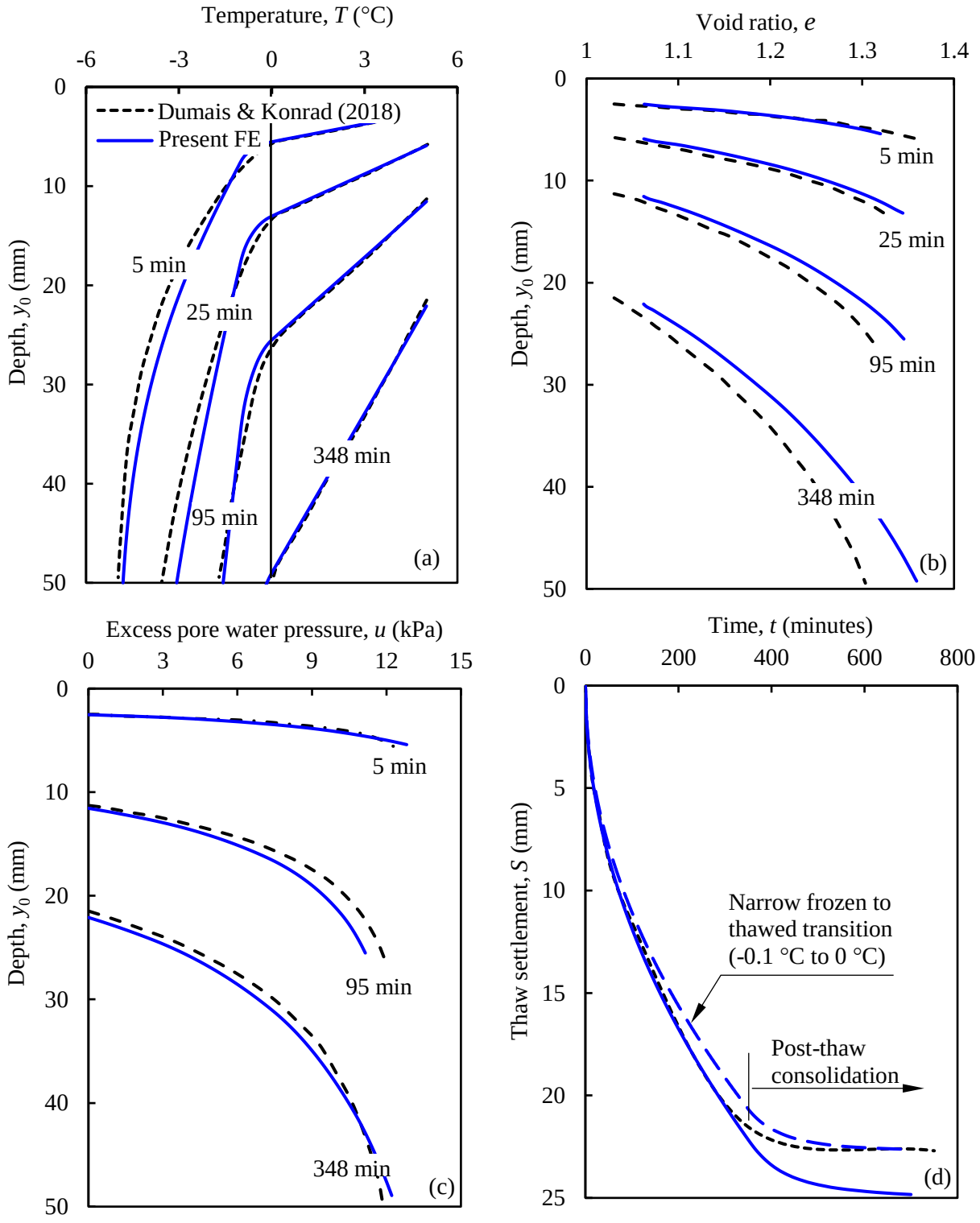

Fig. 6.7. Comparison of present FE results with previous study: (a) temperature distribution; (b) void ratio; (c) excess pore water pressure; and (d) thaw settlement

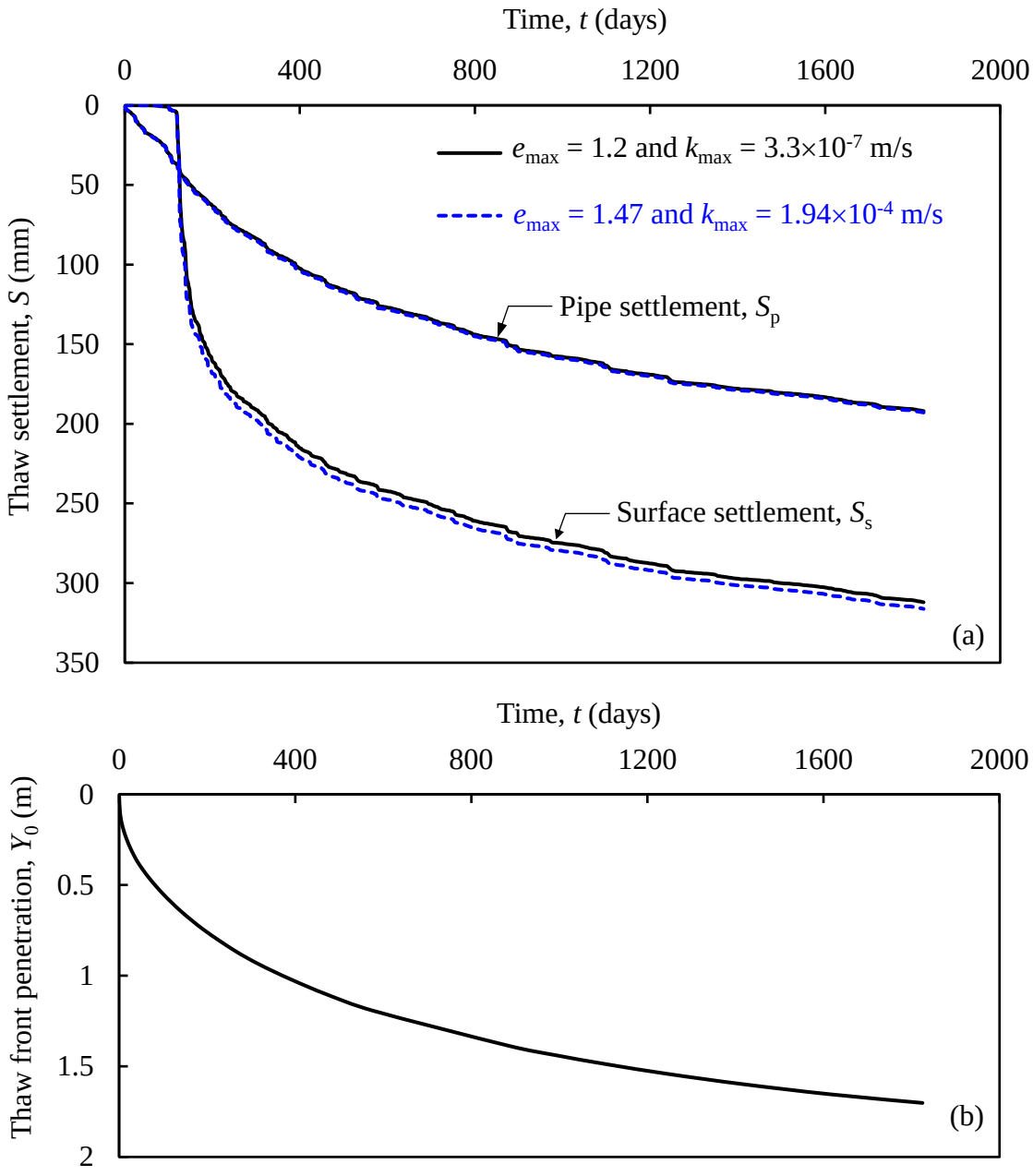

Fig. 6.8. Two-dimensional thawing around pipe: (a) thaw settlement; and (b) thaw front penetration

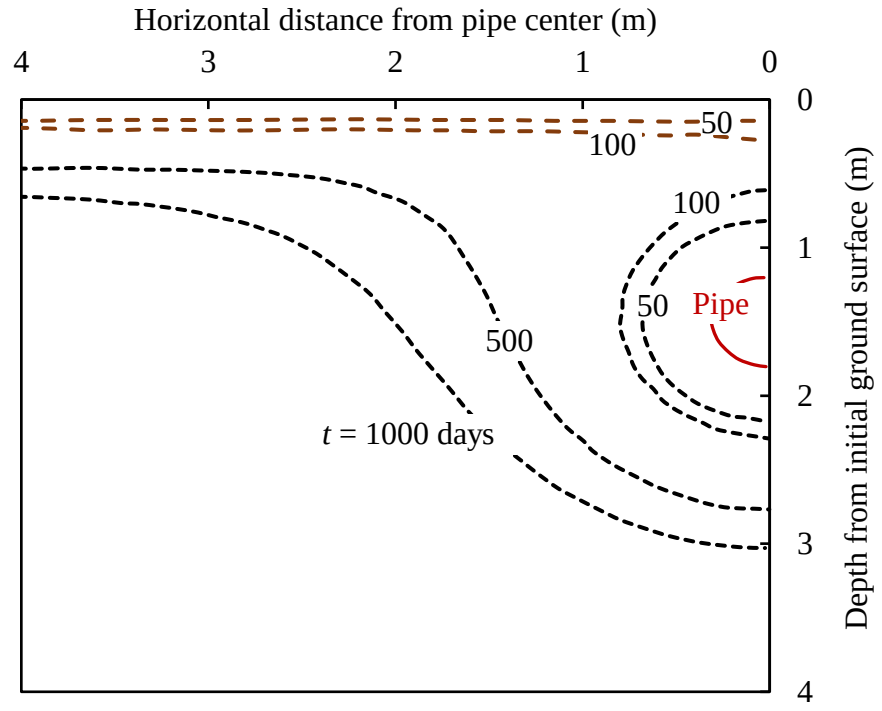

Fig. 6.9. Location of thaw front at different time

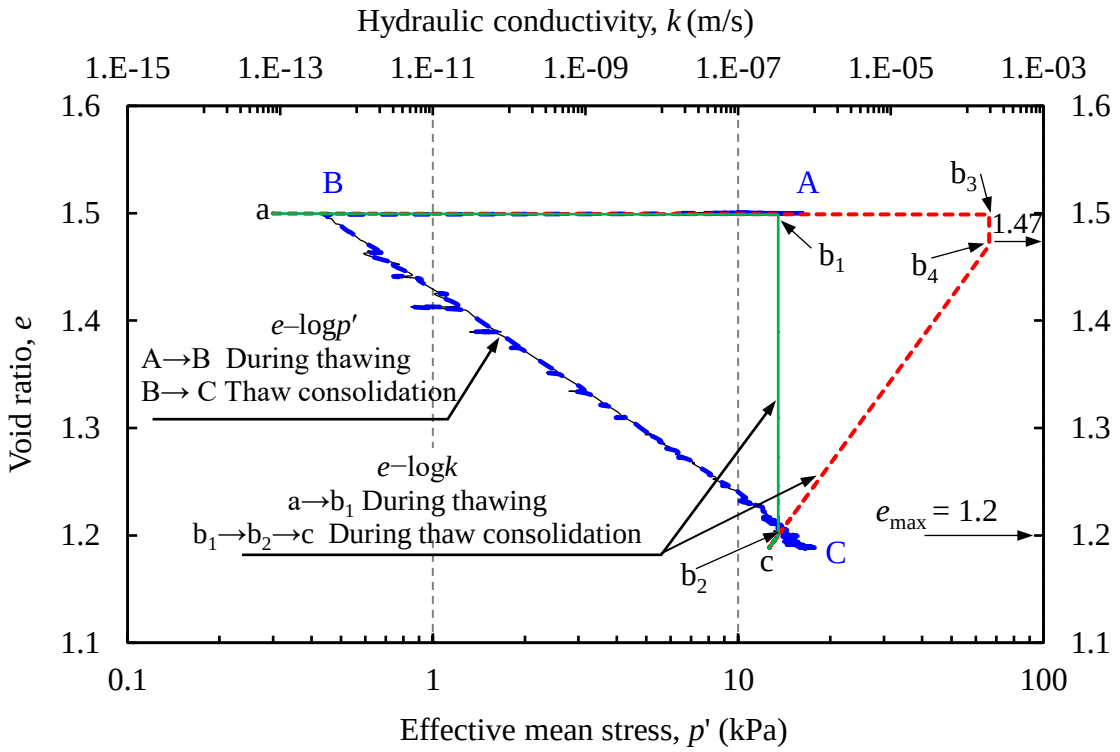

Fig. 6.10. FE calculated mean effective stress and hydraulic conductivity of an element directly below the pipe center at y_0 = 0.9 m

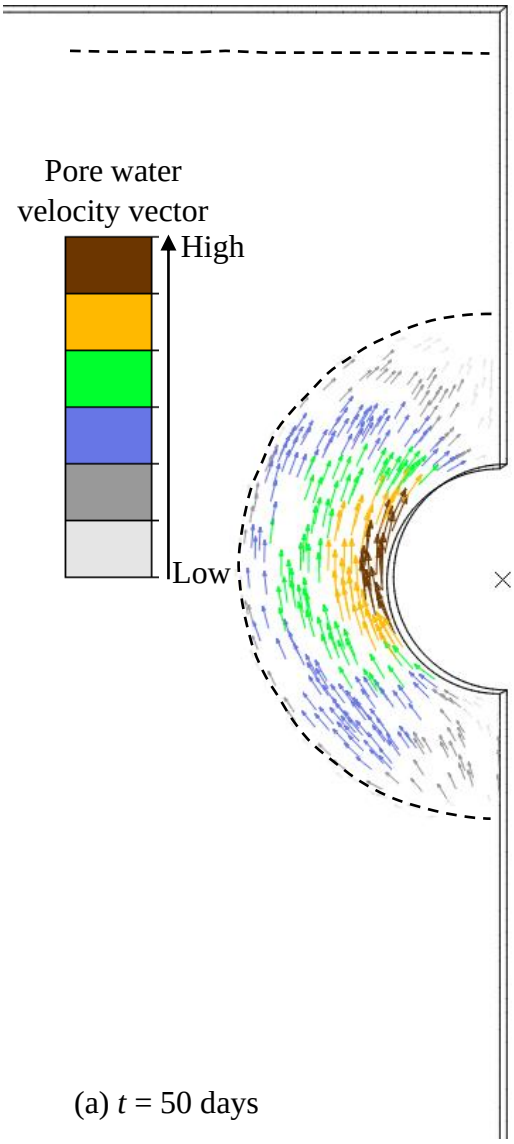

(a) t = 50 days

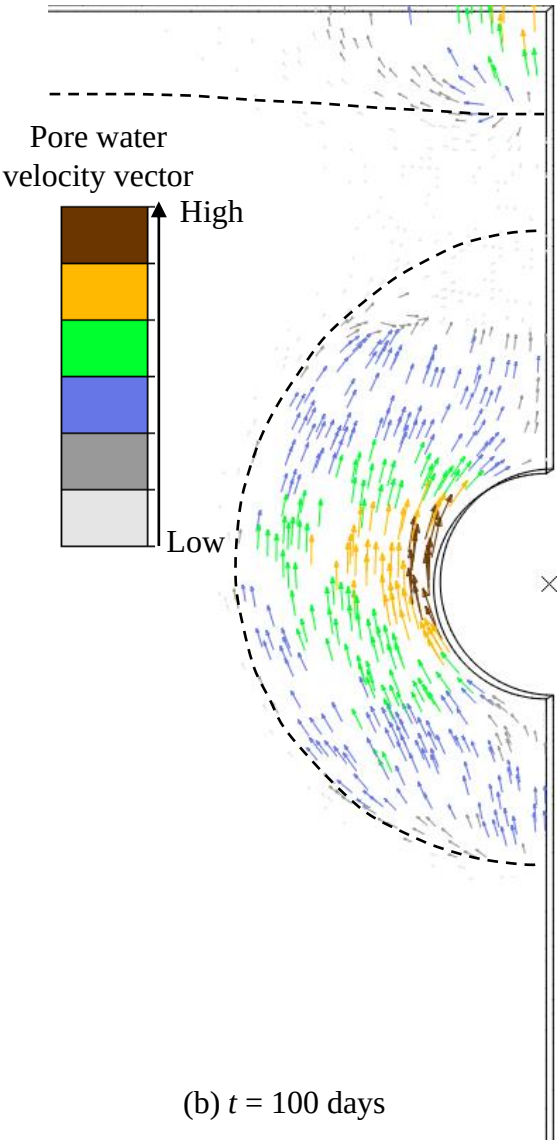

(b) t = 100 days

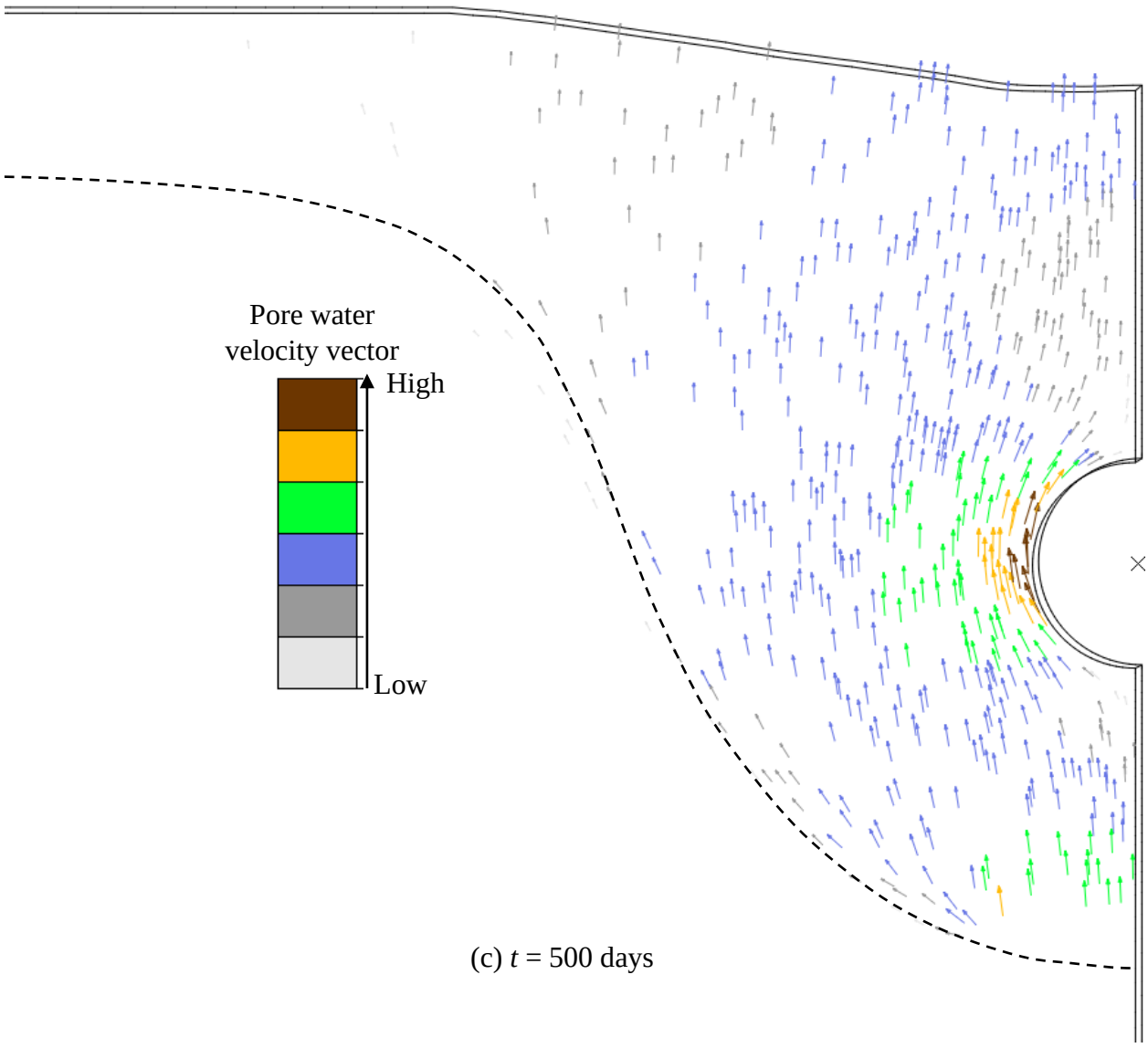

(c) t = 500 days

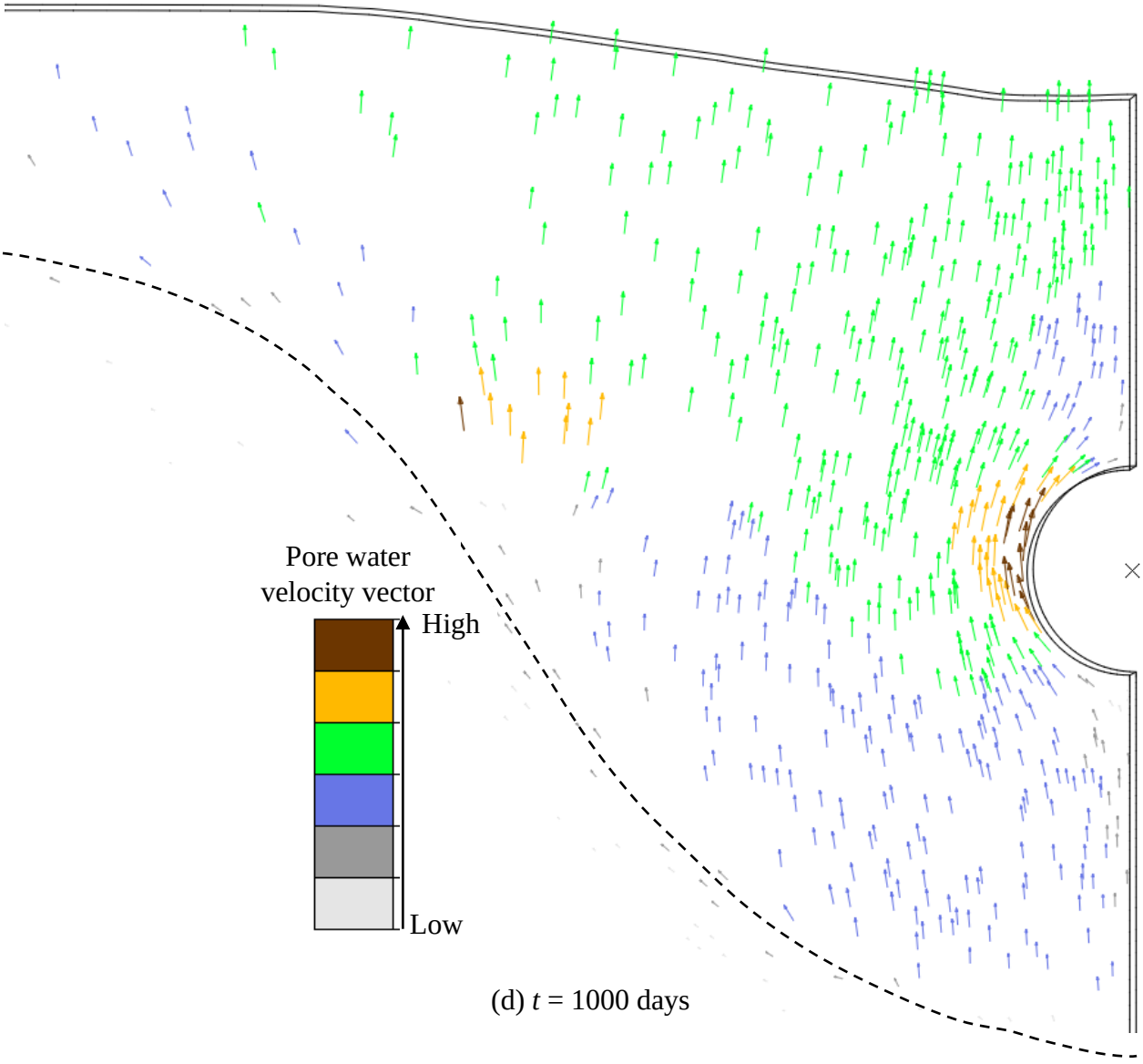

Fig. 6.11. Pore water flow vectors at different time intervals (e_{max} = 1.2 and k_{max} = 3.3×10^{-7} m/s)

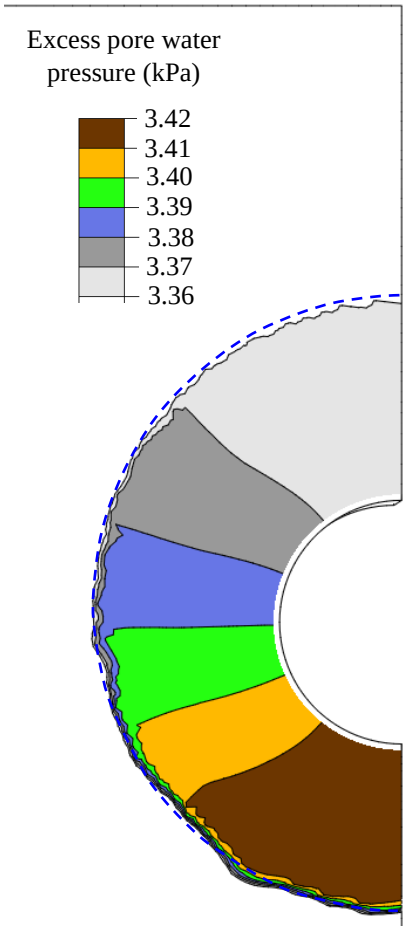

Fig. 6.12. Excess pore water pressure around the pipe after 50 days

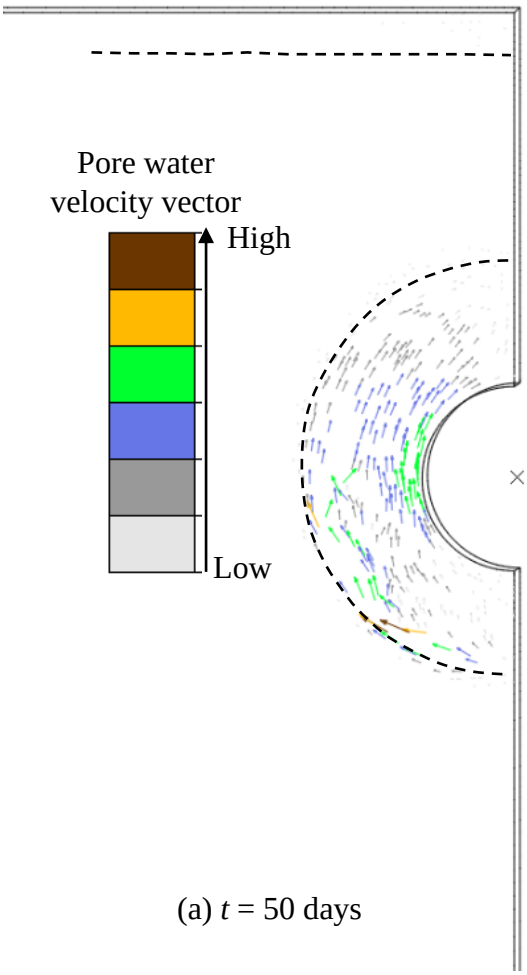

(a) t = 50 days

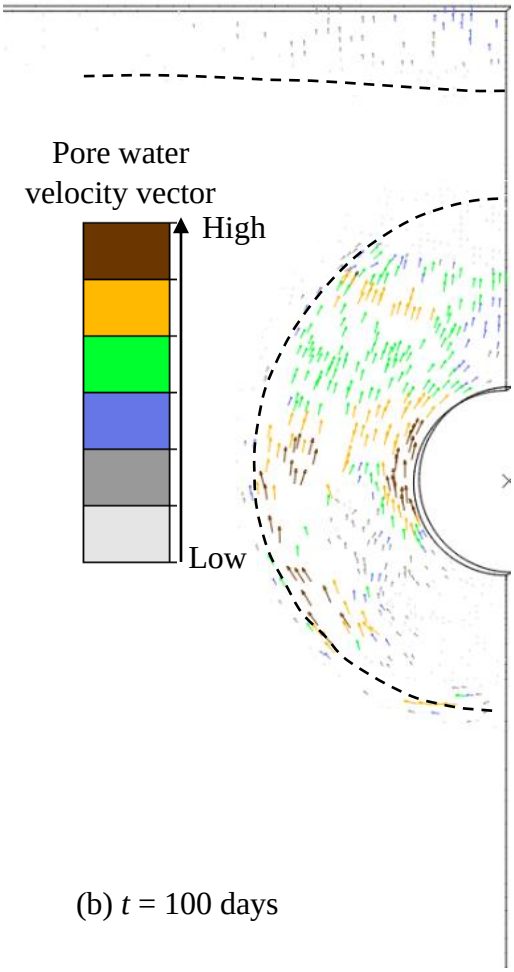

(b) t = 100 days

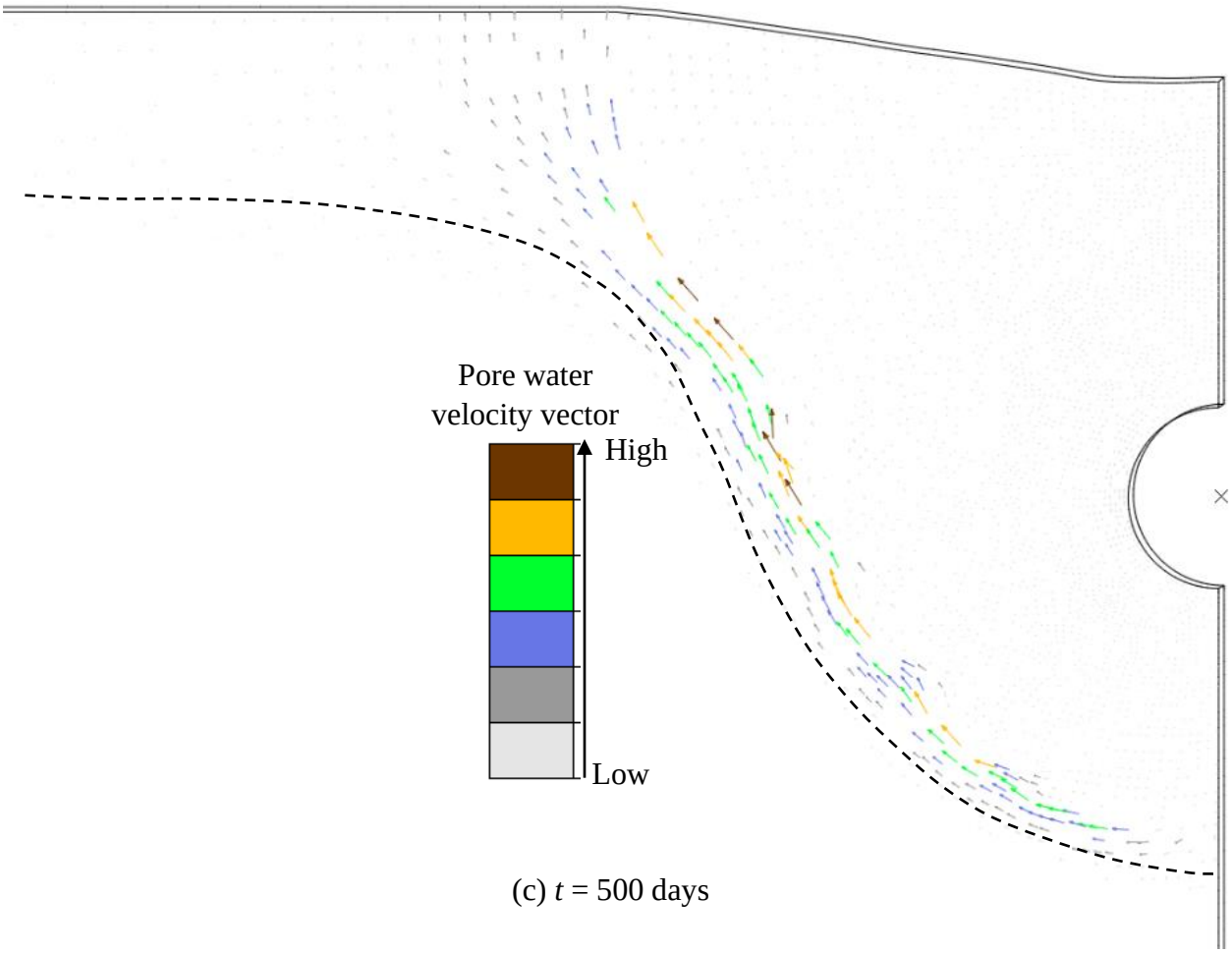

(c) t = 500 days

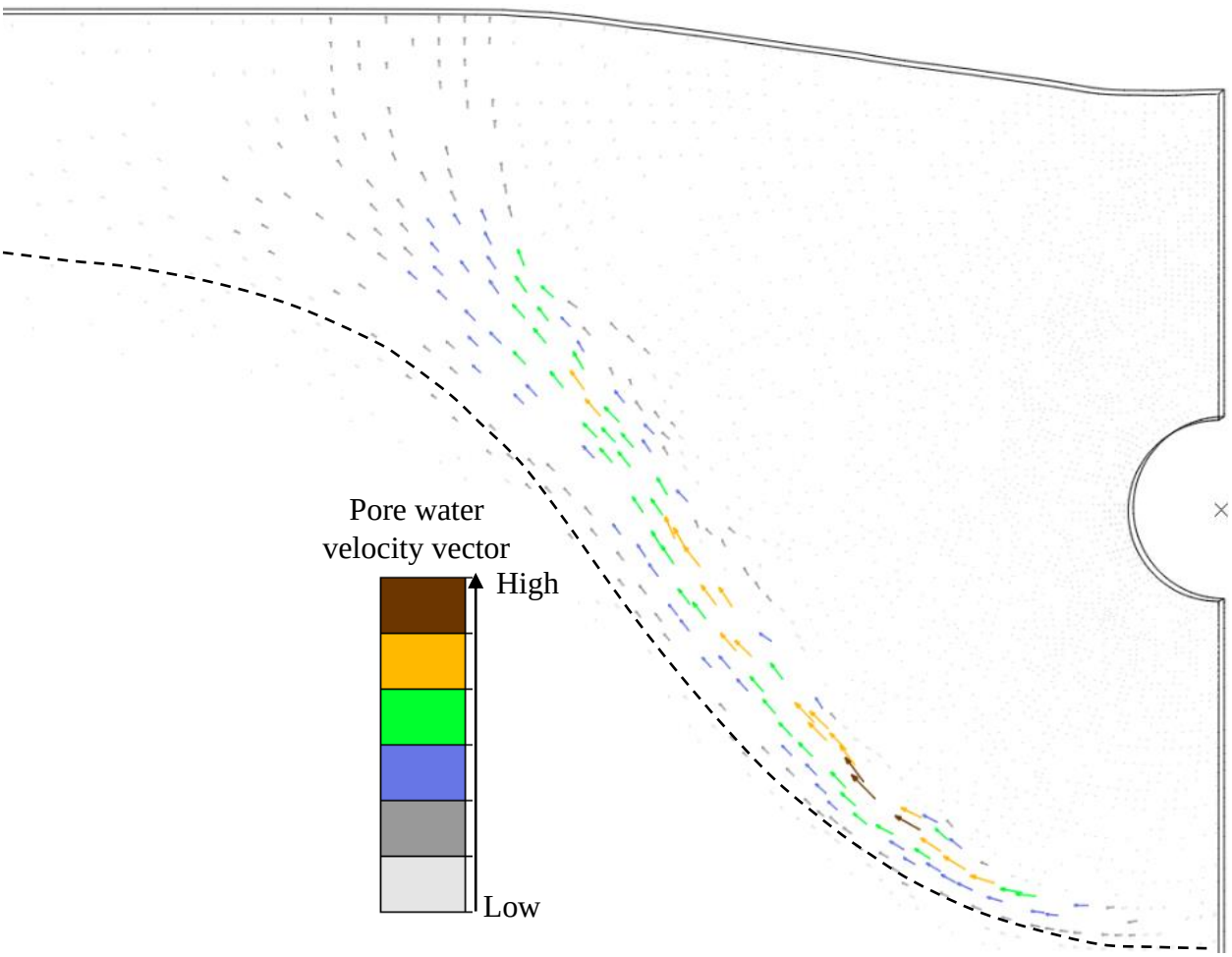

(d) t = 1000 days

Fig. 6.13. Pore water flow vectors at different time intervals (e_{max} = 1.47 and k_{max} = 1.94×10^{-4} m/s)

Table 6.1. Mechanical properties used in Set-II and Set-III analysis with nonlinear soil model

Parameter	Values
Thawed soil	
Young's modulus, E'(MPa)	10
Poisson's ratio, v	0.25
Hydrostatic yield stress immediately after thawing, p'_{b0} (kPa)	$0.003^{(II)}$, $0.5^{(III)}$
Cap shape parameter, R_1	0.5
Slope of e–lnp' in elastic region, κ	$0.021^{(II)}$, $0.011^{(III)}$
Slope of e–lnp' in plastic region, λ	$0.21^{(II)}$, $0.11^{(III)}$
Slope of e-log$k$ line, C_k	$0.305^{(II)}$, $0.098^{(III)}$
Void ratio at maximum hydraulic conductivity, e_{max}	$2.6^{(II)}$, 1.2 & $1.47^{(III)}$
Maximum hydraulic conductivity, k_{max} (m/s)	$4.05\times10^{-4(II)}$, 3.3×10^{-7}& $1.94\times10^{-4(III)}$
Angle of internal friction, ϕ' (°)	25
Cohesion, c' (kPa)	$0.001^{(II)}$, $0.1^{(III)}$
Frozen soil	
Initial void ratio, e_f	$2.83^{(II)}$, $1.5^{(III)}$
Specific gravity, G_s	$2.65^{(II)}$, $2.67^{(III)}$
Bulk density (kg/m^3)	$1{,}431^{(II)}$, $1{,}668^{(III)}$
Young's modulus, E'_f (MPa)	1,200
Poisson's ratio, v_f	0.25
Hydrostatic yield stress, p'_{bf} (kPa)	40×10^3
Cap shape parameter, R_{1f}	0.5
Hydraulic conductivity, k_f (m/s)	1×10^{-14}
Angle of internal friction, ϕ'_f (°)	25
Cohesion, c'_f (kPa)	14×10^3
Pipe material	

Density (kg/m^3)	7,850$^{(III)}$
Young's modulus, E_p (MPa)	$2\times10^{5(III)}$
Poisson's ratio, ν_p	0.3$^{(III)}$

Note: Superscripts II & III are the values for Sets-II & III analyses

Table 6.2. Thermal properties used in FE analysis

Parameter	Values
Thermal conductivity of soil skeleton, λ_s (W/m°C)	2.1
Thermal conductivity of water, λ_w (W/m°C)	0.6
Thermal conductivity of ice, λ_i (W/m°C)	2.24
Specific heat of soil skeleton, c_s (J/kg°C)	836
Specific heat of water, c_w (J/kg°C)	4,184
Specific heat of ice, c_i (J/kg°C)	2,100
Latent heat of water, L' (J/kg)	334,720
Fraction of total water that remains unfrozen in frozen soils, W_u	$0.1^{(I, III)}$, $0.3^{(II)}$
Liquidus temperature, T_{lw} (°C)	0
Solidus temperature, T_{sw} (°C)	$-3^{(I)}$, $-1^{(II, III)}$
Thermal conductivity of pipe material, λ_p (W/m°C)	$52^{(III)}$
Specific heat of pipe material, c_p (J/kg°C)	$434^{(III)}$

Note: Superscripts I, II & III are the values for Sets-I, II & III analyses

Table 6.3. Parameters used in one-dimensional Set-I analysis with linear soil model

Parameter	Value			
	S1	S2	S3	S4
Initial void ratio, e_f	2.6			
Specific gravity, G_s	2.67			
Bulk density (kg/m^3)	1464			
Frozen soil Young's modulus, E_f' (MPa)	1200			
Frozen soil Poisson's ratio, v_f	0.25			
Thawed soil Young's modulus, E' (MPa)	1.0	1.0	1.0	0.1
Thawed soil Poisson's ratio, v	0.25			
Initial ground temperature, T_g (°C)	-5			
Top surface temperature, T_s (°C)	5	20	20	20
Volume compressibility of thawed soil, m_v (m^2/kN) ×10^{-4}	8.33	8.33	83.3	83.3
Hydraulic conductivity of thawed soil, k (m/s) ×10^{-9}	1	1	1	10
Calculated parameters for analytical solution				
Constant, α (m/s$^{1/2}$) ×10^{-5}	16.45	36.6	36.3	36.1
Coefficient of consolidation, c_v (m^2/s) ×10^{-8}	12.2	12.2	1.22	12.2
Thaw consolidation ratio, R	0.24	0.52	1.64	0.52

CHAPTER 7:

Conclusions and Recommendations for Future Research

7.1 Conclusions

Experimental and numerical investigations of frost heave and thaw settlement of pipelines under constant and cyclic temperatures of the pipeline and ground surfaces are presented in this thesis. Some general conclusions that can be drawn from the whole thesis are presented below. The problem-specific conclusions and practical implications are discussed at the end of Chapters 3–6 and Appendices A and B.

Chapter 3 presents an experimental evaluation of pipeline heave and settlement based on the results of 14 model pipes' tests in a geotechnical centrifuge. The tests were conducted for seasonal variations of pipe and ground surface temperatures after an initial period of chilling. Five types of displacement responses are found, depending upon the test conditions and pipeline operating temperature. The practical implications of such responses are discussed based on the expected operating conditions of a chilled gas pipeline between two compressor stations. In general, cyclic pipeline temperatures during operation reduce the total frost heave and heave rate, compared to those expected in a scenario of operating under continuous sub-zero pipe temperatures. This implies that seasonally varying pipeline temperatures might reduce the frost heave of chilled gas pipelines. However, seasonal thawing and refreezing of thawed soil under cyclic operating conditions could make the process more complex and could alter the pipeline–soil interaction behaviour.

Chapter 4 presents a two-dimensional coupled thermo-mechanical FE model to simulate the frost heave around buried chilled pipelines. In addition to the freezing of the in-situ water, the Konrad-Morgenstern segregation potential model is implemented in a commercial finite element

program using user subroutines to calculate the water migration to the freezing front and the resulting volumetric expansion due to the formation of ice lenses. The mechanical behaviour of frozen and unfrozen soils is defined using simplified elastic-plastic models considering the key influencing factors, including temperature and the volumetric ice fraction in the frozen soil. The frost heave behaviour of the control and deep burial sections of the Calgary full-scale test is simulated using the developed FE model. The FE calculated heave and frost front penetration show a good agreement with the observed results. Although the discrete ice lens formation is not modelled explicitly, the predicted moisture growth from the present continuum approach matches the observed behaviour in the full-scale tests. The long-term heave response (up to 20 years) is simulated, where the pipe heaved 1 m or more in some cases, which were not performed in previous numerical studies. The reduction of heave rate after the final ice lens formation and associated warming at the base of the ice lens is discussed.

The developed FE techniques for frost heave modelling in Chapter 4 are used in Chapter 5 to perform a comprehensive parametric study. The analyses are performed for a range of soil properties, burial depths, and thermal boundary conditions, as expected in the pipeline's right-of-way. Based on the FE results, the influence of these key factors on frost heave is discussed. The importance of segregation freezing temperature, stress effects on segregation potential, and stress–strain behaviour of frozen soils in frost heave modelling is discussed.

Chapter 6 and Appendix B present a coupled thermo-hydro-mechanical FE modelling of thaw consolidation. Firstly, one-dimensional FE analyses are performed for thaw and post-thaw consolidation of a semi-infinite soil column under self-weight and a combination of self-weight and a surcharge. Constant volumetric compressibility and hydraulic conductivity of the thawed soil are used in these simulations. The FE results are compared with a decoupled analytical solution

that has been developed based on the small-strain linear consolidation theory. Comparison between the small-strain decoupled approach and the current FE approach shows that the small-strain solution underestimates the thaw depth, excess pore water pressure generation and thaw settlement, especially when thaw settlement is significant with respect to thaw depth. Secondly, FE models are developed to simulate a laboratory thaw consolidation test one-dimensionally and the thawing around a warm pipeline buried in permafrost in two-dimensional conditions, by implementing nonlinear void ratio–effective stress–hydraulic conductivity relationships for thawed soils. In these simulations, a modified Drucker–Prager Cap model is used to implement the nonlinear stress–strain behaviour of thawed soils. The calculated thaw settlement and the variation of temperature, pore water pressure and void ratio during thawing match well with the available numerical simulation results presented in a previous study, which indicates that the developed FE modelling technique can successfully simulate the thaw consolidation, even for highly nonlinear hydromechanical conditions. Two-dimensional FE modelling of thawing around warm pipelines can simulate the generation of excess pore water pressure due to thawing and its dissipation through the thawed soil. During dissipation, the pore water flow concentrates along the curved thaw front when a high hydraulic conductivity of thawed soil at the low-stress level is considered. The simulation results indicate that the assumption of one-dimensional thaw consolidation for pipelines (i.e., both heat and moisture flow in the vertical direction), as used in previous studies, might be questionable for the highly nonlinear consolidation behaviour of ice-rich soils.

7.2 Recommendations to Future Research

The present study successfully investigated many aspects of frost heave and thaw settlement around buried pipelines; however, there are some limitations, as discussed in Chapters 3–6. The following are some issues that could be addressed in future.

i. Centrifuge tests used in this study are limited and are performed on uniform soil beds. The effects of backfill materials, varying soil layer, degree of saturation, initial ground temperature and seasonal ground surface temperature need to be investigated.

ii. For cyclic temperature at the pipeline and ground surface, frost heave and thaw settlement might occur every year. Finite element simulations could be performed, incorporating both processes in a common framework.

iii. Limited laboratory test results are available on clayey silts (highly frost susceptible), especially in the frozen state close to 0 °C and at low-stress levels, which could have a significant effect on frost heave.

iv. Many uncertainties exist in estimating compressibility and hydraulic conductivity of thawed soil at the low-stress level. Advanced laboratory testing and mathematical models are required to be developed.

v. Some centrifuge experiments and field evidence show the formation of an air void above the pipe during thaw consolidation. The mechanisms of this void formation are not well-understood. This could be investigated, and then the mechanisms could be implemented in a FE program for better simulation of thaw consolidation.

vi. Free-field frost heave and thaw settlement are investigated in the present study. Further studies are required for structural analysis of the pipeline around the interface between two soils having different freezing and thawing characteristics.

REFERENCES

Aldaeef, A.A., and Rayhani, M.T. 2018. Impact of ground warming on pile-soil interface strength in ice-poor frozen soils. *In* Proceedings of the 71st Canadian Geotechnical Conference, Edmonton, Alberta, Canada, 7p.

Andersland, O. B., and Ladanyi, B. 2004. Frozen ground engineering. Wiley and Sons, New Jersey, USA.

Anderson, D.M., and Tice, A.R. 1972. Predicting unfrozen water contents in frozen soils from surface area measurements. Highway Research Record, **393**(2): 12–18.

Anderson, D.M., Tice, A.R., and McKim, H.L. 1973. The unfrozen water and the apparent specific heat capacity of frozen soils. *In* 2nd International Conference on Permafrost, Yakutsk, USSR, pp. 289–295.

Arenson, L.U., Azmatch, T.F., Sego, D.C., and Biggar, K.W. 2008. A new hypothesis on ice lens formation in frost-susceptible soils. *In* Proceedings of the 9th International Conference on Permafrost, Fairbanks, Alaska, pp. 59–64.

Arenson, L.U., and Springman, S.M. 2005. Mathematical descriptions for the behaviour of ice-rich frozen soils at temperatures close to 0 C. Canadian Geotechnical Journal, **42**(2): 431–442.

Arenson, L.U., Springman, S.M., and Sego, D.C. 2007. The rheology of frozen soils. Applied Rheology, **17**(1): 12147-1–12147-14.

Black, P.B. 1995. Applications of the Clapeyron equation to water and ice in porous media, CRREL Report 95–6, Hanover, NH, USA: US Army Corps of Engineers.

Burgess, M., Nixon, J., and Lawrence, E. 1998. Seasonal Pipe Movement in Permafrost Terrain, KP2 Study Site, Normal Wells Pipeline. *In* Proceedings 7th International Conference on Permafrost, Yellowknife, Canada, pp. 23–27.

Carlson, L.E., Ellwood, J.R., Nixon, J.F., and Slusarchuk, W.A. 1982. Field test results of operating a chilled, buried pipeline in unfrozen ground. *In* Proceedings of the 4th Canadian Permafrost Conference, Calgary, Alberta, pp. 475–480.

Carlson, L.E., and Nixon, J.F. 1988. Subsoil investigation of ice lensing at the Calgary, Canada, frost heave test facility. Canadian Geotechnical Journal, **25**(2): 307–319.

C-CORE. 2012. Modelling of Thaw-Settlement Related to Mo'he-Daqing Crude Oil Pipeline, C-CORE Report R-12-080-928, NL, Canada: C-CORE.

CGS (Canadian Geotechnical Society). 2006. Canadian Foundation Engineering Manual (CFEM), Richmond, British Columbia, Canada: Canadian Geotechnical Society.

Chalmers, B., and Jackson, K.A. 1970. Experimental and theoretical studies of the mechanism of frost heaving, CRREL Report 199, Hanover, NH, USA: US Army Corps of Engineers.

Chamberlain, E.J., and Gow, A.J. 1979. Effect of freezing and thawing on the permeability and structure of soils. Engineering Geology, **13**: 73–92.

Clark, J.I., and Phillips, R. 2003. Centrifuge modelling of frost heave of arctic gas pipelines. *In* Proceedings of the 8th International Permafrost Conference, Zurich, Switzerland, pp. 21–24.

Colt-KBR (Colt Engineering Corporation and Kellogg Brown & Root). 2003. Conceptual geotechnical/geothermal design basis, WP-005-D1-2, Rev. B. Calgary, Alberta, Canada: Colt Engineering Corporation and Kellogg Brown & Root.

Côté, J., and Konrad, J.M. 2005. A generalized thermal conductivity model for soils and construction materials. Canadian Geotechnical Journal, **42**(2): 443–458.

Coutts, R.J. 1991. Development of a two-dimensional finite element model to calculate temperatures and stresses in frost susceptible soil around a chilled pipeline. M.Sc. thesis, University of Waterloo, Ontario, Canada.

Dallimore, S.R. 1985. Observations and predictions of frost heave around a chilled pipeline. M.A. thesis, Carleton University, Ottawa, Ontario, Canada.

Dumais, S. 2019. Modelling large thaw consolidation deformations. Ph.D. thesis, University of Laval, Quebec, Canada.

Dumais, S., and Konrad, J.-M. 2018. One-dimensional large-strain thaw consolidation using nonlinear effective stress–void ratio–hydraulic conductivity relationships. Canadian Geotechnical Journal, **55**(3): 414–426.

Dumais, S., and Konrad, J.-M. 2019. Large-strain nonlinear thaw consolidation analysis of the Inuvik warm-oil experimental pipeline buried in permafrost. Journal of Cold Regions Engineering, **33**(1): 04018014.

Eigenbrod, K.D. 1996. Effects of cyclic freezing and thawing on volume changes and permeabilities of soft fine-gained soils. Canadian Geotechnical Journal, **33**(4): 529–537.

Eigenbrod, K.D., Knutsson, S., and Sheng, D. 1996. Pore-water pressures in freezing and thawing fine-grained soils. Journal of Cold Regions Engineering, **10**(2): 77–92.

Everett, D.H. 1961. The thermodynamics of frost damage to porous solids. Transactions of the Faraday Society, **57**: 1541–1551.

Farouki, O.T. 1981a. The thermal properties of soils in cold regions. Cold Regions Science and Technology, **5**(1): 67–75.

Farouki, O.T. 1981b. Thermal properties of soils, CRREL Monograph 81-1. Hanover, NH, USA: US Army Corps of Engineers.

Foriero, A., and Ladanyi, B. 1995. FEM assessment of large-strain thaw consolidation. Journal of Geotechnical Engineering, **121**(2): 126–138.

Fukuda, M., Kim, H., and Kim, Y. 1997. Preliminary results of frost heave experiments using standard test sample provided by TC8. *In* Proceedings of International Symposium on Ground Freezing and Frost Action in Soils, Edited by S. Knuttson, A.A. Balkema, Brookfield, Balkema, Netherlands. pp. 25–30.

Gautier, D.L., Bird, K.J., Charpentier, R.R., Grantz, A., Houseknecht, D.W., Klett, T.R., Moore, T.E., Pitman, J.K., Schenk, C.J., Schuenemeyer, J.H., and Sørensen, K. 2009. Assessment of undiscovered oil and gas in the Arctic. Science, **324**(5931): 1175–1179.

Ghoreishian Amiri, S.A., Grimstad, G., Kadivar, M., and Nordal, S. 2016. Constitutive model for rate-independent behavior of saturated frozen soils. Canadian Geotechnical Journal, **53**(10): 1646–1657.

Gilpin, R. 1980. A model for the prediction of ice lensing and frost heave in soils. Water Resources Research, **16**(5): 918–930.

Grip, N. 1997. Dimensional analysis of numerical solution of the rigid ice model frost heave with hints on how to implement the solution in Matlab. Ph.D. thesis, Luleå University of Technology, Luleå, Sweden.

Harlan, R.L. 1973. Analysis of coupled heat-fluid transport in partially frozen soil. Water Resources Research, **9**(5): 1314–1323.

Hawlader, B.C., Morgan, V., and Clark, J.I. 2004. A simplified solution for frost heave prediction of chilled pipelines. *In* Proceedings of the 12th International Specialty Conference, Edmonton, Alberta, Canada, pp. 16–19.

Hawlader, B.C., Morgan, V., and Clark, J.I. 2006. Modelling of pipeline under differential frost heave considering post-peak reduction of uplift resistance in frozen soil. Canadian Geotechnical Journal, **43**(3): 282–293.

He, R., and Jin, H. 2010. Permafrost and cold-region environmental problems of the oil product pipeline from Golmud to Lhasa on the Qinghai–Tibet Plateau and their mitigation. Cold Regions Science and Technology, **64**(3): 279–288.

Huang, S.L., Bray, M.T., Akagawa, S., and Fukuda, M. 2004. Field investigation of soil heave by a large diameter chilled gas pipeline experiment, Fairbanks, Alaska. Journal of Cold Regions Engineering, **18**(1): 2–34.

Hwang, C.T. 1977. On quasi-static solutions for buried pipes in permafrost. Canadian Geotechnical Journal, **14**(2): 180–192.

IORVL. 2004. Inuvik Gas Pipeline Lessons Learned. Report IORVL-128C, Calgary, Alberta, Canada: Imperial Oil Resources Venture Limited.

Japan Geotechnical Society. 2003. Test method for frost heave susceptibility of soils. 0172-2003., Tokyo, Japan: Japan Geotechnical Society.

Johansen, O. 1975. Thermal conductivity of softs. Ph.D. thesis, University of Trondheim, Trondheim, Norway. CRREL Draft English Translation 637. Hanover, New Hampshire, USA: US Army Corps of Engineers.

Johnson, K., 1995. The Canol pipeline: a cold region project with no future. *In* Proceedings of Annual Conference of the Canadian Society for Civil Engineering, Ottawa, Canada, pp. 315–323.

Johnson, E.R., and Hegdal, L.A. 2008. Permafrost-related performance of the Trans-Alaska oil pipeline. *In* Proceedings of 9th International Conference on Permafrost, Fairbanks, Alaska, USA, pp. 857–864.

Ketcham, S.A., Black, P.B., and Pretto, R. 1997. Frost heave loading of constrained footing by centrifuge modeling. Journal of Geotechnical and Geoenvironmental Engineering, **123**(9): 874–880.

Kim, K. 2011. Multi-dimensional frost heave modeling with SP porosity growth function. Ph.D. thesis, University of Alaska Fairbanks, Alaska, USA.

Konrad, J.-M. 1980. Frost heave mechanics. Ph.D. thesis, University of Alberta, Edmonton, Alberta, Canada.

Konrad, J.-M. 1987a. Procedure for determining the segregation potential of freezing soils. Geotechnical Testing Journal, **10**(2): 51–58.

Konrad, J.-M. 1987b. The influence of heat extraction rate in freezing soils. Cold Regions Science and Technology, **14**(2): 129–137.

Konrad, J.-M. 1988. Influence of freezing mode on frost heave characteristics. Cold Regions Science and Technology, **15**(2): 161–175.

Konrad, J.-M. 1989a. Effect of freeze–thaw cycles on the freezing characteristics of a clayey silt at various overconsolidation ratios. Canadian Geotechnical Journal, **26**(2): 217–226.

Konrad, J.-M. 1989b. Physical processes during freeze-thaw cycles in clayey silts. Cold Regions Science and Technology, **16**(3): 291–303.

Konrad, J.-M. 1994. Sixteenth Canadian Geotechnical Colloquium: frost heave in soils: concepts and engineering. Canadian Geotechnical Journal, **31(**2): 223–245.

Konrad, J.-M. 1999. Frost susceptibility related to soil index properties. Canadian Geotechnical Journal, **36**(3): 403–417.

Konrad, J.-M. 2005. Estimation of the segregation potential of fine-grained soils using the frost heave response of two reference soils. Canadian Geotechnical Journal, **42**(1): 38–50.

Konrad, J.-M., and Morgenstern, N.R. 1980. A mechanistic theory of ice lens formation in fine-grained soils. Canadian Geotechnical Journal, **17**(4): 473–486.

Konrad, J.-M., and Morgenstern, N.R. 1981. The segregation potential of a freezing soil. Canadian Geotechnical Journal, **18**(4): 482–491.

Konrad, J.-M., and Morgenstern, N.R. 1982a. Prediction of frost heave in the laboratory during transient freezing. Canadian Geotechnical Journal, **19**(3): 250–259.

Konrad, J.-M., and Morgenstern, N.R. 1982b. Effects of applied pressure on freezing soils. Canadian Geotechnical Journal, **19**(4): 494–505.

Konrad, J.-M., and Morgenstern, N.R. 1984. Frost heave prediction of chilled pipelines buried in unfrozen soils. Canadian Geotechnical Journal, **21**(1): 100–115.

Konrad, J.-M., and Samson, M. 2000. Hydraulic conductivity of kaolinite-silt mixtures subjected to closed-system freezing and thaw consolidation. Canadian Geotechnical Journal, **37**(4): 857–869.

Konrad, J.-M., and Seto, J.T.C. 1994. Frost heave characteristics of undisturbed sensitive Champlain Sea clay. Canadian Geotechnical Journal, **31**(2): 285–298.

Konrad, J.-M. and Shen, M. 1996. 2-D frost action modeling using the segregation potential of soils. Cold Regions Science and Technology, **24**(3): 263–278.

Ladanyi, B., and Shen, M. 1993. Freezing pressure development on a buried chilled pipeline. *In* Proceedings of International Symposium on Frost in Geotechnical Engineering, Anchorage, Alaska, USA, pp. 23–33.

Li, G., Jing, H., Volkov, N., Ma, W., and Wang, F. 2018. Centrifuge Model Test on Performance of Thermosyphon Cooled Sandbags Supporting Warm Oil Pipeline Buried in Thawing

Permafrost. *In* Proceedings of China-Europe Conference on Geotechnical Engineering, Vienna, Austria, pp. 1380–1384.

Li, H., Lai, Y., Wang, L., Yang, X., Jiang, N., Li, L., Wang, C., and Yang, B. 2019. Review of the state of the art: interactions between a buried pipeline and frozen soil. Cold Regions Science and Technology, **157**: 171–186.

Ma, W., Zhang, L., and Yang, C. 2015. Discussion of the applicability of the generalized Clausius–Clapeyron equation and the frozen fringe process. Earth-Science Reviews, **142**: 47–59.

Michalowski, R.L. 1993. A constitutive model of saturated soils for frost heave simulations. Cold Regions Science and Technology, **22**(1): 47–63.

Miller, R.D. 1972. Freezing and heaving of saturated and unsaturated soils. Highway Research Record, **393**(1): 1–11.

Miller, R.D. 1978. Frost heaving in non-colloidal soils. *In* Proceedings of the 3rd International Conference on Permafrost, Edmonton, Alberta, Canada, pp. 707–713.

Miller R.D. 1980. Freezing phenomena in soils. *In* Applications of Soil Physics, Edited by D. Hillel, Academic Press, New York. pp. 254–299.

Miller, R.D. 1990. Scaling of freezing phenomena in soils. *In* Scaling in Soil Physics: Principles and Applications, Edited by D. Hillel and D. E. Elrick, Soil Science Society of America, Madison, Wisconsin, pp. 1–11.

Miyata, Y., and Akagawa, S. 1998. An experimental study of dynamic solid-liquid phase equilibrium in a poroius medium. JSME International Journal Series B Fluids and Thermal Engineering, **41**(3): 590–600.

Morgan, V., Clark, J., Hawlader, B., and Zhou, J. 2004. Prediction of long-term frost heave of chilled gas pipelines by centrifuge modeling. *In* Proceedings of 5th International Pipeline Conference, Calgary, Alberta, Canada, pp. 2429–2435.

Morgan, V., Hawlader, B., and Zhou, J. 2006. Mitigation of frost heave of chilled gas pipelines using temperature cycling. *In* Proceedings of 6th International Pipeline Conference, Calgary, Alberta, Canada, pp. 927–931.

Morgenstern, N.R., and Nixon, J.F. 1971. One-dimensional consolidation of thawing soils. Canadian Geotechnical Journal, **8**(4): 558–565.

Morgenstern, N.R., and Nixon, J.F. 1975. An analysis of the performance of a warm-oil pipeline in permafrost, Inuvik, NWT. Canadian Geotechnical Journal, **12**(2): 199–208.

Morgenstern, N.R., and Smith, L.B. 1973. Thaw–consolidation tests on remoulded clays. Canadian Geotechnical Journal, **10**(1): 25–40.

Nishimura, S., Gens, A., Olivella, S., and Jardine, R.J. 2009. THM-coupled finite element analysis of frozen soil: formulation and application. Géotechnique, **59**(3): 159–171.

Nixon, J.F. 1973. The consolidation of thawing soils. Ph.D. thesis, University of Alberta, Edmonton, Alberta, Canada.

Nixon, J.F. 1975. The role of convective heat transport in the thawing of frozen soils. Canadian Geotechnical Journal, **12**(3): 425–429.

Nixon, J.F. 1983. Practical applications of a versatile geothermal simulator. Journal of Energy Resources Technology, **105**(4): 442–447.

Nixon, J.F. 1986. Pipeline frost heave predictions using a 2-D thermal model. ASCE Research on Transportation Facilities in Cold Regions, pp. 67–82.

Nixon, J.F. 1991. Discrete ice lens theory for frost heave in soils. Canadian Geotechnical Journal, **28**(6): 843–859.

Nixon, J.F. 1992. Discrete ice lens theory for frost heave beneath pipelines. Canadian Geotechnical Journal, **29**(3): 487–497.

Nixon, J.F., and Burgess, M. 1999. Norman Wells pipeline settlement and uplift movements. Canadian Geotechnical Journal, **36**(1): 119–135.

Nixon, J.F., and McRoberts, E.C. 1973. A study of some factors affecting the thawing of frozen soils. Canadian Geotechnical Journal, **10**(3): 439–452.

Nixon, J.F., and Morgenstern, N.R. 1973a. The residual stress in thawing soils. Canadian Geotechnical Journal, **10**(4): 571–580.

Nixon, J.F., and Morgenstern, N.R. 1973b. Practical extensions to a theory of consolidation for thawing soils. *In* Proceedings of 2nd International Conference on Permafrost, Yakutsk, USSR, pp. 369–377.

Nixon, J.F., and Morgenstern, N.R. 1974. Thaw–consolidation tests on undisturbed fine-grained permafrost. Canadian Geotechnical Journal, **11**(1): 202–214.

Nixon, J.D., Saunders, R., and Smith, J. 1991. Permafrost and thermal interfaces from Normal Wells pipeline ditchwall logs. Canadian Geotechnical Journal, **28**(5): 738–745.

Nixon, J.F., Sortland, K.A., and James, D.A. 1990. Geotechnical aspects of northern gas pipeline design. *In* Proceedings of 5th Canadian Permafrost Conference, Quebec City, Quebec, Canada, pp. 299–307.

Northwest Alaskan Pipeline Company. 1981. Preliminary report Fairbanks frost heave test facility. 168p.

Oswell, J.M. 2011. Pipelines in permafrost: geotechnical issues and lessons. Canadian Geotechnical Journal, **48**(9): 1412–1431.

Oswell, J.M., and Tchekhovski, A. 2005. Discussion of "Field investigation of soil heave by a large diameter chilled gas pipeline experiment, Fairbanks, Alaska" by Scott L. Huang, Matthew T. Bray, Satoshi Akagawa, and Masami Fukuda. Journal of Cold Regions Engineering, **19**(1): 30–36.

Parameswaran, V.R., and Jones, S.J. 1981. Triaxial testing of frozen sand. Journal of Glaciology, **27**(95): 147–155.

Patterson, D.E., and Smith, M.W. 1981. The measurement of unfrozen water content by time domain reflectometry: Results from laboratory tests. Canadian Geotechnical Journal, **18**(1): 131–144.

Paulin, M.J., Nixon, D., and Lanan, G.A. 2002. Environmental Loadings and Geotechnical Considerations for the Northstar Offshore Pipelines. *In* Proceedings of the 4th International Pipeline Conference, Calgary, Alberta, Canada, pp. 2085–2092.

Penner, E. 1959. The mechanism of frost heaving in soils. Highway Research Board Bulletin, **225**: 1–22.

Penner, E. 1986. Aspects of ice lens growth in soils. Cold regions science and technology, **13**(1): 91–100.

Peppin, S.S., and Style, R.W. 2013. The physics of frost heave and ice-lens growth. Vadose Zone Journal, **12**(1): 1–12.

Phillips, R., Clark, J.I., and Hanke, R. 2001. Centrifuge Modelling of Pipeline Frost Heave. I*n* Proceedings of 54th Canadian Geotechnical Conference, Calgary, Alberta, Canada, 8p.

Phillips, R., Clarke, J.I., and Hanke, R. 2002. Pipeline frost heave modelling. *In* Proceedings of International Conference on Physical Modelling in Geotechnics, St. John's, NL, Canada, pp. 313–318.

Piercey, G., Volkov, N., Phillips, R., and Zakeri, A. 2011. Assessment of frost heave modelling of cold gas pipelines. *In* Proceedings of 2011 Pan-Am Geotechnical Conference, Toronto, Ontario, Canada, 8p.

Rajani, B., and Morgenstern, N. 1994. Comparison of predicted and observed responses of pipeline to differential frost heave. Canadian Geotechnical Journal, **31**(6): 803–816.

Rempel, A.W., Wettlaufer, J.S., and Worster, M.G. 2004. Premelting dynamics in a continuum model of frost heave. Journal of fluid mechanics, **498**: 227–244.

Rempel, A.W. 2007. Formation of ice lenses and frost heave. Journal of Geophysical Research: Earth Surface, **112**(F02S21).

Rowley, R.K., Watson, G.H., Wilson, T.M., and Auld, R.G. 1973. Performance of a 48-in. warm-oil pipeline supported on permafrost. Canadian Geotechnical Journal, **10**(2): 282–303.

Seligman, B.J. 2000. Long-term variability of pipeline–permafrost interactions in north-west Siberia. Permafrost and Periglacial Processes, **11**(1): 5–22.

Selvadurai, A.P.S. 1988. Mechanics of soil-pipeline interaction. *In* Proceeding of Annual Conference Canadian Society for Civil Engineering, Calgary, Alberta, Canada, pp. 151–173.

Selvadurai, A.P.S., Hu, J., and Konuk, I. 1999. Computational modelling of frost heave induced soil–pipeline interaction: II. Modelling of experiments at the Caen test facility. Cold Regions Science and Technology, **29**(3): 229–257.

Selvadurai, A.P.S., and Shinde, S.B. 1993. Frost heave induced mechanics of buried pipelines. Journal of Geotechnical Engineering, **119**(12): 1929–1951.

Slusarchuk, W.A., Clark, J.I., Nixon, J.F., Morgenstern, N.R., and Gaskin, P.N. 1978. Field test results of a chilled pipeline buried in unfrozen ground. *In* Proceedings of 3rd International Conference on Permafrost, Edmonton, Canada, pp. 878–883.

Slusarchuk, W.A., Watson, G.H., and Speer, T.L. 1973. Instrumentation around a warm oil pipeline buried in permafrost. Canadian Geotechnical Journal, **10**(2): 227–245.

Smith, L.B. 1972. Thaw consolidation tests on remoulded clays. Ph.D. thesis, University of Alberta, Edmonton, Alberta, Canada.

Taber, S. 1929. Frost heaving. The Journal of Geology, **37**(5): 428–461.

Thomas, H.R., Cleall, P., Li, Y.C., Harris, C., and Kern-Luetschg, M. 2009. Modelling of cryogenic processes in permafrost and seasonally frozen soils. Géotechnique, **59**(3): 173–184.

Tice, A.R., Anderson, D.M., and Banin, A. 1976. The prediction of unfrozen water contents in frozen soils from liquid limit determinations. CRREL Report 76–8, Hanover, NH, USA: US Army Corps of Engineers.

Tsytovitch, N.A. 1975. The Mechanics of Frozen Ground. McGraw-Hill, New York, 426p.

Tsytovich, N.A., Zaretskii, Y.K., Grigor'eva, V.G., and Ter-Martirosyan, Z.G. 1965. Consolidation of thawing soils. *In* Proceedings of 6th International Conference on Soil Mechanics and Foundation Engineering, Toronto, Universoty of Toronto Press, pp. 390–394.

Ueda, H.T., Garfield, D.E., and Haynes, F.D. 1977. The Canol Pipeline Project. A Historical Review. CRREL SR 77–34, Hanover, NH, USA: US Army Corps of Engineers.

Wang, Y.P., Li, G.Y., Jin, H.J., Lu, L.Z., He, R.X., and Zhang, P. 2016. Thermal state of soils in the active layer and underlain permafrost at the kilometer post 304 site along the China-Russia Crude Oil Pipeline. Journal of Mountain Science, **13**(11): 1984–1994.

Wang, F., Li, G., Ma, W., Mu, Y., Zhou, Z., and Mao, Y. 2018. Permafrost thawing along the China-Russia crude oil pipeline and countermeasures: a case study in Jiagedaqi, Northeast China. Cold Regions Science and Technology, **155**: 308–313.

Watson, G.H., Rowley, R.K., and Slusarchuk, W.A. 1973. Performance of a warm-oil pipeline buried in permafrost. *In* Proceedings of 2nd International Conference on Permafrost, Yakutsk, USSR, pp. 759–766.

Yang, D., and Goodings, D.J. 1998. Predicting frost heave using FROST model with centrifuge models. Journal of Cold Regions Engineering, **12**(2): 64–83.

Yao, X., Qi, J., and Wu, W. 2012. Three dimensional analysis of large strain thaw consolidation in permafrost. Acta Geotechnica, **7**(3): 193–202.

Yu, F., Guo, P., Lai, Y., and Stolle, D. 2019. Frost heave and thaw consolidation modelling. Part 1: A water flux function for frost heaving. Canadian Geotechnical Journal, **57**(10): 1581–1594.

Yu, F., Guo, P., Lai, Y., and Stolle, D. 2020. Frost heave and thaw consolidation modelling. Part 2: One-dimensional thermohydromechanical (THM) framework. Canadian Geotechnical Journal, **57**(10): 1595–1610.

Zhou, G.Q., Hu, K., Shang, X.Y., and Zhou, J.S. 2009. Test and numerical simulation on frost heave in frozen soils in intermittent freezing mode. Procedia Earth and Planetary Science, **1**(1): 512–518.

Zhou, Y., and Zhou, G. 2012. Intermittent freezing mode to reduce frost heave in freezing soils — experiments and mechanism analysis. Canadian Geotechnical Journal, **49**(6): 686–693.

Zhu, M. 2006. Modeling and simulation of frost heave in frost-susceptible soils. Ph.D. thesis, University of Michigan, Ann Arbor, Michigan, USA.

APPENDIX A

Stress–strain behaviour of a clayey silt in triaxial tests

This paper has been published in the 68th Canadian Geotechnical Conference, GeoQuebec 2015. The first author conducted most of the research work presented in this paper. He also prepared the draft manuscript. The other authors supervised the research and reviewed the manuscript.

Stress–strain behaviour of a clayey silt in triaxial tests

Dayarathne, R.S., Hawlader B.C.
Memorial University, St. John's, NL, Canada

ABSTRACT
Frost heave is one the major issues in the design of pipelines in cold regions. The pipelines generally traverse through a variety of soils. Among the different types of soil, clayey silt has been identified as one of the highly frost susceptible soils. In the analyses of pipeline–soil interaction due to frost heave, the stress–strain behaviour of both unfrozen and frozen soil is equally important. In the current research program, centrifuge physical modeling and finite element analysis will be performed to examine the effects of frost heave on chilled gas pipelines. While a large number of laboratory test results on different sands and clays are available in the literature, laboratory tests on clayey silt, which is highly frost susceptible, are very limited. In this paper, some triaxial and consolidation test results on clayey silt are presented, which could be used to understand its constitutive behaviour. The soil used in this experimental program is same as the soil used for centrifuge physical modeling. Comparing test results with typical behaviour of sand and clay in the critical state framework, some similarity and differences are highlighted.

RÉSUMÉ
Soulèvement par le gel est un des enjeux majeurs de la conception de pipelines dans les régions froides. Les pipelines traversent généralement à travers une variété de sols. Parmi les différents types de sol, limon argileux a été identifié comme l'un des sols sensibles hautement gel. Dans les analyses d'interaction pipeline-sol en raison de soulèvement par le gel, le comportement contrainte-déformation des deux sol non gelé et non gelé est tout aussi important. Dans le programme de recherche en cours, la modélisation physique centrifugeuse et l'analyse des éléments finis seront effectuées pour examiner les effets du soulèvement par le gel sur les gazoducs réfrigérés. Alors qu'un grand nombre de résultats de tests de laboratoire sur différents sables et argiles sont disponibles dans la littérature, des essais en laboratoire sur limon argileux, qui est très sensible au gel, sont très limitées. Dans cet article, certains résultats de tests triaxiaux et de consolidation sur limon argileux sont présentés, qui pourrait être utilisée pour comprendre son comportement constitutif. La terre utilisée dans ce programme expérimental est le même que le sol utilisé pour la modélisation physique centrifugeuse. En comparant les résultats des tests avec un comportement typique de sable et d'argile dans le cadre d'état critique, une certaine similitude.

1 INTRODUCTION

Frost heave is a process in which soil freezing causes moisture flow. It has significant effects on the design of chilled gas pipelines that pass through variety of soils along its route. All types of soil are not frost susceptible. Previous studies showed that clayey silt is one of the highly frost susceptible soil (Andersland and Ladanyi 2004). Various attempts have been taken in the past to understand the mechanisms involved in frost heave and its effects on pipeline design. Based on one-dimensional model test results, frost heave models have been proposed by a number of researchers (Konrad and Morgenstern 1984; Nixon 1991). Large-scale tests, such as Calgary full-scale test, Caen frost heave test, have been also conducted in the past to improve the knowledge and design methodologies of large-diameter chilled gas pipelines in discontinuous permafrost. Physical modeling of frost heave has been also conducted using geotechnical centrifuge, which is less expensive than full-scale tests (Ketcham et al. 1997; Yang and Goodings 1998; Clark and Philips 2003; Morgan et al. 2004; Morgan et al. 2006; Piercey et al. 2011).

The mathematical models developed from model test results have been also implemented in numerical models for analysis of frost heave. For example, the Segregation Potential (SP) model proposed by Konrad and Morgenstern (1984) has been implemented in a FE code (Konrad and Shen 1996) and finite difference code (Nixon 1991). The stress–strain behaviour of both frozen and unfrozen soil influences the response of pipeline subjected to frost heave, which has to be given in numerical models. The stress–strain behaviour of unfrozen soil is the focus of the present study. Most of the previous studies assumed that unfrozen soil behaves as an elastic material (Konrad and Shen 1996; Ladanyi and Shen 1993; Michalowski and Zhu 2006, Shen and Ladanyi 1991). In a recent study, Nishimura et al. (2009) used the critical state model to simulate the response of both frozen and unfrozen soil as shown in Fig. 1. In this model, the yield surface expands with decrease in temperature below the freezing point.

At this stage, a question is whether clayey silt, which is highly frost susceptible, behaves elastically for the range of stress around the pipeline, and/or they also follow the critical state framework as suggested by Nishimura et al. (2009). Although limited, some recent studies (e.g. Nocilla et al. 2006) showed that the silt behaves as '*transitional materials'* in one-dimensional and triaxial loading conditions.

In the present research program, physical and numerical modeling will be performed to understand better the frost heave mechanisms under chilled gas pipelines. In the following section, a brief introduction of frost heave modeling using geotechnical centrifuge is given first. After that a series of laboratory consolidation and triaxial tests results on the soil used for these centrifuge tests are presented to examine the constitutive behaviour of this soil in unfrozen condition.

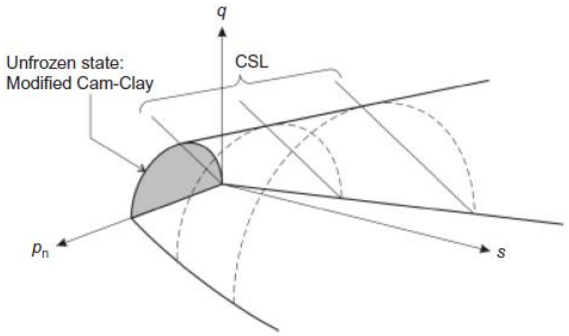

Figure 1. Critical state model for frozen and unfrozen soils (Nishimura et al. 2009)

2 CENTRIFUGE MODELING OF FROST HEAVE UNDER CHILLED GAS PIPELINES

A number of centrifuge tests have been performed in the past for frost heave modeling of chilled gas pipelines using the geotechnical centrifuge at C-CORE. It has been shown that the centrifuge test results are consistent with the full-scale test results (Clark and Philips 2003; Morgan et al. 2004; Piercey et al. 2011). In addition to tests on natural frost susceptible soils, a large number of tests have been conducted on Sil-Co-Sil silt and kaolin mix. Based on these centrifuge modeling and one-dimensional frost heave tests, it is found that 75% Sil-Co-Sil silt and 25% kaolin mix are highly frost susceptible. A typical section after a centrifuge frost heave test is shown in Fig. 2. As shown, significant heave occurred with formation of ice lenses. Outside the frozen bulb the soil is unfrozen. The stress–strain behaviour of the unfrozen soil is investigated in the following sections.

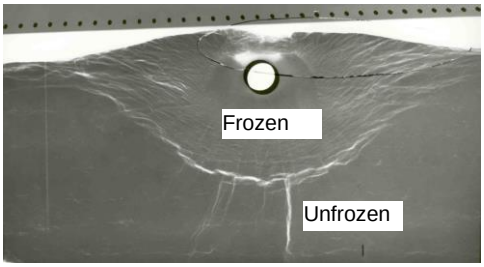

Figure 2. Typical section after centrifuge modeling of frost heave

3 ONE-DIMENSIONAL CONSOLIDATION AND TRIAXIAL TESTS

3.1 Material and Sample Preparation

Two identical reconstituted cylindrical soil blocks were prepared from a mixture of 25% Speswhite kaolin and 75% Sil-Co-Sil silt. The particle size distribution of each material and the mixture are shown in Fig. 3. According to the unified soil classification system this clayey silt can be classified as ML. Other properties of the mixture are summarized in Table 1.

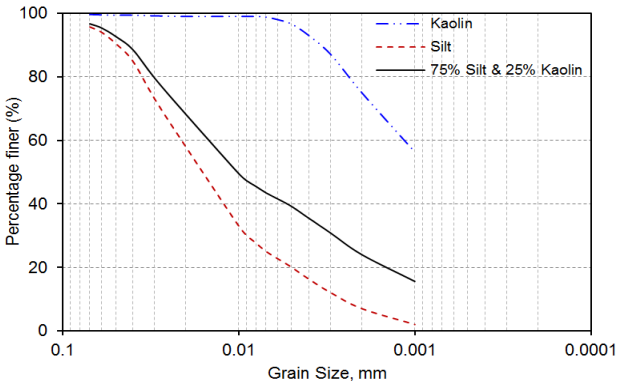

Figure 3. Grain size distributions of materials

By adding water twice the liquid limit (LL) of the mixture, uniform slurry was prepared by thoroughly mixing in a drum type machine mixer for 2 hours, which was then poured into a cylindrical consolidation tub of 300 mm diameter and 350 mm height. Appropriate care was taken to prevent segregation and air entrapping by reducing the drop height and pouring the slurry in three layers with a slight stirring at each layer. The sample was then consolidated on the laboratory floor by applying a vertical pressure from a piston, so that the soil was strong enough to handle. A number of soil samples were then collected from this laboratory floor consolidated soil block using a Shelby tube. The samples were then extruded and the specimens listed in Table 2 are prepared for triaxial (T1–T8) and consolidation (C1–C6) tests. All the tests were conducted according to the ASTM Standards. The moisture content of soil (w) was measured before and after consolidation. As expected, before consolidation initial w was equal to twice of LL. The undrained shear strength was also measured using a Torvane. All the results are summarized in Table 2.

Table 1. Soil properties of mixture

Soil property	75 % Sil-Co-Sil Silt + 25 % Kaolin
Specific gravity	2.65
Sand Content (%)	3
Plastic limit (PL)	22

Liquid limit (LL)	27
Soil type (Unified soil classification)	ML

Table 2. Properties of reconstituted soil samples

Property	Block sample 1	Block sample 2
Final moisture content (%)	24	24
Undrained shear strength (kPa)	27	25
Specimen preparation	C1,T1,T2,T3, T4,T8	C2,C3,C4,C5, C6, T5,T6,T7

3.2 One-dimensional consolidation tests

Six specimens (C1–C6 in Table 2) were prepared for one-dimensional consolidation tests. Soil samples from the Shelby tubes were inserted carefully into the consolidation moulds of 50 mm diameter and 20 mm height, and then the bottom and top surfaces were trimmed off to achieve proper seating. The moisture content of soil at this stage is also measured which represents the initial moisture content for consolidation test results analysis. The consolidation tests were conducted using pneumatic consolidation apparatus having a high accuracy digital display and data acquisition system.

The vertical stress is applied at a load increment ratio of 2 starting from 25 kPa. The samples were loaded up to 3,200 kPa with an unloading-reloading cycle at 400 kPa. Finally, the all the samples were unloaded to 25 kPa.

Figure 4 shows the v–logσ'_v curves for these six consolidation tests, where v is the specific volume (=1+e). In this figure, the initial void ratio (before application of 25 kPa vertical stress) is shown at σ'_v=1.0 kPa in the log scale. As shown, the slope of the curve gradually increases with σ'_v, indicating preconsolidation pressure around σ'_v=100 kPa. However, these curves do not converge to one line (normal compression line, NCL) at large vertical effective stresses, at least up to 3,200 kPa applied in these tests. The vertical difference between the consolidation curves at high stress level might be due to two reasons. First, it could be simply due to inaccurate measurement of initial void ratio. The difficulties in accurate measurement of initial void ratio have been reported in previous studies (e.g. Ponzoni et al. 2014). For their tests, Ponzoni et al. (2014) indicated the accuracy of ±0.05 in the measurement of specific volume. Secondly, the clay-silt mixture tested in the present study might have transitional behaviour as observed by previous researchers from one-dimensional consolidation tests on mixtures of sand, silt and clay (Martins et al. 2001; Nocilla et al. 2006; Ponzoni et al. 2014). Additional tests are required to identify the cause of this difference between the consolidation curves for the soil tested in this study.

3.3 Triaxial Compression tests

Similar to consolidated tests, triaxial tests specimens of 38 mm diameter and 76 mm height were prepared from the Shelby tube soil samples. Initial moisture content was also measured for each specimen from trimmed soil.

A series of consolidated drained and consolidated undrained triaxial compression tests was conducted as listed in Table 3. Tests were conducted using an advanced triaxial system as shown in Fig. 5. In this fully automated system, the cell and back pressures were controlled using the GDS pressure/volume controllers. The axial load was applied using a computer controlled loading system at a specified displacement rate. All the data such as back pressure, cell pressure, pore water pressure, volume change and axial displacement were recorded using a data acquisition system. Further details of test conditions are shown in Table 3.

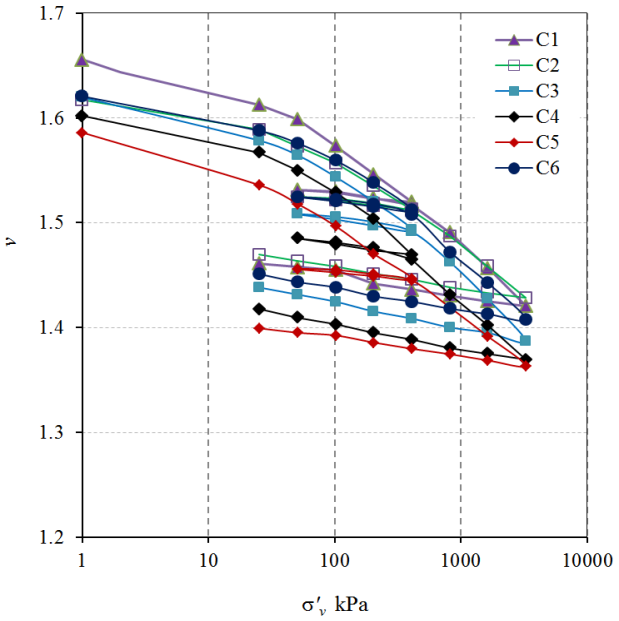

Figure 4. Consolidation test results

3.3.1 Consolidated drained triaxial tests

In tests T1–T4, the soil specimen was consolidated isotropically to the given confining pressure as shown in Table 3 and then sheared by compressing the specimen at 0.005 mm/min of vertical displacement as per ASTM recommendation ($\acute{\varepsilon}$ = 4%/10t_{90}, where t_{90} is the time required to achieve the 90% consolidation).

Figure 6 shows the stress–strain and volume change behaviour of soil during drained shearing. The deviatoric stress gradually increases and reaches the peak approximately at axial strain of 7–11%. After the peak, there is a slight decrease in deviator stress. The initial stiffness of the q–ε_1 curve increases with increase in confining pressure.

The volumetric strain versus axial strain curves in Fig. 6(b) show that the soil specimens first compress with increase in axial strain. For lower confining pressures (e.g. tests T1 and T2) the volume change behaviour changes after the maximum compression and then sample dilates (i.e. ε_v–ε_1 curves go up). In test T1, the ε_v–ε_1 curve does not become horizontal even at the maximum axial strain applied, which implies that the critical state may not be reached in this test. However, in

tests T2 and T3 the ε_v–ε_1 curves become almost horizontal after some dilation. No significant dilation is observed in test T4 where the confining pressure is the maximum. Comparing these curves, it can be concluded that dilative tendency of this soil decreases with increase in confining pressure, which is consistent with previous studies on sand (Jefferies and Been 2006).

A quick drop of q after the peak in the q–ε_1 plot in Test T3 and T4 might be due to strain localization in the failure plane, because any sharp change in volumetric strain was not observed at this level of strain in the ε_v–ε_1 plot. Notice that the volumetric strain is calculated from drained water which came out from the ends of the specimen. Therefore, local shearing along the failure plane may not be seen immediately from drainage of water from the sample. It is to be noted here that some researchers (e.g. Desrues and Viggiani 2004) also recognized such behaviour in sand, and inferred as localization effects which have been verified using stereo photogrammetry analysis.

Table 3. Triaxial test conditions

Test	Confining pressure, σ_c (kPa)	Type of shearing
T1	100	Drained
T2	200	Drained
T3	400	Drained
T4	640	Drained
T5	100	Undrained
T6	100	Undrained
T7	200	Undrained
T8	400	Undrained

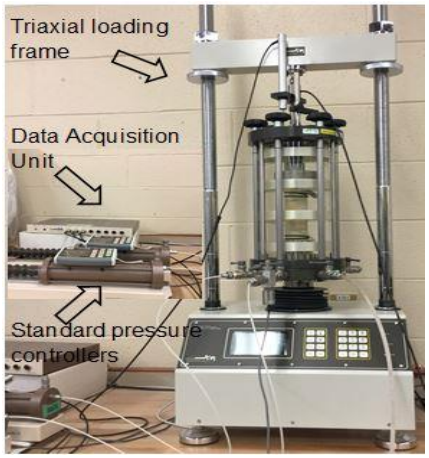

Figure 5. Automated GDS triaxial system

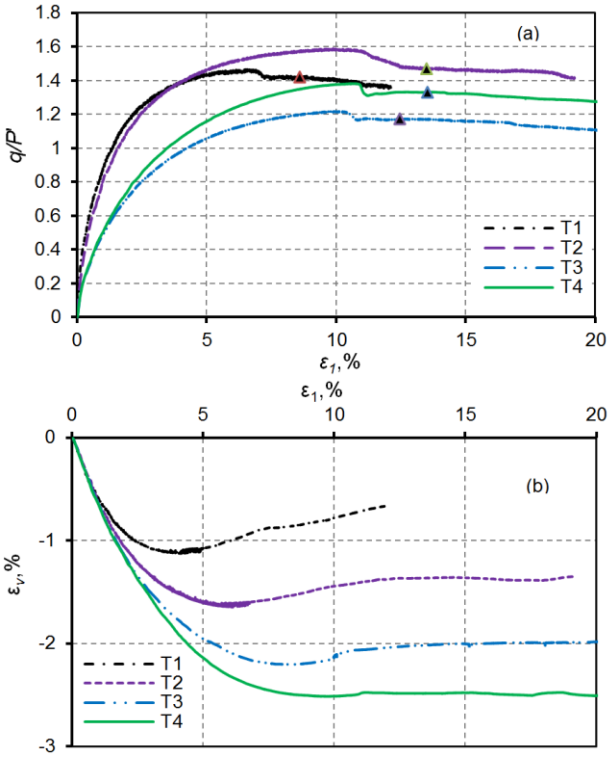

Figure 6. Stress–strain behaviour in consolidation drained tests: (a) deviatoric stress versus axial strain, (b) volumetric strain versus axial strain

3.3.2 Consolidated undrained traixial tests

In tests T5 and T8, the soil specimen was consolidated isotropically to the given confining pressure and then sheared by increasing axial stress in triaxial compression mode in undrained condition. However, in tests T6 and T7, the sample was first consolidated to 400 kPa and then unloaded isotropically to 100 and 200 kPa, respectively, meaning that, overconsolidated specimens were created in triaxial cell before shearing. The sample was then sheared in undrained condition by applying vertical displacement of 0.02 mm/min as per ASTM recommendation ($\acute{\varepsilon}$=4%/10t_{50}, where t_{50} is the time required to achieve the 50% consolidation).

Figure 7 shows the stress–strain and pore pressure change behaviour during undrained shearing. The deviatoric stress gradually increases and reaches the peak approximately at axial strain of 7–12%. All the specimens show a slight decrease in deviatoric stress after the peak, indicating less softening behaviour. The undrained elastic modulus (slope of the q–ε_1 curve) also increases with increase in confining pressure. Similar to drained tests, there is a sharp decrease of q after the peak in tests in T6 and T8, which could be again because of strain localization.

Figure 7(b) shows the developed of excess pore water pressure (u) during undrained shearing. The pore pressure is plotted by normalizing it with confining pressure (σ_c). In all the tests, pore water pressure increases with axial strain and then decreases, which

indicate that the soil specimens initially contract and then dilate after some level of shearing. This could be better visualized from stress path of the samples presented in the following sections.

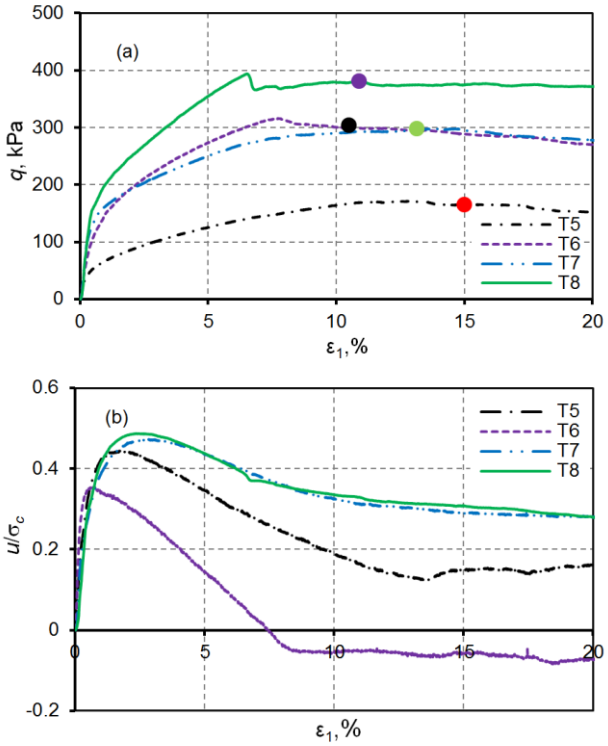

Figure 7. Stress–strain behaviour in consolidation undrained tests: (a) deviatoric stress versus axial strain, (b) normalized excess pore pressure versus axial strain

Although the soil specimens T5 and T8 were sheared from the maximum isotropic consolidation pressure applied in triaxial cell, these specimens also show some dilative behaviour. This could be because of two reasons. Firstly, the lab floor consolidation pressure is higher than the isotropic consolidation pressure in Test T5, which makes the soil specimen over-consolidated. However, in test T8 the sample was consolidated isotropically to 400 kPa, which is higher than the lab floor consolidation pressure. Therefore, the dilative behaviour of T8 is not due to over-consolidation. This could be due to initial void ratio of the specimen as commonly observed in dense sand which shows dilative behaviour although sand might be normally consolidated. Tests T6 and T7 are very similar except for the over-consolidation ratio (OCR) created in triaxial cell—OCR is 4 and 2 in T6 and T7, respectively. Comparing pore pressure variation in T6 and T7 it can be shown that sample T6 shows more dilative behaviour than T7 because the pore pressure decrease in T6 is higher than T7 and after ε_1~7.5% the pore pressure is negative in T6 which has higher OCR. In other words, the stress–strain behaviour of this clayey silt is not exactly same as clay or sand, rather it depends significantly on OCR and initial void ratio, meaning that the behaviour is somewhere between clay and sand.

3.3.3 Effective stress path

Figure 8 shows the effective stress path of the soil specimens during undrained shearing. In tests T5 and T8, the specimens show contractive behaviour initially and then dilative behaviour with a phase change similar to dense sand. However, in the overconsolidated specimens T6 and T7 the undrained stress paths initially move almost vertically, indicating elastic behaviour, followed by a dilation tail similar to T5 and T8. Although authors recognize that it is very difficult to identify the critical state condition from these tests results because the deviatoric stress and pore pressure do not become constant even at large strains. The approximate location of the critical state is shown by the circles in this figure. The specimens T5 and T8, which were not overconsolidated in triaxial cell, reached almost the same stress ratio at the critical state (q/p'=1.1). However, for the overconsolidated soil specimens q/p' could be greater than this value,1.3 in T7 and 1.5 in T6, which means that OCR also significantly influence the behavior of this clayey silt.

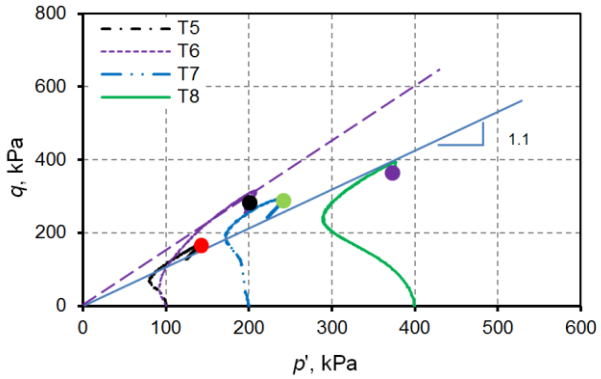

Figure 8. Effective stress path for consolidated undrained triaxial tests

The effective stress paths for the drained tests are shown in Fig. 9. As shown in Fig. 6(a) the deviator stress reaches the peak and then decreases. Moreover, the volumetric strain change with axial strain does not become zero at large strains (Fig. 6b); therefore, the triangles shown in Fig. (6a) are assumed to be at the critical state. The stress state (p',q) at this condition is shown in Fig. 9 by triangles. An average line drawn through these triangles gives the slope of the critical state line of 1.25. For comparison with M obtained from undrained tests without any pre-consolidation in triaxial cell (the lower line in Fig. 8), a line having slope of 1.1 is also drawn in this figure. As shown, the drained tests give slightly higher M.

In summary, the triaxial test results show that there is a discrepancy between the values of M obtained from drained and undrained tests. Nocilla et al. (2006) also recognized such difference in their test on Italian silt mixed with clay.

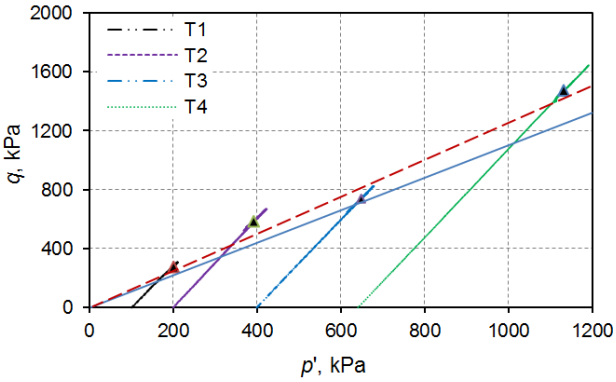

Figure 9. Effective stress path for consolidated drained triaxial tests

4 CONCLUSIONS

From previous studies, it is found that frost susceptibility of 75% sil-co-sil silt and 25% kaolin mixture is comparable to Calgary silt, and therefore this mixture has been used for centrifuge modeling of frost heave behaviour under chilled gas pipelines. In the present study, stress–strain behaviour of this frost susceptible soil is examined from a series of one-dimensional consolidation, triaxial compression tests. One-dimensional consolidation tests show that the consolidation curves do not converge to one line at large vertical effective stress, although the difference between these curves is not very significant. Undrained triaxial compress tests show dilative tendency at large strains. The slope of the critical state line is not constant but varies with drainage condition during shearing (drained or undrained). In other words, unique critical state line the p'–q plane was not obtained for this soil.

Finally, it is to be noted here that above conclusions have been drawn from a limited number of tests. Additional experimental investigation is required for better explanation of the test results presented above.

ACKNOWLEDGEMENTS

The works presented in this paper have been supported by the Research and Development Corporation of Newfoundland and Labrador (RDC) and NSERC. The authors also express their sincere thanks to Shantanu Kar and Anup Fouzder for their help with laboratory testing.

REFERENCES

Andersland, O.B. and Ladanyi, B. 2004. *Frozen ground engineering*, 2nd ed., John Wiley & Sons, Hoboken, New Jersey, USA, 363p

Clark, J.I. and Phillips, R. 2003. Centrifuge modeling of frost heave of Arctic gas pipelines, *8th International Permafrost Conference,* Balkema Publishers, Zurich, Switzerland, 1:152–156.

Desrues, J. and Viggiani, G. 2004. Strain localization in sand: an overview of the experimental results obtained in Grenoble using stereophotogrammetry, *Int. J. Numer. Anal. Meth. Geomech.,* 28:279–321.

Jefferies, M. and Been, K. 2006. *Soil Liquefaction: A Critical state approach*, 1st ed., Taylor & Francis, New York, NY, USA, 479p.

Ketcham, S., Black, P. and Pretto, R. 1997. Frost heave loading of constrained footing by centrifuge modelling, J. Geotech. Eng., ASCE, 123(9):874–881.

Konrad, J. and Morgenstern, N. 1984. Frost heave prediction of chilled pipelines buried in unfrozen soils, *Canadian Geotechnical Journal*, 21(1):100–115.

Konrad, J. and Shen, M. 1996. 2-D frost action modeling using the segregation potential of soils, *Cold regions science and technology*, 24(3):263-278.

Ladanyi, B. and Shen, M. 1993. Freezing pressure development on a buried chilled pipeline, *2nd Int. Symp. on frost in geotechnical engineering*, Anchorage, AK.,23-33.

Martins, F.B., Bressani, L.A., Coop, M.R. and Bica, A. V.D. 2001. Some aspects of the compressibility behaviour of clayey sand, *Canadian Geotechnical Journal*, 38:1177–1186.

Michalowski, R.L. and Zhu, M., 2006. Frost heave modelling using porosity rate function, *Int. J. Numer. Anal. Meth. Geomech.* ,30(8): 703–722.

Morgan, V., Clark, J.I., and Hawlader, B. 2004. Modeling of frost heave of gas pipelines in Arctic conditions, *International Conference on Terrain and Geohazard Challenges Facing Onshore Oil and Gas Pipelines*, Thomas Telford, London, 1: 417–427.

Morgan, V., Hawlader, B., and Zhou, J. 2006. Mitigation of frost heave of chilled gas pipelines using temperature cycling, *6th International Pipeline Conference*, ASME, Calgary, 1:927–931.

Nishimura, S., Gens, A., Olivella, S. and Jardine, R. J. 2009. THM-coupled finite element analysis of frozen soil: formulation and application, *Geotechnique*, 59(3): 159–171.

Nixon, J. 1991. Discrete ice lens theory for frost heave in soils, *Canadian Geotechnical Journal*, 28:843–859.

Nocilla, A., Coop, M. and Colleselli, F. 2006. The mechanics of an Italian silt: an example of transitional behaviour, *Geotechnique*, 56(4):261–271.

Piercey, G., Volkov, N., Phillips, R. and Zakeri, A., 2011. Assessment of Frost Heave Modelling of Cold Gas Pipelines, *Pan-Am CGS Geotechnical conference*,8.

Ponzoni, E., Nocilla, A., Coop, M.R. and Colleselli, F. 2014. Identification and quantification of transitional modes of behaviour in sediments of Venice lagoon, *Geotechnique*, 64(9):694–708.

Shen, M., and Ladanyi, G. 1991. Soil-pipe interaction during frost heaving around a buried chilled pipeline, *6th International Cold Regions Engineering Conference*, West Lebanon, NH. , 11–21.

Yang, D. and Goodings , D.J. 1998. Climatic Soil Freezing Modelled in Centrifuge, *Journal of Geotech. and Geo-environmental Eng. ASCE*, 124(12): 1186-1194.

APPENDIX B

An approach for finite element modeling of one-dimensional thaw consolidation

This paper has been published in the 72nd Canadian Geotechnical Conference, GeoSt.John's 2019. The first author conducted most of the research work presented in this paper. He also prepared the draft manuscript. The other authors supervised the research and reviewed the manuscript.

An approach for finite element modeling of one-dimensional thaw consolidation

Dayarathne, R.S., Hawlader, B.C.
Memorial University, St. John's, NL, Canada
Robert, D.J.
Civil Engineering Department, School of Engineering, RMIT University, VIC 3001, Australia

ABSTRACT
Thawing of permafrost in the North could cause many issues such as the settlement in roads, foundations, pipelines, and slope instability. For a given above-zero temperature at the boundary (e.g., at the ground surface), the excess pore water pressure generates at the thaw front that moves with time depending upon the thermal properties of the soil. The excess pore water pressure generated in the thawed soil dissipates with time, and thaw consolidation occurs. This study presents a finite element (FE) modeling technique that can simulate heat transfer, including the thawing of ice-rich frozen soil, and generation of excess pore water pressure at the thaw front and its dissipation. The FE analyses are performed for a one-dimensional condition, and the results are compared with a simplified analytical technique. The developed FE method could be used for complex boundary value problems such as thawing of frozen soil around a warm buried pipeline.

RÉSUMÉ
La décongélation du pergélisol dans le Nord pourrait poser de nombreux problèmes, tels que le règlement des routes, des fondations, des pipelines et l'instabilité des pentes. Pour une température donnée au-dessus de zéro à la limite (par exemple à la surface du sol), la pression interstitielle en excès génère au front de dégel qui se déplace avec le temps en fonction des propriétés thermiques du sol. L'excès de pression interstitielle généré dans le sol décongelé se dissipe avec le temps et il se produit une consolidation par le dégel. Cette étude présente une technique de modélisation par éléments finis (FE) permettant de simuler le transfert de chaleur, notamment la décongélation d'un sol gelé riche en glace, la génération d'une pression interstitielle excessive dans le front de dégel et sa dissipation. Les analyses FE sont effectuées pour une condition unidimensionnelle et les résultats sont comparés à une technique analytique simplifiée. La méthode FE développée pourrait être utilisée pour résoudre des problèmes complexes liés aux valeurs limites, tels que la décongélation de sol gelé autour d'un pipeline enterré à chaud.

1 INTRODUCTION

Thaw settlement is a major geotechnical design consideration of many infrastructures in cold regions such as highways, airfields and energy pipelines. Ice-rich frozen soils might melt due to seasonal warm temperatures in the spring or by ground warming due to human activities such as flow of warm hydrocarbon in a pipeline.

Upon thawing near the thaw front, the volumetric ice in the forms of pore ice and ice lenses transfers to pore water, which experiences an increase in excess pore water pressure due to the weight of soil and other external loads. The hydraulic conductivity of frozen soil (k_f) is generally several order smaller than that of thawed soil (k_t) (Williams and Burt 1974); therefore, the excess pore water pressure dissipation primarily occurs through thawed soil. In addition to thaw-consolidation settlement, the generated excess pore water pressure could reduce the shear strength of thawed soils which might cause the failure of slopes and foundations (Morgenstern and Nixon 1971; Nixon and Morgenstern 1973).

The dissipation of thaw-induced excess pore water pressure depends on the rate of thawing and hydraulic conductivity of the soil. When thawing occurs at a faster rate, especially in the vicinity of above-zero temperature boundary, the generated excess pore water pressure may not dissipate completely during thawing. The pore pressure dissipation can be modeled using the consolidation theory for unfrozen soil; however, the moving boundary (thaw front) makes the problem complicated. In other words, proper modeling of heat transfer, excess pore water generation and dissipation are required to calculate thaw settlement.

Morgenstern and Nixon (1971) developed an analytical solution for one-dimensional consolidation of thawed soils by extending Terzaghi's one-dimensional consolidation theory. The compressibility of the frozen soil and flow of water through it were neglected. The location of the moving thaw front boundary was modeled using the Neumann solution (Carslaw and Jaegar 1947). Analyses were performed using a small strain approach adopting a linear void ratio (e)–effective stress (σ') relationship together with a constant hydraulic conductivity of thawed soil.

Foriero and Ladanyi (1995) developed a finite-strain approach by extending Gibson's large-strain consolidation theory which also accounts the varying compressibility and hydraulic conductivity during consolidation. Similar to Morgenstern and Nixon (1971), an uncoupled heat transfer analysis was considered to determine the thaw front depth prior to consolidation analysis.

After addressing some of the limitations of the above studies, Dumais and Konrad (2018) developed a coupled

large-strain thaw consolidation model in Lagrangian coordinates. Nonlinear e–σ' and e–k_t relationships were implemented which also considered the volume change when ice transfers to water. Assuming the one-dimensional analysis is valid, Dumais and Konrad (2019) analyzed the thaw consolidation around the Inuvik warm-oil pipeline using the consolidation model developed by Dumais and Konrad (2018).

The objective of this study is to present a finite element modeling approach for one-dimensional thaw consolidation. The generation and dissipation of excess pore water pressure obtained from FE analyses are compared with the analytical solution of Morgenstern and Nixon (1971).

2 PROBLEM DEFINITION

Figure 1 shows the one-dimensional soil sample considered in this study. Initially, at time t = 0, the soil column is frozen having a constant temperature $T = T_g$ (< 0°C) (Fig. 1(a)). A step increase in temperature $T = T_s$ (> 0°C) is applied at the top surface. With time, the thaw front (T = 0°C) moves downward to X(t), and two regions are formed (frozen and thawed), as shown in Fig. 1(b). The frozen region (x > X(t)) is almost incompressible and impermeable as compared to the thawed region. The top surface of the soil domain (x = 0) is considered as a free drainage boundary. When the pore ice and ice lenses melt, the weight of the soil above the thaw front is carried by water that creates an excess pore water pressure (u(x,t)) at the thaw front. The thaw consolidation occurs if the pore water dissipates, which results in settlement of the soil layer (S(t)). In the present study, the thaw depth is measured from the top surface of the soil domain at a given time, which moves with the settlement.

In the field, thaw consolidation might occur either under the self-weight of thawed soils (e.g., spring warming of the frozen ground at the surface) or under combined effects of self-weight and external loads (e.g., frozen ground warming by buried warm oil pipelines). To investigate thaw consolidation under these loading conditions, FE analyses are performed with and without a surcharge (p).

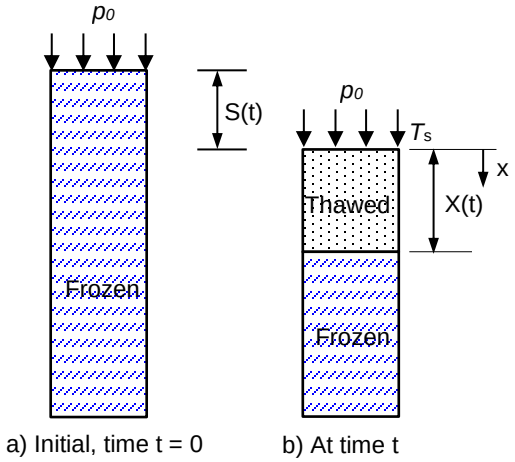

Figure 1. One-dimensional soil domain used in FE analysis

3 FINITE ELEMENT MODELING

Abaqus/Standard FE software is used for modeling coupled pore fluid diffusion and stress analysis along with conduction mode of heat transfer. An initially frozen soil sample of 250 mm high is thawed by a step increase in temperature at the top surface as shown in Fig. 1.

The FE program used in this study allows only linear brick, first-order axisymmetric, and second-order tetrahedron elements for modeling coupled heat transfer with pore fluid diffusion and stress analysis. In this study, the soil column is created using the 8-node linear brick reduced integration fully coupled temperature–pore pressure element (C3D8RPT) available in the software. The soil domain is discretized into 1 mm cubical elements. In order to perform one-dimensional analysis, only one element is used in all horizontal directions.

All the vertical faces are restrained to lateral movement, while the bottom boundary is restrained to vertical movement. For heat and fluid flow, zero heat flux and zero pore fluid flux boundary conditions are applied to all surfaces except for the top surface. A free drainage (zero pore pressure) boundary condition is applied at the top surface.

The initial conditions such as void ratio, degree of saturation and initial ground temperature are defined, and then the numerical analysis is divided into two steps. The geostatic load is applied in the first step to bring the soil domain to the in-situ stress condition. The pore fluid weight is excluded in this step to perform the analysis in terms of excess pore water pressure. In the second step, a step increase in temperature is applied at the top surface. To avoid numerical instability, the temperature is ramped from the initial frozen ground temperature (-5°C) to the targeted value within 1 minute.

3.1 Excess pore water pressure generation

Upon thawing, excess pore water pressure is generated at the thaw front because of the weight of the thawed soil and other external loads. In order to simulate the pore water pressure generation, the volume compressibility and hydraulic conductivity are ramped from the frozen state to the thawed state over a temperature range of -0.5°C to 0°C. In other words, the soil compressibility is very small at a temperature below -0.5°C; however, it becomes a compressible thawed soil at a temperature above 0°C. Similarly, hydraulic conductivity increases from k_f to k_t in this temperature range.

3.2 Model parameters

Table 1 shows the thermal, mechanical and hydraulic parameters used in this study. The hydraulic conductivity of thawed fine-grained soils is generally in a range of 10^{-10} m/s –10^{-7} m/s (Morgenstern and Smith 1973; Nixon and Morgenstern 1974; Konrad 1989). Therefore, a range of hydraulic conductivities from10^{-10} m/s to 10^{-8} m/s is used.

The soil is modeled as a linear elastic material. One-dimensional volumetric compression occurs after thawing. The Young's modulus (E) is obtained from the volume compressibility (m_v) using Eq. (1) for FE input.

$$E = \frac{(1+\nu)(1-2\nu)}{m_v(1-\nu)} \quad [1]$$

where ν is the Poisson's ratio. In this study, $\nu = 0.25$ is used for both frozen and thawed soil. Very small volume compressibility is used for frozen soil (m_{vf} = 6.94x10^{-07} m^2/kN (E = 1200 MPa)), which yields a negligible settlement of frozen soil. On the other hand, the volume compressibility of the thawed soil (m_{vt}) is 3–4 order higher than that of frozen soil (E = 0.1 MPa–1.0 MPa), which implies that settlement mainly occurs in thawed soil (Table 1 and 2).

A total of six cases are simulated for a varying hydraulic conductivity and volume compressibility of the thawed soil, and the temperature boundary conditions. In S1–S3, only the top surface temperature is varied to create different thaw front penetration rates. On the other hand, the hydraulic conductivity and volume compressibility of thawed soils are varied in S4–S6. In all cases, simulation is continued for 58 hours. FE analyses are performed without any surcharge (i.e., only self-weight) and with a surcharge p_0 = 15 kPa.

3.3 Governing heat transfer equations

The heat transfer by conduction is more significant than convective heat transfer during freezing and thawing of fine-grained soils (Nixon 1975). Therefore, the convective part is neglected in this study. The energy balance in conduction mode can be written as:

$$\rho c \frac{\partial T}{\partial t} - L\rho_i \frac{\partial \theta_i}{\partial T} - \nabla(\lambda \nabla T) = 0 \quad [2]$$

where c is the heat capacity of soil by mass, ρ is the density of soil, L is the latent heat of fusion of water per unit mass, ρ_i is the density of ice, λ is thermal conductivity and T is the temperature.

Table 1 shows the thermal properties of the multiphase system (soil skeleton and pore fluid). The phase change of pore water in soil generally occurs over a range of temperature rather than at a specific temperature of 0°C. This range depends on several including salt content, applied load and grain sizes (Lunardini 1988; McKenzie et al. 2007; Gholamzadehabolfazl 2015). In this study, a typical range of -3 °C to 0 °C is considered to model the latent heat.

Table 1. Parameters used in finite element modeling

Soil Skeleton	
Thermal conductivity, λ (W/m°C)	2.1
Specific heat, c (J/kg°C)	836
Density, ρ_s (kg/m^3)	2670
Volume compressibility of frozen soil, m_{vf} (m^2/kN)	6.94x10^{-07}
Volume compressibility of thawed soil, m_{vt} (m^2/kN)	10^{-4}–10^{-3}
Hydraulic conductivity of frozen soil, k_f (m/s)	1x10^{-14}
Hydraulic conductivity of thawed soil, k_t (m/s)	10^{-10}–10^{-8}
Pore fluid	
Thermal conductivity, λ (W/m°C)	0.58
Specific heat, c (J/kg°C)	4186
Density, ρ (kg/m^3)	1000
Latent heat, L (J/kg)	3.34x10^5
Initial conditions	
Void ratio, e	2.6
Degree of saturation, S_r	1.0

Table 2. Soil properties and boundary conditions used in the parametric study

Parameter	S1	S2	S3	S4	S5	S6
T_g (°C)	-5	-5	-5	-5	-5	-5
T_s (°C)	1	5	20	20	20	20
k_t (m/s) x10^{-10}	1	1	1	10	10	100
m_{vt} (m^2/kN) x10^{-4}	8.33	8.33	8.33	8.33	83.33	83.3

4 RESULTS

The present FE model provides the thaw depth (i.e., the location of the 0 °C isotherm), excess pore water pressure and resulting settlements. Therefore, it is not required to determine the thaw depth using an idealized equation as used in the development of previous analytical solutions for thaw consolidation (Morgenstern and Nixon 1971). Thaw consolidation is simulated for both self-weight and a combination of self-weight and applied loads. The FE results are compared with the simplified Morgenstern and Nixon (1971) analytical solution, as described below.

4.1 Analytical solution

Morgenstern and Nixon (1971) developed the thaw consolidation model based on the thaw depth measured from the initial position of the top surface. However, the top surface settles considerably with the progress of consolidation, as presented later in this paper and also shown in other studies (Dumais and Konrad 2018). Therefore, for a better comparison, the FE calculated thaw depth measured from the moving top surface (X(t)) is used. Note that Morgenstern and Nixon (1971) used the Carslaw and Jaegar (1947) solution to calculate the thaw depth as a function of $\sqrt{t}$, which is also valid for FE calculated X(t) as

$$X(t) = \alpha\sqrt{t} \quad [3]$$

where α is a constant determined from heat transfer solution.

Morgenstern and Nixon (1971) also showed that the excess pore water pressure $u(x,t)$ in the thawed soil at a location x at time t is

$$u(x,t) = \frac{p_0}{\mathrm{erf}(R) + \frac{e^{-R^2}}{\sqrt{\pi}R}} \times \mathrm{erf}\left(\frac{x}{2\sqrt{c_{vt}t}}\right) \times \mathrm{erf}\left(\frac{x}{2\sqrt{c_{vt}t}}\right) + \frac{\gamma' x}{1 + \frac{1}{2R^2}} \quad [4]$$

where c_{vt} is the coefficient of consolidation of the thawed soil, p_0 is the surcharge (Fig. 1), γ' is the submerged unit weight of the thawed soil, and R is the thaw consolidation ratio, which is given by

$$R = \frac{\alpha}{2\sqrt{c_{vt}}} \quad [5]$$

The coefficient of consolidation is related to volume compressibility and hydraulic conductivity as

$$c_{vt} = \frac{k_t}{m_{vt}\gamma_w} \quad [6]$$

where γ_w is the unit weight of water.

4.2 Simulations with a surcharge (p_0 = 15 kPa)

In this section, the FE simulations of the six cases listed in Table 2 with a surcharge p_0 = 15 kPa are presented. Figure 2 shows the FE calculated settlement (S(t)) of the soil layer with time. The surcharge causes additional settlement, as compared to only the self-weight cases, as discussed later in Section 4.3.

Figure 2 shows that the maximum settlement during the simulation period is the highest in S6 and the lowest in S1, which is due to the higher surface temperature, hydraulic conductivity and volume compressibility in Case S6 than those compared to Case S1. A higher surface temperature results in a larger thawed zone, while the higher hydraulic conductivity and volume compressibility causes more settlement due to the dissipation of pore water pressure. Note that the excess pore water pressure is not completely dissipated during the simulation period shown in Fig. 2. The post-thaw dissipation is discussed later in Section 4.4.

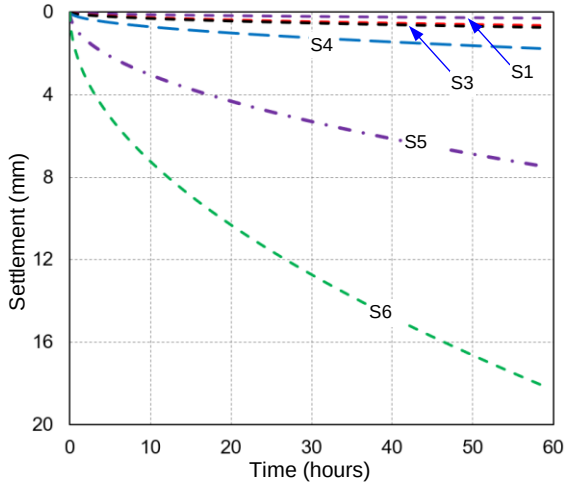

Figure 2. Surface settlement in the simulations with a surcharge p_0 = 15 kPa

The settlement of the soil sample, as compared to the initial height, is not negligible for all the cases. For example, the soil sample settle ~18 mm (8% of the initial height) in case S6 after 58 hours. Therefore, the small-strain assumption, as used by Morgenstern and Nixon (1971), may not be always valid.

Figure 3 shows the pore pressure variation with depth for three time intervals (8h, 16 h and 58 h) for Case S6. In this figure, the vertical axis represents the depth measured from the top surface of the soil sample before settlement (i.e., initial state). As the settlement of the soil sample is considered in the present FE analyses, there is a discrepancy between the analytical solution of Morgenstern and Nixon (1971) and FE analysis in terms of thaw depth. Therefore, to compare the results obtained from FE and analytical solutions, the thaw depth measured from the top of the settled soil sample is used.

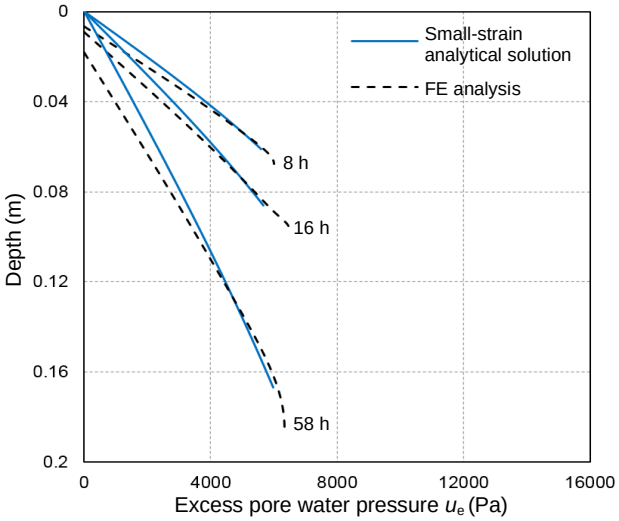

Figure 3. Comparison of excess pore pressure in Case S6 obtained from FE analysis and a small-strain analytical model

Morgenstern and Nixon (1971) presented the thaw consolidation results using the dimensionless thaw consolidation ratio (R) (Eq. 5). The parameters R incorporate the effects of several factors including the coefficient of consolidation (c_{vt}) and heat transfer (α). Plotting the frost front penetration depth in FE analyses with time and fitting the results as Eq. (3), the value of α is obtained for each case (S1–S6 in Table 2). Table 3 shows the calculated values of α. Now, using the values of α and c_{vt}, the thaw consolidation ratio (R) is calculated, as shown in Table 3. Note that the higher the value of R the lower the pore pressure dissipation (i.e., higher excess pore pressure accumulation during thawing).

Table 3. Calculated parameters for analytical solution

Calculated parameters	S1	S2	S3	S4	S5	S6
α ($m/s^{1/2}$) x10^{-5}	5.07	16.4	36.6	36.6	36.3	36.1
c_{vt} (m^2/s) x10^{-8}	1.22	1.22	1.22	12.2	1.22	12.2
R	0.23	0.74	1.66	0.52	1.64	0.52

Figure 4 shows the FE simulated excess pore water pressures(u_e) (dashed lines) with time up to the thaw depth at that time for the six simulation cases. The calculated excess pore pressure using the Morgenstern and Nixon (1971) analytical solution (solid line) is also plotted in this figure. Note that, x = 0 represents the current position of the top surface of the soil sample at a given time for both FE analysis and analytical solution.

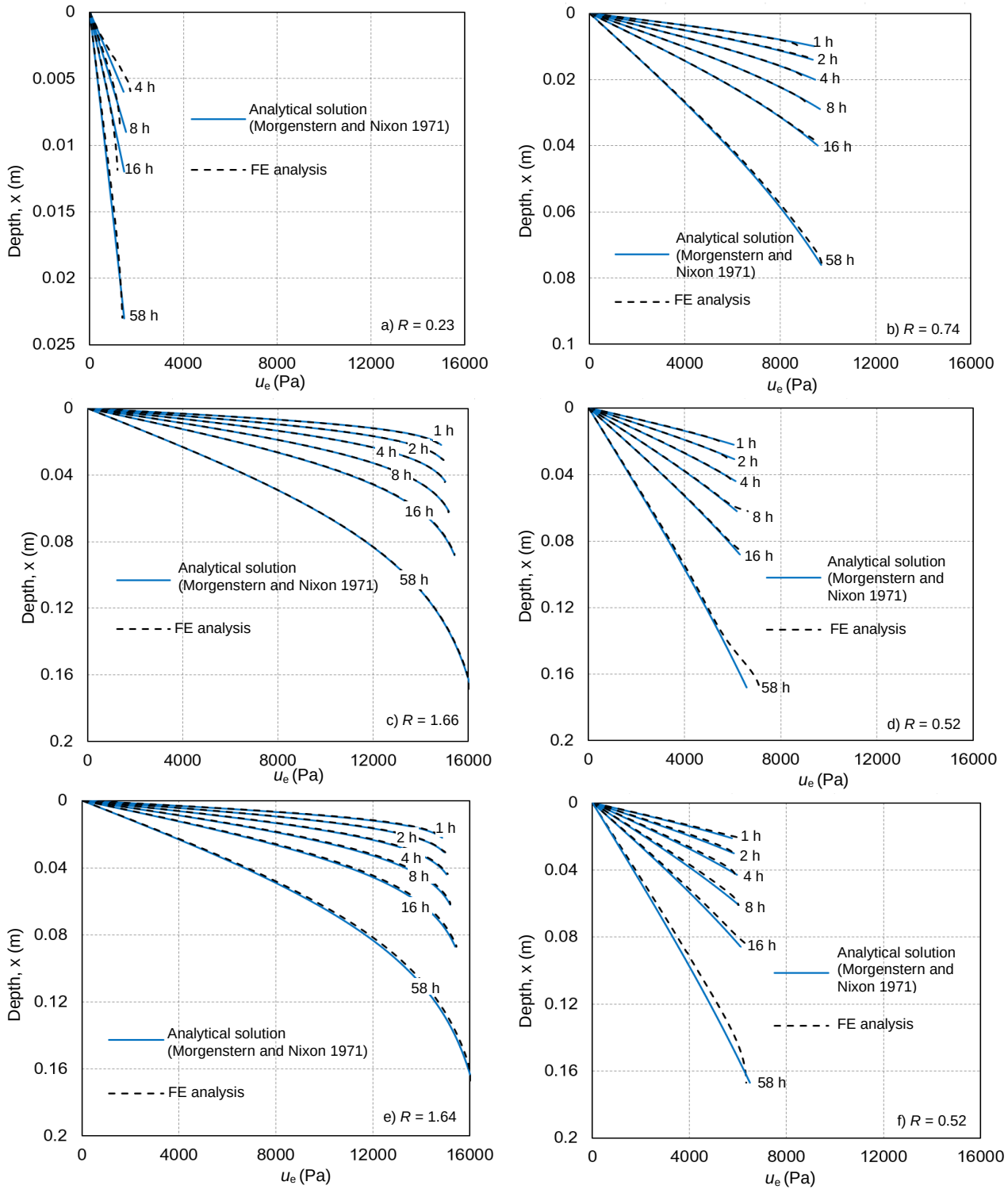

Figure 4. Excess pore water pressure in the soil sample under a surcharge

The FE calculated excess pore water pressure closely matches with the analytical solution, which implies that the FE approach presented in this study can be used successfully for modeling thaw consolidation. Some discrepancies in Case S1 at the early stage of consolidation (≤ 4 h) are primarily due to very small thaw front penetration depth (only few elements) under a low surface temperature (T_s = 1 °C).

4.3 Simulations for only self-weight (p_0 = 0)

In this set of analysis, no surcharge is applied to the top surface; therefore, the consolidation occurs only due to the self-weight of the soil. The other parameters used in these analyses are the same as before (Tables 1 and 2). Figure 5 shows the FE simulated excess pore water pressure (u_e) (dashed lines) for the six simulation cases listed in Table 2. Note that, the surface settlement in this case during thawing is less than that of with a surcharge as discussed in Section 4.2.

Following the same approach described in Section 4.2, the thaw consolidation ratio (R) is calculated from FE results for this case, as shown in Figs. 5(a)–5(f). The excess pore water pressure is then calculated using the Morgenstern and Nixon (1971) analytical solution for these values of R.

Figures 5(a)–5(f) show that the FE calculated u_e increases almost linearly with depth and reaches the maximum at the thaw front. Below this depth where the soil is still frozen, FE analysis calculates some pore water pressure which gradually decreases to zero. This is attributed to the pore fluid diffusion into the frozen soil from the thaw front, although it has a low permeability as compared to the thawed soil (Table 1 and 2). Note that, an impermeable boundary is considered in the analytical solution (Morgenstern and Nixon 1971).

For a case without surcharge (p_0 = 0), the analytical solution for the excess pore water pressure (Eq. (4)) becomes a time-independent linear function of depth (x), where the slope of the linear line depends on R.

$$u(x,t) = \frac{\gamma' x}{1 + \frac{1}{2R^2}} \qquad [7]$$

The solid lines in Fig. 5 shows the excess pore water pressure in the thawed soil during thawing, which match with the FE calculated results. Moreover, the higher the value of R the larger the excess pore water pressure. For example, the maximum u_e is 1400 Pa for R = 1.65 (Fig. 5(c) while it is 550 Pa for R = 0.52 (Fig. 5(d)). Therefore, it can be concluded that the FE modeling approach presented in this study can simulate the process of thaw consolidation.

4.4 Post-thaw consolidation under self-weight

Figure 5 shows that the generated excess pore water pressure does not dissipate completely during thawing. Therefore, consolidation settlement will be continued even if the thaw front does not move further. This process is known as post-thaw consolidation.

FE analysis is performed for the case S2 to calculate the post-thaw consolidation. In this simulation, the heat transfer analysis is stopped after 58 hours, when the thaw front moves ~75 mm; however, the analysis for pore pressure dissipation is continued. Figure 6 shows the pore pressure in the thawed zone with time factor $T = c_{vt}.t/H^2$, where $c_{vt} = 1.22\times10^{-8}$ m^2/s and H is the drainage length which is equal to the thaw depth in this case (= 0.075 m). The pore pressure dissipates with time, and the pore pressure isochrones are very similar to the self-weight consolidation of a soil layer having an impermeable bottom boundary.

5 CONCLUSIONS

Thaw consolidation settlement is one of the major concerns in the cold climates. The effectiveness of an FE modeling approach for thaw consolidation is presented in this study. The FE simulations are performed for a soil sample in one-dimensional condition. Coupled heat transfer, pore water pressure generation and its dissipation are successfully simulated. An idealized soil behaviour—linear void ratio-effective stress relation, constant hydraulic conductivity and heat transfer only by conduction—is considered in order to compare the FE result with the analytical solution developed by Morgenstern and Nixon (1971).

The analyses are performed with and without a surcharge at the top surface of the soil sample in order to simulate effects of self-weight and external loads. It is shown that the present FE approach can successfully simulate the thaw consolidation process.

In terms of practical implication, the FE approach can be modified and used for thaw consolidation with complex boundary conditions, such as moving thaw front boundary or thawing around a buried pipeline.

One of the limitations of this study is that a linear void ratio–effective stress relationship and constant permeability is used for the thawed soil. It is understood that e–σ′ relationship is highly nonlinear, especially at a low-stress level, and hydraulic conductivity decreases with void ratio change during consolidation.

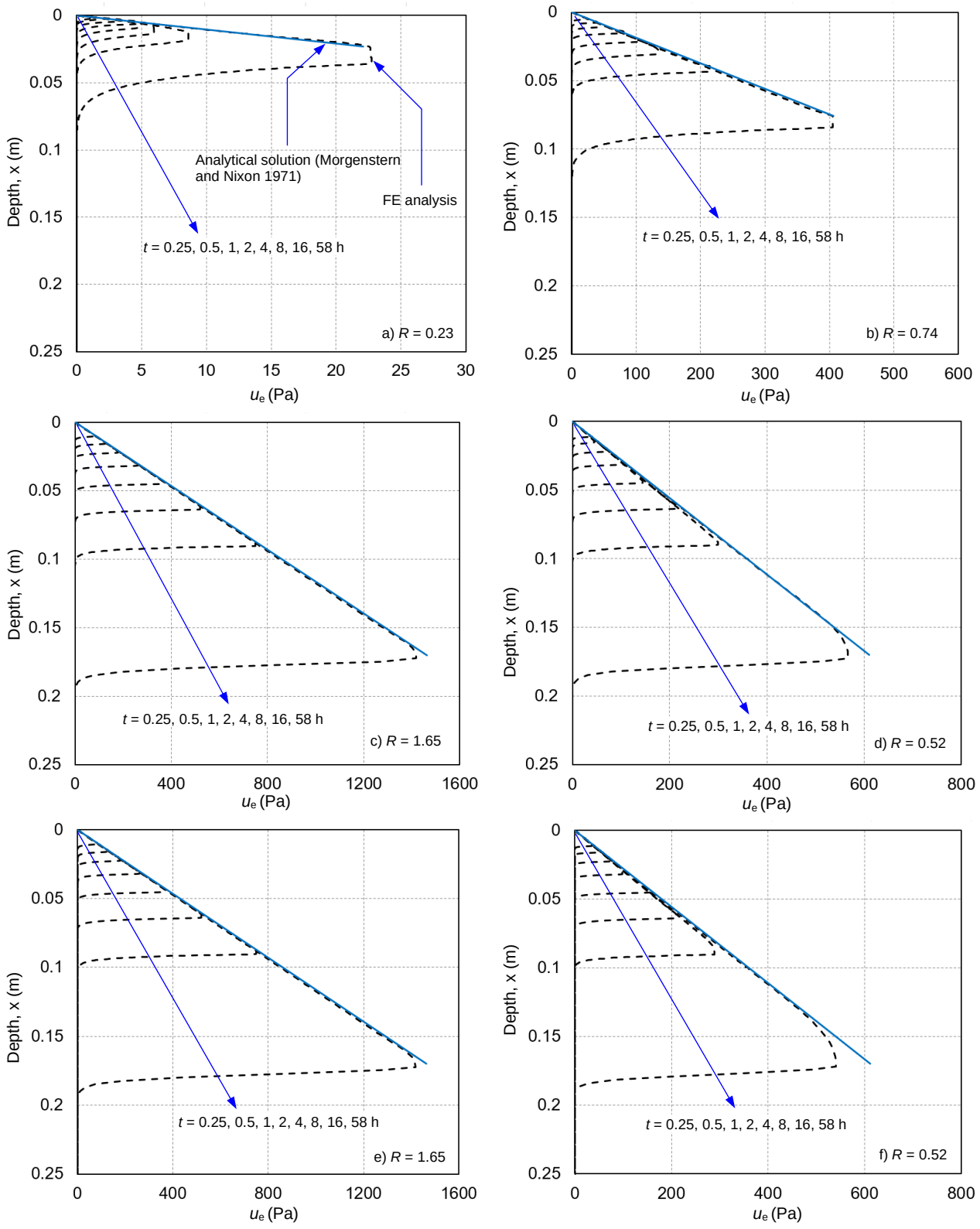

Figure 5. Excess pore water pressure under self-weight

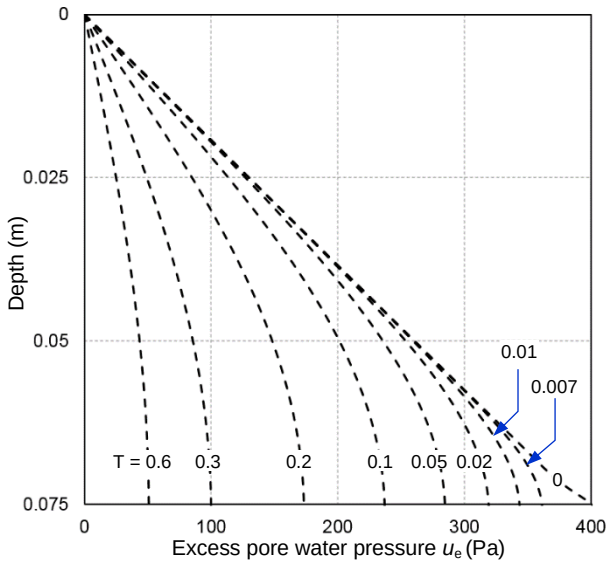

Figure 6. Post-thaw excess pore water pressure dissipation in S2

ACKNOWLEDGEMENTS

The works presented in this paper have been supported by the Natural Sciences and Engineering Research Council of Canada (NSERC), InnovateNL and former Research and Development Corporation of Newfoundland and Labrador (RDC).

REFERENCES

Carslaw, H.S. and Jaegar, J.C. 1947. *Conduction of heat in solids*, 2nd ed., Oxford: Clarendon Press.

Dumais, S. and Konrad, J.-M. 2018. One-dimensional large-strain thaw consolidation using nonlinear effective stress–void ratio–hydraulic conductivity relationships, *Canadian Geotechnical Journal*, 55(3): 414-426.

Dumais, S. and Konrad, J.-M. 2019. Large-strain nonlinear thaw consolidation analysis of the Inuvik warm-oil experimental pipeline buried in permafrost, *Journal of Cold Regions Engineering*, 33(1): 04018014.

Foriero, A. and Ladanyi, B. 1995. FEM Assessment of large-strain thaw consolidation, *Journal of Geotechnical Engineering*, 121(2): 126-138.

Gholamzadehabolfazl, A. 2015. A numerical study of a highway embankment on degrading permafrost, *MSc thesis*, University of Manitoba, Winnipeg, Manitoba.

Konrad, J.-M. 1989. Effect of freeze–thaw cycles on the freezing characteristics of a clayey silt at various overconsolidation ratios, *Canadian Geotechnical Journal*, 26(2): 217-226.

Lunardini, V.J. 1988. *Freezing of soil with an unfrozen water content and variable thermal properties*, CRREL report 88-2, CRREL: Hanover, NH, USA.

McKenzie, J., Voss, C.I. and Siegel, D.I. 2007. Groundwater flow with energy transport and water-Ice phase change: numerical simulations, benchmarks, and application to freezing in peat bogs, *Advances in Water Resources*, 30(4): 966-983.

Morgenstern, N.R. and Nixon, J.F. 1971. One-dimensional consolidation of thawing soils, *Canadian Geotechnical Journal*, 8(4): 558-565.

Morgenstern, N.R. and Smith, L.B. 1973. Thaw–consolidation tests on remoulded clays, *Canadian Geotechnical Journal*, 10(1): 25-40.

Nixon, J.F. 1975. The role of convective heat transport in the thawing of frozen soils, *Canadian Geotechnical Journal*, 12(3): 425-429.

Nixon, J.F. and Morgenstern, N.R. 1973. Practical extensions to a theory of consolidation for thawing soils, Proceedings of *2nd International Conference of Permafrost*, Yakutsk, USSR, 1: 369-377.

Nixon, J.F. and Morgenstern, N.R. 1974. Thaw–consolidation tests on undisturbed fine-grained permafrost, *Canadian Geotechnical Journal*, 11(1): 202-214.

Williams, P.J. and Burt, T.P. 1974. Measurement of hydraulic conductivity of frozen soils, *Canadian Geotechnical Journal*, 11(4): 647-650.